Multi-Objective Optimization and Model-based Predictive Control using State Feedback Linearization for Crystallization

By

Ravi Parekh

A doctoral thesis submitted in partial fulfilment of the requirements for the award of Doctor of Philosophy of Loughborough University

Department of Chemical Engineering

2019

Declaration

I declare that the work presented in this thesis is my own except where acknowledged in the text, and has not been submitted either in whole or in part, for a degree at this or any other institution.

Dedicated to my parents Hemant and Rita, and to my brother Nehal.

Abstract

The ongoing Quality-by-Design paradigm shift in the pharmaceutical industry has sparked a new interest in exploring advanced process control techniques to aid the efficient manufacture of high value products. One important process in the manufacturing is crystallization, a key process in purification of active pharmaceutical ingredients (APIs). There has been little crystallization control research in the area of global input/output linearization, otherwise referred to as state-feedback linearization (SFL). The global linearization allows a nonlinear model to be linearized over the whole domain for which the model is valid and can be embedded into a model predictive controller (MPC). MPC allows the control of a process based on a model which captures the physical understanding and constraints, but a widely reported challenge with the SFL technique is the poor ability of explicitly handling the plant constraints, which is not ideal for a highly regulated production environment such as pharmaceutical manufacturing.

Therefore, the first purpose of this research is to explore the use of SFL and how it can be applied to controlling batch and continuous MSMPR crystallization processes with the incorporation of plant constraints in the MPC (named SFL-Plant constraints). The contribution made from this research is the exploration of the SFL MPC technique with successful implementation of SFL-Plant constraints. The novelty in this method is that the technique builds on existing SFL-MPC frameworks to incorporate a nonlinear constraints routine which handles plant constraints. The technique is applied on numerous scenarios of batch and continuous mixed suspension mixed product removal (MSMPR) supersaturation control of paracetamol in water, both seeded and unseeded, which all show that the SFL-Plant constraints technique indeed produces feasible control over crystallization subject to constraints imposed by limitations such as heat transfer. The SFL-MPC with SFL-Plant constraints was applied to single-input single-output (SISO) and multiple-input multiple-output (MIMO) systems, demonstrating consistent success across both schemes of control. It was also determined that the SFL-Plant constraints do increase the computational demand by 2 to 5 times that of the SFL when unconstrained. However, the difference in absolute time is not so significant, typically an MPC which acted on a system each minute required less than 5 seconds of computation time with inclusion of SFL-Plant constraints. This technique

presents the opportunity to use the SFL-MPC with real system constraints with little additional computation effort, where otherwise this may have not been possible.

A further advancement in this research is the comparison between the SFL-MPC technique to an MPC with a data-driven model - AutoRegression model with eXogenous input (ARX) – which is widely used in industry. An ARX model was identified for batch supersaturation control using a batch crystallization model of paracetamol in isopropyl alcohol (IPA) in gPROMS Formulated Products as the plant, and an ARX model developed in an industrial software for advanced process control – PharmaMV. The ARX-MPC performance was compared with SFL-MPC performance and it was found that although the ARX-MPC performed well when controlling a process which operated around the point the ARX-MPC was initially identified, the capability of tracking the supersaturation profile deteriorated when larger setpoints were targeted. SFL-MPC, on the other hand, saw some deterioration in performance quantified through an increase in output tracking error, but remained robust at tracking a wide range of supersaturation targets, thus outperforming the ARX-MPC for trajectory tracking control.

Finally, single-objective and multi-objective optimization of a batch crystallization process is investigated to build on the existing techniques. Two opportunities arose from the literature review. The first was the use of variable-time decision variables in optimization, as it appears all pre-existing crystallization optimization problems to determine the ideal crystallization temperature trajectory for maximising mean-size are constructed of piecewise-constant or piecewise-continuous temperature profiles with a fixed time step. In this research the time-step was added as a decision variable to the optimization problem for each piecewise continuous ramp in the crystallization temperature profile and the results showed that for the maximisation of mean crystal length in a 300-minute batch simulation, when using 10 temperature ramps each of variable length resulted in a 20% larger mean size than that of 10 temperature ramps, each over a fixed time length. The second opportunity was to compare the performance of global evolution based Nondominated Sorting Genetic Algorithm – II (NSGA-II) with a deterministic SQP optimization method and a further hybrid approach utilising first the NSGA-II and then the SQP algorithm. It was found that for batch crystallization optimization, it is possible for the SQP to converge a global solution, and the convergence can be guaranteed in the shortest time with little compromise using the hybrid

method if no information is known about the process. The NSGA-II alone required excessive time to reach a solution which is less refined. Finally, a multi-objective optimization problem is formed to assess the ability to gain insight into crystallization operation when there are multiple competing objectives such as maximising the number weighted mean size and minimizing the number weighted coefficient of variation in size. The insight gained from this is that it is more time efficient to perform single-objective optimization on each objective first and then initialize the multi-objective NSGA-II algorithm with the single-objective optimal profiles, because this results in a greatly refined solution in significantly less time than if the NSGA-II algorithm was to run without initialization, the results were approximately 20% better for both mean size and coefficient of variation in 10% of the time with initialization.

Contents

List of figures

List of tables

Acknowledgements

I would like to begin by thanking my mum, dad and brother for their love and support, as well as my extended family. Also, thanking my closest friends Ashley Lawrence and Rajen Mistry for their friendship and support.

I express my appreciation and gratitude to my supervisors; Professor Chris Rielly and Dr Brahim Benyahia; who provided me with this opportunity to become a PhD researcher at Loughborough University. I thank you for your support and guidance, for helping me develop personally and professionally as a researcher and an engineer; and for allowing me to collaborate with other institutions and industrial partners during my time as a researcher.

I thank and acknowledge David Lovett, John Mack and Furqan Tahir from Perceptive Engineering Ltd for allowing me to pursue a collaborative project and providing me with guidance and support as well as the industrial advanced process control platform to investigate and compare the performance between the MPC technique I used in the core of my research with the MPC technique used in industry with data-driven modelling.

I thank and acknowledge the International Institute for Advanced Pharmaceutical Manufacturing (I2APM), along with Associate Professor Rohit Ramachandran for enabling my secondment at Rutgers University. I thank Nirupaplava Metta for her guidance and support during my secondment where I investigated the effects of moisture content of high-shear granulated particles on the milled particle size distribution using a conical screen mill.

I thank and acknowledge Dr Ian Houson and Dr Johan Remmelgas for enabling a further secondment with AstraZeneca in Gothenburg, Sweden and Macclesfield, UK. I also thank the extended team at AstraZeneca of Pirjo Tajarobi, Mats Josefson, Olof Svensson, Mike Quayle, Kristina Roos-Rydell, Gavin Reynolds, Steve Holland, Sean Clifford, Jeff Parry and Nick Pedge for the opportunity to explore in-line PAT for monitoring properties of twin-screw granulation.

With that, I thank EPSRC and the Doctoral Training Centre in Continuous Manufacturing and Crystallization (CMAC) for funding the research I have documented herein.

I thank my friends from Loughborough; Iyke Onyemelukwe, Akos Borsos, Zhuang Sun and Monalie Bandulasena; as well as my CMAC cohort for their friendship and the many great moments we had over the four years together and the much-needed comic relief! I also acknowledge and thank the wider research group at Loughborough, particularly Qinglin, Elena, Keddon, Dimitrios. Emmanuel, Sharleigh, Gurinder and David Odetade.

1 Introduction

1.1 Background

The pharmaceutical industry has traditionally been based on flexible batch processes which have been operated primarily based on past human experience, observation and testing. The pharmaceutical product development pipeline consists of four stages. The first stage is the initial research and drug discovery where hundreds or thousands of drug candidates are screened and based on criteria that feedback from clinical trial requirements, many drug candidates will be eliminated as potential drugs. The second phase is the clinical trials where the most promising drugs will be tested in increasing numbers of patients. This stage will usually bring the number of drug candidates down to one which is put forward for the third phase, regulatory review. During the clinical trials, further research and consideration will be given to developing manufacturing methods to produce the drugs, and the scale of production will increase from tens of volunteers to thousands, requiring a robust procedure to manufacture the drug in larger equipment or with a greater throughput. The final phase is the post approval research and monitoring once the drug enters production and is released to market. Underlying in these four phases are extensive costs from researching thousands of candidates, the clinical trials and building robust manufacturing techniques in the existing manufacturing paradigm. This can lead to drugs becoming approved for a therapy but the manufacturing methods for the efficiently producing the drug are seldom considered because there is a great reliance on existing batch production techniques in the industry. However, there are greater efficiencies and other benefits to be seen by investing in continuous manufacturing. These issues have invoked a paradigm shift in the way drug research and development is being undertaken in industry, and specifically when considering the manufacturing process, a greater appreciation has been gained for continuous manufacturing techniques in place of batch. The preliminary analysis of continuous manufacturing methods in the industry appear to offer benefits such as streamlining drug production processes and thus reduce plant size/footprint, production times and to increase purity, yield and efficiency; leading to an overall reduction in cost. Although these are the theoretical benefits of continuous manufacturing, given the principles of production at a theoretical steady state, there are numerous challenges that must be overcome for regulatory compliance and for purity and drug efficacy compliance. It is important to quantify how sensitive these

production methods are to disturbances and to ensure that the defined steady state is also compliant. This is steadily bringing a need for robust and advanced process control strategies and collectively this is bringing a paradigm shift to the pharmaceutical industry known as Quality by Design (QbD). The focus of this research is to explore optimization advanced process control applications in pharmaceutical manufacturing with the aim to contribute towards the advancement into QbD.

1.2 Research methodology

The research undertaken in this thesis is based *in-silico* using modelling, simulation, optimization and control techniques to address the optimization and controllability of nonlinear chemical processes such as pharmaceutical crystallization. Recent and ongoing advancement of computer processing capabilities has enabled further exploration of numerical optimization and control methods in research. This research builds on a global input-output feedback linearization technique which is used to transform a nonlinear input-output model into a linear one through a coordinate transformation of the model into a new domain. The technique is then applied to realistic control scenarios in the pharmaceutical industry such as controlling a batch supersaturation trajectory through a full batch or maintain a continuous MSMPR number-weighted mean crystal size at steady state. The linearization technique is applied to continuous MSMPR crystallization models for different input/output objectives, and the resulting linearized model is embedded into a model predictive controller. The MPC is used to execute control over a process by making informed changes to the process using the model to predict the process behaviour. The inherent functionality of a traditional MPC is the ability to handle constraints of the system, such as in a crystallization process the cooling or heating rate will not exceed specified limits due to heat transfer limitations, but this is a greater challenge for the SFL based MPC because the coordinate transformation results in loss of plant visibility in the MPC – this will be overcome with the development of a routine that builds on existing constraints handling routines that have been used for SFL-MPC elsewhere. The methodology is focussed on using mathematical computation software that is widely available in the research environment – MATLAB – and exploring potential new capabilities of existing numerical techniques. Finally, a comparative study is also considered to compare the SFL-MPC to a data-driven technique. The purpose of this is to assess the performance benefit of using SFL-MPC, and to introduce mismatch by

implementing a low-order model in the SFL-MPC and a higher order model solved using finite volume method in an external software, which is to be controlled using industrial advanced process control software.

1.3 Aims and objectives

The aim of this research is to investigate the development of an advanced process control technique based on a global linearization method, and its applicability in the effective control of pharmaceutical crystallization processes. The objectives were:

1. Develop single and multi-objective optimization strategies for crystallization to:
    a. Explore the use of time steps as decision variables in place of fixed time steps which are commonplace in literature for crystallization. Identify if there is a benefit to variable time-steps, such a larger number-weighted crystal mean-size in a maximization optimization problem.
    b. Compare the performance and quality of optimal solution from the stochastic Nondominated Sorting Genetic Algorithm – II (NSGA-II) compared to a deterministic sequential quadratic programming (SQP) algorithm and a hybrid approach which begins with NSGA-II to provide SQP with an initial guess which will be refined.
    c. Explore the performance of multi-objective optimization and determine if the quality of the optimal solution can be improved in a shorter time by initializing the NSGA-II multi-objective optimization problem to maximize the crystal mean-size and minimize the coefficient of variation in size.
2. Develop a state feedback linearization model predictive controller (SFL-MPC) for a single-input single-output (SISO) crystallization processes.
3. Extend the state feedback linearization MPC capabilities by exploring the ability to implement valid constraints (SFL-Plant constraints) on the control problem and determine the performance and feasibility of using MPC with the SFL-Plant Constraints method.
4. Extend and validate the state feedback linearization MPC to multiple-input multiple-output crystallization processes and apply the SFL-Plant constraints technique to assess feasibility of MPC.

5. Develop a data-driven autoregression model with exogenous input (ARX) for use in MPC and compare the ARX-MPC with SFL-MPC on a batch seeded crystallization system to assess the performance benefits of SFL-MPC.

1.4 Main contribution of this work

This research has three main novelties. The first is in applying the global input/output state feedback linearization technique and applying it to model predictive control for continuous MSMPR crystallization. The SFL-MPC has already been applied to batch crystallization elsewhere. The implementation in SISO continuous number-weighted mean-size control is also a novelty. The insights gained from tuning the batch and continuous MSMPR SFL-MPC for supersaturation control also has not been reported elsewhere.

The developed SFL-Plant constraints technique is a nonlinear constraints routine which has been developed based on pre-existing an SFL constraints-handling framework for MPC, but the routine that was developed for directly handling plant constraints in an SFL-MPC is novel. This work primarily bridges a gap in using global input/output linearization on crystallization and implementing the linearized model in an MPC. Various attempts have been made at constraints handling with compromises from either generating infeasible constraints due to the coordinate transformation from SFL, computational inefficiency of nonlinear constraints routines. The proposed method in this research is usable in real-time applications. The application of the constraints on SISO and MIMO configurations of batch and continuous MSMPR crystallization for supersaturation and mean-size control is a new contribution.

A comparative study on the performance comparison of ARX-MPC and SFL-MPC is also a new contribution, applied to batch crystallization in an industrial simulation environment using an industrial advanced process control software – PharmaMV.

Finally, minor contributions include the insights gained in the comparison of global-stochastic and local-deterministic optimization methods applied to batch crystallization optimization by introducing a new set of decision variables that does not appear to have been used previously. The most common optimization problems appear to optimize a piecewise-constant or piecewise-continuous temperature profile to maximise the crystal size in a process, but the piecewise profiles tend to have a fixed time-step. In this case the time-step was introduced as a decision variable to explore if the optimal mean-size of the same model and same batch

length can be improved. Furthermore, insights were gained into the performance and quality of optimization solution between the NSGA-II, SQP and hybrid optimization when applied to batch crystallization to maximise the mean-size. Also, in the use of true multi-objective optimization of batch crystallization process to determine the optimum crystallization trajectory for maximising crystal mean size whilst also minimising the coefficient of variation of size, it was realised that initialization with single-objective optimization can play an important role in obtaining a better optimization result in shorter computation time.

1.5 Thesis structure

The following is a summary of the remaining chapters in this thesis:

Chapter 2. Literature review: This chapter introduces and reviews: pharmaceutical crystallization process; the kinetics and mechanisms with associated modelling techniques; the population balance model and solution techniques; batch and continuous MSMPR crystallization modelling; subsequent optimization in single and multi-objective forms for batch crystallization; process control applications with a focus on model predictive control; and applications of state-feedback linearization and constraints techniques of SFL both in crystallization and other fields to explore the research opportunities of implementing techniques used elsewhere to crystallization.

Chapter 3. Multi Objective Optimization of Batch Crystallization: An introductory study is conducted on optimization applications for crystallization using piecewise-constant and piecewise-continuous decision variables. The uses of local (SQP), global (NSGA-II) and hybrid optimization methods are considered for offline optimization. The results from the three approaches are compared and assessed for potential use in online control systems. Multi-objective optimization using a global NSGA-II is also used to assess how the competing objectives in crystallization will impact the operation and performance of crystallization, while initialization is used in multi-objective optimization to establish if optimization can be performed more efficiently and yield improved optimization results.

Chapter 4. Single-Input Single-Output State Feedback Linearization, Tuning and SFL-Plant Constraints for Crystallization: The use of input-output linearization with state-feedback is used to linearize the nonlinear crystallization model, and the new model is then used for control in an MPC. This chapter introduces how to perform this linearization for a single-input

single-output (SISO) system and applies the technique to the crystallization model. The MPC is also introduced in detail and the SFL is embedded into the MPC with the introduction of the SFL-MPC framework. The challenges in performing this transformation and various drawbacks to using this as a model for control are also discussed. A comprehensive tuning is performed on the SFL-MPC system to complete the controller design. The method for constraints handling is developed and discussed. The SFL-Plant constraints routine is then tested in a series of short crystallization scenarios to establish if they technique can be applied to batch and continuous MSMPR crystallization to produce feasible control. Finally, the SFL-MPC technique is implemented for batch supersaturation control and continuous MSMPR supersaturation control and mean-size control, with the discussion focussed on control of the crystallization process.

Chapter 5. Multiple-Input Multiple-Output Model Predictive Control with State Feedback Linearization and Decoupling for Crystallization: The MIMO SFL technique which extends the SISO SFL technique is described, introducing a decoupling procedure. A continuous MSMPR crystallization process is used for supersaturation and mean size control by manipulation of jacket temperature and seed loading in the MIMO SFL MPC. The SFL-Plant constraints technique described in chapter 4 is applied to the MIMO system to assess the applicability of the technique to MIMO SFL MPC.

Chapter 6. Comparative Study of SFL-MPC and ARX-MPC applied to Seeded Batch Crystallization: A comparison is made between the SFL-MPC already developed in previous chapters, and an industrially adopted modelling technique used in MPC – the data driven ARX modelling. The two models are then implemented through an industrial software for advanced process control – PharmaMV – to control a batch seeded crystallization plant running in gPROMS Formulates Products which is solved using a finite volume method, thus introducing some mismatch between the plant and model. The ARX model is identified at a supersaturation of 1.1, and then applied to control a batch to a relative supersaturation target of 1.1, 1.25 and 1.4 to be compared with SFL-MPC at the same conditions.

2 Literature review

2.1 Introduction

The purpose of this chapter is to investigate and review the field of crystallization modelling, simulation, optimization and control to understand the advances in the field and to identify research opportunities that will be explored in this research. The crystallization process and the underlying kinetic mechanisms are introduced to discuss the methods and approaches used for modelling crystallization. Model-based crystallization optimization and control techniques are also reviewed. The chapter is concluded with the identified research opportunities that will be investigated further in the following chapters.

2.2 Crystallization, Solubility and Supersaturation

Crystallization is a phase change of atoms or molecules from a dissolved liquid state in solution into a solid and highly ordered crystalline state; crystallization is primarily used as a purification process to recover a desired material from a solution, usually with the presence of impurities (Mullin, 2001; Ulrich *et al.*, 2001; Veesler and Puel, 2015). The solubility is a thermodynamic equilibrium state defined as the maximum quantity of solute that can be dissolved in a solvent at a defined temperature and pressure. When the quantity of solute in solution is equal to the solubility, the solution is saturated with solute. To perform crystallization, it is first necessary to identify the solubility curve of a chosen solute and solvent system.

The solubility curve is dependent upon the solute, solvent(s) and type of crystallization process. The solubility curve is obtained experimentally by establishing how much solubility of solute at multiple different conditions (Hefter and Tomkins, 2003). For example, a cooling crystallization solubility curve will be determined by establishing how much solute can be dissolved in solvent at multiple pre-determined temperatures, then these points are used to construct a continuous function which represents the solubility for the system (Mullin, 2001; Veesler and Puel, 2015; Gao *et al.*, 2017). For the purposes of modelling and simulation of crystallization, the solubility curve will not be determined experimentally in this research, but rather, a candidate crystallization system will be chosen whose solubility curve is already provided and validated in literature.

The solubility curve is most often represented as a second order polynomial or as an exponential function of temperature, as per equations Equation 2-1 and Equation 2-2.

$$C^* = A_0 + A_1 T + A_2 T^2 \qquad \textit{Equation 2-1}$$

$$C^* = A_0 \exp A_1 T \qquad \textit{Equation 2-2}$$

The driving force behind crystallization is supersaturation, where the solution is driven from a stable under-saturated or completely saturated condition into a state of being thermodynamically over-saturated. At this point, the mass of solute that remains dissolved in the system is greater than theoretical solubility at the same conditions. The supersaturation can be represented as a function of solute concentration and the solubility, and can either be the absolute supersaturation Equation 2-3, the supersaturation ratio Equation 2-4, or the relative supersaturation as defined in Equation 2-5.

$$S = C - C^* \qquad \textit{Equation 2-3}$$

$$S_r = \frac{C}{C^*} \qquad \textit{Equation 2-4}$$

$$\sigma = \frac{C - C^*}{C^*} \qquad \textit{Equation 2-5}$$

where C is the concentration of solute in solution and C^* is the solubility at the same temperature, S is absolute supersaturation and S_r is supersaturation ratio, and σ is the relative supersaturation. There are multiple modes of operating crystallization from a solution: cooling, anti-solvent and evaporative are three examples. In cooling crystallization, supersaturation can be created by cooling the solution (Ulrich *et al.*, 2001), in anti-solvent crystallization it is created by adding anti-solvent to the solution thus reducing the solubility of solute in the solution mixture, and in evaporative crystallization the solvent is evaporated thus creating a supersaturated solution by increasing solute concentration through reduction of solvent mass. There exists a large body of research on anti-solvent and cooling crystallization, and some authors have also studied the combination of both methods (Yang and Nagy, 2014b, 2014a), which will be referenced throughout the discussion, but the focus

of this research will be on cooling crystallization. This decision was made when reviewing the literature to select a candidate crystallization system for the optimization and control activities in this research, it was found that a couple of cooling crystallization system models were used extensively for prediction, optimization and control activities, these will be detailed later.

The crystallization process is often represented in a phase diagram, for cooling crystallization this diagram is a plot of concentration vs temperature as shown in Figure 2-1.

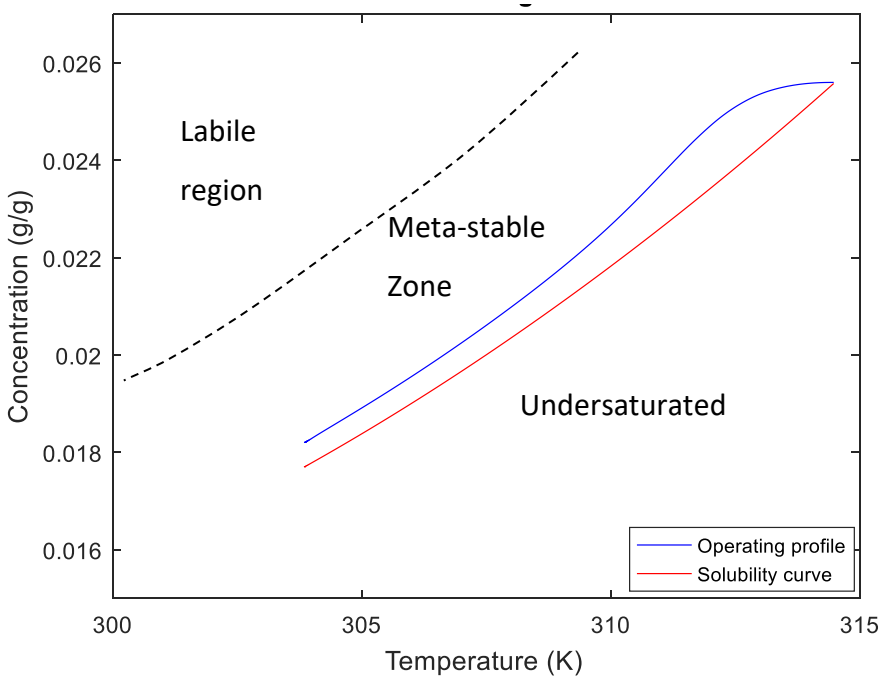

Figure 2-1 Crystallization Phase Diagram regions

The solubility curve is the boundary between the undersaturated and supersaturated regions, where the former is below and to the right, and the latter is above and to the left. The supersaturated region for crystallization can be further split into a meta-stable zone and a labile region, whose boundary (black curve) is the meta-stable limit and is determined by the crystallization kinetic mechanisms. The significance of this is that operating in the meta-stable zone allows for better control of the crystal size distribution by preferentially growing existing crystals and suppressing the nucleation of new crystals (Zhang *et al.*, 2015; Xiong *et al.*, 2018). Conversely, if the crystallization process enters into the labile region the dominant kinetic mechanism will be nucleation. The operating profile curve in Figure 2-1 is an example of a

cooling crystallization trajectory operating in the meta-stable zone, where the starting point is at 314.5 K and the process is cooled to 304 K.

Choosing a candidate crystallization system for the basis of this research is important to ensure all the necessary model parameters for chemical and physical properties of the crystallization system are available for simulation. One popular crystallization system is paracetamol in water (P/W), whose parameter identification has been performed by (Nagy, Fujiwara, *et al.*, 2008). The identification was for nucleation and size independent growth, both in the form of power law kinetics, and the identified parameters were the constants and exponents of the nucleation and growth rate equations (kinetic equations are introduced in 2.2.1 and 2.2.2). This model has been used extensively in further research by Nagy *et al.* (2008a) for comparing the performance of temperature and concentration crystallization control, further by Brown and Ni (2012) in a continuous oscillatory baffled crystallizer (COBC) to determine meta-stable zone width, particle size and number density using a video imaging technique, and also by Acevedo *et al.* (2017) to evaluate the performance of direct nucleation control (DNC) of a continuous mixed-suspension mixed-product removal (MSMPR) crystallizer. Paracetamol crystallization kinetic parameter identification has also been reported in isopropyl alcohol (IPA) (Granberg and Rasmuson, 1999), ethanol (Mitchell and Frawley, 2010), and IPA/water mixture (Hojjati and Rohani, 2006a, 2006b). Data for other pharmaceutical APIs including ibuprofen have also been reported (Manrique and Martinez, 2007; Kitak *et al.*, 2015), therefore there are multiple systems available to choose from. However, the extensive use of the paracetamol/water crystallization system in literature has led to the selection of this system. The model for this system has been validated with crystallization experiments, and the model has also been used for control in an MPC (Nagy *et al.* 2008a). The model for this system will be used for simulation, optimization and control studies.

Now the crystallization process has been described, the mechanisms for crystallization will be introduced with a review on kinetic models that have been reported in literature. There are four main kinetic mechanism that determine the crystal size distribution at the end of the process; nucleation, growth, agglomeration and breakage (Mullin and Nývlt, 1988). Every unique solute and solvent/mixture system is also uniquely impacted by each of the four kinetics.

2.2.1 Nucleation

Nucleation is the formation of a new phase in a system. In crystallization, it is when the solid crystalline material is first formed from dissolved solute. However, as described by Mullin (2001), it is not immediately possible to determine when nucleation occurs because the phenomenon occurs on a size scale that is beyond the lower detection limit of widely used sensors and analytical devices (Mitchell, Frawley and Ó'Ciardhá, 2011). There are two commonly accepted theories of how nuclei form in solution. The first is the classical theory, where molecules are constantly interacting with each other in solution and begin to amass until a critical mass is reached, at which point a crystal is formed. The second is the theory that a cluster of free-moving molecules forms in solution and when a critical size is reached, the cluster then rearranges into a highly ordered structure to form a crystal (Mohan & Myerson 2002; Izmailov et al. 1999).

Nucleation is split into primary homogeneous, primary heterogeneous and secondary homogeneous nucleation. Primary homogeneous nucleation is the spontaneous nucleation of crystals in a supersaturated solution absent of other crystals or foreign particles or surfaces. Therefore, the driving force for crystal formation is solely the supersaturation of the system (Pöllänen *et al.*, 2006). Conversely, primary heterogeneous nucleation is induced by foreign particles but not crystals of the desired material. The foreign particles provide a surface upon which nucleation can occur more readily than in homogeneous nucleation (Garside, 1982). Secondary nucleation is the formation of new crystals in the presence of existing crystals of the desired material.

	Mechanism	**Equation**	***Reference***
1	Primary Homogeneous	$B = k_b S^b$	(Mullin and Nývlt, 1988)
2	Primary Homogeneous	$B = k_{b,hom} \exp\left(-\frac{16\pi\sigma^3 v^2}{3k^3T^3(ln(\sigma_s+1))^2}\right)$	(Mullin, 2001)
3	Primary Heterogeneous	$B = k_{b,het} \exp\left(-\frac{16\pi\sigma^3 v^2 f(\varphi)}{3k^3T^3(ln(\sigma_s+1))^2}\right)$	(Söhnel and Garside, 1988)
4	Secondary	$B = k_b S^b \mu_2$	(Garside and Davey, 1980)

5	Secondary	$B = k_b \exp\left(-\frac{\Delta E}{T}\right)\sigma_s^b \mu_3^k$	(Helt and Larson, 1977)
6	Secondary	$B = k_b \sigma_s^b \ \mu_3 (L_{min})^j$	(Matthews, Miller and Rawlings, 1996)

Table 2-1 – Summary of Nucleation Kinetic Equations

Nucleation mechanisms can be represented by kinetic equations in a crystallization model. There are multiple forms of primary and secondary nucleation kinetics, the most notable are shown in Table 2-1. In this table, B is the nucleation rate, S and σ are previously defined forms of supersaturation. The second equation in the table includes parameters v for the molecular volume and T for solution temperature, as well as the Boltzmann constant k. The third equation extends the second by inclusion of a function $f(\varphi)$ as a correction factor for the presence of foreign surfaces. The fourth equation is an extension of the first by inclusion of the second moment; μ_i are the i^{th} moments (introduced in section 2.5); for a surface area dependent nucleation rate. Furthermore, equation 5 is an Arrhenius-type equation capturing the activation energy ΔE, and finally the last equation contains a length attribute L_{min}, as a minimum length for which secondary nucleation will occur. All other parameters are fitting parameters whose values are identified by using experimental data and parameter estimation techniques.

For a given crystallization system, it is first important to determine which form(s) of nucleation are most prevalent, to aid in equation selection. Then it is also important to consider the kinetic parameters that must also be identified as parameter identification can lead to a significantly large number of experiments (Matthews, Miller and Rawlings, 1996), which may not be possible to perform due to limitations in time and material availability.

The occurrence of secondary nucleation is important when considering potential nucleation in a seeded system (Chianese, Di Berardino and Jones, 1993; Bakar, Nagy and Rielly, 2009). One of the challenges with this form of nucleation is the newly formed crystals are much smaller than those which existed already in the system. As noted by Beck *et al.* (2009), the size distribution has adverse effects on downstream processes such as a larger pressure requirement during filtration. Therefore, reducing and controlling secondary nucleation is important particularly when crystallization processes are seeded.

Selection of a suitable equation for use in simulation will be based on the dominant mechanisms for the chosen P/W system. Primary homogenous nucleation has reported, therefore primary heterogeneous nucleation will not be considered. Primary homogeneous and secondary homogeneous equations will be important for the cases of unseeded and seeded crystallization, these two forms of nucleation do occur in the chosen crystallization system as it was reported by Nagy, Fujiwara *et al.* (2008) that when determining the kinetics for primary nucleation, there will be some uncertainties in the results due to the potential presence of secondary homogeneous nucleation. The identified model for primary nucleation reported by Nagy *et al.* (2008a) shows the use of equation 1 in Table 2-1. Therefore, this equation will be adopted for this research. Conversely, secondary nucleation has not been studied as extensively with the P/W system and consequently, equation 4 in Table 2-1 has been considered which is also a power law, with the addition of a new term, the second moment which is introduced in section 2.4. The secondary nucleation equation will be used for seeded systems while accepting the results may not exactly replicate a real system undergoing secondary nucleation. However, this decision is made with some confidence because of the way a seeded crystallization is operated, the aim of this type of crystallization is to grow the seed crystals and suppress nucleation. Therefore, the effects of secondary nucleation will ideally be reduced enough that they will not significantly impact the overall simulation results.

2.2.2 Growth

If a system is supersaturated and crystals are present, the crystals will grow. A widely accepted mechanism for growth is two stage crystal growth as described by (Mullin, 2001). The first stage is the transportation of solute to an available growth sites on the surface of a crystal. The second is the adsorption of solute onto the crystal. This two-stage mechanism results in crystal growth generally being rate limiting in crystallization. A simple schematic of where crystal growth can occur is shown in Figure 2-2. This schematic shows the face of a crystal being developed where A is a flat surface of the face, B is a step between faces and C is a kink on each step. Solute molecules can be considered as blocks, and when a solute block is transported to the surface, it may either adsorb onto the surface directly (D), it could occupy a vacancy in the edge (E), adsorb to a kink (C) or fill a surface vacancy (F). How the solute block joins onto the surface though is largely governed by the solute orientation and position.

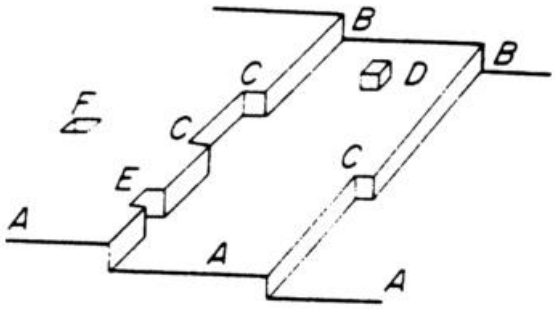

Figure 2-2. Schematic of crystal surface growth showing flat surfaces (A), steps (B), kinks (C), surface-adsorbed growth units (D), vacancies in edges (E) and vacancies in surfaces (F) (Mullin, 2001)

A couple of first principle models that are discussed by Mullin (2001) include the diffusion rate controlled kinetic equation (Equation 2-6).

$$\frac{dm}{dt} = k_m A(S) \qquad \textit{Equation 2-6}$$

where m is the mass of solids deposited on the surface of the crystal, A is the surface area of the crystal and k_m the coefficient of mass transfer. The mass transfer coefficient is very large for small boundary layers, leading to very high growth rate predictions. An alternative is the two-step model for mass transport (Equation 2-7) and adsorption (Equation 2-8) (Ulrich *et al.*, 2001).

$$\frac{dm}{dt} = k_D A(C - C_i) \qquad \textit{Equation 2-7}$$

$$\frac{dm}{dt} = k_r A(C_i - C^*) \qquad \textit{Equation 2-8}$$

where C is the concentration in the bulk of the solution, C_i is the concentration at the boundary layer from the crystal surface, C^* is the crystal surface concentration, k_D is the coefficient of mass transfer by diffusion and k_r is the rate constant for surface reaction. However, further issues with these equations are the difficulty in measuring C_i and the suggested linear gradient across the stagnant boundary layer to the surface of the crystal as defined by Equation 2-8, this is highly unlikely to be the case (Coulson *et al.*, 1964). Fortunately, there are empirical equations which can be used to model the growth kinetics.

As shown in Table 2-2, multiple different forms of equations are available in literature and have been used in various studies of crystal growth. Equation 1 is an empirical power law equation to represent growth (G) as a function of supersaturation (S). This is only suitable for size independent growth, but this equation was later extended to equation 2 with a further parameter γ, and the length of the crystal L, to incorporate size dependent growth. The third equation also include size dependent growth by inclusion of the crystal length, but this time raised to an exponent p which is another fitting parameter. The final equation is another Arrhenius type equation, similar to the fifth equation in Table 2-1 for nucleation. All other parameters are fitting parameters whose values are again obtained through a parameter identification technique using experimental data.

	Mechanism	**Equation**	***Reference***
1	Size Independent Growth	$G = k_g S^g$	(Beckmann and Randolph, 1977; Choong and Smith, 2004)
2	Size Dependent Growth	$G = k_g S^g (1 + \gamma L)$	(Garside and Jančić, 1978; Ma, Tafti and Braatz, 2002; Granberg and Rasmuson, 2005)
3	Power Law Growth	$G = k_g S^g L^p$	(Garside, 1984)
4	Arrhenius type growth	$G = k_g \exp\left[-\frac{\Delta E_G}{RT}\right] \sigma_s^g$	(Rawlings, Miller and Witkowski, 1993)

Table 2-2 – Summary of Growth Kinetic Equations

There are also other growth kinetic equations that have also emerged, one from Larsen et al. (2006) which incorporates surface defects into the equation, but the defects are not easy to measure in practice. Further from Rawlings et al. (1993) there is a semi-empirical Arrhenius-type equation which incorporates activation energy and temperature. The concluding remarks on the rate equation selection are similar to that of primary homogeneous nucleation. Empirical models have been used in research mainly due to limitations of measuring some of the parameters required for theoretical and first principle models, and in many cases the empirical models appear to be sufficiently accurate over the intended operating ranges.

In selecting the growth equations to use, there are two examples for paracetamol crystallizations in water (Nagy, Fujiwara, *et al.*, 2008), and paracetamol crystallization in solvent mixtures of water, acetone and toluene (Granberg and Rasmuson, 2005) which use equation 1 in Table 2-2. This equation will be used for further studies.

2.2.3 Agglomeration

The physical combining of multiple existing crystals into a larger mass in a crystallization system is called agglomeration. The main mechanism by which agglomeration occurs is when crystals in the system experience different degrees of shear, causing crystals to collide and shear against each other and combine together (Mumtaz *et al.*, 1997; David *et al.*, 2003; Porru and Özkan, 2017). The surface shearing can cause adsorption of molecules between the crystals, such as a molecule on one crystal's face adheres to the neighbouring crystal, or when some dissolved solute is trapped between the two faces it may also adsorb onto both faces simultaneously (Mumtaz *et al.*, 1997). When monitoring changes to a crystal size distribution (CSD), agglomeration has a dual effect as agglomeration of two or more crystals will result in an agglomerate whose size is much greater than the original crystals, but also the number of particles is reduced because two or more crystals combine into one agglomerate. When modelling a crystal size distribution with a population balance model (introduced in section 2.4), the most common way of handling agglomeration is to split the CSD into size intervals or bins, and then perform a balance on each bin (Georgieva, Meireles and Feyo de Azevedo, 2003; Faria *et al.*, 2008). Then, agglomeration of small crystals into larger crystals will be seen as a death of the smaller crystals from their original bin sizes and a birth of the larger crystal in its corresponding size bin. Number based population balances will not be sufficient here because multiple crystals will merge together to form one larger crystals, so the birth and death rates must be quantified in a quantity that is conserved, such as mass (Hulburt and Katz, 1964; Georgieva, Meireles and Feyo de Azevedo, 2003).

While agglomeration is a reported issue with paracetamol crystallization (Fujiwara *et al.*, 2002), the parameters for agglomeration have seldom been reported because the mechanism is likely dependent on shear rates which are system specific and not included in typical crystallization models. There have been some investigations of paracetamol agglomeration in pure and mixed solvent systems (Ålander, Uusi-Penttilä and Rasmuson, 2004; Ålander and Rasmuson, 2005), the most notable is by Alander *et al.* (2004), but has been seldom-used for

further modelling and simulation. For this reason, agglomeration will not be considered in the crystallization model.

2.2.4 Breakage

The final crystallization kinetic mechanism is breakage, the destruction of one crystal into smaller crystals or fragments. Crystal breakage can be common in crystallization, especially where an agitated vessel is used because the impeller speed required to suspend crystals and maintain a homogeneous mixture is often also enough to cause a crystal to fracture if the crystal is impacted by the impeller (Mazzarotta, 1992; Cornehl *et al.*, 2014; Szilágyi, Agachi and Lakatos, 2015). Similarly, collisions between crystals at high speeds can also cause fracture. In some cases where crystals have a needle-like morphology where one dimension is significantly longer than the others, they can also experience high levels of shear stress along the length of the crystal and these torqueing forces can also be enough to break the crystals (Lekhal *et al.*, 2004; Antonyuk, Palis and Heinrich, 2011; Grof *et al.*, 2011). Breakage is undesirable in a crystallization process, much like agglomeration, because it results in undesirable changes to the CSD such as the production of fines or broadening a narrow or unimodal crystal size distribution (Randolph, 1969).

Modelling the breakage is similar to the modelling of agglomeration, however in the case of breakage a single large crystal results in two or more smaller crystals. Therefore, the breakage of a large crystal results in the death of a crystal from a large size bin and the birth of two or more crystals in smaller bins. Paracetamol crystal breakage is another mechanism that is rarely reported and is also highly dependent on the operating conditions such as the crystal concentration, or number of crystals in the system, as well as fluid shear rate and agitation rate which increases the likelihood of collisions of crystal to crystal, crystal to wall and crystal to impeller (Kadam, Kramer and ter Horst, 2011; Kulkarni, Meekes and Ter Horst, 2014; Briuglia, Sefcik and ter Horst, 2018). Typically, the shapes of crystals that are prone to breakage under the aforementioned conditions generally are crystals which are long and thin, needle-like. This information along with the few reports of paracetamol breakage in crystallization give the indication that breakage is likely not a dominant mechanism given P/W is a low concentration system. For this reason, breakage is also not considered in the model for P/W crystallization.

2.3 Modelling Crystallization Processes

Models are used to mathematically represent a process, and models have a variety of uses from predictive control systems (García, Prett and Morari, 1989b), to simulating a process and even being used as a surrogate to a process for estimating process properties that would otherwise be difficult to measure from the real process (Boukouvala and Ierapetritou, 2013). In chemical process, models can be in the form of steady state models or dynamic models. Steady state models are used to determine where a continuous process will operate at steady state, whereas dynamic models are useful to represent how a continuous process will respond to changes in operation, or how a batch process will change with time. Crystallization modelling has been reported widely. Typically, crystallization model equations are selected and certain parameters in the model require identification. The identification can be performed from a small selection of experiments, to explore the design space of the crystallization process. This use of models can lead to further process understanding or decision making *in silico*, reducing the requirement for performing many experiments thus reducing cost and waste of material. For models that can converge fast results, there is an added benefit of reducing time to obtain results.

Models can be formulated purely from theoretical understanding, be derived purely from empirically derived relationships, or a combination of both. Formulating models from theoretical understanding encapsulates as much generality as possible in the model (Tulleken, 1993). This provides the most comprehensive model structure for a process and can be applied for production of any material. However, this type of model encapsulates every mechanism for the process and in most cases, not all mechanisms are required, so this approach leads to an over-engineered model. This is especially the case for the chosen P/W system where nucleation and growth kinetic equation have been determined as the dominant mechanisms. First principle models also require resources and time to develop, and parameter identification can also be impractical or impossible using conventional experimental techniques and technologies. Some examples of information that is impossible to quantify are: the exact onset of nucleation, the exact number of crystals in a system, the exact crystal size distribution in a system. These data are currently only measured in situ using a probe or sensor in a fixed point. The alternatives, empirical or semi-empirical models derived from experimental work, are a favourable modelling option in this instance

(Matthews, Miller and Rawlings, 1996). Empirical models are completely derived from experimental relationships, consequently the validity of these models does not extend beyond the design space or operating region over which the model was identified (Akaike, 1974; Johansson, 1993). Furthermore, the model will be system-specific and may not be transferrable to other systems. The semi-empirical approach balances the empirical approach with the first principles approach using a modular structure, whereby the model structure can be standardised using a set of general equations, but the kinetic equations can be system-specific and transferrable. Then, when the solute/solvent system is changed, the pertinent kinetics can be identified and incorporated into the model.

The models that have been widely accepted for reliably modelling a crystallization process include a population balance, mass and energy balances, and the relevant kinetic equations for the solute and solvent, given the type of crystallization (Beckmann and Randolph, 1977; Ma and Braatz, 2003).

2.4 Population Balance Modelling

It may be sufficient in some cases to model a crystallization process using the traditional mass and energy balances, and limited system information such as the crystal yield can be obtained from such a simplified model. However, an important property in crystallization is the actual crystal size distribution (CSD). The size, shape and distribution of crystals will have an impact on the downstream unit operations (Beck *et al.*, 2009; Benyahia, Lakerveld and Barton, 2012). Therefore, when considering the modelling of crystallization processes, capturing the evolution of the crystal size distribution (CSD) or the statistical moments of the CSD is important. One of the challenges with modelling CSDs is that there can be millions of crystals in small volume systems and tracking the size of every crystal will be computationally demanding and unrealistic to model in real time. One of the most widely accepted methods of tracking the size distributions of disperse phases is using the population balance equation (PBE) (Randolph and Larson 1971). The PBE has been adopted by the crystallization community to model a CSD, and the balance is written in terms of a property of the crystal system, usually a crystal length or volume (Ramkrishna, 2000), referred to as the internal coordinate for the PBE. There are multiple ways to perform crystallization, and each system will also have unique kinetics for nucleation, growth, agglomeration and breakage. Hence, a one-model-fits-all approach is not viable, especially when considering controllability of mean

crystal size or the entire CSD in crystallization. Therefore, using the semi-empirical approach for population balance modelling allows compatibility with as many or few kinetic equations as required. Another consideration for modelling the CSD is to consider the time taken to converge results; it is important to solve the model in a short time without compromising on accuracy of results or time to simulate, predict and control a process (Rawlings, Miller and Witkowski, 1993; Matthews, Miller and Rawlings, 1996).

Modelling, of size distributions and otherwise, can be achieved with three different approaches (Groppi *et al.*, 1995; Jang *et al.*, 2014):

1) Fully distributed parameter modelling where the system is split into many small parts and each is solved separately.
2) Compartmentalised lumped parameter models where a system is split into multiple discrete parts which each have their own model, useful in cases where there are distinct zones of a process whose dominant mechanism is different from adjacent zones.
3) Overall lumped parameter model which only require the solution of a small set of integro-PDEs. This approach is computationally fast, which is usually critical for control applications on real systems.

$$\frac{\partial f_n(L)}{\partial t} = \delta(L - r_0)B + \frac{\partial[G(L)f_n(L)]}{\partial L} + \int_L^{\infty} b(L,\lambda)g(\lambda)f_n(\lambda)d\lambda$$

$$+\frac{L^2}{2}\int_0^L \frac{F\left[(L^3-\lambda^3)^{\frac{1}{3}},\lambda\right] f_n\left[(L^3+\lambda^3)^{\frac{1}{3}}\right] f_n(\lambda)}{(L^3-\lambda^3)^{\frac{2}{3}}} d\lambda \qquad \textit{Equation 2-9}$$

$$-g(L)f_n(L) - f_n(L)\int_0^{\infty} F(L,\lambda)f_n(\lambda)d\lambda$$

The PBE is shown in Equation 2-9, and is valid for a well-mixed batch crystallization system. Here, $f_n(L)$ is the number density function, which is the number of crystals within a size range $(0,\infty)$ per unit mass or unit volume of solvent/solution. B is the nucleation rate and G the growth rate, F is the aggregation kernel, g the breakage kernel and b the daughter particle distribution, $\delta(L - r_0)$ is the Dirac delta function. The PBE forms a framework for modelling particulates in processes such as crystallization. Furthermore, coupling PBEs with mass and

energy balances provides a suitable framework for modelling crystallization for control (Rawlings et al., 1992). The PBE will be used to model crystal size distribution in this research alongside the nucleation and growth mechanisms. The next step is to determine the best method to solve the PBE.

2.5 Numerical techniques for solving the PBEs

There are many numerical techniques that can be used to solve the population balance equation. Each have their benefits and drawbacks and three selected techniques that have been commonly used in published research will be discussed:

1. Standard method of moments (SMOM)
2. Quadrature method of moments (QMOM)
3. Direct numerical solutions using finite volume method

2.5.1 Standard method of moments

The standard method of moments (SMOM) is simple and widely used as a solution for PBEs. Moments are a statistical way of representing some of the main CSD attributes (Diaconis, 1987). Often for crystallization, only the first four moments are used for convenience, because when the characteristic length (length of a single crystal dimension) is chosen to be the PBE internal coordinate, μ_0 represents the total number of crystals, μ_1 the sum of the characteristic length of all the crystals, μ_2 the total surface area and μ_3 the total volume occupied by all the crystals (Ramkrishna, 2000; Vollmer and Raisch, 2006). The moments may also be represented as quantities per unit volume or per unit mass of solvent, as seen in research from Nagy *et al.*, (2008). The SMOM method transforms the PBE from Equation 2-9 by multiplying the equation by L^k and integrating between the bounds of 0 and ∞; thus, the kth moment is defined as:

$$\mu_k(t) = \int_0^\infty f_n(L,t)L^k dL \qquad \text{where } k = 0, 1, 2, \dots, \infty \qquad \textit{Equation 2-10}$$

This transformation allows the PBE to be represented by a set of moment equations (Randolph and Larson 1971; Hulburt and Katz 1964). By performing this transformation, the PBE transforms into the following form, for the kth moment:

$$\frac{d\mu_k}{dt} = \int_0^\infty L^k B\delta(L - r_0)dL + \int_0^\infty kL^{k-1}G(L)f_n(L)dL$$

$$+ \int_0^\infty L^k \int_0^\infty g(\lambda)b(L,\lambda)f_n(\lambda)d\lambda dL$$

$$- \int_0^\infty L^k g(L)f_n(L)dL \qquad \text{Equation 2-11}$$

$$+\frac{1}{2}\int_0^\infty f_n(L)\int_0^\infty F(L,\lambda)(L^3+\lambda^3)^{\frac{k}{3}}f_n(L)d\lambda dL$$

$$-\int_0^\infty L^k f_n(L)\int_0^\infty F(L,\lambda)f_n(L)d\lambda dL$$

In Equation 2-11, the first term is nucleation and second is growth, following by birth due to breakage, death due to breakage, birth due to aggregation and death due to aggregation. In this form, the PBE is more difficult to solve as the closure cannot be found for the equation, but there is a simple case of crystallization for which this PBE can also be simplified. For a crystallization where nucleation and size independent growth are declared as the dominant kinetics, the breakage and aggregation kinetics can be considered as negligible. Subsequently, applying the SMOM results in closure of Equation 2-11 and reduces the PDE into a system of ODEs. The chosen nucleation and growth mechanism equations defined in the prior discussion indeed fits these requirements, so the SMOM is a viable approach for solving the PBE in this research. For batch crystallization, the first four moment equations from this closure are the system of ODEs shown in Equation 2-12 to Equation 2-15.

$$\frac{d\mu_0}{dt} = B \qquad \text{Equation 2-12}$$

$$\frac{d\mu_1}{dt} = G\mu_0 + Br_0 \qquad \text{Equation 2-13}$$

$$\frac{d\mu_2}{dt} = 2G\mu_1 + Br_0^2 \qquad \text{Equation 2-14}$$

$$\frac{d\mu_3}{dt} = G\mu_2 + Br_0^3 \qquad \text{Equation 2-15}$$

The moments of the distribution are obtained using this method and can provide useful information about the crystallization system. However, there are further limitations, the first of which is the reconstruction of the real distribution from these moments is not numerically stable. Obtaining a reliable CSD shape using SMOM is therefore not possible because it requires the solution of every moment from 0 to infinity, thus an infinite number of ODEs must be solved. Inversion approaches have been proposed (Randolph and Larson 1971) but are seldom used, and alternative approaches combining the moments with method of characteristics have also shown success in rebuilding the CSD (Aamir *et al.*, 2009; Aamir, 2010) but would require further computational effort in calculating the method of characteristics. However, contrary to the absence of the full CSD, with the lower order moments it is possible to quantity some important characteristics of the CSD. Some of these include (Shen, Chiu and Wang, 1999):

1. Variance

$$\sigma_{var}^2 = \frac{\mu_2}{\mu_0} - \frac{\mu_1^2}{\mu_0^2} \qquad \textit{Equation 2-16}$$

2. Coefficient of variation

$$c.v. = \frac{\sigma_{var}}{L_m} = \sqrt{\frac{\mu_0 \mu_2}{\mu_1^2} - 1} \qquad \textit{Equation 2-17}$$

3. Number-based mean size or L_{10}

$$L_{10} = \frac{\mu_1}{\mu_0} \qquad \textit{Equation 2-18}$$

4. Weight-based mean size or L_{43}

$$L_{43} = \frac{\mu_4}{\mu_3} \qquad \textit{Equation 2-19}$$

These quantities can allow the tracking of average crystal size and the width of the crystal size distribution for unimodal distributions in one characteristic size dimension. These quantities may not be desirable for representing multi-modal CSD. Furthermore, for single dimension

PBE, the crystal shape cannot be accurately represented. However, modelling crystal shape is not important for paracetamol crystals in a P/W system (Meimaroglou, Roussos, and Kiparissides 2006; Randolph and Larson 1971). The most significant limitation with this method is that crystallization systems are quite complex; primary and secondary nucleation and size independent growth is a very limiting case because there will likely be agglomeration and breakage as well as size dependent growth in many crystallization systems. The ability to model these effects is therefore lost using the SMOM technique and the subsequent model predictions may also be unreliable. On the other hand, this method is useful for obtaining a simple model for crystallization to perform optimization and investigate control applicability. Moreover, for the P/W crystallization system, results using this method have been reported frequently in publications so the method will also be used in this research. For crystallization systems where other mechanisms need to be considered, another moments-based solution can be used; the quadrature method of moments (QMOM) as described next.

2.5.2 Quadrature method of moments

The QMOM was first proposed by McGraw (1997). It is a specific case of the generic weighted residual approach which uses the Gaussian quadrature approximation from quadrature theory to approximate integrals in terms of a set of weights (w_i) and abscissas (L_i), e.g. the moments may be written as:

$$\mu_j(t) = \int_0^{\infty} f_n(L,t)L^j dL = \sum_{i=1}^{Ns} w_i L_i^k \qquad \text{where } j = 0, 1, 2, \dots, \infty \qquad \textit{Equation 2-20}$$

A solution method for Equation 2-20 was proposed by McGraw (1997), based on the product difference algorithm (PDA) (Gordon, 1968) and allows an explicit calculation of the weights from the moments, which averts the closure problem from SMOM for cases involving agglomeration and breakage. The PDA calculates the weights (w_i) and abscissas (L_i) from moments by solving Equation 2-20, where N is the number of quadrature points. Alternatively these can be determined by direct solution of the set of non-linear equations using a differential-algebraic equation (DAE) solver (Gimbun, Nagy and Rielly, 2009).

The application of QMOM to the PBE results in Equation 2-21. Here, the closure problem is eliminated and this equation has been used by Marchisio et al. (2003a), Marchisio et al. (2003b) and Marchisio & Fox (2005) in aggregation and breakage processes coupled with

computation fluid dynamics (CFD). It has also been used with the method of characteristics by Aamir et al. (2009) and Aamir (2010) to track the evolution of the full crystal size distribution. From the perspective of monitoring a process, these techniques do work in tracking the full CSD, but the challenges lie in using this technique for process control. The ability to control the exact CSD is difficult in a crystallization process (Liu *et al.*, 2011) because the exact size and number distribution cannot be measured accurately enough, *in situ*.

An infinite number of quadrature points would lead to the weights and abscissas tracking every point on the CSD. Therefore, with a greater number of quadrature points, it is likely that the solution will also be more accurate, but conversely calculating a solution becomes more computationally intensive and hence a trade-off needs to be made because the PDA becomes infeasible to use when N is greater than 8 (John and Thein, 2012).

$$\frac{d\mu_k}{dt} = \delta(0,k)B + k\sum_{i=1}^{N} w_i L_i^{k-1} G(L_i) + \sum_{i=1}^{N} w_i g(L_i) b(k, L_i) + \frac{1}{2}\sum_{i=1}^{N} w_i \sum_{j=1}^{N} w_j \left(L_i^3 + L_j^3\right)^{\frac{k}{3}} F\left(L_i, L_j\right) - \sum_{i=1}^{N} w_i g(L_i) L_i^k - \sum_{i=1}^{N} w_i L_i^k \sum_{j=1}^{N} w_j F(L_i, L_j) \qquad \textit{Equation 2-21}$$

While it has already been discussed how crystals can be distributed in size, they can also be distributed in shape. For crystal shape characterisation and tracking, it is possible to extend the PBE to two dimensions with two internal coordinates, one used to characterise a length and the other to characterise width, and the QMOM can be used to solve this form of PBE. These types of models with more than one internal coordinate will be referred to as multi-

dimensional models. The QMOM has been used by Qamar et al. (2009) for solving a batch crystallization model with nucleation, size-dependent growth, agglomeration, breakage and dissolution. The case studies presented by the author included nucleation and growth with fines dissolution simulation, as well as pure agglomeration, pure breakage and combined agglomeration and breakage. While it is difficult to assess the author's claim that all results performed similar to those when using a finite volume scheme, the results for each problem do follow the trends one would expect from theoretical principles, such as increases in the value of the first moments due to agglomeration, and decrease in the same moments due to breakage. Furthermore, The QMOM was used by Szilágyi et al. (2015) recently for the simulation of two-dimensional (2D) analysis of crystal shape. In particular, the author discusses the development of the 2D population balance model for continuous cooling crystallization of high aspect ratio crystals. Primary and secondary nucleation, non-linear size dependent growth and size dependent breakage along the crystal length (the first internal coordinate) are presented. Using a 2D PBE, they determine a nonlinear and unclosed moment equations system for bivariate mixed moments of length and width of crystals which are closed using the QMOM. This is an important advancement because the earlier modelling of crystallization systems was primarily focussed on the accuracy of methods like QMOM. The results show a wider applicability to more realistic crystallization modelling by considering the crystal shape. Continuing along this line of research, QMOM is a useful method to extend the model capabilities in capturing real system information. There are few examples of QMOM based models in controllers. The QMOM is slightly more computationally expensive than the SMOM but is still efficient for lumped parameter systems as compared to higher resolution schemes such as finite volume method.

The concluding remarks on QMOM is that while it would be useful to demonstrate a control application with this solution method, the additional complexity created by inclusion of the PDA far outweighs the system it is being used to predict and control. While the ability to include agglomeration and breakage is useful, these mechanisms have not been characterised for the chosen P/W system to a great level of accuracy. Consequently, it appears that using the SMOM in place of the QMOM is the better solution for the P/W system, but QMOM should be considered for crystallization systems where agglomeration or breakage

mechanisms are dominant, and where the parameters of the kinetic equations for these mechanisms have been identified to a suitable degree of accuracy.

2.5.3 Finite Volume Method

The finite volume method (FVM) is one of many direct numerical solution approaches to solving the PBE. Other direct numerical solution approaches include the finite difference and finite element method, as well as high resolution algorithms (Gunawan et al. 2004) and the lattice Boltzmann method (Majumder et al. 2012a; Majumder et al. 2012b; Majumder & Nagy 2013), but the FVM is a technique that has been used extensively for solving partial differential equations (Eymard, Gallouët and Herbin, 2000; Peiró and Sherwin, 2005). The FVM was first introduced by Koren (1993) as an upwind advection solution method. The FVM discretises the spatial domain into a set of nodes and uses piecewise functions to approximate derivatives of the distribution function. The method was developed from the finite difference method (FDM) to achieve a more accurate mass balance. The interval over which the PDE is to be calculated is first discretised to form a set of points, this is common to both techniques, and each point in the discretisation is called a node. The FVM performs calculations using the mid-points between adjacent nodes as opposed to using the node itself as in the FDM. The FVM uses a flux limiter, which is used in high resolution schemes to prevent the effects of discontinuities, shocks and sharp changes in the solution between nodes, thus improving the mass balance accuracy. This method can be applied to multiple dimensions as required but each new dimension increases the order of magnitude of calculations required (Ma et al. 2002; Gunawan et al. 2004). The FVM enables tracking of the entire crystal size distribution, and with the increases in computation efficiency in recent years, using FVM in controllers for real-time operation could be a strong possibility in the future. However, for the case of exploring control applications in the chosen P/W crystallization system, the use of this technique would over-estimate the accuracy of the solution and it would not be possible to verify the actual CSD evolution *in-situ*. Therefore, the additional computational effort in simulating and calculating a whole CSD to ultimately find the values of simplified parameters such as a CSD mean size and width/variance would be impractical.

Concluding the discussion on the use of PBE modelling and applications on crystallization, using SMOM to solve the PBE for the chosen system is the selected approach because:

1) The dominant mechanisms in the P/W system are suitable for use with SMOM
2) The computation cost of using QMOM or FVM is greater, for a greater accuracy in a solution which cannot be practically verified from either publications or *in-situ* in experiments, so a higher quality of result cannot be guaranteed using these techniques
3) The research aims to focus on optimization and control; the compatibility of the chosen technique is important. SMOM offers a simple solution for the PBE which has been used for optimization and control, as will be discussed in the following sections. In comparison, the inclusion of a PDA for QMOM, or coupling with method of characteristics, or a higher order FVM schemes will be more computationally demanding.

2.6 Batch Cooling Crystallization Modelling

In the literature, the most commonly used model for batch crystallization using SMOM is defined by Equation 2-22 to Equation 2-31 (Shen, Chiu and Wang, 1999). The first four equations are the moments balances for a constant volume system, obtained by solving the population balance using SMOM. The remaining equations are the mass and energy balances, nucleation and growth kinetic equations and the solubility equation which is represented as a second order polynomial function of temperature.

$$\frac{d\mu_0}{dt} = B \qquad \textit{Equation 2-22}$$

$$\frac{d\mu_1}{dt} = G\mu_0 + Br_0 \qquad \textit{Equation 2-23}$$

$$\frac{d\mu_2}{dt} = 2G\mu_1 + Br_0^2 \qquad \textit{Equation 2-24}$$

$$\frac{d\mu_3}{dt} = 3G\mu_2 + Br_0^3 \qquad \textit{Equation 2-25}$$

$$\frac{dC}{dt} = -k_v\rho_c(3G\mu_2 + Br_0^3) \qquad \textit{Equation 2-26}$$

$$\frac{dT}{dt} = -\frac{3\rho_c k_v G\mu_2 \Delta H}{\rho c_p} - \frac{UA_c}{\rho V c_p}(T - T_j) \qquad \textit{Equation 2-27}$$

$$B = k_b(S)^b \quad \text{Equation 2-28}$$

$$G = k_g(S)^g \quad \text{Equation 2-29}$$

$$S = C - C^* \quad \text{Equation 2-30}$$

$$C^*(T) = A_0T^2 - A_1T + A_2 \quad \text{Equation 2-31}$$

This is a lumped parameter model, which is accurate based on the following assumptions:

- The batch vessel is well-mixed and thus every unit volume of the batch reactor will contain the same chemical, thermodynamic and particulate composition; each element experiencing the same nucleation and growth rates.
- The volume constant throughout the batch; the volume of crystals generated in the solution will not significantly change the working volume.

These assumptions are valid for P/W system because Paracetamol has a relatively low solubility in water, but for highly soluble systems, the change in volume from crystallization can also be modelled using a volumetric balance equation.

In batch crystallization, the nucleation and growth rates can be highly nonlinear, especially nucleation which can have a very large exponent in the power law. This crystallization model also contains time varying conditions, the supersaturation and heat transfer will not be constant throughout the batch, resulting in changes nucleation and growth as the batch crystallization advances. In large systems where the well-mixed assumption cannot be upheld, these properties may also vary with position in a system (Mullin and Nývlt, 1988; Bakar, Nagy and Rielly, 2009).

2.7 Continuous Cooling Crystallization Modelling

Continuous methods of crystallization have existed for many years, but the optimization and control of these methods for pharmaceutical processing is relatively new (Nagy and Braatz, 2012). The main applications of PBE with continuous crystallization have been for mixed suspension mixed product removal (MSMPR) and continuous oscillatory baffled crystallizers (COBCs) (Powell *et al.*, 2015; Yang and Nagy, 2015; Liu *et al.*, 2019). The MSMPR is a vessel with continuous flow in and out, and is modelled under the following assumptions:

1. The volume is constant volume, which can be maintained provided that in and out volumetric flows are equal (perfect level control)

2. The vessel is well-mixed so the concentration can be assumed as uniform throughout the volume and the out-flow concentration is equal to system concentration. The crystals will also be fully fluidised and the out-flow crystal size distribution is considered to be the same as the CSD in the vessel.

The COBC on the other hand is a tubular reactor with baffles and uses axial oscillations to generate near-plug-flow behaviour; plug flow theoretically has perfect radial mixing zones which move along the axial direction with little to no axial diffusion (Ni and Liao, 2008). Perfect plug flow is an ideal case for continuous crystallization and should in theory produce a consistent CSD when the process is at steady state with constant feed and operating conditions and absence of disturbances. Without a baffled oscillatory setup, plug flow requires very high flow rates in a tubular system and the time limitations of crystal growth would mean the process would have to also be very long to achieve a good product yield (Lawton *et al.*, 2009; Brown and Ni, 2012; Onyemelukwe *et al.*, 2018). The COBC is designed to reduce the system length and achieve some representative results, but is also suffers from some axial dispersion (Onyemelukwe *et al.*, 2018). In crystallization modelling, the COBC has been modelled as a series of MSMPR systems with dispersive transport between each MSMPR in the series to account for the oscillatory behaviour (Jiang et al. 2012; Powell et al. 2015; Su et al. 2015; Ochsenbein et al. 2015). In summary, there are already a couple of continuous crystallization systems to investigate and some reliable models have been provided for these systems but these models would require further development for the COBC systems due to their uniqueness. The MSMPR system models are a version of a continuous stirred tank reactor (CSTR) with a particle suspension. As CSTR models have been widely used and accepted as reliable, the MSMPR models are likely to also be the most reliable among the options available for continuous crystallization. The MSMPR model equations are defined here, where the structure is the same as for the batch crystallization system, this form reduces to the batch system when the volumetric flow in F_{in} and out F_{out} are set to 0:

$$\frac{d\mu_0}{dt} = B + \frac{F_{in}}{V}\mu_{0in} - \frac{F_{out}}{V}\mu_0 \qquad \textit{Equation 2-32}$$

$$\frac{d\mu_1}{dt} = \mathrm{G}\mu_0 + Br_0 + \frac{F_{in}}{V}\mu_{1in} - \frac{F_{out}}{V}\mu_1 \qquad \textit{Equation 2-33}$$

$$\frac{d\mu_2}{dt} = 2\mathrm{G}\mu_1 + Br_0^2 + \frac{F_{in}}{V}\mu_{2in} - \frac{F_{out}}{V}\mu_2 \qquad \textit{Equation 2-34}$$

$$\frac{d\mu_3}{dt} = 3\mathrm{G}\mu_2 + Br_0^3 + \frac{F_{in}}{V}\mu_{3in} - \frac{F_{out}}{V}\mu_3 \qquad \textit{Equation 2-35}$$

$$\frac{dC}{dt} = -\mathrm{k_v}\rho_c(3\mathrm{G}\mu_2 + Br_0^3) + \frac{F_{in}}{V}C_{in} - \frac{F_{out}}{V}C \qquad \textit{Equation 2-36}$$

$$\frac{dT}{dt} = -\frac{3\rho_c k_v G\mu_2 \Delta H}{\rho c_p} - \frac{UA_c}{\rho V c_p}(T - T_j) + \frac{F_{in}}{V}T_{in} - \frac{F_{out}}{V}T \qquad \textit{Equation 2-37}$$

$$\frac{dV}{dt} = F_{in} - F_{out} \qquad \textit{Equation 2-38}$$

2.8 Optimization methods for crystallization

Optimization techniques can be split into local approaches and global approaches. These two approaches serve different purposes, local approaches are usually deterministic approaches and often gradient based, which converge to a local maxima or minima. The following is a definition of an optimization problem:

$$\min_u J = f(u)$$

Subject to:

$$Au = 0$$
$$Bu \leq 0$$
$$c(u) = 0$$
$$d(u) \leq 0$$

Where, J is the cost that is to be minimised using the decision variables or inputs u, and the cost is some function of the input $f(u)$. The cost function is subject to four constraint where A is a matrix of scalars which defines a linear equality constraint, B is a matrix of scalars which defines a linear inequality constraint, $c(u)$ defines a nonlinear equality constraint function and $d(u)$ defines a nonlinear inequality constraint function. Considering a minimisation cost, the path is usually determined by first evaluating a cost function for a user-supplied initial guess or starting point. The surrounding points are then evaluated and whichever direct appears to be reducing the cost function (in a minimisation problem) is then chosen by the optimizer. This path is followed until subsequent points cease to reduce the cost, then the optimizer terminates and returns the current point as the minimum. The greatest drawback

with this method is that even if the design space is small, a local solution cannot be considered to be the global solution for a cost function unless it is validated against a global optimization problem, unless if it is known that only one minimum exists (Törn and Žilinskas, 1989; Pardalos and Romeijn, 2013). Therefore, if the target is to find an optimal solution and be highly confident that it is global, a global optimization technique must be used in most cases.

One established global optimization approach is the genetic algorithm (GA), which is a class of evolutionary optimization algorithms, and although there are other forms of global optimization algorithm, they broadly follow similar principles in finding a solution. One particular GA, Non-Dominated Sorting Genetic Algorithm (NSGA-II), randomly generates a population of initial points across the whole design space and this population is referred to as the first generation (Davis, 1991). Once the objective function is evaluated for every individual in this population, the first generation will have a spread of cost function values. The minimum cost value of this first generation is then used to generate a new second generation of points using the same population size, which will be clustered closer to where the minimum cost appears to be, thus refining the solution. This process is repeat until the cost function value returns a global solution which satisfies a set of conditions set for the optimization problem, or until a predefined maximum number of generations, defined by the user, have been evaluated. The algorithm evolves through the design space to converge onto the global minimum (Deb *et al.*, 2000).

Although the global solution may be of interest, consideration should be given to how critical it is to find this in place of a local solution because global optimization techniques like NSGA-II are only viable in offline optimization. Global techniques are computationally expensive because they involve a random evolving search. In contrast the deterministic approaches already are following an intuitive path to the minimum and can do so with fewer function evaluations, resulting in shorter evaluation time, which is desirable for control (Suh and Hollerbach, 1987; Pardalos and Romeijn, 2013). Therefore, the deterministic approaches will be preferred for online optimization in a control system, but either approach could be chosen for offline analysis. The comparison between local and global approaches have been performed in fields outside crystallization and pharmaceutical production such as for robotic manipulators (Kazerounian and Wang, 1987) and oil wells (McDonald *et al.*, 2007) but there appears an opportunity to explore this comparison when applied to a crystallization process.

It is widely reported that the critical quality attributes (CQAs) in crystallization are purity, yield, morphology and size distribution (Gao *et al.*, 2017). These CQAs are routinely quantified in practice, and there are often one or multiple operating profiles in a crystallization process that will result in a product with desirable characteristics but finding these experimentally can be a laborious and expensive process. Often, the APIs being investigated are also of very high value so to avoid waste, having as few experiments as possible is ideal. Optimization using a crystallization model is one route to finding the optimal production trajectory, where a model can be identified from a few experiments and then used to find an optimal solution to maximise one or more CQAs. The optimal solution can then be implemented in an experiment for validation (Sarkar, Rohani and Jutan, 2006; Trifkovic, Sheikhzadeh and Rohani, 2008).

In this way, optimization approaches can be employed to maximise purity, yield, crystal size or to minimise cost, ideally resulting in an operating profile that can be used for production and lead to the same or comparable CQAs. However, there are numerous drawbacks to modelling and despite the increased understanding in this research area, there are many challenges to overcome (Nagy, Chew, *et al.*, 2008a; Castagnoli *et al.*, 2010; Nagy *et al.*, 2013). Firstly, there are no mechanistic models that truly and fully encapsulate every quality attribute and important measurable property in a crystallization process. Morphology is still only approximated by two-dimensional growth modelling and using an aspect ratio to determine general shape differences in crystals (Eggers *et al.*, 2009; Schorsch, Vetter and Mazzotti, 2012; Yang, Ma and Wang, 2012; Borsos, Majumder and Nagy, 2014). The effects of an impurity on CSD have been modelled by Borsos (2015) where the author selected a preferred impurity adsorb onto a crystal face and inhibit growth, thus successfully controlling the crystal shape. However, there is still a demand for a model which characterises how localised and undesirable impurities are captured within the crystal structure and the subsequent impact on the CSD. Impurities are likely to exist in real systems that would become incorporated into the crystal structure, this is an undesirable outcome and is difficult to quantify in a crystallization model.

Models in crystallization have been used for predicting and optimizing crystallization process behaviour and while there are many advances that will still need to be made for models to be more reliable and accurate, overall the use of these crystallization models in optimization has yielded reliable prediction of process behaviour, supported with experimental results.

2.9 Multi-Objective Optimization for Crystallization

The use of the NSGA-II can be extended to multi-objective optimization. This form of optimization is one where there is a set of two or more competing objectives, and it is desired to discover how both objectives can be met. The main outcome will be the set of nondominated solutions known as Pareto set; a set of the best trade-offs or compromise solutions for the two objective functions. Graphically, the Pareto front defines the boundary of the feasible region of the optimization problem, as shown in Figure 2-3.

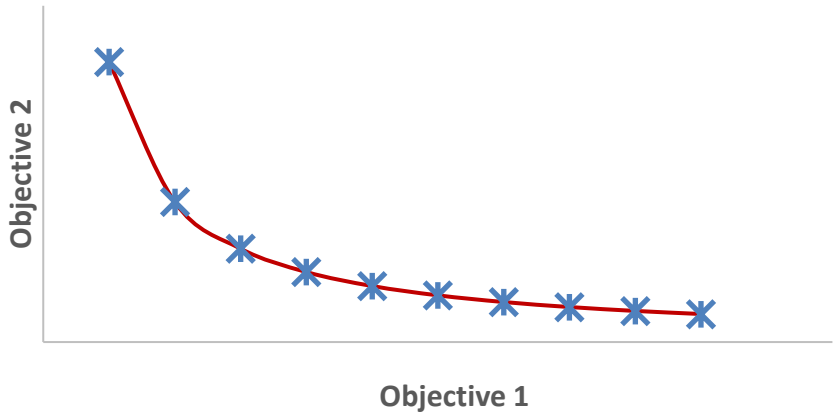

Figure 2-3 – Feasible region and Pareto front

In Figure 2-3 is an arbitrary representation for pareto output to provide further context of how this form of optimization can be useful. The red pareto front will host the set of solutions from the optimization problem and defines the boundary of the feasible region for the two objectives. The blue markers represent each of the Pareto optimal solutions.

The use of multi-objective optimization for seeded batch crystallization was explored by Sarkar et al. (2006) and is the most notable example in crystallization optimization research. The volume-based mean size was calculated from the moments Equation 2-19, and similarly the volume-based coefficient of variation in size was expressed using Equation 2-17. A third moment was also expressed in terms of nucleation and seed growth. Three constrained multi-objective optimization problems were explored to:

1) Maximise the volume-based mean size and minimise the third moment due to nucleation.
2) Maximise the volume-based mean size and minimise batch operation time.
3) Maximise the volume-based mean size and minimise the coefficient of variation.

In all cases the temperature profile and mass of seed were the decision variables and there were constraints imposed on the temperature profile limits and seed mass, and the temperature profile was piecewise linear, defined by Equation 2-36.

$$T(t) = T(k) + \frac{T(k+1) - T(k)}{t_f/P}(t - t_k) \qquad \textit{Equation 2-39}$$

where k is the interval, t is time and P is the number of equal intervals in the profile. The temperature profile over the range [0, t_f] was divided into P equal intervals. The results demonstrated how each scenario presented a Pareto set of solutions. However, there is an opportunity to explore the multi-objective optimization problem by incorporating the interval length into the decision variables rather than enforcing equal time intervals, because the cooling profiles in the results appeared to follow a nonlinear cooling profile constructed of piecewise linear temperatures. Observing the optimal cooling profile for a P/W system disclosed by Nagy *et al.* (2008a), the optimal solution appears to be smooth and the same smoothness cannot be achieved from the fixed time period for each temperature gradient. Furthermore, a comprehensive study of citric acid anhydrate crystallization (Hemalatha *et al.*, 2018) includes a similar multi-objective optimization to maximise the number weighted mean size and minimise the coefficient of variation, subject to cooling rate and limit constraints. One profile from the Pareto set was then implemented as a cooling policy in a citric acid anhydrate batch crystallization, and the results showed good agreement between the predicted mean size and coefficient of variation with those that were obtained from the batch. However, the authors opted to use a piecewise constant temperature profile as the decision variables for the multi-objective optimization, despite the prior research which used a piecewise linear profile the piecewise constant profiles hold the temperature of the crystallization process at a fixed value over each successive time period.

A further study on the multi-objective optimization of seeded anti-solvent crystallization in isothermal conditions (Trifkovic, Sheikhzadeh and Rohani, 2008) also uses the same approach of applying a multi-objective optimization to establish the cooling profile for a seeded batch crystallization process to obtain desired CSD characteristics, and the optimal profile was implemented in an experiment which yielded comparable results. Finally, multi-objective optimization for targeting crystal shape and size of paracetamol and potassium dihydrogen

phosphate (KDP) were also studied by Acevedo *et al.* (2015) with a similar outcome where the experimental results supported the optimization output.

In conclusion, single objective and multi-objective optimization have been on crystallization optimization and two opportunities identified are investigating the difference between local and global single-objective optimization on the P/W system using the optimal profile from Nagy *et al.* (2008a) as a point of reference, to observe the difference between the optimal piecewise-constant and piecewise-linear cooling obtained using a global single-objective optimization, and to incorporate the time period for the piecewise-linear cooling profile as a decision variable in single and multi-objective optimization.

2.10 Control methods for crystallization

There are two main forms of control methods in crystallization literature: model-free and model based. Model free methods use existing data from the crystallization system to follow a trajectory and require little computation effort. The manipulated variables are able to be changed quickly. Supersaturation control has proven to be a good way of controlling a crystallization process in the phase diagram as supersaturation drives nucleation and growth, the two main crystallization mechanisms in the P/W system (Bakar et al. 2009a; Bakar et al. 2009b). The use of supersaturation control in a model-free approach has been investigated and proved to be a suitable control implementation (Saleemi 2011; Saleemi et al. 2012a; A. Saleemi et al. 2012b). Another form of control for crystallization is direct nucleation control (DNC) where a focussed-beam reflectance measurement (FBRM) probe is used to monitor the change in number of crystals in the system and if there is a sharp increase in crystals. DNC works by heating the process to dissolve the most recently generated crystals, then subsequently cooling to produce further growth, with the aim being to obtain a unimodal and narrow crystal size distribution and dissolving any secondary nucleation and fines as they appear. Though this approach is useful, it lacks the ability to forward predict behaviour, so the product that will exit the unit at the end of the process cannot be predicted from this type of control approach, it is a reactive control approach. This is an important limitation because the CSD from crystallization will affect downstream processes, so maintaining a consistent product is important to ensure consistent downstream productivity and regulatory compliance of the product. Another drawback with specific types of model-free controllers such as PID controllers is the requirement to tune the controller. Often it is difficult to tune

these types of controller as the tuning parameters cannot be derived through intuition and must be found from testing and qualification.

Early work in crystallization control by Shen *et al.* (1999) forms a comparison between three types of model based and one model-free controller. The model-based controllers are a globally linear controller (GLC), a generic model controller (GMC) and a multi-model MPC, meanwhile the model-free controller is a PI controller. An optimal cooling profile was determined based on a weighted cost function to maximise the weight-based mean size whilst minimising secondary nucleation in the seeded system and reducing the coefficient of variation, to obtain an optimal cooling profile. The profile is then used in each of the respective controllers to track the temperature trajectory. The outcome saw that all the model-based approaches performed significantly better than the model-free PI approach.

Nagy (2008) presented an important comparison between the performance of temperature control and concentration control of a batch crystallization process. Using temperature control, the end of the batch is more sensitive to the variation in the nucleation exponent which can lead to undesirable nucleation and fines, also the temperature profile must be optimized and is a time dependent curve with a specified end-time. However, concentration control only depends on the temperature of the process and can therefore have variable batch end-times leading to a more consistent yield between batches. In lab experiments, the temperature disturbances resulted in an immediate difference between the two control methods, and concentration control appeared to be a better strategy because it was not fixed to follow a strict temperature profile. The modelling, optimization and subsequent implementation of optimal control profiles from the model-based approach in this paper lead well into the implementation of model predictive control implementations for concentration control.

There are many examples which also show the advantages of model-predictive approaches over model-free, each suggesting the advantages occur because there exists an underlying relationship that is captured in a reliable model that can better inform the controller of the actions that should be taken (García, Prett and Morari, 1989a; Nagy and Braatz, 2003; Damour *et al.*, 2010; Yang and Nagy, 2015). Model prediction is used to predict the controlled output trajectory over a future horizon, based on current state of the system and future inputs. This

is important when considering integrated processes and how the crystal size distribution will look at the outlet of the crystallizer. If the shape of the distribution can be predicted accurately, the properties for downstream processing may be correlated to the CSD and could inform the time required for subsequent process operations. Similarly, with accurate models, the CSD may be controlled to within pre-defined boundaries to ensure the CSD at the outlet is always consistent and will almost guarantee consistent filtration performance (Benyahia et al., 2012). Another key advantage would be unlocking further information about compromises that can be made in the process. For example, there is a drive to produce crystals that are as monodisperse as possible with large size and narrow CSD as this is believed to give the best filtration properties. However, with greater process information, it may not be necessary to form crystals as big as possible with as narrow CSD as possible as this may lead to undesirably long crystallization times and may require other downstream activities such as milling to regulate the crystal sizes down for blending, granulation and tableting. Therefore, an integrated system of multiple unit operations being combined into a single control scheme with an MPC could be used to optimization process characteristics such as minimization of production time whilst maintaining high purity and yield. These are all areas that should be explored, specifically to establish what criteria should be put in place to ensure high productivity and consistent steady-state performance in industrial continuous crystallization.

2.11 Model Predictive Control

Model predictive control is one of the more popular forms of model-based advanced process control and has been applied to pharmaceutical production over multiple processes in recent years. (Antwerp & Braatz 2000; Braatz 2004; Forgione et al. 2015; Mesbah et al. 2009). The dynamic optimization problem can be of the following form:

$$\min_{u} J = Q \sum_{i=1}^{N_p} \left(y_i - y_{i,setpoint}\right)^2 + R \sum_{l=1}^{N_c} \Delta u_l^2$$

Subject to:

$$Au = 0$$
$$Bu \leq 0$$
$$c(u) = 0$$
$$d(u) \leq 0$$

This optimization problem includes some dynamic information from a model, where the model input is u and output is y. The output error is defined as the difference between the

output and the setpoint, in this cost function the difference is squared to ensure a positive magnitude of error but similarly the absolute error can be used. The cost function then evaluates the output error over a time period or prediction horizon of size N_p and where necessary also includes a cost associated with changing the input value (Δu) over an input horizon N_c. The latter is useful when input changes may involve mechanical parts which are prone to wear and failure. Given there are two components to the cost function, the weighting matrices Q and R are introduced to complete the cost function, allowing the ability to change the influence of the output error or input changes on the overall cost. Finally, because dynamic optimization involves prediction of future output and input trajectories, this cost function uses the model (which captures the input-output behaviour) to optimize the future inputs in order to minimise the output error, thus converging the output onto a reference or target trajectory.

Garcia et al. (1989) have formed the first major review of linear MPC and its application mainly to the oil and gas industry. Applications of nonlinear MPC (NMPC) for nonlinear processes such as polymerisation and nonlinear batch processes like crystallization were also investigated (Nagy & Agachi, 1997), demonstrating successful control in tracking temperature profiles to a reference trajectory in polyvinyl chloride polymerisation, as well as temperature and concentration tracking in crystallization (Nagy & Agachi 1997; Nagy & Braatz 2003; Nagy & Braatz 2012). Since then, NMPC has gained momentum in crystallization with a variety of methods of NMPC emerging including the use of an efficient direct multiple shooting algorithm, which was compared to other NMPC techniques for solving a distillation column control problem (Diehl et al. 2002; Allgöwer et al. 2004; Nagy 2003; Nagy & Braatz 2003; Raff et al. 2006). NMPC has been investigated for batch crystallization, some forms of continuous MSMPR and even for multi-objective optimization and control for shape and size, all with much success (Acevedo, Tandy and Nagy, 2015).

One dynamic optimization approach that is an alternative to MPC is Pontryagin's Maximum Principle (PMP). This method is used to find the best possible control input to advance a process or system from one state to the next in the presence of state and input constraints (Vollmer and Raisch, 2003), but the challenge is to define a system in a structure that can be solved using PMP. Vollmer and Raisch (2003) discuss the properties of a batch cooling crystallization model, defining how using a scaled time instead of real time transforms the

model into one which exhibits orbital flatness whilst retaining physical meaning from the process. Hofmann and Raisch (2010) used this model structure to then define an optimization problem using PMP. The crystallization problem they solved was to obtain a specified crystal mass (defined by the third moment) at the end of a batch in as short a time as possible, by growing seed crystals and suppressing secondary nucleation. They apply an assumption that the mass of secondary nucleation crystals will be so small that it will have negligible impact on the overall mass balance, and from their results it is clear that for most cases of their crystallization system, this assumptions is valid. The other notable benefit of this method is the very fast computational time, in which they state an implementation in MATLAB solves a single optimization problem within 0.04 seconds.

The extensive research in this area does leave some unexplored avenues, including an area of linear MPC which can be further explored too. In 2011 and since, some research emerged using linear MPC and a global linearization method applied to the nonlinear system. The global linearization method is an input/output linearization discussed in the next sub-section of this literature review (Jansens and Hof, 2009; Jansen, 2011; Vissers, Jansen and Weiland, 2011). The authors linearized a batch crystallization process and implemented the model into an MPC for supersaturation control, and demonstrated that the MPC was capable of tracking the supersaturation profile despite model uncertainties and growth parameter uncertainty. However, the greatest limitation of this technique is that it was only applied to a single-input single-output system and was unable to handle bounds or constraints from the crystallizer. This is an important limitation for crystallization control because the heat transfer to large volume systems is limited, so achieving large temperature changes in short time is not possible.

Industrial applications often rely on process data and statistics (Qin and Badgwell, 2003) and for continuous processes operating at steady state, data driven models can be used for model predictive control. Data-driven models are typically identified from plant testing (Tulleken, 1993) by treating a process as a black box and subjecting the plant to a set of input changes while observing the outputs, thus establishing the cause-effect relationships on the process. The dynamic data collected from plant can be used to identify low-order regression models, one example is an AutoRegressive model with eXogenous input (ARX) (Jansson, 2003), and the model can then be qualified for use in control of critical parameters on the plant. This

type of MPC has been used in wastewater treatment, oil and gas, fine chemicals and consumer packed goods industries (Qin and Badgwell, 1997), with emerging use in pharmaceutical manufacturing, therefore there is an opportunity to explore this type of MPC in pharmaceutical crystallization control.

There are other noteworthy uses of advances predictive control and MPC are firstly the use of an iterative learning control which utilises batch to batch variability to update the operating profile for future batches to meet a desired crystallization end-point (Sanzida and Nagy, 2013). The supersaturation profile is successfully adjusted after each batch, but it is not clear how sensitive this adjustment in profile is to batch variability, particularly in the case of a single bad batch which produces poor produce due to unintentional seeding, poor raw material quality or unusually high impurity. Furthermore, an application of MPC on combined cooling and anti-solvent 2-stage MSMPR crystallization has also been explored, to control crystal size and yield (Yang and Nagy, 2014b, 2014a). The MIMO system controlled was controlled by PID and NMPC, where the NMPC was found to have a superior performance particular with regards to disturbance rejection. Despite these success cases some areas remain unexplored, such as the COBC style continuous crystallization MPC, and higher dimensional population balance models for accurate shape control. The research into MPC and NMPC thus far has primarily been used SMOM. Therefore, more complex systems with QMOM or FVM could also be explored using these methods, providing bounds and constraints can be applied successfully. Therefore, this is a balance between the benefit of time saving from the linearized MPC and the time used to formulate the MPC to see if it is truly a better approach than NMPC.

2.12 Linearization techniques

2.12.1 Local Linearization

Linearization methods are categorised into either local or global. Local techniques linearize around a defined operating point and are commonly used because they can be implemented with minimal effort (Hartman, 1963). However, the main drawback for this technique is a reduced accuracy in predicting the behaviour of a nonlinear system at conditions that are far from the operating point used for linearization. This drawback can also be accentuated by the degree of nonlinearity in the dynamics, i.e. the more nonlinear the system dynamics the more

inaccurate the prediction will be. This can be detrimental to process control given the control decisions are made using the linearized system. Fortunately, global linearization techniques exist which can alleviate the concerns of using a linear model for controlling nonlinear processes.

2.12.2 Global Linearization

Global linearization methods were first applied onto nonlinear systems by Gilbert and Ha (1984). They considered state variable transformations using a state feedback control law. The method transforms a nonlinear input-state process into a linear input-state model. The terminology used here, nonlinear input-state, simply implies the relationship of the process input to states is nonlinear. However, there is a drawback in that a linear input-state model does not guarantee reliable output prediction because the state-output system may also be nonlinear. This drawback led to an alternative feedback linearization framework developed by Kravaris and Chung (1987) for single-input single-output (SISO) systems by considering the input-output. The aim was to develop a framework for global linearization for solving control problems. Applying this linearization to a nonlinear system, a new linear system can be identified as shown in Figure 2-4 (Mesbah *et al.*, 2010). The state feedback linearization (SFL) block contains a control law which uses the states of the nonlinear plant, x, with the input to the linear system, v, to obtain the input to the plant, u. The plant may also be affected by disturbances or uncertainties (d) and the output of the plant is y. The SFL and nonlinear plant together create a linear system, which can be controlled by MPC. However, the SFL is the states of the plant and the inputs to the plant are within the linear system and are not intuitively accessed directly by the MPC.

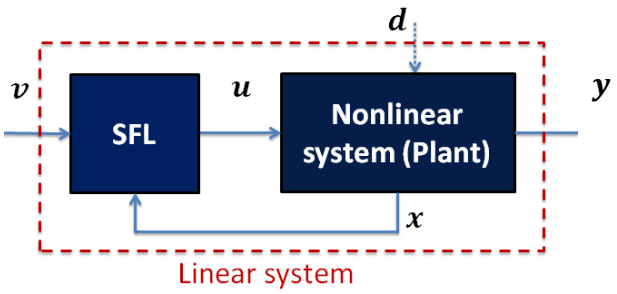

Figure 2-4 Linearization schematic of a nonlinear plant using state-feedback linearization

The output from the nonlinear system is mapped to the MPC input v using the states and the plant input u using Lie derivatives. The transformation means the states are not accessible in

the MPC because they are inside the linear system, and this is the system that the MPC would control. Therefore, the MPC would find the changes in v required to converge output y to a reference trajectory.

This linearization technique has been applied to the batch crystallization model and MPC performance has been evaluated by Jansen (2011) and Vissers, Jansen and Weiland, (2011). The output of the system was supersaturation, and the input to the plant was the temperature of the coolant in the jacket. They evaluated the performance of the controller with a growth parameter mismatch and uncertainty between the MPC and process model which mimicked the crystallization system, to establish if MPC was sufficiently robust to control the process. The results show that the MPC is able converge the supersaturation trajectory onto the reference throughout the simulation, but the input profile varies significantly based on the growth parameter and uncertainty. Furthermore, there was an unsuccessful attempt made to calculate constraints on feedback linearization input, v.

For multiple-input multiple-output control with linearization, there have been implementations of MIMO control with SFL outside pharmaceutical crystallization, namely in proton exchange membrane fuel cells (Chang and Chen, 2014) resulting in the successful proportional-integral control of the process. Similarly, there is a MIMO implemented on MSMPR crystallization but again using a PID controller in place of an MPC (Quintana-hernandez et al. , 2012), the control objectives were to stabilize the third moment and crystallization temperature, and both were successfully achieved with the model-free controller. This shows the possibility of extending the SFL to a MIMO system for crystallization.

2.12.3 Methods for Applying Constraints to Global Linearization

If a global linearization is to be used for MPC, an important requirement is the ability to translate the real process constraints to the MPC, so as to not lose an important function of MPC, the ability to accurately model and predict feasible future input moves for a process. In literature, a few successful attempts have been made on applying constraints to a feedback linearization optimization problem. Two techniques introduced by Kurtz and Henson (1996) and further detailed by Kurtz and Henson (1998) discuss how the SFL control law can be used to identify the state-dependent constraints at each interval that the MPC is executed. In the

first technique, named constant constraint technique (CCT), the constraints are calculated for the next immediate MPC input, v, using the most recent states, $\boldsymbol{x}$,and these constraints are applied on v across the entire horizon. The second technique named variable constraint technique (VCT) uses the horizon of v from the previous time the MPC was executed to estimate the future states, $\boldsymbol{x}$. These future states make it possible to calculate the future inputs into the process (u), using the SFL control law. In both techniques, the constraints on the first input in the horizon will be correct and given that this is the only input from the MPC that is implemented onto the plant, this trade-off has been accepted knowing that the horizon prediction may not be accurate or reliable. However, this is a major drawback for MPC because the important characteristic of MPC is the ability to predict how the trajectory will evolve over the future horizon. Therefore, infeasible horizon prediction is arguably of little to no use.

Kurtz and Henson (1996) also disclose that the method to ensure exact constraints would be to create a constraint calculation strategy which uses the nonlinear system's real states but this route wasn't chosen by the authors as it would be relatively computationally inefficient compared to even nonlinear MPC, hindering the real-time capabilities. This claim can now be challenged with advances in computational efficiency, as it may now be possible to form a more computationally demanding constraints calculation strategy whilst also maintaining the ability for real-time operation.

Further advances have since been made by Van Soest, Chu and Mulder (2006) in using a similar technique to CCT and VCT, using the constraint techniques on a MIMO SFL with decoupling. Deng, Becerra and Stobart (2009) also explored the capabilities of constraint implementation using artificial neural networks (ANN), but the technique appears computationally demanding and requires large training sets of data to train the ANN, even then the constraint selection was not reliable. Furthermore, this application was in the aerospace domain and the viability of using ANNs in pharmaceutical crystallization control would require new datasets to be formed.

The most recent advance by Schnelle and Eberhard (2015) introduces a constraint mapping technique for SFL again based on VCT but they introduce the use of recursively calculating the future plant states and using them to dynamically update the VCT constraints technique with

the constraints on the MPC input. The advantage of this technique is that the constraints will be valid throughout the entire horizon, which means the prediction horizon will be the most accurate of all the previous techniques discussed. However, this method could be improved upon if there was a method to directly constrain the plant states and inputs without the need to convert them into the MPC input constraints.

One solution to implementing plant constraints across the entire prediction horizon could lie in the use of the Sequential Quadratic Programming (SQP) algorithm in optimization. Boggs and Tolle, (1995) introduce the SQP algorithm and state that SQP has the ability to solve nonlinear control problems with nonlinear constraints by using an iterative approach which is capable of converging a feasible optimal solution. This optimization algorithm therefore presents an opportunity to address the problem of handling real plant constraints, by coupling the SFL transformation with the nonlinear state space system into nonlinear constraints function. The SQP algorithm can then be employed to solve the control problem on the state feedback linearized system subject to the nonlinear constraints function.

In summary, this method for linearization poses some complications with bounding and constraints on the real inputs to the nonlinear system, but there is sufficient motivation to explore this area and find a solution. This form of linearization would make it possible to use MPC with a globally linearized model for crystallization and the offline linearization method would only need to be performed once. This is advantageous over local linearization around one or multiple operating points. The ability to linearize a model over its whole design space is an appealing idea for control application.

2.13 Conclusions

Although there are a lot of modelling and control applications for crystallization already, many are quite simple and applied to batch crystallization, meanwhile the more advanced applications are very niche. There are a lot of publications with NMPC and relatively few with MPC on crystallization. Research into using continuous MSMPR is also becoming more prevalent. There is still a lot of space in the field for more advanced modelling techniques to be applied in higher dimensions to construct cases of more realistic problems, addressing complex crystals shapes and breakage/aggregation problems. There is also scope to incorporate a lot of the computationally demanding approaches such as FVM which were too

expensive a few years ago but now could be viable given the performance increases of computers. Further, in terms of model-based control there are gaps for controlling modelled crystallization approaches with greater than 1 dimension. There are very few papers in the field on multi-objective optimization, especially in regard to crystallization.

Based on this review, the areas that have been chosen for the main focus of subsequent research are firstly the further exploration of multi-objective optimization by exploring the optimization of cooling crystallization temperature trajectory and incorporating a decision variable that allows the interval of the temperature profile ramp rate to be optimized per piecewise linear cooling stage. The other area of focus is the use of global input-output linearization for batch and continuous crystallization, the constraint applications of this technique in both SISO and MIMO control problems, and the application of this technique in a model predictive controller. Furthermore, as the linearization approach is global, an investigation into global vs local optimization is also important to determine which approach should be used for optimization in the MPC.

3 Multi Objective Optimization of Batch Crystallization

In this chapter, three optimization studies are performed on batch crystallization to address the opportunities that were realised in the literature review. The first is a study on piecewise constant and piecewise linear decision variables for optimization of a batch crystallization temperature profile, to compare how the two forms of decision variable affect the batch temperature trajectory and the number based mean size of the CSD at the end of the batch. The second optimization study compares three optimization techniques, the first is the Nondominant Sorting Genetic Algorithm – II, the second is deterministic sequential quadratic programming optimization, and the final is a hybrid combination, to again assess the differences in batch crystallization optimization. The final study is a multi-objective optimization to obtain a Pareto set for maximising the number weighted mean size and minimising coefficient of variation of the CSD, using a previously unused combination of decision variables to define the temperature profile – the temperature gradients and time steps per gradient.

3.1 Materials and methods

A model-based optimization technique requires a mathematical model and the formulation of the optimization problem which requires a cost function and a set of constraints. This section will first introduce the mathematical model of the crystallization process, and subsequently discuss the selection of decision variables to maximise the number-weighted mean crystal length (referred to as L_{10} or mean length). Also discussed are the optimization problems for a single objective using local, global and a multi-objective optimization.

3.2 Batch crystallization modelling approach

In chapter 2 various methods of modelling and solving a crystallization system have been discussed which can be applied to batch cooling crystallization. The model for batch cooling crystallization is a system of differential and algebraic equations (DAEs) comprising a population, mass and energy balance, kinetic equations for crystallization mechanisms and thermodynamic relationships for solubility (Shen, Chiu and Wang, 1999; Nagy, Chew, *et al.*, 2008b).

A population balance is used to quantify and track the crystal size distribution (CSD). The standard method of moments (SMOM) is chosen as the method of quantifying and tracking

the CSD. The main drawback is that the SMOM is only valid for nucleation and size independent growth rates, but this is acceptable for the chosen crystallization system. The paracetamol in water (P/W) system which has been modelling, identified and optimized in literature by Nagy et al (2008) is chosen because the product and process remain relevant within the pharmaceutical industry at the time of writing. The kinetic data for nucleation and size independent growth have been provided for this system (Nagy, *et al.*, 2008). The batch crystallization moments equations are shown from Equation 3-2 to Equation 3-5 for the first to fourth moments and Equation 3-6 shows the mass balance.

$$\frac{\partial(\mathrm{n(L)})}{\partial t} = \delta(L - r_0)B + \frac{\partial[G(L)n(L)]}{\partial L} \qquad \textit{Equation 3-1}$$

$$\frac{d\mu_0}{dt} = B \qquad \textit{Equation 3-2}$$

$$\frac{d\mu_1}{dt} = G\mu_0 + Br_0 \qquad \textit{Equation 3-3}$$

$$\frac{d\mu_2}{dt} = 2G\mu_1 + Br_0^2 \qquad \textit{Equation 3-4}$$

$$\frac{d\mu_3}{dt} = 3G\mu_2 + Br_0^3 \qquad \textit{Equation 3-5}$$

$$\frac{dC}{dt} = -k_v\rho_c(3G\mu_2 + Br_0^3) \qquad \textit{Equation 3-6}$$

In Equation 3-1, the breakage and agglomeration functions have been excluded given they are not required for SMOM. In these equations, n is the number distribution, L is the length of crystals, r_0 is the initial nucleus radius, B is the nucleation rate, G is the growth rate and μ_0, μ_1, μ_2 and μ_3 are the zeroth to third moments respectively, and are defined per unit mass of solvent. The concentration C is the concentration of paracetamol in solution, k_v is the shape factor of paracetamol which is 0.24 and ρ_c is the crystal density 1296 kg/m^3 (Nagy, Fujiwara, *et al.*, 2008). The moments represent the properties of the CSD. The first four moments (zeroth to third) are used here. The first, second and third moments represent the total length, total surface area and total volume of the crystals respectively, all per mass of solvent.

Dividing these by the zeroth moment obtains more useful information such as the L_{10} mean size of crystals, the average surface area per crystal and average volume per crystal, respectively.

No energy balance has been included in this model because the optimization will be on the crystallization temperature trajectory. This can also be viewed as if there is perfect heat transfer to the crystallizer. This case study considers unseeded systems, so the initial conditions of all the moments are 0. The initial condition of concentration is 0.256 g/g (paracetamol/water). The nucleation and growth kinetics are defined by the power laws shown in Equation 3-7 and Equation 3-8. The supersaturation (S) is calculated using Equation 3-9 where C is the concentration from the model and C^* is the solubility. The solubility is simplified to a second order polynomial relationship with temperature as shown in Equation 3-10 (Nagy *et al.*, 2008b). This relationship is applicable for the temperature range of crystallization from 320 K to 290 K. All temperature in the optimizations of this case study are set to start at 315 K and end at 295 K. In the power law Equation 3-7, the value for k_b is $e^{45.8}$ min^{-1} g^{-1} and b is 6.2. In Equation 3-8, k_g is $e^{-4.1}$ m min^{-1} and g is 1.5 (Nagy, Fujiwara, *et al.*, 2008).

$$B\ (min^{-1}g^{-1}) = k_b(S)^b \qquad \textit{Equation 3-7}$$

$$G(m\ min^{-1}) = k_g(S)^g \qquad \textit{Equation 3-8}$$

$$S\ (g/g) = C - C^* \qquad \textit{Equation 3-9}$$

$$C^*(g/g) = 1.5846 \times 10^{-5}T^2 - 9.0567 \times 10^{-3}T + 1.3066 \qquad \textit{Equation 3-10}$$

3.3 Dynamic optimization methods

Three main optimization techniques will be used, a stochastic genetic algorithm (NSGA-II) (Deb *et al.*, 2000), a deterministic gradient based method and a hybrid method which utilises first the NSGA-II to begin the optimization, and feeds the solution of this into the initial guess of the deterministic approach. Each method is used to solve the same optimization problem which is to maximise the crystal mean size for given start and end temperatures for

crystallization of paracetamol in water. The cooling rates and temperature limits are bounded and where possible the optimization configuration is also set to be identical in all cases.

3.3.1 Genetic Algorithm (stochastic)

The first optimization method which will be used is the NSGA-II. This method requires no input or initial guess for a temperature profile and uses the entire decision variables domain defined by the upper and lower bounds for the temperature. The genetic algorithm adopts the principles of biological evolution and selection to solve an optimization problem. Firstly, the decision space is defined by specifying the bounds and constraints on the decision variables. The NSGA-II requires specification of the population size, the maximum number of generations and optimization tolerance; the generations and tolerance define the optimization end criteria. The population size is the number individuals representing the decision variables that will be used to evaluate the cost function in each generation, which initially are randomly generated by the NSGA-II algorithm. After evaluating the cost function for the whole population of the first generation, the DVs in the population which give the minima (or maxima) are then used as parents to generate new individuals for the next generation (offspring), the decision variable with improved characteristics. Subsequent generations will be generated according to same principle. If successful, the process will converge to the global minimum or maximum where the best individual in the last population represents the optimal set of the decision variables (Deb *et al.*, 2000).

In the optimization problem of the crystallization process, each member or individual of the population is a temperature profile that runs for 300 minutes, begins at 315 K and ends at 295 K, set according to the profiles disclosed by Nagy *et al.* (2008a). The generations will then evolve the population by refining and reducing the domain until a global temperature profile is found which maximises the crystal mean size. In the event of a nonconvex optimization problem, there is a chance that the previous population's minimum cost value was at a local minimum, presenting a possible risk of converging to that solution. This is usually not an issue with the genetic algorithm because of a property called 'diversity' (Winston, 2015). A higher diversity will enable the genetic algorithm to randomly generate individuals in each population that aren't based on the parent but are actually in other areas in the domain. So, if the algorithm is not already converging onto the global solution, with enough generations there is a greater chance that this diversity effect will eventually find the global minimum.

Many preliminary test runs of the genetic algorithm have determined that the default settings for MATLAB's genetic algorithm (2014b) are sufficient for exploring the entire domain for the purposes of crystallization optimization. This process continues for a user-defined number of generations, a large number of generations are preferred (Sarkar, Rohani and Jutan, 2006), until finally an optimized profile is obtained. This is computationally demanding but the advantage is that no input guess is required and the entire domain is searched with convergence onto the global optimum.

3.3.2 Deterministic method

In contrast to the genetic algorithm, a deterministic approach requires a valid initial guess which determines the outcome of the final solution. As a result, the deterministic method requires some prior knowledge of the system for an informed initial guess in order to converge to the global solution, otherwise the optimization process will converge to local solutions particularly if the problem possesses the property of non-convexity, i.e. the objective space has many local solutions. Several methods can be used to solve constrained optimization problems such as the interior point and sequential quadratic programming (SQP) (Boggs and Tolle, 1995). An optimization tool or function called `fmincon` in MATLAB, which allows several optional local deterministic optimization methods, is used to solve the optimization problem (Equation 3-12 and Equation 3-13), the sequential quadratic programming (SQP) algorithm is used to solve the optimizations in this study. The main advantage of this method over NSGA-II is the lower number iterations required and as a result is not as computationally intensive (Törn and Žilinskas, 1989).

3.3.3 Hybrid optimization technique

The adopted hybrid method is a combination of the NSGA-II with SQP in `fmincon`. The method first employs the genetic algorithm to randomly generate the population of initial profiles, and each is evaluated using the optimization function to narrow down the search space and begin to converge onto the global solution. Then there is a handover phase once the genetic algorithm has evaluated, the best final profile is used as the initial guess for SQP to refine the optimal solution (Deb, Lele and Datta, 2007). This has been chosen as a test method to combine the advantages of the genetic algorithm's convergence to a global solution without any prior guesses or user input, with the computationally inexpensive SQP approach that should use the genetic algorithm result as an initial guess and almost guarantee

faster convergence to the global solution as compared to a pure genetic algorithm optimization (Gao *et al.*, 2008). The decision must be made on how many individuals will be considered in the population and through how many generations the genetic algorithm will evolve. The hybrid optimization will be used to explore the advantages gained from both methods and the benefits will be quantified mainly through difference in computation time differences with the other two methods.

3.4 Decision Variables Comparison for Optimization

There are two types of decision variables (DVs) used to construct the temperature profile. The first is a pairing of time steps and constant temperatures (Hemalatha *et al.*, 2018), the second is a pairing of time steps and linear cooling ramps (Sarkar, Rohani and Jutan, 2006). These are defined as piecewise-constant (*PC*) and piecewise-linear (*PL*) respectively. The PC approach uses an optimizer to find the optimal sequence of constant temperatures for each time step in the batch crystallization, and the temperature profile is then constructed, as shown in Figure 3-1a. The temperature step changes at each time step are only bounded by the maximum and minimum temperatures and the optimizer is set up such that the temperature is held or reduced but heating Is not allowed. The PL approach uses an alternative approach with a sequence of gradients (α) with the corresponding time periods for which each temperature ramp is active (Figure 3-1a, blue). Similarly to PC, the ramp rate is held for the respective time period, and it is ensured that the ramps will not exceed the lower bound temperature of 295 K by imposing the following condition:

$$\sum_i \alpha_i \Delta t_i = 315\ K - 295\ K \qquad \textit{Equation 3-11}$$

In this equation α_i is the gradient for which a positive value is a cooling ramp and a zero value is to hold temperature (as seen in Figure 3-1b) over the time period Δt_i (1 interval) so by multiplying both together it is possible to obtain the temperature change over the time period of Δt_i. Summing the entire sequence of gradients over each respective time period can then ensure that the sum does not exceed the difference between the start and end temperatures. Further as there is a constraint on the gradient to prevent heating, so all the values of α_i in the summation will always be greater than or equal to 0, thus the profile will always cool from 315 K to 295 K.

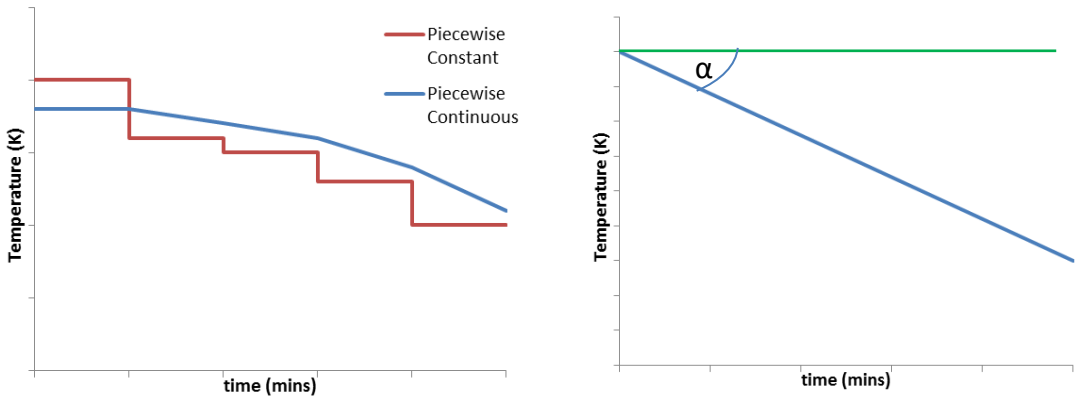

Figure 3-1 a) Piecewise constant vs piecewise linear for a whole profile (left), b) Defining piecewise continuous gradients for one time interval (right).

The method of optimization that will be used for decision variable selection is the NSGA-II because a global solution is desired for both problems. Additionally, with the DVs being so different, using a deterministic approach would require two unique initial guesses for the optimizer, one for each DV case, which will not be identical. There is also a chance that one or both of these optimization problems are nonconvex in the feasible region, and the nonconvexity affects the ability to find the global optimum with a deterministic approach (Henrion and Lasserre, 2004). The purpose of this test is to see how step changes in the temperature profile will affect the final number weighted (L_{10}) mean length in this simple batch cooling crystallization problem, and moreover to understand the benefits to employing a more robust cooling profile with gentle ramp rates as opposed to sharp step changes in temperature as will be experienced with the PC approach.

3.4.1 DV Comparison Optimization Case Study

For this optimization study the crystallization process will run for 300 minutes in every simulation, with a fixed time step of 30 minutes. This means that the optimization has 10 equal sized time steps which require 10 decision variables that must be optimized (one for each time step); for piecewise-constant these DVs are 10 constant temperature values, and for piecewise-linear trajectory the DVs are 10 gradients for cooling. The optimization problem for the PC is as follows:

$$\max \frac{\mu_1}{\mu_0} \qquad \textit{Equation 3-12}$$
$$s.t.\ 295 \leq T(K) \leq 315$$
$$T(t_0) = 315\ K$$

$$T(t_{end}) = 295\ K$$
$$T(t_i) \leq T(t_{i-1})$$

Similarly, the optimization problem for PL is:

$$\max \frac{\mu_1}{\mu_0} \qquad \textit{Equation 3-13}$$
$$s.t. 295 \leq T(K) \leq 315$$
$$T(t_0) = 315\ K$$
$$T(t_{end}) = 295\ K$$
$$0 \leq \alpha \leq 30$$

The optimization will maximise the L_{10} mean length and the NSGA-II parameters are summarised in Table 3-1.

Case	Optimization Method	Population size (GA)	Generations (GA)	Absolute Tolerance
PC	NSGA-II	150	50	1 x 10^{-5}
PL	NSGA-II	150	50	1 x 10^{-5}

Table 3-1 – NSGA-II Optimization Parameters for PC vs PL Comparison

The settings above were determined by performing optimization under a range of settings to gain insight into how set up the NSGA-II to solve this problem. The model allows tracking of some statistics which are related to the CSD and quantified using the moments such as the final average crystal size and the width of the distribution quantified by coefficient of variation. In the ideal case, the final crystal mean size (L_{10}) will be large whilst maintaining a narrow coefficient of variation in size. Also, any large nucleation rates that occur after the first instance of nucleation event will be considered undesirable and should be avoided to prevent the generation of fines which would be reflected by a larger coefficient of variation in the moments. It is desired to see the growth kinetic dominate nucleation, which can be confirmed by tracking the L_{10} trajectory which should increase throughout the crystallization process, a decrease in L_{10} in a supersaturation system would signify that nucleation of new smaller particles are resulting in a reduction of the number weighted mean size (when breakage is not an active mechanism). The criteria used for determining which decision variables are best for this offline optimization problem are:

- The DVs which result in the best overall mean size at the end of the batch,
- The optimal solution which reduces the occurrences of large spikes in the nucleation rate throughout the batch.

The best decision variables will then be taken forward to the next section which aims to compare the local and global optimization approaches for an identical optimization problem.

3.4.2 Decision Variable Comparison Results

The optimization solution for the PC temperature profile case is shown in Figure 3-2 and the final L_{10} mean size was 76 µm. The solution for PL case is shown in Figure 3-3 and the final optimization length was 106 µm. The PC case shows a series of step changes in temperature with the first step change being the largest from just under 315 K to 309 K as seen in Figure 3-2h. This results in a sharp increase in nucleation rate seen in Figure 3-2e at 50 minutes. Each subsequent step change in temperature also results in a further nucleation event which can be seen by the sharp peaks in Figure 3-2e. These nucleation events could result in a multi-modal CSD, though this cannot be verified using the SMOM. Another indication of multiple peaks in the CSD is the zeroth moment data in Figure 3-2a. Each time the line plateaus, nuclei have been formed and held until the next spike in nucleation rate. Looking at this in conjunction with Figure 3-2b (mean size), and Figure 3-2f (growth plot), there is crystal growth occurring throughout the batch after the initial nucleation event, therefore during each plateau of the zeroth moment curve all the crystals will continue to grow. The global solution is different for PC than for PL and this is why the final L_{10} is so small in comparison to the PL optimization. If the number of DVs are increased towards an infinite number, the optimization would be more comparable with PL because an infinite number of step changes would likely lead to numerous gradual step changes as opposed to the large and aggressive step changes seen in this case, thus giving the appearance of a smoother temperature profile.

The PL optimization results were directly comparable to published work and therefore were validated against the work by Nagy et al (2008). In Figure 3-3h, the temperature profile reaches 295 K within 250 minutes. Figure 3-3b shows that the L_{10} mean size also seems to plateau towards the end. The nucleation and growth rates in Figure 3-3e and Figure 3-3f respectively have similar trends to each other which is unsurprising given that both kinetic equations are power law functions of the supersaturation. The main difference is that initially

the zeroth moments (representing number of crystals) is 0 so nucleation must first occur to generate some crystals and increase the zeroth moment. Subsequently, the optimum temperature profile appears to favour growth, making this the dominant mechanism over nucleation for the remainder of the simulation. The most apparent advantage over the PC case is that PL results in a smoother cooling profile with fewer DVs and as a result the phase diagram in Figure 3-3g appears to show one large nucleation event which is succeeded predominantly by growth. There are a few further maxima in the nucleation curve in Figure 3-3e but these do not result in the same characteristic increases in the zeroth moment that were seen in Figure 3-3e for PC. These nucleation spikes do appear to occur whenever the rate of cooling changes. The behaviour can be attributed to the correlation of ramp rate to change in supersaturation, which affects the nucleation rate. One possible solution to prevent these nucleation spikes would be to decrease the time step and increase the number of temperature ramps (DVs) with the overarching aim to refine the temperature profile and reduce large step changes in temperature. Alternatively, from observing the optimum profile from Nagy et al. (2008a), it appears that the optimum cooling profile is nonlinear and smooth, and by fixing the time step for each ramp it may not be possible to obtain such a smooth profile. Therefore, instead of enlisting more ramps in the DV, it may be better to consider incorporating the time periods for each ramp as a DV instead. The optimizer may be allowed the freedom to then alter the duration of each ramp and obtain an overall smoother cooling profile.

The computational time for both optimizations was approximately 15 minutes, but the PL approach resulted in a much smoother temperature profile and significantly larger L_{10} mean size. This coupled with the nucleation trends in the PC results determine that the PL results are preferable. In order to a similar result from the PC approach, the number of decision variables would have to be increased and coupled with a shorter time period between temperature changes. However, the computation time would likely increase because 50 generations of 150 may not be sufficient to converge on the global solution when increasing the number of decision variables. This was observed in prior optimizations when determining the settings for this optimization test. Finally, the temperature profile optimized here is that of the crystallization solution. As such, some of the large temperature step changes from the PC optimal solution would be difficult to achieve in reality because typically crystallization

temperature is controlled by manipulating fluid temperature in the vessel's jacket and achieving large changes in temperature are heat transfer limited. So, although this case performs less desirably, replicating it in practice would also be difficult.

3.4.3 Decision Variable Comparison Conclusion

Overall, when comparing the two decision variables as used in these two cases, the PL case is the best option. The temperature profile is achievable, and the smoother temperature profile also results in a smooth supersaturation profile for the batch. To achieve a significantly smoother temperature profile from the PC approach, the number of decision variables would have to be increased, leading to greater computation time. For the optimization case studies, the PL approach will be used and the time periods will be included as decision variables to allow the optimizer to further refine the temperature profile in search of the optimal solution.

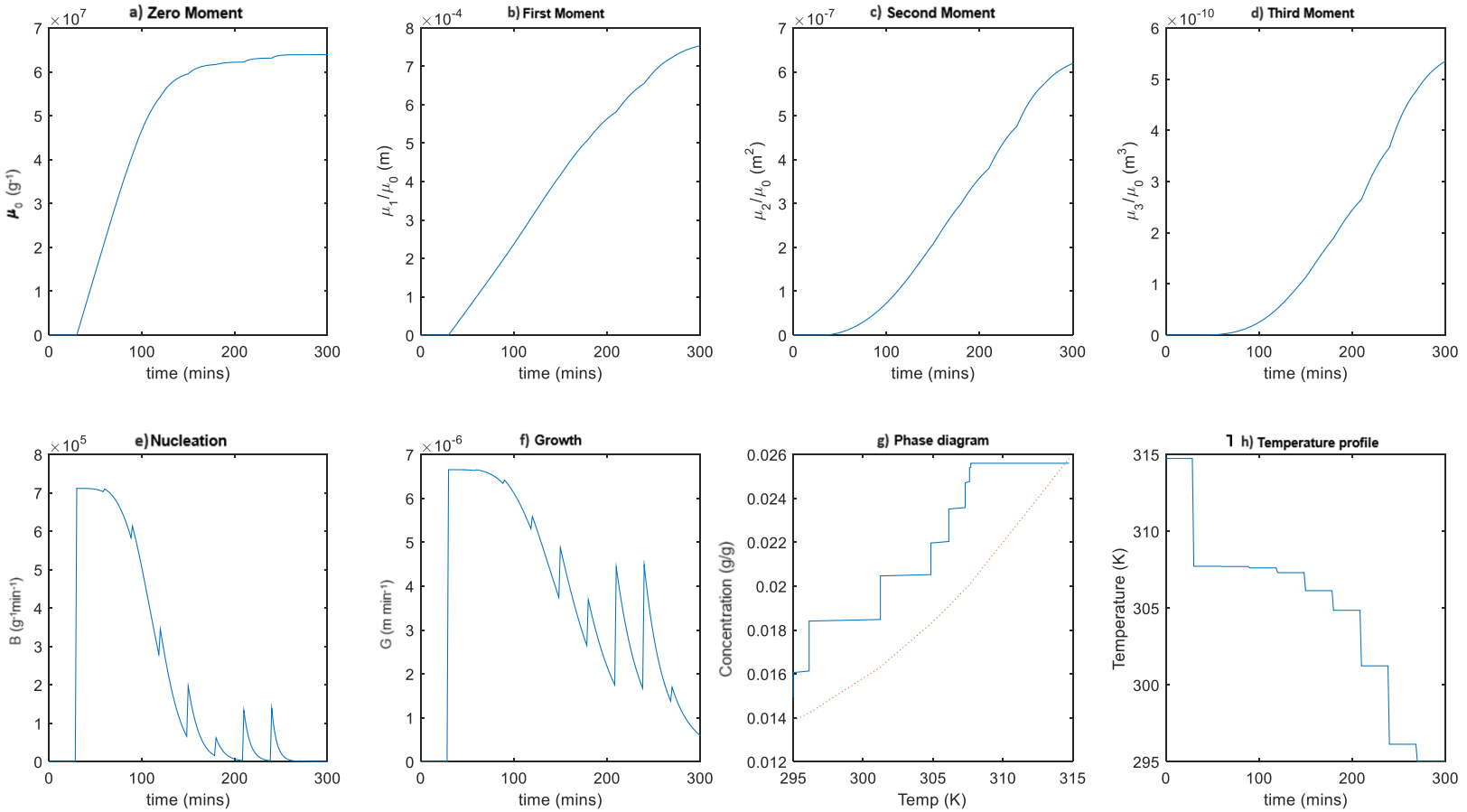

Figure 3-2 – Piecewise constant optimization output: a) Zeroth moment vs time, b) L_{10} mean size profile (maximisation objective), c) Mean surface area profile, d) Mean crystal volume profile, e) Nucleation rate profile, f) Growth rate profile, g) Crystallization phase diagram trajectory, h) Optimized temperature profile.

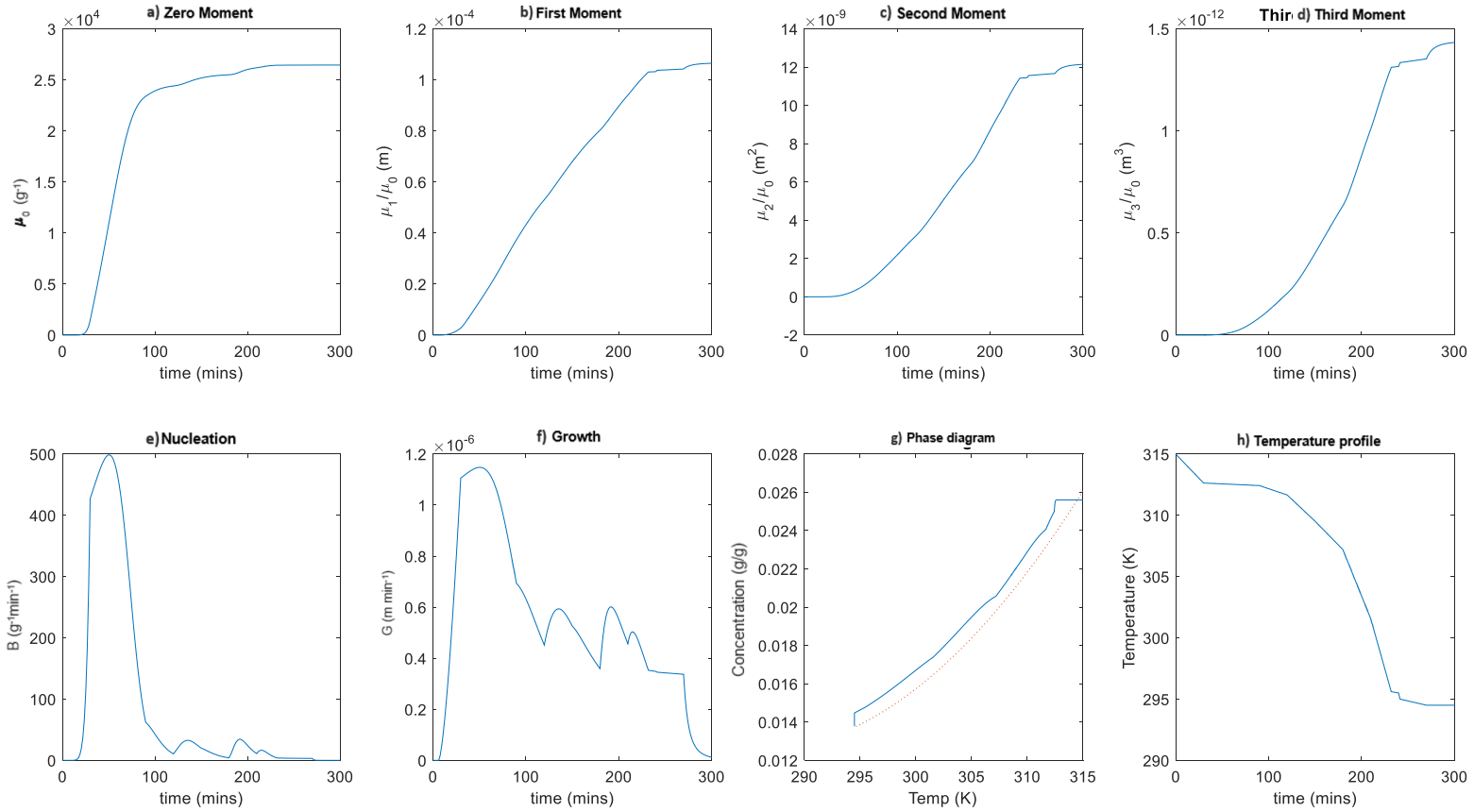

Figure 3-3 – Piecewise continuous optimization output: a) Zeroth moment vs time, b) L_{10} mean size profile (maximisation objective), c) Mean surface area profile, d) Mean crystal volume profile, e) Nucleation rate profile, f) Growth rate profile, g) Crystallization phase diagram trajectory, h) Optimized temperature profile

3.5 Batch Crystallization Optimization Study

A comparison will be made between the 3 optimization methods on the same objective function and model using identical options for the optimizations where possible. The genetic algorithm requires no initial guess. Here, the time periods have also been incorporated as decision variables. Therefore, there are 50 DVs comprised of 25 time periods and 25 temperature gradients. This new optimization problem allows the time periods to be varied so if there are long periods of time where it would be ideal to hold the temperature in the crystallizer, the optimizer can achieve this with 1 temperature gradient observed over 1 long time period, allowing the remaining DVs to be used to refine the temperature profile. A new linear equality constraint is added to ensure that all time steps always add up to 300 minutes. The optimization will run for 250 generations for a population size of 600.

The SQP optimization is used with the same constraints but with two initial guesses, whose values are provided in Table 3-2.

Initial guess	$\boldsymbol{\alpha}$	$\boldsymbol{\Delta t}$
1	$\alpha_{1,25} = 0.8$	$\Delta t_{1-25} = 12$
2	$\alpha_{1,25} = 0.8$	$\Delta t_{1-24} = 1 \quad \Delta t_{25} = 276$

Table 3-2 – Initial guesses for Two SQP Optimization Cases

The initial guesses are both linear cooling profiles with a fixed gradient. The first cooling profile consists of 25 equal time periods. The second initial guess consists of the first 24 time-steps being equal and 1 minute long, followed by one very long time step at the end at 276 minutes (totalling 300 minutes). These initial conditions were chosen to exploit any potential local solutions that may be converged using this deterministic optimization approach. The prior results from decision variable analysis section showed the global solution temperature profile from the PL case appears to be nonlinear where the initial half of the batch cools at a slower rate than the final half of the batch. The second initial guess is to test the SQP optimization algorithm and see when the majority of the batch time is subject to a fixed ramp, if the optimizer can reduce this time significantly enough to converge the same solution as the first SQP case, or even the global solution. Finally, the hybrid method starts without the initial guess and uses the NSGA-II for 10 generations comprised of 100 individuals to create an initial guess for the SQP optimization which then completes the optimization, ideally

converging to the global solution. All optimization parameters have been summarised in Table 3-3.

Case	Optimization Method	Population size (GA)	Generations (GA)	Absolute Tolerance
1	Genetic Algorithm	250	600	1×10^{-5}
2	*SQP*	-	-	1×10^{-5}
3	*SQP*	-	-	1×10^{-5}
4	Genetic Alg. + *SQP*	100	10	1×10^{-5}

Table 3-3 – Summary of settings for optimization test problem

The performance criteria for this study is first the time to converge a solution and secondly the quality of solution. The quality of the solution relates to how well the mean size is maximised and then looking at other data such as undesired spikes in the nucleation trend, total number of crystals in the crystallizer at the end of the process and if the growth remains the dominant mechanism after the initial nucleation. The aim is to produce few and large crystals so these key performance indicators are sufficient to decide which approach is best for online optimization in a real-time control system too.

3.5.1 Optimization Case Study Results

The key performance indicators from the results of each optimization case in this study are summarised in Table 3-4.

Case	Optimization Computation Time (mins)	L_{10} Mean Size	Maximum Rate of Nucleation ($min^{-1}\ g^{-1}$)	Zeroth Moment at end of batch
1	300	117	280	19900
2	25	125	225	16100
3	25	80	3050	6700
4	30	125	225	16100

Table 3-4 Summary of KPI values from all four cases.

3.5.1.1 Genetic Algorithm Optimization Results

The optimization results obtained with the genetic algorithm optimization are shown in Figure 3-4. This optimization required 300 minutes (5 hours) of computing time. There is one initial peak in nucleation between 50 and 100 minutes with multiple less prominent increases in nucleation rate throughout the batch (Figure 3-4e). The ideal scenario would be the zeroth moment increasing to a plateau resulting from the peak in nucleation and subsequently dropping to a low and fixed value until the end of the process. This would give confidence

that the CSD would be unimodal with small coefficient of variation in size. However, the zeroth moment in this result is increasing throughout the crystallization process due to the sustained nucleation rate throughout the process. The mean length increases almost linearly after the initial nucleation and at end of crystallization the final mean size is 117 µm (Figure 3-4b). Comparing this to the PL optimal solution from the DV comparison case study where the time steps were fixed, the added flexibility of allowing the optimizer to use time steps as decision variables has indeed resulted in a larger mean size. Furthermore, in the phase diagram (Figure 3-4g), the crystallization trajectory does not reach the solubility curve at the end so the final state of the batch is still supersaturated and further growth may indeed have been possible. The final temperature constraint to achieve a system temperature of 295 K was satisfied but an increased hold time would be necessary to fully crystallize the remaining material which results in the batch ending in a supersaturated state. One improvement to this would be to incorporate a yield target for the batch as has been implemented in other studies (Sarkar, Rohani and Jutan, 2006).

3.5.1.2 Deterministic Optimization Results

In comparison to NSGA-II, when using SQP with the first set of initialization values in Table 3-1, the optimizer converges a solution (Figure 3-5) within 25 minutes of computation time. The solution is similar to that of the genetic algorithm, though the resulting temperature profile here is smoother it is assumed that the initial guess has converged onto the global optimal solution. The optimized temperature profile (Figure 3-5h) shows faster cooling from 315 K to 312.5 K at the start of batch when compared to the prior case. The batch also ends at the low temperature constraint of 295 K but the system is still supersaturated so further growth occurs until the end of the 300-minute process. There is one dominant nucleation event early in the batch (Figure 3-5e) thereafter the nucleation rate drops drastically and stabilises at a much lower rate. The zeroth moment does not plateau (Figure 3-5a) but is very smooth compared to the solution using the NSGA-II; it is suspected that the continuous nucleation of new crystals will be broadening the distribution but it is likely to remain more unimodal than for the temperature profile produced by the genetic algorithm because of this smoothness. However, this cannot be confirmed from the current results using SMOM. The growth rate after the first nucleation peak is close to constant (Figure 3-5f) and the mean size evolves almost linearly to a final size of 126 µm (Figure 3-5b).

Figure 3-6 shows the optimization result in the case the optimizer is provided with the second initial guess from Table 3-1. The temperature profile (Figure 3-6h) shows that the final time step was decreased from 276 mins to under 200 minutes, but as the temperature profile does not match the results from the prior 2 cases, this is likely not converging onto the global solution. The initial supersaturation led to a single dominant nucleation peak (Figure 3-6g and e) which is an order of magnitude greater than the previous 2 solutions. The growth rate is also not uniform beyond the first nucleation event (Figure 3-6f) which translates into a final mean size of 80 µm, much lower than the global solution. However, it is observed that the zeroth moment (Figure 3-6a) did reach a plateau in this local solution, so after an initial burst of nucleation the optimizer was able to prioritise maximisation of crystal size. In the phase diagram (Figure 3-6g) the batch supersaturation trajectory also operated closer to the saturation curve after the initial nucleation peak.

3.5.1.3 Hybrid Optimization Results

The hybrid method required 30 minutes of computation to converge and the final results are shown in Figure 3-7. The results are exactly as shown for the first guess using SQP. The interpretation of this that as the genetic algorithm will be converging to the global minimum, and the point where the NSGA-II terminate, the best individual which is provided to the SQP as the initial guess will begin near the global solution, so it gives confidence that this result is indeed the global optimal solution for the optimization problem. Furthermore, the additional time required by the hybrid method appears to be a good compromise when there is not enough information known about the system to determine a reliable starting guess for SQP.

3.5.2 Batch Crystallization Optimization Conclusion

The selected optimization problems lead to the conclusion that for optimizations on systems with little or no prior knowledge, the hybrid method is likely the best approach, but with systems that are well understood or well researched, SQP is a reliable alternative for single objective optimization when it is desired to converge onto the global solution. The long time period for the genetic algorithm paired with the relatively coarse results shown in this study is not considered desirable for optimization despite running to a global solution without an initial guess. However, the advantages of the genetic algorithm will be seen when extending the study from single-objective to multi-objective optimization, as will be discussed next.

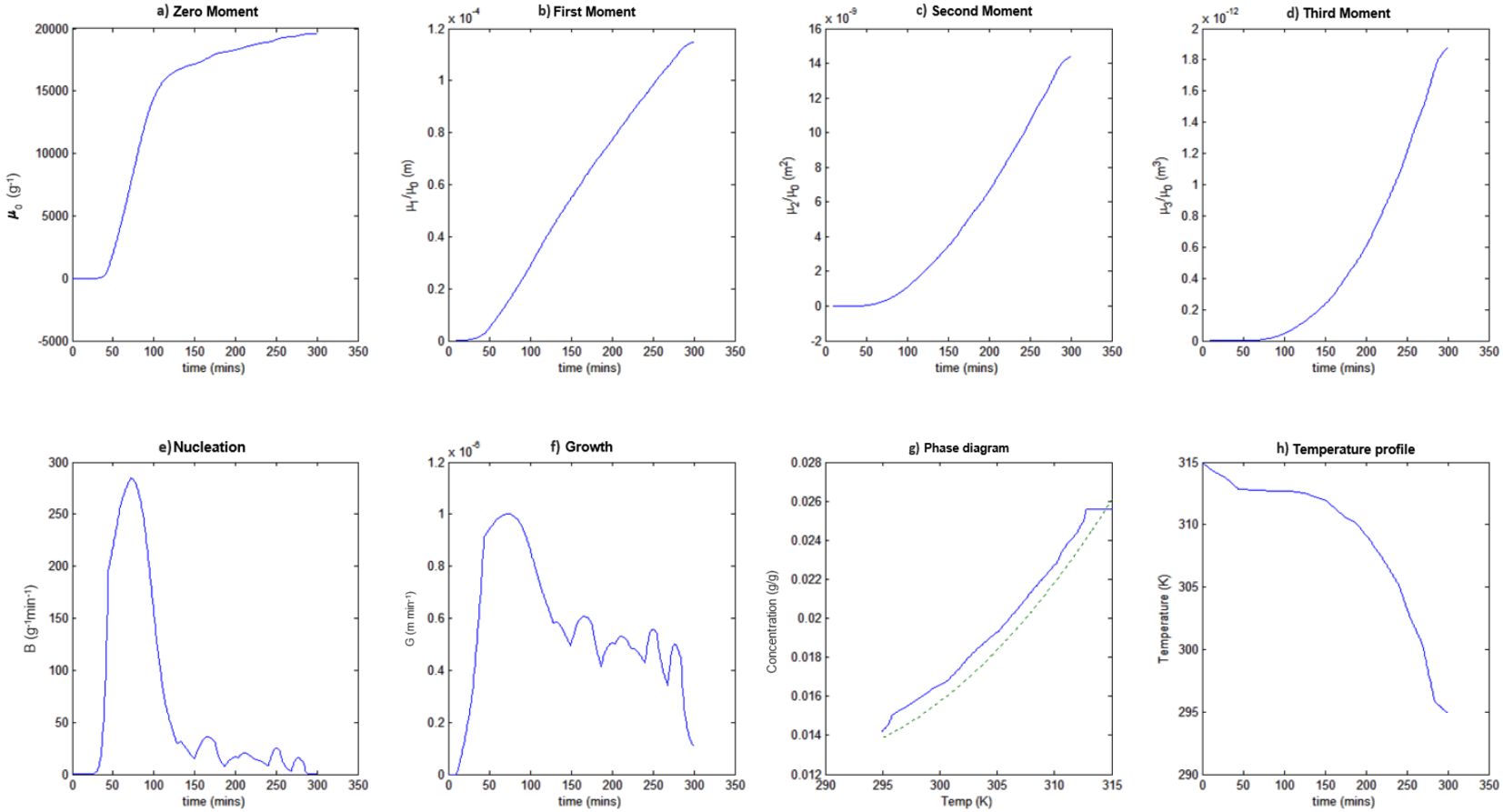

Figure 3-4 – NSGA-II Optimization Output: a) Zeroth moment vs time, b) L_{10} mean size profile (maximisation objective), c) Mean surface area profile, d) Mean crystal volume profile, e) Nucleation rate profile, f) Growth rate profile, g) Crystallization phase diagram trajectory, h) Optimized temperature profile.

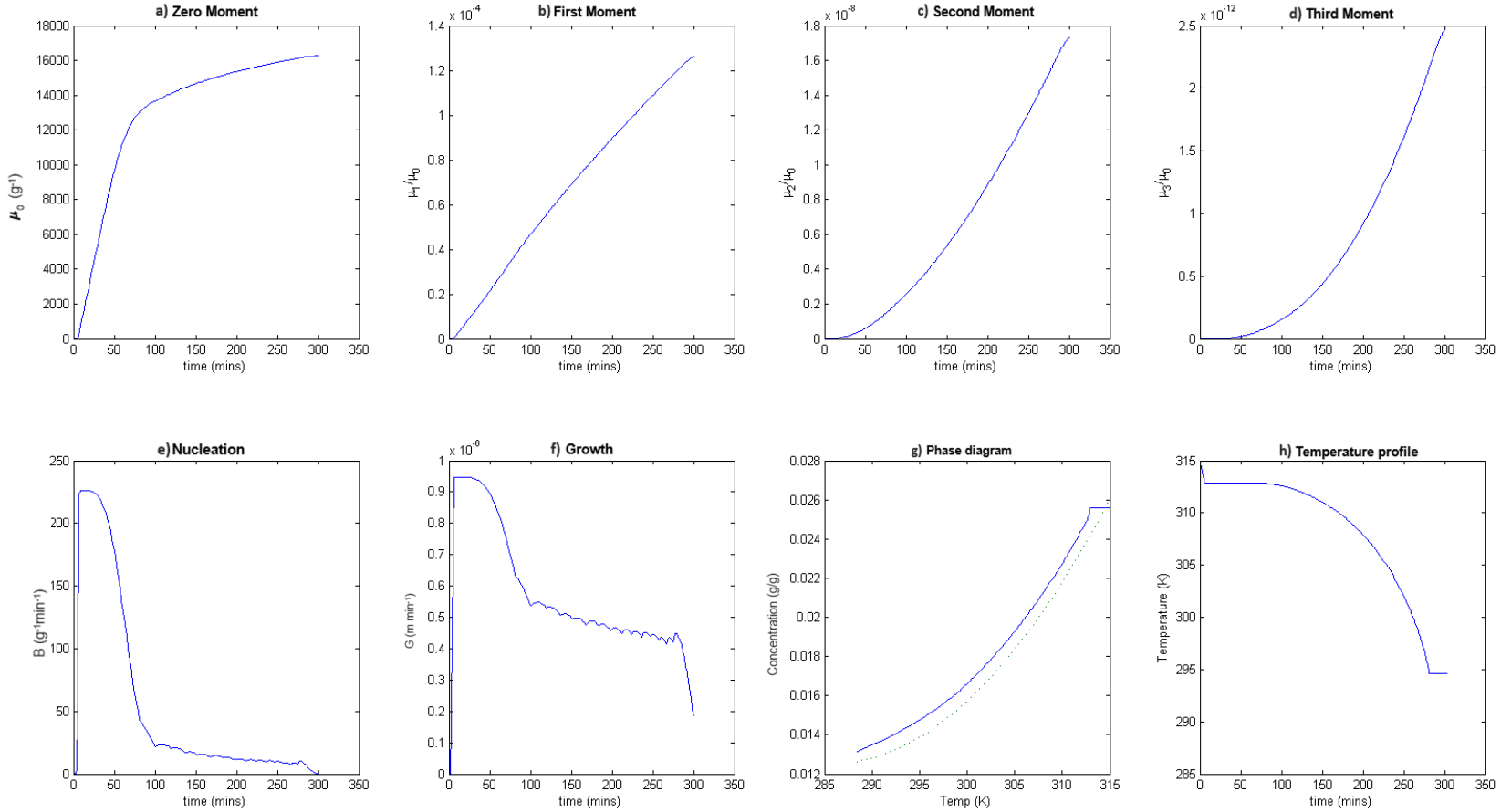

Figure 3-5 – SQP Case 1 Optimization Output: a) Zeroth moment vs time, b) L_{10} mean size profile (maximisation objective), c) Mean surface area profile, d) Mean crystal volume profile, e) Nucleation rate profile, f) Growth rate profile, g) Crystallization phase diagram trajectory, h) Optimized temperature profile.

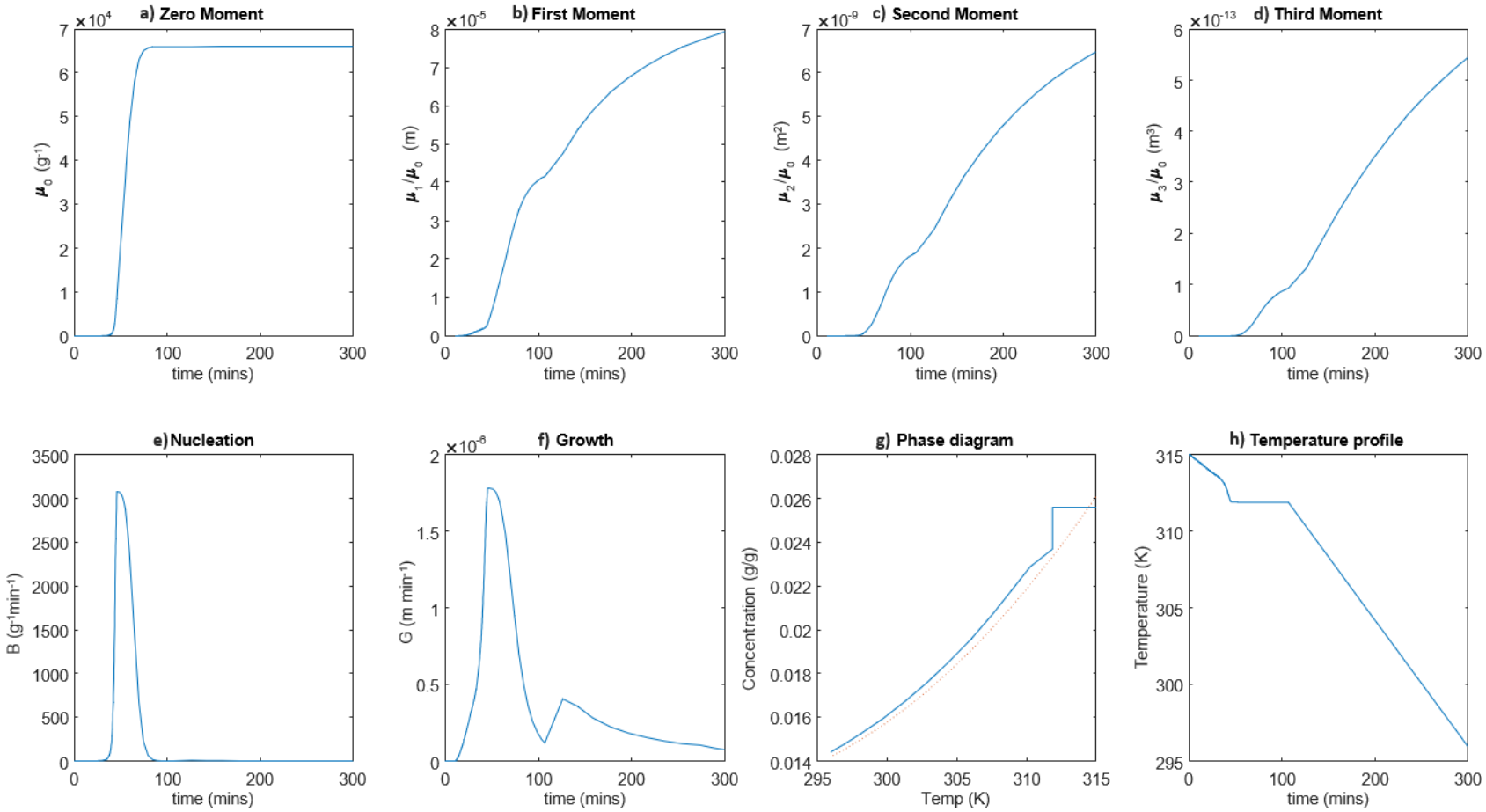

Figure 3-6 – SQP Case 2 Optimization Output: a) Zeroth moment vs time, b) L_{10} mean size profile (maximisation objective), c) Mean surface area profile, d) Mean crystal volume profile, e) Nucleation rate profile, f) Growth rate profile, g) Crystallization phase diagram trajectory, h) Optimized temperature profile.

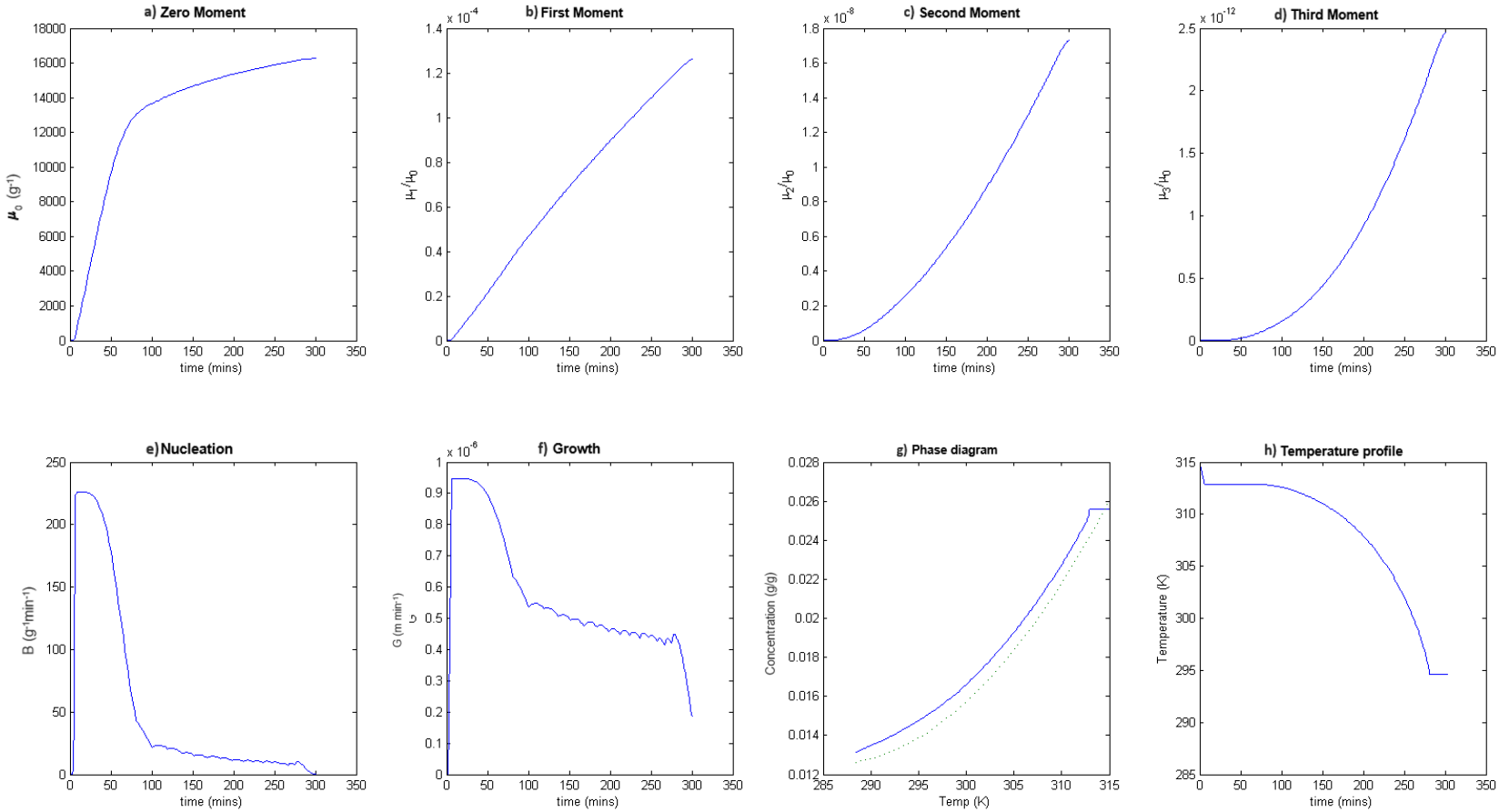

Figure 3-7 – Hybrid Optimization Output: a) Zeroth moment vs time, b) L_{10} mean size profile (maximisation objective), c) Mean surface area profile, d) Mean crystal volume profile, e) Nucleation rate profile, f) Growth rate profile, g) Crystallization phase diagram trajectory, h) Optimized temperature profile.

3.6 Multi-objective Optimization

The discussion thus far has focussed on single objective optimization, but in reality there are many CQAs in pharmaceutical production and it would be desirable to target more than one objective from optimization and control. Single-objective optimization can be used when it is known to what extent each of the different objectives should be achieved, by using a weighted optimization approach, one example of this is seen in Shen et al. (1999) where a cost function is introduced with a weighted objectives on the mean size, crystal mass and suppression of nucleation. However, qualitative understanding of a process can be gained by an alternative method of multi-objective optimization where objectives are competing or contradictory and an ideal solution cannot be found. The aim of multi-objective optimization is to find a set of trade-off solutions and thus understand the many ways in which two or more competing objectives can be achieved. The NSGA-II is capable of performing multi-objective optimization, and the algorithm will be used to maximise crystal length and minimise the crystal size distribution width because these two are known to be competing objectives (Benyahia *et al.*, 2011; Acevedo, Tandy and Nagy, 2015; Hreiz *et al.*, 2015; Lakerveld *et al.*, 2015). The outcome of this optimization will not lead to one unique solution but many compromise or a trade-off solutions. In MATLAB, the function `gamultiobj` is based on the NSGA-II, and is used to solve the multi-objective optimization problem.

One option that is available with the genetic algorithm is seeding. As seeding is terminology that is also used for crystallization, to avoid conflict of terms, seeding of a genetic algorithm will be referred to as initialisation. Initialisation is the process of providing the initial population of the genetic algorithm with one or more defined individuals. The remaining individuals in the population are generated through the random selection performed by the algorithm.

3.6.1 Multi-objective Optimization Case Study

This case study consists of 2 optimization problems and the population size and generations are specified in Table 3-5. There are 50 DVs (25 time periods and 25 corresponding temperature gradients). The first case is without initialisation, whereas the second case is initialised with two profiles. The two profiles are obtained by performing a single objective optimization first on the maximisation of mean size, and secondly on the minimization of

coefficient of variation, using the same DVs but using the SQP method and the first initial guess from Table 3-2.

Case	Population size (GA)	Generations (GA)	Absolute Tolerance
1	200	60	1×10^{-5}
2	200	60	1×10^{-5}

Table 3-5 – Summary of settings for optimization test problem

The second multi-objective genetic algorithm case is initialised with these two profiles to determine if initialisation shows a performance benefit when using multi-objective optimization, such as an improved solution or reduced time to converge a solution. The CSD width is quantified by the coefficient of variation which can be obtained by the zeroth, first and second moments as shown in Equation 3-14 (Shen et al, 1999, Aamir, 2010). This together with maximising the number weighted mean size will define the optimization problem for this case study.

$$c.v. = \frac{\sigma_{var}}{L_m} = \sqrt{\frac{\mu_0 \mu_2}{\mu_1^2} - 1} \qquad \textit{Equation 3-14}$$

The optimization problem is defined in Equation 3-15.

$$\begin{aligned} &\max \frac{\mu_1}{\mu_0} \\ &\min \sqrt{\frac{\mu_0 \mu_2}{\mu_1^2} - 1} \\ &s.t. 295 \leq T(K) \leq 315 \\ &T(t_0) = 315\ K \\ &T(t_{end}) = 295\ K \\ &t_f = 300\ mins \\ &0 \leq \alpha_i \left(-\frac{K}{min}\right) \leq 30 \\ &1 \leq \Delta t_i (mins) \leq 300 \end{aligned} \qquad \textit{Equation 3-15}$$

3.6.2 Multi-objective results and discussion

The multi-objective optimization results for the first case without initialisation are presented in Figure 3-9. Here, a Pareto fraction value of 35% is used which means from all the individuals in a given generation, the best 35% are plotted in the Pareto plot. For each generation, the Pareto front (the boundary on which the Pareto set lies in Figure 3-8) should move closer to the boundary of the feasible region for these two objectives until a final Pareto set is found with no further improvement to both objectives. The two Pareto points on the extremes of the Pareto front are known as the anchor points, which should be comparable to the single-objective optimization solution of each respective objective.

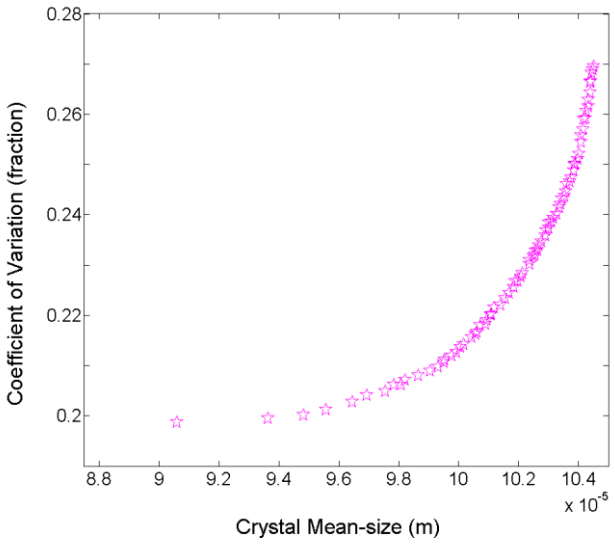

Figure 3-8 - The multi-objective Pareto plot for maximising crystal mean size and minimising coefficient of variation

The results show how increasing crystal size results in an increasing distribution width, quantified by coefficient of variation. Specifically, the maximum mean size seen here is 104 µm for which the coefficient of variation is 0.27, whereas the minimum coefficient of variation of 0.198 results in a corresponding mean size of larger than 90.6 µm. This information can be used to select an operating profile based on one of these Pareto points for further analysis or experimental validation. One drawback of this approach is that the Pareto required 4 hours of computation to achieve the results shown in Figure 3-8, but the best mean size result of 104 µm was significantly lower than the previously seen values of 117 µm for the genetic algorithm with single objective optimization.

In an attempt to improve on this result, the second multi-objective optimization is initialised with the temperature profiles resulting from two single-objective optimizations, one for maximising L_{10} mean size and the other for minimising coefficient of variation. The single-objective optimizations were performed with lower tolerances on error than the previous case study to reduce the time to converge a solution. The initialised multi-objective genetic algorithm converged the results shown in Figure 3-9 in 40 minutes of computation time, 30 minutes of this time was used for both single objective optimization and 10 minutes for the multi-objective optimization. With a new maximised mean size of 124 µm and minimised coefficient of variation of 0.16, initialisation of the multi-objective optimization with single-objective optimization profiles would be the preferred way to handle this optimization problem, as can be seen in the Pareto front in Figure 3-9. This Pareto solution is much further to the right in the objective space than the Pareto from the previous multi-objective case and it is suspected that the first case was also evolving towards the solution of the second case but was terminated soon before it could reach the same Pareto due to the number of individuals and generations not being sufficiently large enough. However, with a time of 4 hours to converge the previous case, and 40 minutes for the current case, it appears that the current approach to multi-objective optimization is a better use of resources and time.

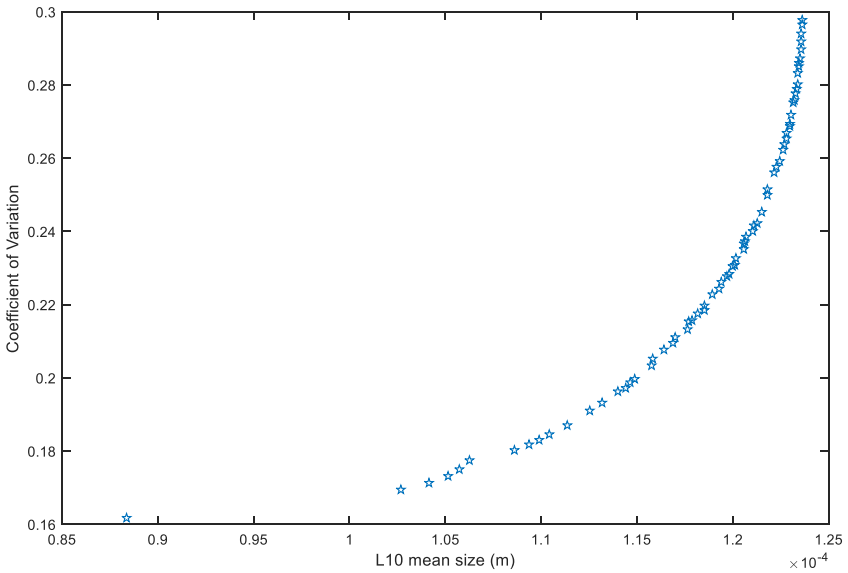

Figure 3-9 – Multi-objective Pareta plot when initialised with single-objective optimization profiles

The temperature profiles for the Pareto set of the second case are provided in Figure 3-10. The insight gained from these trends is that the initial cooling phase differs between the two

objectives. The dark blue profile was obtained from single-objective optimization of mean size, and the red profile from coefficient of variation reduction. After the initial 50 minutes of the simulation, the remaining profiles from the Pareto appear to be bounded by the two single objective profiles for much of the temperature profile except for the initial 50 minutes prior to nucleation.

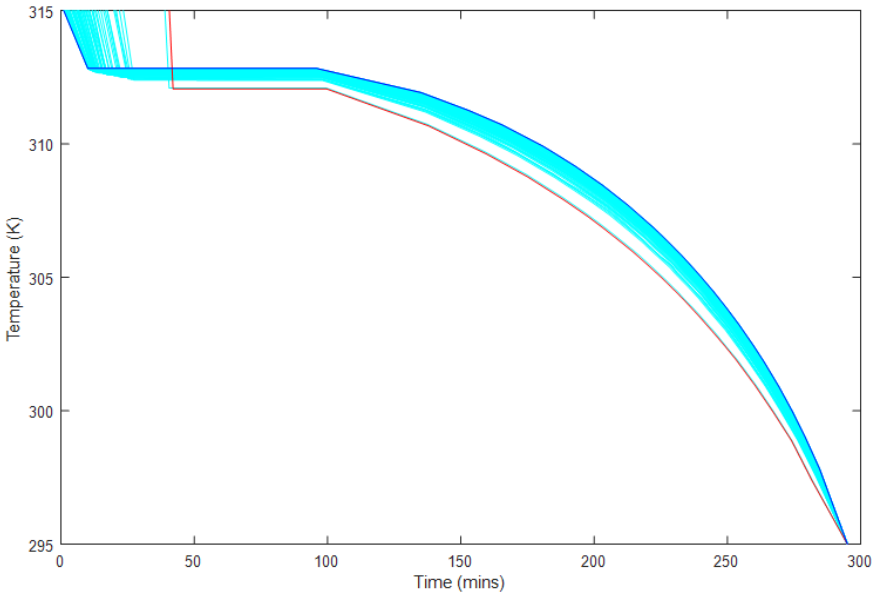

Figure 3-10 – Temperature profiles for the Pareto set obtained from Multi-Objective Optimization with Initialisation – Blue profile from single objective maximisation of mean size, Red profile from single-objective minimisation of coefficient of variation, Cyan profiles from intermediate points in the Pareto front.

A further consideration to be made here is that while the Pareto plot can be used to determine the region in which the process can be operated to give the best compromise solution of these two objectives, there would also need to be some profile selection criteria in place if automatic selection of a profile is desired, such as for real-time control. For systems with higher degree of nonlinearities and objective functions whose correlation isn't as obvious as for this system, it may be useful to use multi-objective optimization to highlight any nonconvexity in the Pareto too. However, for this simple batch crystallization simulation, a weighted single-objective approach would suffice in selecting an operating profile and using the deterministic SQP would also be sufficient in place of the NSGA-II.

3.7 Conclusion

Three areas of optimization are considered in this chapter; the selection of decision variables, the method of single objective optimization and the use of multi-objective optimization.

Piecewise-constant and piecewise-linear decision variables were used to optimize a cooling crystallization temperature profile. The initial and final temperatures were constrained to fixed values with a fixed total time of 300 minutes for the batch, to compare optimization results for maximising the mean crystal length (number weighted). The PL decision variables were found to give a much smoother crystallization profile which appeared to prevent undesired nucleation events in simulation. However, the temperature profiles were subject to fixed time steps which appeared to limit the final mean size obtained, so a new approach was implemented to allow the time steps to be decision variables in the optimization. The resulting difference was a mean size increase from 106 to 117 μm.

The comparison was then made between a global stochastic genetic algorithm optimizer, a local deterministic SQP algorithm and a hybrid combination of both to understand benefits and drawbacks of each and whether a deterministic or hybrid approach would be sufficient to converge the global solution in short times to be considered for a real-time approach. It was found that in the case of cooling batch crystallization optimization, the local approach converged fast results but in both cases the solutions were different. The first case was found to be the global solution, confirmed after the hybrid optimization obtained the same results. Additionally, the genetic algorithm required more time on average and didn't converge to the same exact solution as the deterministic of hybrid method, but rather a coarser solution that appeared to require further refinement. This comparison revealed that using the SQP algorithm for optimization with a suitable initial guess will provide a fast optimization result with little compromise on the quality of the solution.

Finally, the multi-objective optimization for crystal mean size and coefficient of variation using the genetic algorithm provides a Pareto that is useful for understanding the relationship between the two objectives, but the optimization approach is computationally demanding taking over 4 hours to converge before terminating because 60 generations had been surpassed. Performing single-objective optimizations first and injecting the profiles as a starting point for the multi-objective optimization yielded optimization results in a shorter period of time and the Pareto was closer to the feasible region boundary than the previous case. Determining these relationships between quality attributes is important, but it should be restricted to being an offline activity as it is unlikely to be a feasible to implement this form

of optimization in real-time without some decision-making criteria for selecting a profile in the Pareto.

4 Single-Input Single-Output State Feedback Linearization, Tuning and SFL-Plant Constraints for Crystallization

4.1 Introduction

This chapter explores the use of state-feedback linearization (SFL) with a model predictive control (MPC) policy to control batch and continuous crystallization processes, while introducing a novel nonlinear constraints function for the MPC that can be implemented using a sequential quadratic programming (SQP) optimization algorithm to provide feasible constrained solutions. The single-input single-output (SISO) control problem in this study is for supersaturation control of crystallization. Supersaturation control is chosen as the control policy based on insights gained from Nagy et al. (2008) who disclose that temperature profile tracking is sensitive to disturbances or changes in operating conditions. While others have used properties of the CSD to formulate the objective function (see Chapter 5 for an example of this approach), obtaining accurate live CSD information *in-situ* remains a measurement challenge in crystallization, so for control purposes, using supersaturation control is comparatively more transferrable to a real batch process.

The global linearization technique developed by Kravaris and Chung (1987) will be introduced and applied to transform a nonlinear input-output crystallization model into a linear input-output model and a state-feedback control law for MPC. The MPC will be introduced and the input-output model from SFL-MPC declared. The developed MPC will then be iteratively tuned to achieve a desirable output response from batch and continuous modes of operation, gaining insight into how tuning parameters affect controller performance of the globally linearized model. Finally, the constraints handling technique, named SFL-Plant constraints, will be introduced and tested in further batch and continuous control scenarios. The outcome will be to assess if SFL-Plant constraints have been implemented successfully by validating the inputs are all feasible, and to further assess differences in controller performance, as defined by tracking errors of the controller (Shen et al, 1999).

4.2 State-Feedback Linearization for SISO systems

The SFL is an offline technique that can be applied to single-input single output (SISO) systems. The desired input and output variables must be selected to perform this technique, because it is designed for input-output linearization (Kravaris and Chung, 1987). This technique was

specifically devised for control systems in which input-output linearization was desired, because the pre-existing technique of input-state linearization did not guarantee in input-output linearization if there were nonlinearities between the states and outputs. The state space form is used throughout for model and control representation. To begin, the nonlinear model of the process can be represented in nonlinear state-space form:

$$\dot{\boldsymbol{x}} = \boldsymbol{f}(\boldsymbol{x}) + \boldsymbol{g}(\boldsymbol{x})\boldsymbol{u}$$
$$\boldsymbol{y} = \boldsymbol{h}(\boldsymbol{x})$$

Equation 4-1

where $\boldsymbol{x}$ is the vector of states, $\boldsymbol{y}$ is the vector of output and $\boldsymbol{u}$ is the vector of inputs, $\boldsymbol{f}(\boldsymbol{x})$, $\boldsymbol{g}(\boldsymbol{x})$ and $\boldsymbol{h}(\boldsymbol{x})$ are vector functions. The system can be represented in continuous state-space form or in a discrete form. Discrete state space is useful for when data is not continuously obtained but is instead obtained at discrete time points, ideally with a constant time step. This type of data is often referred to as time-series data. The discrete state space form is (Haddad, 2008):

$$\boldsymbol{x}(k+1) = \boldsymbol{f}\big(\boldsymbol{x}(k)\big) + \boldsymbol{g}\big(\boldsymbol{x}(k)\big)\boldsymbol{u}(k)$$
$$\boldsymbol{y}(k) = \boldsymbol{h}(\boldsymbol{x}(k))$$

Equation 4-2

Where k is the discrete time point in the time-series. The next step is to perform a transformation which aims to linearize the output of the system ($\boldsymbol{y}$) to the input ($\boldsymbol{u}$), hence the name input-output linearization. The methodology for input-output linearization requires the introduction of:

- Lie derivatives – to be performed for determining the input-output linearization
- Relative order – this is the order of the input-output linearization
- Control law – constructed using both the Lie derivatives and the relative order; also includes the tuning parameters for input-output control.

Generally, Lie derivatives are used in differential geometry, a branch of mathematics, to evaluate the changes in a tensor field along the flow defined by a vector field. In the context of input-output linearization, Lie derivatives are the changes of the output $\boldsymbol{h}(\boldsymbol{x})$ with respect to each of the states multiplied by the dynamics matrix $\boldsymbol{f}(\boldsymbol{x})$, or the input matrix $\boldsymbol{g}(\boldsymbol{x})$ (more details can be found in Kravaris & Chung (1987)):

$$L_f \boldsymbol{h}(\boldsymbol{x}) = \sum_i^N \frac{\partial \boldsymbol{h}}{\partial x_i} f(x_i) \qquad \text{Equation 4-3}$$

Where N is the number of states in the vector $\boldsymbol{x}$. Similarly, for L_g:

$$L_g \boldsymbol{h}(\boldsymbol{x}) = \sum_i^N \frac{\partial \boldsymbol{h}}{\partial x_i} g(x_i) \qquad \text{Equation 4-4}$$

This is a special case of vector multiplication where one of the vectors is a state-based derivative vector. In both cases, the derivative vector is the derivative of $\boldsymbol{h}(\boldsymbol{x})$ with respect to each element of $\boldsymbol{x}$. Hence the Lie derivative, when expanded, results in the following equation:

$$L_f \boldsymbol{h}(\boldsymbol{x}) = \frac{\partial \boldsymbol{h}}{\partial x_1} f(x_1) + \frac{\partial \boldsymbol{h}}{\partial x_2} f(x_2) + \cdots + \frac{\partial \boldsymbol{h}}{\partial x_N} f(x_N) \qquad \text{Equation 4-5}$$

The Lie derivative can be performed successively too, so much like with $\boldsymbol{h}(\boldsymbol{x})$, the derivative vector can be developed with respect to another vector such as the previous Lie derivative $L_f h$. This expands into the following (Oguchi, Watanabe and Nakamizo, 2002):

$$L_{\boldsymbol{f}} L_f \boldsymbol{h}(x) = \frac{\partial L_f \boldsymbol{h}}{\partial x_1} f(x_1) + \frac{\partial L_f \boldsymbol{h}}{\partial x_2} f(x_2) + \cdots + \frac{\partial L_f \boldsymbol{h}}{\partial x_N} f(x_N) \qquad \text{Equation 4-6}$$

And with this the k^{th} derivative can also be defined:

$$L_f L_f^k \boldsymbol{h}(\boldsymbol{x}) = \frac{\partial L_f^k \boldsymbol{h}}{\partial x_1} f(x_1) + \frac{\partial L_f^k \boldsymbol{h}}{\partial x_2} f(x_2) + \cdots + \frac{\partial L_f^k \boldsymbol{h}}{\partial x_N} f(x_N) \qquad \text{Equation 4-7}$$

The same can be applied for the vector $\boldsymbol{g}(\boldsymbol{x})$ in place of $\boldsymbol{f}(\boldsymbol{x})$. This gives the ability to successively find Lie derivatives, which are used for input-output linearization.

The relative order, r, is the minimum number of successive Lie derivatives required to obtain an explicit and non-zero relationship between the input and output (Kravaris and Chung, 1987). The relative order is therefore unique to a model input-output combination. There are two conditions that must be met to determine the relative order:

$$L_g L_f^k \boldsymbol{h}(\boldsymbol{x}) = 0 \qquad k = 0, 1, \ldots, r-2 \qquad \text{Equation 4-8}$$

$$L_g L_f^{r-1} \boldsymbol{h}(\boldsymbol{x}) \neq 0 \qquad \text{Equation 4-9}$$

The first condition is in place to ensure that r is obtained from the minimum number of derivatives. The second condition ensures when r is determined and implemented, the Lie derivative of relative order r results in a non-zero value thus ensuring an input-output relationship. The use of the $\boldsymbol{g}(\boldsymbol{x})$ and $\boldsymbol{f}(\boldsymbol{x})$ matrices are in an affine-in-control representation because the aim is to find the relationship between the input and output, hence the input vector function is isolated in the nonlinear state space formulation. From the state space system, the function $\boldsymbol{g}(\boldsymbol{x})$ is related to the input, and $\boldsymbol{h}(\boldsymbol{x})$ is defined as the output. The states in a state space formulation define the relationship between the inputs and outputs. Hence the definition of the Lie derivative can be interpreted here as when the output is differentiated with respect to each state and multiplied by the respective input that affects each state, what is obtained is how the output varies with respect to changes in the input; which can also be regarded as the output sensitivity to the inputs, coupled with the state-derived dynamics of the process. Therefore, a zero value would appear if either of the following happens for all the terms in the Lie derivative:

1) The output is not sensitive to changes in a state
2) The states which do show output sensitivity are not affected by the input

Then, if a non-zero value appears, there is a connection between the output and the input through the states. As the states play an important role in forming this relationship, they must also be used in the control law, hence the *state-feedback* linearization. When the above conditions are not satisfied for the first Lie derivative, the next Lie derivative must be found, and this is where the $\boldsymbol{f}(\boldsymbol{x})$ matrix is introduced. The $\boldsymbol{f}(\boldsymbol{x})$ in state space is the dynamics matrix, it is used to describe how the states change with respect to their existing values and inputs. Consequently, if the output is not directly affected by the input through the states alone, the dynamic changes in states will be used to determine if there exists an input-output relationship for the system. It is also possible that a relationship may not exist, to prevent this from occurring it is best to perform plant tests and cause-effect analysis or sensitivity analysis to ensure the selected inputs would indeed have an effect on the outputs. Finally, given the order of the system is r, the control law can be established. The control law (φ) is (Kravaris and Chung, 1987):

$$u = \varphi(\boldsymbol{x}, v) = \frac{v - \sum_{k=0}^{r} \beta_k L_f^k \boldsymbol{h}(\boldsymbol{x})}{\beta_r L_g L_f^{r-1} \boldsymbol{h}(\boldsymbol{x})} \qquad \textit{Equation 4-10}$$

Where u is the plant input, v is the model input and β are controller tuning parameters. The β parameters are have two important roles in this approach in that they determine the effects of the model input v on the plant input u, because the β parameters are linked to the state-feedback parameters in the control law. Furthermore, this transformation will be used to determine a state-feedback linearized model in section 4.3, where it is shown that the β parameters form the linear state-space model that is used in the MPC. This is because the transformation captures the plant input and plant state information in the linearization to form a system using a new arbitrary input, the MPC input v, and the β parameters which together capture the evolution of the process output y. Therefore, selection of appropriate values for these parameters is critical to the MPC performance and control law. The plant and model inputs are scalars in the control law because one value of model input is used to obtain one plant input. This control law is an explicit equation which determines the plant input from the model input and plant states. The control law is used to convert the MPC model input into the plant input. The MPC model is the linear state space model derived using the aforementioned SFL methodology and the MPC uses the model to optimize the future plant inputs to keep the output for the process on track to a trajectory or setpoint. The introduction and functionality of MPC is discussed in section 4.3.

There are certain conditions which must be met for the SFL to be used for process control; the control law should be non-zero and the SFL should have a relative order greater than 0. To guarantee this, the input must cause some effect on the output. Fortunately, the identification of a suitable input and output is possible using techniques such as sensitivity analysis (Fysikopoulos *et al.*, 2018) to ensure input-output controllability. Moreover, supersaturation control was selected for the study because of the abundance of successful supersaturation control in literature (Vissers, Jansen and Weiland, 2011; Saleemi, Rielly and Nagy, 2012).

4.2.1 Crystallization Model Linearization

The continuous MSMPR seeded crystallization model is described by Equations 4-11 to 4-20. In this model, the absolute supersaturation S is the controlled or output variable and the manipulated or input variable is the jacket temperature T_j.

$$\frac{d\mu_0}{dt} = B + \frac{F_{in}}{V}\mu_{0in} - \frac{F_{out}}{V}\mu_0 \quad \textit{Equation 4-11}$$

$$\frac{d\mu_1}{dt} = \mathrm{G}\mu_0 + Br_0 + \frac{F_{in}}{V}\mu_{1in} - \frac{F_{out}}{V}\mu_1 \quad \textit{Equation 4-12}$$

$$\frac{d\mu_2}{dt} = 2\mathrm{G}\mu_1 + Br_0^2 + \frac{F_{in}}{V}\mu_{2in} - \frac{F_{out}}{V}\mu_2 \quad \textit{Equation 4-13}$$

$$\frac{d\mu_3}{dt} = 3\mathrm{G}\mu_2 + Br_0^3 + \frac{F_{in}}{V}\mu_{3in} - \frac{F_{out}}{V}\mu_3 \quad \textit{Equation 4-14}$$

$$\frac{dC}{dt} = -\mathrm{k_v}\rho_c(3\mathrm{G}\mu_2 + Br_0^3) + \frac{F_{in}}{V}C_{in} - \frac{F_{out}}{V}C \quad \textit{Equation 4-15}$$

$$\frac{dT}{dt} = -\frac{3\rho_c k_v G\mu_2 \Delta H}{\rho c_p} - \frac{UA_c}{\rho V c_p}(T - T_j) + \frac{F_{in}}{V}T_{in} - \frac{F_{out}}{V}T \quad \textit{Equation 4-16}$$

$$B = k_b(S)^b \quad \textit{Equation 4-17}$$

$$G = k_g(S)^g \quad \textit{Equation 4-18}$$

$$S = C - C^* \quad \textit{Equation 4-19}$$

$$C^*(T) = A_0T^2 - A_1T + A_2 \quad \textit{Equation 4-20}$$

where *F* is the volumetric flow, *V* is the volume of the crystallizer, μ_{in} are the moments of the seed distribution, U is the heat transfer coefficient, A is the surface area for heat transfer, c_p is the specific heat capacity of the crystallization system, ρ is the density of the solvent and ΔH_c is the heat of crystallization. This model is used to represent the continuous MSMPR and batch crystallizers in a series of control scenarios. When the flow rates are set to 0, the model is valid for batch crystallization. The crystallization model can be represented in the nonlinear state space form previously disclosed in Equation 4-1, where the system vectors are as follows:

$$\boldsymbol{x} = [\mu_0\ \mu_1\ \mu_2\ \mu_3\ C\ T]^T \qquad \textit{Equation 4-21}$$

$$\boldsymbol{u} = \left[0\ 0\ 0\ 0\ 0\ T_j\right]^T \qquad \textit{Equation 4-22}$$

$$\boldsymbol{f}(\boldsymbol{x}) = \begin{bmatrix} B + \frac{F_{in}}{V}\mu_{0in} - \frac{F_{out}}{V}\mu_0 \\ \mathrm{G}\mu_0 + Br_0 + \frac{F_{in}}{V}\mu_{1in} - \frac{F_{out}}{V}\mu_1 \\ 2\mathrm{G}\mu_1 + Br_0^2 + \frac{F_{in}}{V}\mu_{2in} - \frac{F_{out}}{V}\mu_2 \\ 3\mathrm{G}\mu_2 + Br_0^3 + \frac{F_{in}}{V}\mu_{3in} - \frac{F_{out}}{V}\mu_3 \\ -\mathrm{k_v}\rho_c(3\mathrm{G}\mu_2 + Br_0^3) + \frac{F_{in}}{V}C_{in} - \frac{F_{out}}{V}C \\ -\frac{3\rho_c k_v G\mu_2 \Delta H}{\rho c_p} - \frac{UA_c}{\rho V c_p}(T) + \frac{F_{in}}{V}\ T_{in} - \frac{F_{out}}{V}T \end{bmatrix} \qquad \textit{Equation 4-23}$$

$$\boldsymbol{g}(\boldsymbol{x}) = \begin{bmatrix} 0 \\ 0 \\ 0 \\ 0 \\ 0 \\ \frac{UA_c}{\rho V c_p} \end{bmatrix} \qquad \textit{Equation 4-24}$$

$$y = \boldsymbol{h}(\boldsymbol{x}) = C - C^*(T) \qquad \textit{Equation 4-25}$$

This is in the continuous nonlinear form. The SFL technique described will now be applied to the batch and continuous MSMPR crystallization model. The control problem for supersaturation control will be considered, where the temperature of the coolant will be used as the manipulated variable. The absolute supersaturation is defined as the output, as per Equation 4-26.

$$y = \boldsymbol{h}(\boldsymbol{x}) = C - C^* \qquad \textit{Equation 4-26}$$

The crystallizer solution concentration, C, is the fifth state, $x_{5,}$ and the solubility C^* is a function of the crystallizer temperature which is the sixth state, x_6, (Equation 4-21). The relative order must be found by satisfying the following two conditions (Kravaris and Chung, 1987):

$$L_g L_f^k \boldsymbol{h}(\boldsymbol{x}) = 0 \qquad k = 0, 1, \dots, r-2$$
$$L_g L_f^{r-1} \boldsymbol{h}(\boldsymbol{x}) \neq 0$$

Therefore, beginning with $k = 0$:

$$L_g L_f^0 \boldsymbol{h}(\boldsymbol{x}) = L_g \boldsymbol{h}(\boldsymbol{x})$$
$$L_g \boldsymbol{h}(x) = \sum_i^N \frac{\partial \boldsymbol{h}}{\partial x_i} g(x_i)$$

where N = 6 because there are 6 states, and expanding gives

$$L_g \boldsymbol{h}(\boldsymbol{x}) = \frac{\partial \boldsymbol{h}}{\partial x_1} g(x_1) + \frac{\partial \boldsymbol{h}}{\partial x_2} g(x_2) + \frac{\partial \boldsymbol{h}}{\partial x_3} g(x_3) + \frac{\partial \boldsymbol{h}}{\partial x_4} g(x_4) + \frac{\partial \boldsymbol{h}}{\partial x_5} g(x_5) + \frac{\partial \boldsymbol{h}}{\partial x_6} g(x_6)$$

Given $\boldsymbol{g}(\boldsymbol{x}) = \begin{bmatrix} 0 \\ 0 \\ 0 \\ 0 \\ 0 \\ \frac{UA_c}{\rho V c_p} \end{bmatrix}$, substituting into the above equation results in:

$$L_g \boldsymbol{h}(\boldsymbol{x}) = 0 + 0 + 0 + 0 + 0 + \frac{\partial \boldsymbol{h}}{\partial x_6} \frac{UA_c}{\rho V c_p}$$

And substituting $\boldsymbol{h}(\boldsymbol{x}) = C - C^*(T)$,

$$\frac{\partial \boldsymbol{h}}{\partial x_6} = -\frac{dC^*}{dT} = 2A_0 T + A_1$$

Hence, the first Lie derivative results in a non-zero value:

$$L_g \boldsymbol{h}(\boldsymbol{x}) = (2A_0 T + A_1) \times \frac{UA_c}{\rho V c_p} \neq 0$$

Therefore when $\boldsymbol{k = 0}$, the final condition of $\boldsymbol{L_g L_f^{r-1} h(x) \neq 0}$ is satisfied.

This concludes that for supersaturation control using jacket temperature, the relative order of the system is r = 1, because the first Lie derivative results in a non-zero value. Specifically, the input-output linearization has transformed the nonlinear model defined by Equations 4-11 to 4-20 into a linear input-output model with a relative order of 1. Hence, the control law becomes:

$$u = \varphi(\boldsymbol{x}, v) = \frac{v - \sum_{k=0}^{r} \beta_k L_f^k h(x)}{\beta_r L_g L_f^{r-1} h(x)} = \frac{v - \beta_0 h(x) - \beta_1 L_f h(x)}{\beta_1 L_g h(x)} \qquad \textit{Equation 4-27}$$

The Lie derivative $L_f \boldsymbol{h}(\boldsymbol{x})$ is found using the same procedure as above, by substituting the $\boldsymbol{f}(\boldsymbol{x})$ vector in place of the $\boldsymbol{g}(\boldsymbol{x})$ vector. Now it is clear that there are two β parameters in conjunction with one MPC input v that will form the linear state-space model for the MPC (shown in section 4.3.2). It is now possible to represent the SFL model in a linear state-space form, but because the linear model will be used for control in a model predictive controller, the MPC will be introduced first.

4.3 Model Predictive control

A linear model predictive controller has been developed for SFL and the full structure of the MPC is described in this section. The structure for SISO MPC without bounds or constraints will first be introduced, then further expanded to incorporate bounds and constraints. Traditional linear MPC has the inherent capability of handling bounds and constraints (García, Prett and Morari, 1989b), so loss of this functionality is not desirable for advanced process control. This is the main reason for the emphasis on constraints handling in this research.

The requirements to build an MPC and the objectives of an MPC are first described here. To construct an MPC, first a mathematical model is identified and validated to accurately and reliably predict the behaviour of a real system which is to be controlled (Matthews, Miller and Rawlings, 1996). The model is presented in a linear state-space form compatible with the MPC. Once the model is integrated into the MPC, the process states $\boldsymbol{x}$ and measured outputs $\boldsymbol{y}$ are transferred to the controller from the plant. The MPC then uses the model and an optimizer to determine the optimal inputs $\boldsymbol{u}$ for the future. The optimal path depends on the control problem, represented as the optimizers cost function. Typically, the control problem will be to follow the reference trajectory of the output $\boldsymbol{y_{ref}}$, which is achieved by comparing the predicted output from the MPC (prediction horizon) to the reference and minimizing the error between them. The sequence of inputs (control horizon) will be returned from the optimisation, the first input from this control horizon is implemented on the plant. Thus, the controller has two stages, an optimisation stage and an implementation stage.

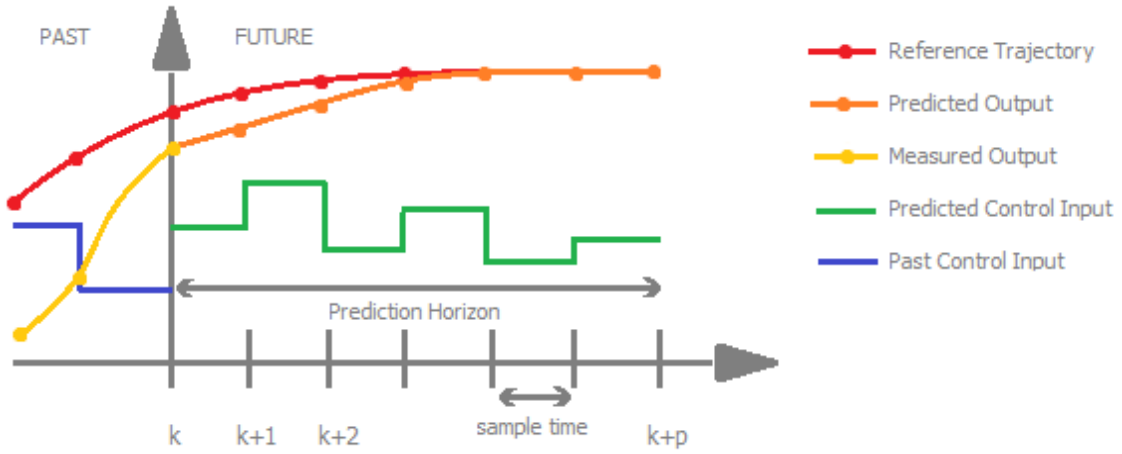

Figure 4-1. Schematic for discrete-time Model Predictive Control

The method of implementing or scheduling an MPC is now described (García, Prett and Morari, 1989b), aided with the schematic of MPC shown in Figure 4-1. Assuming the current time is k, the past and current information about the inputs and outputs are known, in addition to any other measured information from the process (states). When the controller is invoked at time k, the data is passed to the controller to begin the optimisation stage. Once the objective function is minimised and a control horizon is obtained, the controller will then implement the first of the inputs from the control horizon onto the plant until time $k+1$. This procedure is repeated at each interval of $k, k+1, k+2, \dots, k+n$. Usually the optimization step requires a significant amount of computation time and uses a discrete state-space model of the system. The time interval (sample time in Figure 4-1) which determines how often the controller is invoked will be decided based on the plant, model and controller's computational efficiency. This feature of the MPC also results in the capability to reject process disturbances.

The continuous linear state-space form of the MPC model is:

$$\dot{\boldsymbol{x}}_{\boldsymbol{m}} = A_c \boldsymbol{x}_{\boldsymbol{m}} + B_c \boldsymbol{u} \qquad \textit{Equation 4-28}$$

$$\boldsymbol{y} = C_c \boldsymbol{x}_{\boldsymbol{m}} \qquad \textit{Equation 4-29}$$

Here, A_c, B_c and C_c are matrices of scalars for the continuous model (denoted by the subscript c) resulting in a linear system, $\boldsymbol{x}_{\boldsymbol{m}}$ is a vector of states $\boldsymbol{x}$ with the value of $\boldsymbol{y}$ appended to the

end of the vector. Usually, the MPC input and output are measurable variables, but the states may not be directly measured. One solution to this is to implement a state observer in order to calculate or approximate the values of the states in the system. In this research a state observer has not been implemented, as it is assumed that the state information is accessible via direct measurement. This is a reasonable assumption for crystallization concentration and temperature states which are commonly measured from solution, but for the method of moments states this would be more difficult to measure directly. It may also be possible to use process analytical technologies to approximate particle size *in-situ* and thus deduce the states of the moments. It is understood that this is a limitation and for application on a real system, a state observer would be beneficial.

Sophisticated linearization approaches such as SFL have enabled the transformation and control of nonlinear processes without the need for elaborate nonlinear MPC algorithms that are substantially more computationally demanding (Corriou and Rohani, 2002). These continuous state space formulations use the ODE forms of the state equations directly. The systems can be converted to discrete-time state space by applying a discretization in the time domain, such as setting a time period. The discrete-time approach is convenient when a controller must wait for new process measurements before actuating changes to the process. For example, if new process data is measured at 30 s intervals, setting the time period to be less than 30 s will mean the controller will actuate a new input before the changes from the last input have been observed through new measurements. Furthermore, the model defined in Equation 4-28 and Equation 4-29 is an absolute model which uses the absolute values of the states and inputs to determine the output. A better approach is to use a relative or incremental model which observes the changes in states and inputs instead (Haber, 1992). The linearized system discrete-time state-space formulation is introduced by first defining the changes in states $\Delta \boldsymbol{x}$ and changes in input $\Delta \boldsymbol{u}$:

$$\Delta \boldsymbol{x}(k+1) = \boldsymbol{x}(k+1) - \boldsymbol{x}(k) \qquad \textit{Equation 4-30}$$

$$\Delta \boldsymbol{u}(k) = \boldsymbol{u}(k) - \boldsymbol{u}(k-1) \qquad \textit{Equation 4-31}$$

$$\boldsymbol{x_m}(k) = [\Delta \boldsymbol{x}(k)^T \; \boldsymbol{y}(k)]^T \qquad \textit{Equation 4-32}$$

Here, $\Delta \boldsymbol{x}(k+1)$ is the change in the states from instant k to $k+1$, and similarly for $\Delta \boldsymbol{u}(k)$ this is the change in $\boldsymbol{u}$ from $k-1$ to k, these can also be referred to as incremental states and inputs. The $\Delta \boldsymbol{u}$ can also be called the *move* because it is the amount by which the previous value of $\boldsymbol{u}$ is moved. Additionally, $\boldsymbol{x_m}(k)$ refers to the vector of state changes $(\Delta \boldsymbol{x}(k))$ and also includes the output $\boldsymbol{y}(k)$, at instant k. Based on these definitions, the discrete-time state space formulation of Equation 4-30 and Equation 4-31 are:

$$\boldsymbol{x_m}(k+1) = A\boldsymbol{x_m}(k) + B\Delta \boldsymbol{u}(k) \qquad \textit{Equation 4-33}$$

$$\boldsymbol{y}(k) = C\boldsymbol{x_m}(k) \qquad \textit{Equation 4-34}$$

In the discrete form, the A, B and C matrices differ from the continuous form but can be obtained through conversion. Moreover, these matrices are not the same as those for a linear state-space model because as shown in Equation 4-32 the vector $\boldsymbol{x_m}$ is not the same as $\boldsymbol{x}$; this will be revisited when the SFL MPC framework is introduced in section 4.4. There is a function built into MATLAB for this conversion ***(c2dm)*** and variants of this function also exist in the field of signal processing and are well defined and widely accepted (Tretter, 1976; Ogata, 1995). The ***c2dm*** function uses a defined time-step to convert a continuous form state space model's A_c, B_c and C_c matrices to discrete form A, B and C respectively. Furthermore, $\boldsymbol{x_m}(k+1)$ is the value of the states at the next point in the horizon, the future prediction. This can be extended to the length of the output prediction horizon N_p. Additionally, the number of control points in the control horizon (N_c) is usually less than N_p. The full horizon of inputs will range from $\Delta \boldsymbol{u}(k)$ to $\Delta \boldsymbol{u}(k+N_c)$. The vector of $\Delta \boldsymbol{u}$ is the control horizon. The output vector is $\boldsymbol{y} = [y(k), y(k+1) \dots\ y(k+N_p)]$. This is also determined from the state vector $\boldsymbol{x_m}$ using the matrix C.

The linear state space form can be used to calculate each value in the prediction horizon directly, and can subsequently be simplified for the output prediction. For the output prediction, the following equations can be used to find the predicted outputs:

$$\boldsymbol{y}(k+1|k) = CA\boldsymbol{x}(k) + CB\Delta \boldsymbol{u}(k) \qquad \textit{Equation 4-35}$$

$$\boldsymbol{y}(k+2|k) = CA^2\boldsymbol{x}(k) + CAB\Delta \boldsymbol{u}(k) + CB\Delta \boldsymbol{u}(k+1) \qquad \textit{Equation 4-36}$$

$$\boldsymbol{y}(k+3|k) = CA^3\boldsymbol{x}(k) + CA^2B\Delta\boldsymbol{u}(k) + CAB\Delta\boldsymbol{u}(k+1) + CB\Delta\boldsymbol{u}(k+2)$$ *Equation 4-37*

Or more generally:

$$\boldsymbol{Y} = \boldsymbol{F}\boldsymbol{x}(k) + \boldsymbol{\Phi}\Delta\boldsymbol{U}$$ *Equation 4-38*

Where

$$\boldsymbol{Y} = \left[\boldsymbol{y}(k+1|k)\ \boldsymbol{y}(k+2|k) \dots \boldsymbol{y}\left(k+N_p\middle|k\right)\right]^T$$ *Equation 4-39*

$$\Delta\boldsymbol{U} = [\Delta\boldsymbol{u}(k)\ \Delta\boldsymbol{u}(k+1) \dots\ \Delta\boldsymbol{u}(k+N_c-1)]^T$$ *Equation 4-40*

As shown, the output horizon $\boldsymbol{y}$ can be linked directly to the current states $\boldsymbol{x}(k)$ and the current and future input changes used as decision variables by the optimizer. This means no further future states are required for the prediction horizon calculation and thus the computation burden can also be reduced by calculating the prediction horizon in a single matrix-multiplication calculation shown in Equation 4-39. One important point on the use of $\Delta\boldsymbol{u}$ instead of $\boldsymbol{u}$ is that this is the change in input from the previous to current step. Given that the time step is constant, $\Delta\boldsymbol{u}$ is the rate of change of input and the $\Delta\boldsymbol{u}$ vector will be optimised in the traditional MPC approach. Furthermore, constraints can be applied directly on $\Delta\boldsymbol{u}$ to ensure rates of change on the input are not violated, which is useful for when the input is the temperature of a cooling jacket where the rate of change in temperature is limited by heat transfer (Sarkar, Rohani and Jutan, 2006). Also, the time period is known so $\Delta\boldsymbol{u}$ can be used to obtain $\boldsymbol{u}$, thus there is an ability to bound $\boldsymbol{u}$ within limits to avoid infeasible values, such as temperatures being outside the feasible range for the coolant. Equation 4-35 to Equation 4-37 and further can be simplified into the form shown in Equation 4-38 where $\boldsymbol{Y}$ is related to $\boldsymbol{x}(k)$ and $\Delta\boldsymbol{U}$ by the matrices $\boldsymbol{F}$ and ϕ. These matrices are shown here:

$$\boldsymbol{F} = \begin{bmatrix} CA \\ CA^2 \\ CA^3 \\ \vdots \\ CA^{N_p} \end{bmatrix}$$ *Equation 4-41*

$$\boldsymbol{\Phi} = \begin{bmatrix} CB & 0 & 0 & \cdots & 0 \\ CAB & CB & 0 & \cdots & 0 \\ CA^2B & CAB & CB & \cdots & 0 \\ \vdots & \vdots & \vdots & \ddots & \vdots \\ CA^{N_p-1}B & CA^{N_p-2}B & CA^{N_p-3}B & \cdots & CA^{N_p-N_c}B \end{bmatrix}$$

Equation 4-42

These matrices can be obtained from the already identified state-space model as each element of $\boldsymbol{F}$ and $\boldsymbol{\Phi}$ are simply multiples of A, B and C matrices (Wang, 2009a). Calculating these matrices from the discrete state-space model in the MPC will enable the calculation of the prediction horizon and optimization of the control horizon in an MPC. Therefore, the next step is to define the discrete state-space model for crystallization.

4.3.1 Linear State-Space Models for Control

The linear discrete state-space SFL model is now defined given the control law has been determined and the MPC model form has been discussed. The symbols used here are different to that of the nonlinear state-space form to differentiate the inputs and states in the SFL model from the plant model.

$$\begin{aligned} \boldsymbol{\xi}(k+1) &= A_d\boldsymbol{\xi}(k) + B_d\boldsymbol{v}(k) \\ \boldsymbol{y}(k) &= C_d\boldsymbol{\xi}(k) \end{aligned}$$

Equation 4-43

where, $\boldsymbol{\xi}$ is the state vector, $\boldsymbol{y}$ the output and $\boldsymbol{v}$ the input. The expanded continuous form of this model is shown in Equation 4-44 and Equation 4-45, this form is used to identify the matrices of the continuous form state-space model first because the SFL parameters can substituted into the model.

$$\dot{\boldsymbol{\xi}} = \begin{bmatrix} 0 & 1 & \cdots & 0 & 0 & 0 \\ \vdots & \vdots & \ddots & \vdots & \vdots & \vdots \\ 0 & 0 & \cdots & 1 & 0 & 0 \\ 0 & 0 & \cdots & 0 & 1 & 0 \\ 0 & 0 & \cdots & 0 & 0 & 1 \\ -\frac{\beta_0}{\beta_r} & -\frac{\beta_1}{\beta_r} & -\frac{\beta_2}{\beta_r} & \cdots & -\frac{\beta_{r-2}}{\beta_r} & -\frac{\beta_{r-1}}{\beta_r} \end{bmatrix} \boldsymbol{\xi} + \begin{bmatrix} 0 \\ \vdots \\ 0 \\ 0 \\ 0 \\ \frac{1}{\beta_r} \end{bmatrix} \boldsymbol{v}$$

Equation 4-44

$$\boldsymbol{y} = [1 \quad 0 \quad 0 \quad \cdots \quad 0 \quad 0\,]\boldsymbol{\xi}$$

Equation 4-45

The β tuning parameters appear in the model as well as the control law. As stated by Kravaris and Chung (1987), these parameters must be tuned to achieved a desired controller

performance and control response, but the values are arbitrary and selection is not as routine as that of other control techniques such as PID. However, as shown by Shen *et al.* (1999), the input-output behaviour of the closed loop system is governed by:

$$\sum_{k=0}^{r} \beta_k \frac{d^k y}{dt^k} = v \qquad \textit{Equation 4-46}$$

Applying the transfer function to this form gives the transfer function of the closed loop system (Vissers *et al.,* 2011) as shown:

$$G_l(s) = \frac{y(s)}{v(s)} = \frac{1}{\beta_r s^r + \beta_{r-1} s^{r-1} + \cdots + \beta_1 s + \beta_0} \qquad \textit{Equation 4-47}$$

The denominator is set equal to 0 to determine the poles of the system, therefore the β parameters define the poles of the system and to ensure controller stability, one requirement is that the poles must have negative real parts. Thus, the β tuning parameters must be positive real numbers. This is the only condition that has been defined in literature. Further challenges lie with selecting values for the parameters because they exist in the model's dynamics matrix A as well as the control law.

One notable limitation of the SFL model is the inability to capture the state information of the process. The SFL model is identified entirely from the input-output relationship, but the output alone forms the model along with the tuning parameters. The model does not capture the dynamics of the process that traditional MPC models would. Moreover, the control input v is used to determine the plant input u but the latter is state-dependent, thus v does not directly correlate to u resulting in difficulties to implement of bounds and constraints from the real system into the SFL model (Kurtz and Henson, 1996); this is addressed in section 4.8.

4.3.2 Linearized SFL Model for Crystallization Supersaturation Control

The SFL model for continuous seeded MSMPR crystallization that is used in the MPC is defined by Equation 4-43 where β_0 and β_1 are the tuning parameters, based on the relative order r equal to 1, valid for supersaturation control using the coolant temperature of the crystallizer as the manipulated variable (Equations 4-11 to 4-20).

$$\xi_{(k)} = \left[-\frac{\beta_0}{\beta_1}\right] \xi_{(k-1)} + \left[\frac{1}{\beta_1}\right] v_{(k)}$$
$$y_{(k)} = [1]\, \xi_{(k-1)}$$

Equation 4-48

4.4 SISO MPC with SFL

The single-input single-output MPC with SFL framework will now be introduced. To remain consistent with the state space equations already defined for SFL, the MPC state space equations are rewritten using the same variables from the SFL. The schematic for MPC with SFL is shown in Figure 4-2. In this schematic, the SFL control law and nonlinear plant are considered together as an overall linear system whose output is controlled by the MPC and the input to the linear system is the input to the SFL control law v. Two further changes are made to the state space equation. Firstly, the state space defined by Equation 4-33 and Equation 4-34 have been expanded to show how A, B and C matrices are defined from the discrete model matrices from Equation 4-43. The expanded forms are in Equation 4-49 and Equation 4-50 (Wang, 2009b). The SFL model's state space equations also have their own expanded controllable form because the states are different, this results in the expanded form shown in Equation 4-51 and Equation 4-52, which can be used interchangeably with the original form.

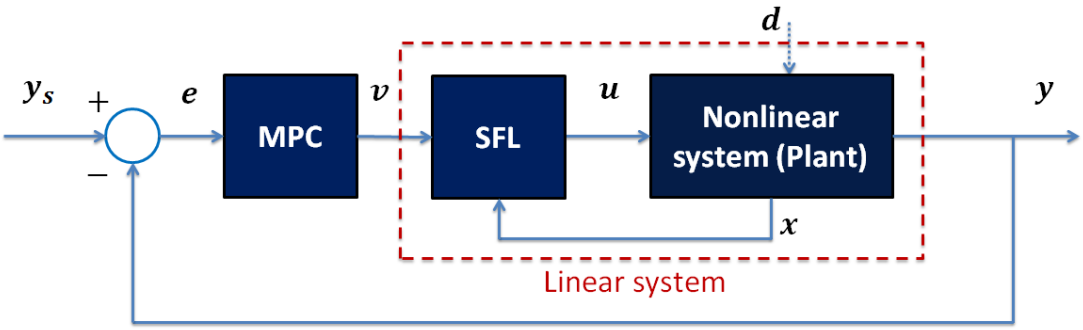

Figure 4-2 Schematic of MPC with the linearized system

$$\begin{bmatrix}\Delta x(k+1)\\ y(k+1)\end{bmatrix} = \begin{bmatrix}A_d & o_m^T\\ C_d A_d & 1\end{bmatrix}\begin{bmatrix}\Delta x(k)\\ y(k)\end{bmatrix} + \begin{bmatrix}B_d\\ C_d B_d\end{bmatrix}\Delta u(k)$$

Equation 4-49

$$y(k) = \begin{bmatrix}o_m^T & 1\end{bmatrix}\begin{bmatrix}\Delta x(k)\\ y(k)\end{bmatrix}$$

Equation 4-50

$$\begin{bmatrix}\Delta\xi(k+1)\\ y(k)\end{bmatrix} = \begin{bmatrix}A_d & 0\\ C_d & I\end{bmatrix}\begin{bmatrix}\Delta\xi(k)\\ y(k-1)\end{bmatrix} + \begin{bmatrix}B_d\\ 0\end{bmatrix}\Delta v(k)$$

Equation 4-51

$$y(k) = \begin{bmatrix} C_d & I \end{bmatrix} \begin{bmatrix} \Delta\xi(k) \\ y(k-1) \end{bmatrix} \qquad \text{Equation 4-52}$$

The main difference between these two state space forms other than the state space matrices is that the output defined in Equation 4-50 expands out to $y(k) = y(k)$ which is often stated for completeness. The output is traditionally obtained from Equation 4-49 instead because this equation holds the dynamics and input data which is used to calculate the output. However, for the SFL model the output is obtained directly from the output equation (Equation 4-52). This is because $y(k)$ is now dependent on the state changes $\Delta\xi(k)$ where in the prior case it was not a function of $\Delta x(k)$ because o_m^T is a vector of zeros (Wang, 2009b). So Equation 4-52 can be read as the new output ($y(k+1)$) which is obtained from the changes in output ($\Delta\xi(k) = \frac{dy_k}{dt}$) added to the previous output ($y(k)$). This now defines the full structure of the MPC with SFL that can be used for controlling a nonlinear plant. For the crystallization model for supersaturation control, the system equations can be populated since it is known that the relative order is 1:

$$\begin{aligned} \xi_{(k)} &= \begin{bmatrix} 1 & 1 \\ 0 & -\beta_0/\beta_1 \end{bmatrix} \xi_{(k-1)} + \begin{bmatrix} 0 \\ 1/\beta_1 \end{bmatrix} \Delta v_{(k)} \\ y_{(k)} &= \begin{bmatrix} 1 & 1 \end{bmatrix} \xi_{(k-1)} \end{aligned} \qquad \text{Equation 4-53}$$

The SLF MPC algorithm requires initialisation with Equation 4-53 before the MPC can begin to control the plant. To complete the definition of the MPC, the objective function must be defined and the tuning parameters must be selected.

4.5 MPC with SFL Objective Function

The MPC Equation 4-54 shows the cost function J used by the optimization algorithm for MPC:

$$J = Q \sum_{i=1}^{N_p} \left(y_{i,predicted} - y_{i,setpoint}\right)^2 + R \sum_{l=1}^{N_c} \Delta v_l^2 \qquad \text{Equation 4-54}$$

where Q and R are weighting matrices that facilitate the prioritisation of minimising the error in output prediction and minimising the changes to the input, respectively. This is one of the advantages for using MPC; the input changes are a part of the optimization problem and if large changes in the input are undesirable, as is the case for mechanical equipment where excessive changes can lead to wear and failure, the objective function weightings can be

tuned to prevent excessive changes to the inputs. The weighting of R is determined through tuning, and the weight of R can be tuned relative to Q in such a way that the cost function will be more influenced by the input changes Δv, which usually results in a slower convergence of the output onto a reference trajectory. Conversely, a larger relative weight of Q results in the cost function prioritising setpoint convergence and thus, large changes in input may be made by the MPC. Although u is the real plant input, recalling from Figure 4-2, the MPC acts upon the linear system which includes the coupled control law with the plant. Therefore, the actual input from the MPC is v (through calculation of Δv) which is then used to calculate u using the control law $\varphi(\boldsymbol{x}, v)$. The objective function which defines the MPC control problem is Equation 4-55.

$$\min_{v} J = Q \sum_{i=1}^{N_p} \left(y_i - y_{i,setpoint}\right)^2 + R \sum_{l=1}^{N_c} \Delta v_l^2 \qquad \textit{Equation 4-55}$$

Subject to:

$$u_{min} \leq u = \varphi(\boldsymbol{x}, v) \leq u_{max}$$

$$\Delta u_{min} \leq \Delta u = \varphi(\boldsymbol{x_i}, v_i) - \varphi(\boldsymbol{x_{i+1}}, v_{i+1}) \leq \Delta u_{max}$$

Given:

$$\boldsymbol{x}$$
$$\dot{\boldsymbol{x}} = \boldsymbol{f}(\boldsymbol{x}) + \boldsymbol{g}(\boldsymbol{x})\boldsymbol{u}$$

In this objective function, there are real plant constraints in $\boldsymbol{u}$ which must be satisfied and can be done so by applying the inverse transformation of the control law, φ^{-1}. To perform this transformation, the objective function is also supplied with the states of the real plant, $\boldsymbol{x}$ as well as the nonlinear plant. The use of this will be explained in section 4.8 when SFL-Plant constraints are introduced.

4.6 Simulation data

Table 4-1 shows the data used for all crystallization simulations. The data used were obtained from the paracetamol crystallization system described by Nagy et al (2008).

Constant	Value	Units
$\boldsymbol{k_b}$	$e^{45.8}$	$min^{-1}g^{-1}$
$\boldsymbol{b}$	6.2	-
$\boldsymbol{k_g}$	$e^{-4.1}$	$m\ min^{-1}$

g	1.5	-
r_0	0	m
k_v	0.24	-
ρ_c	1296	kgm^{-3}
V	1	L
UA_c	545.21	$J\ min^{-1}\ K^{-1}$

Table 4-1 – Parameter values used to represent Crystallization Properties

Constant	Value	Units
C_{in}	0.0256	g/g
$C_{initial}$	0.0256	g/g
$T_{initial}$	315	K
Δt	1	min
N_p	5	-
N_c	5	-

Table 4-2 – Supplementary Crystallization Control Simulation Data

Further data for the simulation are provided in Table 4-2 for variables and parameters which are constant across all simulation scenarios. The prediction horizon N_p and control horizon N_c are both set to 5 based on a trade-off between having enough points to determine the output prediction trajectory and reducing the computation cost. Typically, the horizon is set to the number of samples over which a closed-loop response converges to the setpoint and from performing some initial simulations it was found that the shortest closed loop response occurred in 5 samples from the point the MPC was active. The horizon lengths are also typically set prior to tuning the MPC weights, hence they have been specified now, prior to simulation. A larger prediction and control horizon result in more decision variables in the optimization stage of the MPC and a longer trajectory whose errors must be calculated to be minimised. The remaining simulation data are not included in these two tables, as they are scenario-specific and are disclosed with each simulation scenario in the following sections.

4.7 Tuning of the SFL-MPC parameters

This section focusses on the selection of the SFL β tuning parameters for batch and start-up of continuous MSMPR crystallization alongside tuning the cost function weighting matrices Q and R. The former are important for determining the controller dynamics, whereas the latter are important for tuning the controller objective. Typically, the tuning of an MPC would entail tuning the cost function weights of the inputs and outputs as well as tuning the horizon lengths, because a longer prediction and control horizon will result in a larger computation cost. The purpose of the prediction and control horizon is to allow sufficient prediction into the future to establish the direction of the process output. However, this section primarily aims to tune the β parameters whose tuning is not trivial, so in this case a horizon of 5 is chosen for both because it offers a trade-off between fast computation and enough future points to determine the trajectory of the predicted output.

The β parameters were identified using an iterative approach because as stated by Kravaris and Chung (1987), these parameters are arbitrary. Others who have used the SFL technique for control, namely Shen *et al.* (1999) and Vissers *et al.* (2011) all appear to have used an iterative approach for selection of these parameters. It is possible to ensure the control response is stable by ensuring the tuning parameters are selected such that the poles of the closed loop system have negative real parts. Stability is therefore guaranteed by ensuring the tuning parameters have positive real values, as discussed previously. Two sets of scenarios have been devised to establish how the tuning parameters affect the controller response; one for a batch crystallization and one for continuous crystallization. Furthermore, for each set of scenarios there are also response tests for when the objective function weights (Q and R) are adjusted. The scenarios will be used for tuning parameter selection first using an iterative approach for selecting the β parameters based on selection criteria to be defined in section 4.7.2. Once the best β parameters are selected, they will be used to select the objective function weights for the controller based on another separate criterion. This same procedure is applied for batch crystallization and continuous crystallization tuning. The purpose of using this approach is to gain greater insight into β parameters and how they affect the controller response.

4.7.1 Crystallization Scenarios

The purpose of each scenario is to observe how the tuning parameters affect the ability of the MPC to converge onto a fixed absolute supersaturation setpoint of 0.0002g/g for batch and 0.0006 g/g for continuous MSMPR crystallization. For each scenario, the crystallization is first initialised according to the parameters in Table 4-1 and Table 4-2, and the system will run in open loop for 2 time periods (each time period is Δt) to generate measured data that can be used in the SFL MPC initialisation. The 2 time periods of data are required because the changes in output are required, and the change can only be calculated when 2 points have been measured. From the third time period the plant will be in closed loop control with the SFL MPC. The output response will be considered from the beginning of simulation.

4.7.2 Controller Response and Tuning Selection Criteria

The criteria for tuning parameter selection are based on two properties: overshoot and settling time. In this study, the reference trajectory is a fixed absolute supersaturation value that is scaled in order to be considered as 100%, and there is a band that is defined between 95% to 105% of the reference trajectory which will be referred to as the acceptance region. If the output trajectory enters and remains within this region the output will be regarded as converged onto the reference trajectory. The overshoot is defined as the output response exceeding its target, in this case the target is the reference trajectory. For tuning parameter selection, overshoot is considered as a state that either does occur or does not occur, though it can be quantified too (Shinskey, 1996), the decision was made to refer to overshoot as a state because the aim is to prevent overshoot for supersaturation control. The importance of this is supersaturation overshoot can lead to the crystallization trajectory entering the labile region resulting in nucleation and generation of fines. To avoid this, overshoot must be avoided. The occurrence of overshoot in this study is defined as the instance where the output response exceeds both the reference trajectory and acceptance region limit (Figure 4-3).

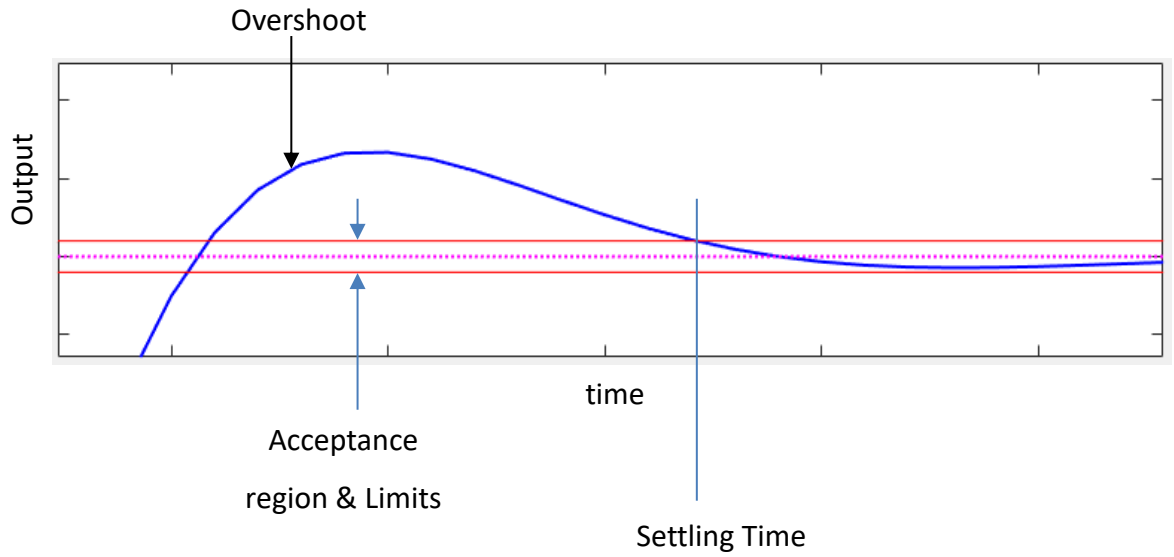

Figure 4-3 Overshoot, Settling time and Acceptance Region

The settling time is defined as the time required for the output response to be within pre-defined limits; it is the time until the output is considered to be converged onto the target or reference trajectory (Shinskey, 1996). In this study the limits are defined by the boundaries of the acceptance region. The overshoot and settling time are shown diagrammatically in Figure 4-3; the overshoot occurs because the output trajectory exceeded the upper limit. The criteria for tuning parameter selection are:

1) The tuning parameters must prevent overshoot of the output trajectory with respect to the reference trajectory, thus the output response must either be critically damped or over-damped.
2) The tuning parameters must minimise the output settling time.

Moreover, the tuning parameters β_0 and β_1 must be tuned independently, but to compare the performance of each pair of β parameters, the decision was made to also define a ratio of tuning parameters (Equation 4-56) because it captures the value of both parameters. The settling time is then plotted against tuning parameter ratio to gain further insight into how settling time is affected by each pair of β parameters.

$$Tuning\ Param\ Ratio = \beta_1/\beta_0 \qquad \textit{Equation 4-56}$$

Further to tuning parameter section, the objective function weights for the reference trajectory tracking, Q, and input moves weight, R, must also be determined. The criterion for these weights is:

- Minimise the output settling time whilst also considering the relative weight of Q and R. One weight should not dominate the other for a small reduction settling time.

To compare the settling time with respect to a unified objective function weighting, the values of both weights are combined into the objective function weighting ratio (Equation 4-57). The settling time is plotted against this ratio when assessing the above criterion.

$$Weighting\ Ratio = Q/R \qquad \textit{Equation 4-57}$$

The equation for output error is defined in **Equation 4-58**. The KPIs are introduced in Table 4-3.

4.7.3 Controller Key Performance Indicators

The key performance indicators (KPIs) often used for assessing and comparing controller performance are based on the error of the controller, which is defined in Equation 4-58 as the error between the measured output and the reference trajectory. A list of the common KPIs and the equations for each are shown in Table 4-3. The integral square error will be used as the primary KPI, but others will be referenced as necessary when used. The use of these KPIs is commonplace when comparing performance of controllers and has been used by Shen *et al.* (1999) when comparing performance of different types of MPC.

$$\boldsymbol{\varepsilon = y_{meas} - y_{ref}} \qquad \textit{Equation 4-58}$$

KPI	Equation	Comments
Integral Square Error (ISE)	$\int_0^t \varepsilon^2\, dt$	The ISE is sensitive to setpoint error due to the squared term. Large values of ISE will result if the output does not converge to the reference trajectory.
Integral Absolute Error (IAE)	$\int_0^t \lvert\varepsilon\rvert\, dt$	The IAE is less sensitive than the ISE. The IAE can provide the absolute error for comparison between scenarios.
Integral Time Absolute Error (ITAE)	$\int_0^t t\lvert\varepsilon\rvert\, dt$	The ITAE is the time weighted version of the IAE and has greater sensitivity to errors that occur later in the process. This will be useful to determine if the output

		trajectory deviated from reference late in the simulation.
Standard Deviation of the Error (SDE)	$\sigma = \sqrt{\frac{\sum_{i=1}^{n}(y_i - y_{i,setpoint})^2}{n-1}}$	The standard deviation of the output error, to measure the variability of the output error over the simulation
Settling time (t_{set})	-	As defined in the prior section.

Table 4-3 – Key Performance Indicators

4.7.4 Batch Crystallization SFL-MPC Tuning

The tuning parameters were determined iteratively for batch seeded crystallization using the settings defined in Table 4-4, additionally the seed loading was 0.5 gL^{-1} with a number weighted mean size of 10 µm, both values were converted to moments to determine the initial values for the moment equations in the plant model (Equations 4-11 to 4-15). The supersaturation setpoint is set to 0.0002 g/g. Fourteen scenarios were required for the tuning parameter selection starting from the β_0 and β_1 parameters in scenario 1 and changing the value of one parameter in each subsequent scenario until scenario 14 where a value of 2.5 is selected β_0 and 5 for β_1 were selected. This scenario satisfied the criteria for no overshoot and shortest settling time of 11 minutes. Some insights into the effects of tuning parameter ratios on settling time are shown in Figure 4-4. Of the first 14 scenarios, it was possible to determine the tuning parameter ratios and then plot these according to the absolute value of β_1 for which 3 unique values were used; 1, 5 and 10, as per Figure 4-4. The markers are coloured red where there was an overshoot and green where there was no overshoot.

Scenario	β_0	β_1	β_1/β_0	Q	R	ISE	Settling time (mins)	Overshoot
1	1	1	1	1	1	1.37E-06	8	Yes
2	1	5	5	1	1	1.64E-06	16	Yes
3	1	10	10	1	1	2.06E-06	24	Yes
4	5	1	0.2	1	1	1.37E+68	-	Yes
5	2	1	0.5	1	1	7.73E-05	26	Yes
6	5	5	1	1	1	1.39E-06	25	No
7	5	10	2	1	1	1.62E-06	26	No
8	10	5	0.5	1	1	3.95E-06	72	Yes
9	10	10	1	1	1	1.73E-06	76	No
10	4	10	2.5	1	1	1.66E-06	18	No
11	3	10	3.33	1	1	1.87E-06	12	No
12	2	10	5	1	1	1.74E-06	22	Yes

13	0.5	5	10	1	1	1.48E-06	17	Yes
14	2.5	5	2	1	1	1.45E-06	11	No
15	2.5	5	2	5	1	1.35E-06	7	No
16	2.5	5	2	10	1	1.33E-06	6	No
17	2.5	5	2	1	5	1.48E-06	32	No
18	2.5	5	2	1	10	1.86E-06	58	No

Table 4-4 Summary of Batch Scenarios for Tuning SFL Parameters and Objective Function Weights

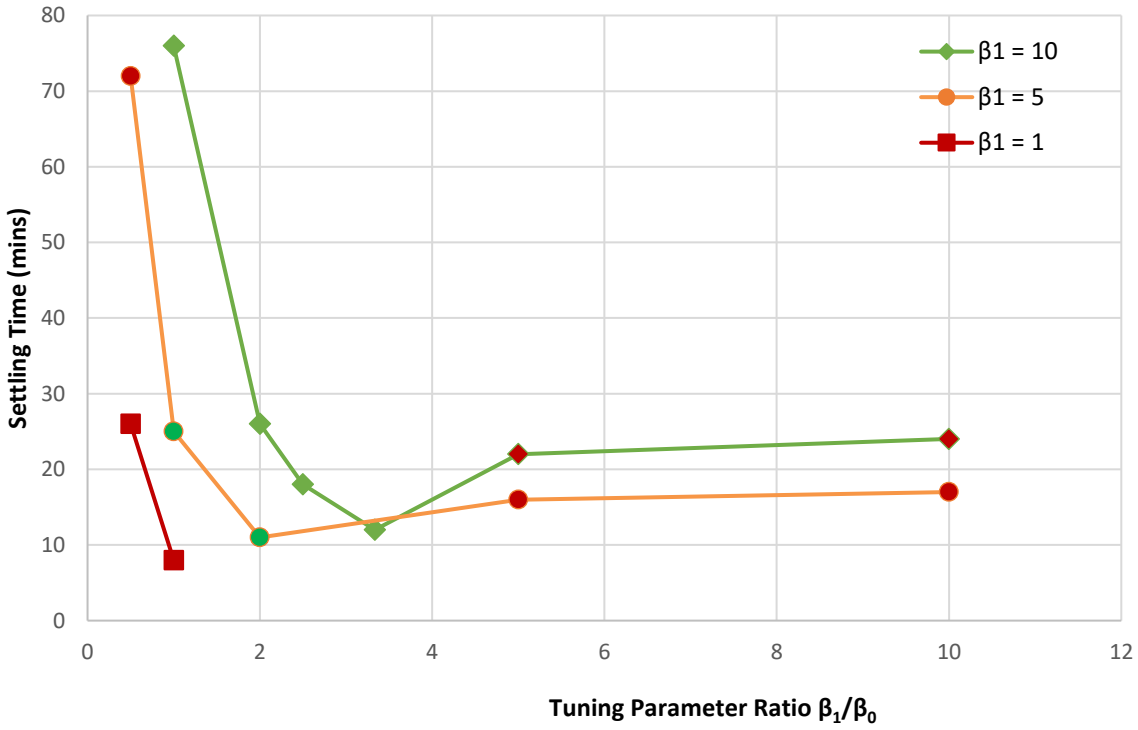

Figure 4-4 Effects of Tuning Parameter Ratio on Settling Time for Batch Crystallization

The information gained from this trend is that for each value of β_1 there exists a tuning parameter ratio at which the settling time is the shortest. Where the value of β_1 is 5, the shortest settling time is 11 minutes and occurs at a tuning parameter ratio of 2. Similarly, where β_1 is 10, the shortest settling is 12 minutes at a tuning parameter ratio of 3.33. The ratio for minimum settling time is not conclusively determined for β_1 = 1. Of all the scenarios with no overshoot, the ISE for scenario 6 was shorter than scenario 14, but the settling time was longer by 14 minutes in scenario 6, this is because the MPC increased the output close to the setpoint in two time steps but then had a very sluggish response as it converged onto the setpoint. The output response from scenario 14 is shown in Figure 4-5, where the

supersaturation (output) trajectory is shown plotted against the coolant temperature (input) for the first 100 minutes of simulation. The simulation begins at a supersaturation less than 0 because the initial condition of the batch seeded system is under-saturated. When the system enters closed-loop control at 3 minutes, there is a large drop in the input temperature to drive the process into a supersaturated state. In the subsequent time steps, the temperature increases to reduce the rate of change in supersaturation and settle on the reference trajectory of 0.0002 g/g, then the temperature profile gradually decreases as the batch progresses because the supersaturation is being consumed for crystal growth until the end of the 100-minute simulation.

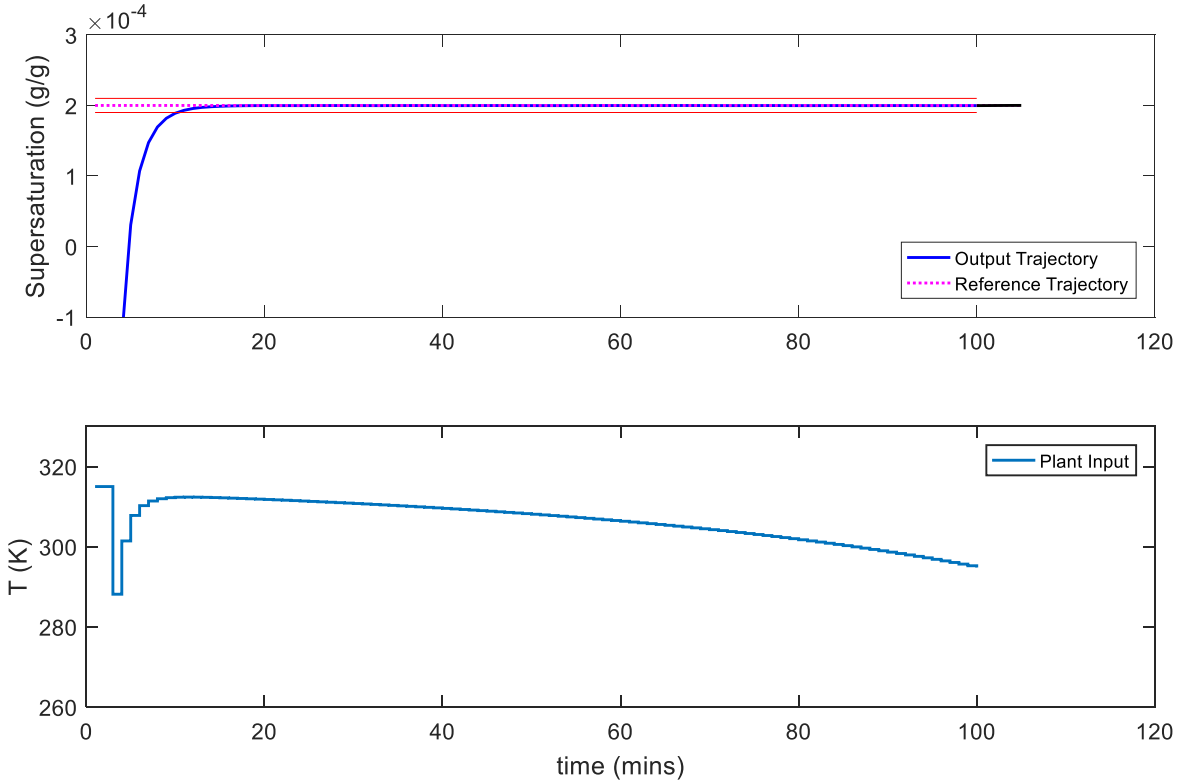

Figure 4-5 Output Response from Scenario 14 showing Output (Supersaturation) Response and Input (Coolant Temperature) profile from MPC for β_0 = 2.5 and β_1 = 5

Scenarios 15 to 18 in Table 4-4 were used in conjunction with scenario 14 to identify the objective function weights that satisfy the objective weight criterion. The trend in Figure 4-6 shows the settling time against the objective function weighting ratio. There were no overshoots when changing the weightings and it can be concluded that by increasing the weight of Q relative to R, the settling time of the controller can be decreased to a limit. It is assumed that the limit will be at a value where Q is infinitely large compared to R; in a

scenario where R is close or equal to 0. The selected values of Q and R are 5 and 1, respectively, from scenario 15. Indeed, scenario 16 evaluated the shortest settling time of 6 minutes as opposed to 7 minutes for scenario 15, but it was decided that the relative increase in Q from 5 to 10, for a 1-minute gain in settling time does not satisfy the criterion. With the chosen weightings, the objective function is therefore prioritising reference trajectory tracking, but there is still a significant weighting on the MPC input moves.

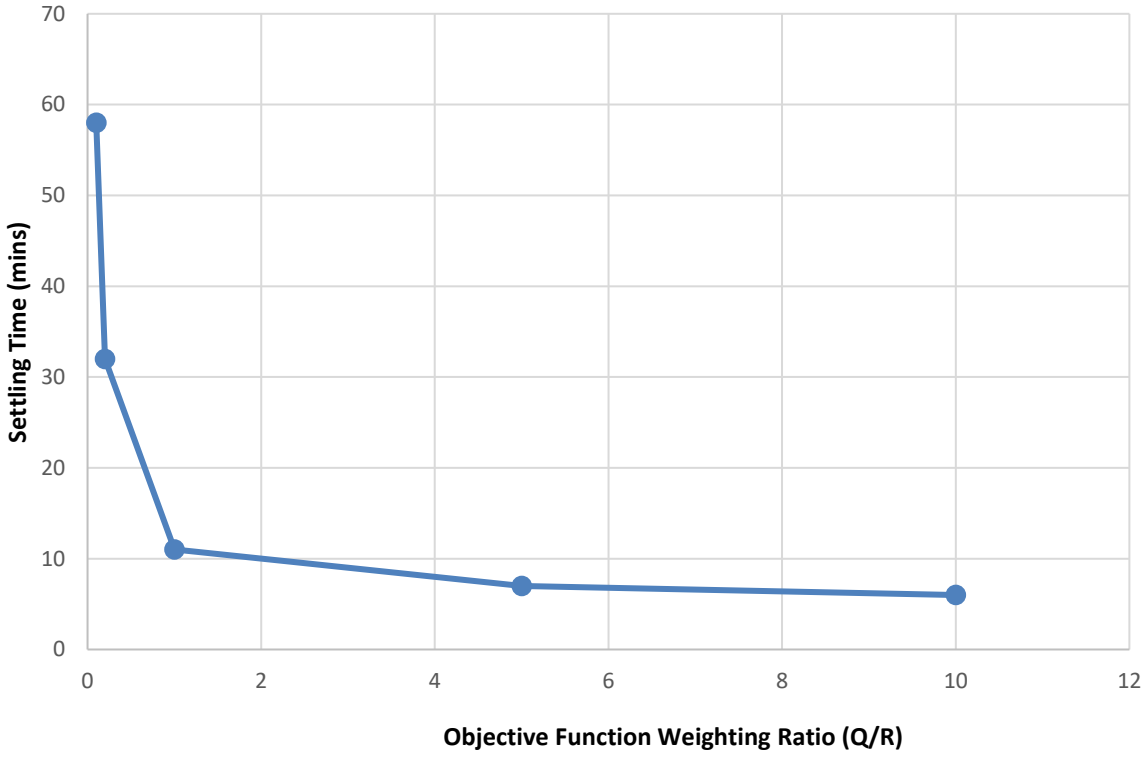

Figure 4-6 – Settling Time against Objective Function Weighting Ratio (Q/R) for Batch Crystallization

4.7.5 Continuous Crystallization SFL-MPC Tuning

The continuous seeded MSMPR crystallization tuning for the β parameters required 12 scenarios (Table 4-5) with the same procedure as for batch crystallization. The seed loading and seed size were also the same as for batch. The feed flow rate and temperature are also disclosed in Table 4-5, the feed concentration is provided in Table 4-2 and the feed also has a seed distribution with the same loading of 0.5 gL^{-1} and 10 µm mean crystal size, again converted to moments for initializing the crystallizer model. The initial jacket temperature is at 350 K. Scenario 12 shows the chosen values of 0.5 for β_0 and 1 for β_1, resulting in the lowest settling time of all scenarios with no overshoot. The ISE in this case was also smallest for scenario 12, showing the overall best performance in converging onto the supersaturation

setpoint and maintaining it throughout the simulation. The effects of tuning parameter ratios on settling time are shown in Figure 4-7, with the markers coloured in red where there was an overshoot and green where there was no overshoot. The tuning parameter ratios were again categorised based on the value of β_1 being equal to 1, 5 and 10.

Scenario	β_0	β_1	$\frac{\beta_1}{\beta_0}$	Q	R	Feed flow rate (ml min^{-1})	Feed Temp. (K)	ISE	Settling Time (mins)	Over-shoot
1	1	1	1	1	1	70	305	5.83E-07	9	No
2	1	5	5	1	1	70	305	6.08E-07	11	No
3	1	10	10	1	1	70	305	6.84E-07	14	No
4	5	1	0.2	1	1	70	305	2.78E+62	-	Yes
5	2	1	0.5	1	1	70	305	2.09E-05	26	Yes
6	5	5	1	1	1	70	305	1.66E-06	27	No
7	5	10	2	1	1	70	305	1.79E-06	30	No
8	10	5	0.5	1	1	70	305	4.95E-06	72	No
9	10	10	1	1	1	70	305	4.73E-06	77	No
10	0.5	10	20	1	1	70	305	6.05E-07	13	No
11	0.5	5	100	1	1	70	305	5.40E-07	11	No
12	0.5	1	2	1	1	70	305	4.69E-07	7	No
13	0.5	1	2	5	1	70	305	4.14E-07	6	No
14	0.5	1	2	10	1	70	305	4.02E-07	5	No
15	0.5	1	2	1	5	70	305	6.79E-07	9	No
16	0.5	1	2	1	10	70	305	8.01E-07	11	Yes

Table 4-5 Summary of Continuous Crystallization Scenarios for Tuning Parameter Selection

The trend differs to that of the batch tuning scenarios and there did not appear to be a ratio at which the settling time was shortest. Instead, increasing the tuning parameter ratio decreases the settling time for a given value of β_1 within the range of values that were testing in the 12 scenarios. However, one similarity with the batch tuning scenarios is that at a given tuning parameter ratio, the settling time is short for smaller values of β_1. No settling time was obtained from scenario 4 because the output response was unstable, as quantified by the value of ISE which is significantly larger than that of the other scenarios. The output response from scenario 12 is shown in Figure 4-8 with the output (supersaturation) trajectory shown with the corresponding input (coolant temperature) profile as manipulated by the MPC.

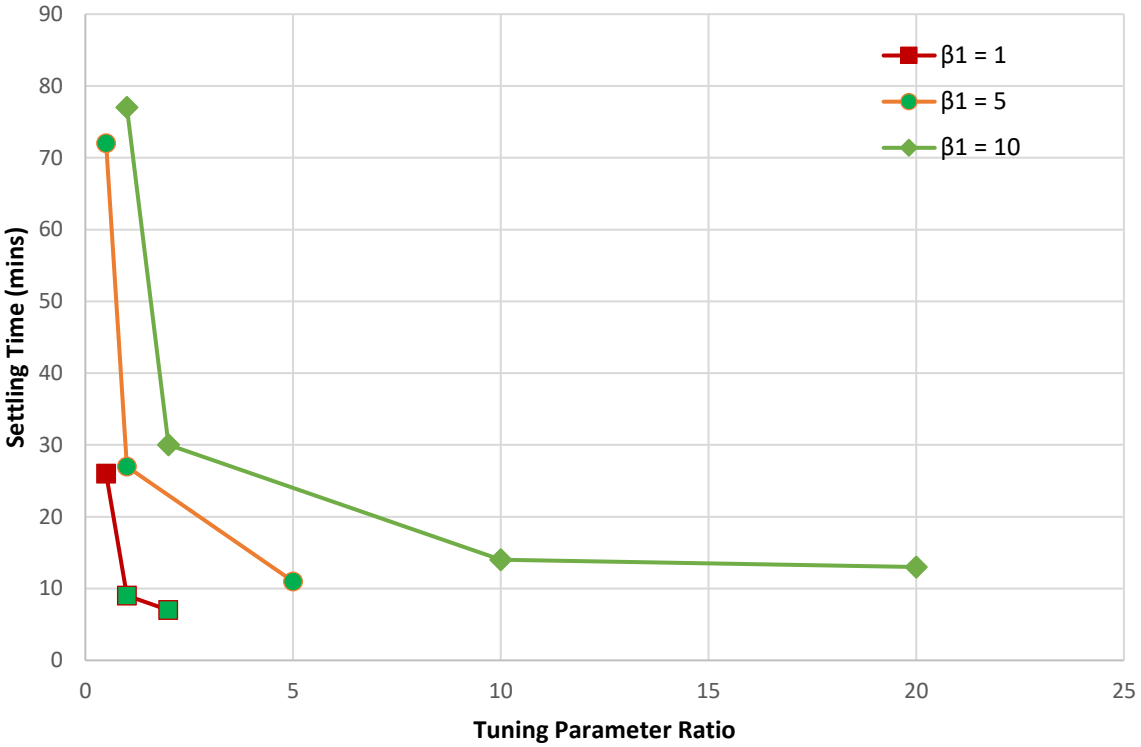

Figure 4-7 Effects of Tuning Parameter Ratio β_1/β_0 on Settling Time for Continuous Crystallization

Recalling the first 2 minutes of the simulation are in open-loop, the initial increase in the supersaturation occurs because the feed temperature of 305 K is lower than the initial conditions in the MSMPR at 315 K resulting in an immediate cooling of the crystallizer contents. When the MPC is activated at the 3rd interval, it establishes the rate of increase in the output trajectory and responds by increasing the temperature input to slow down the rate of change. However, the initial step in this unconstrained simulation results in a very large change in temperature which reduces supersaturation for 1 time-interval before continuing to converge onto the supersaturation setpoint. For the remaining 100 minutes, the temperature of the coolant steadily decreases to a steady state temperature, this decrease is caused by the transience in the crystallizer because the initial state is different to the steady state due to the operating conditions.

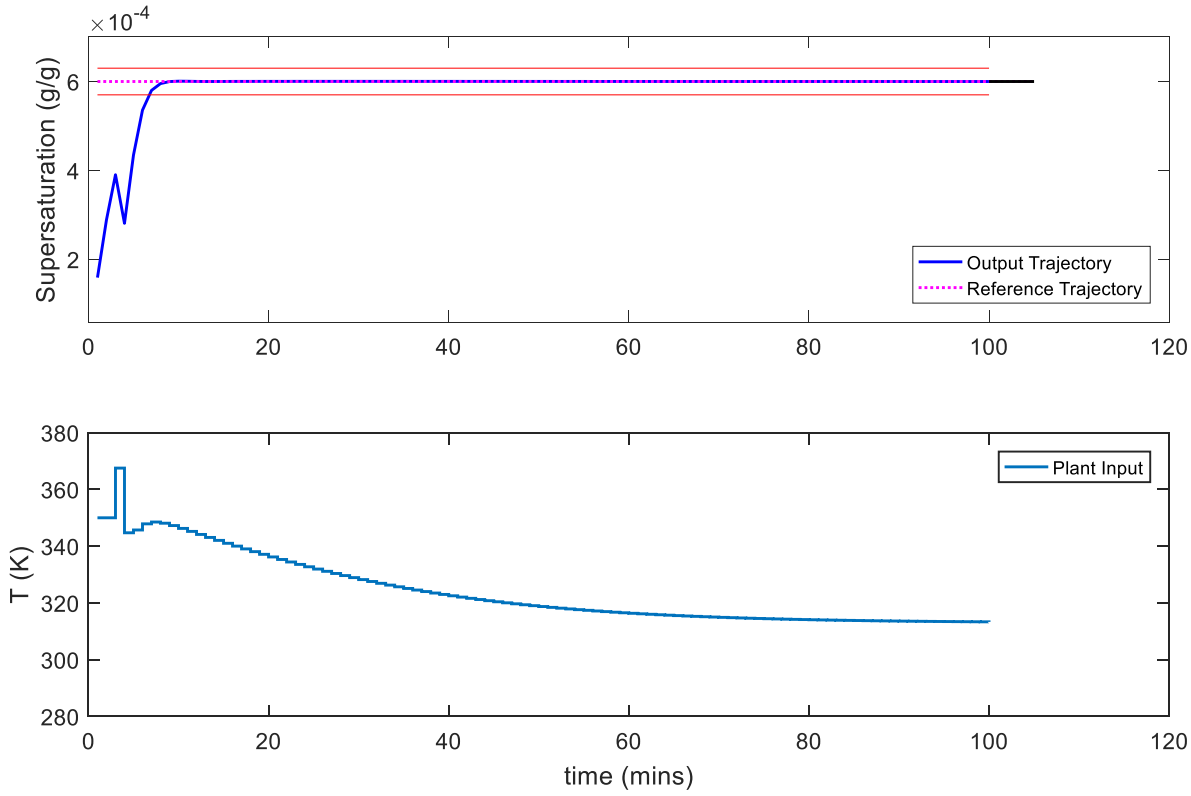

Figure 4-8 Output Response from Scenario 12

Scenarios 13 to 16 were used in conjunction with scenario 12 to identify the objective function weights that satisfy the objective weight criterion. The trend in Figure 4-9 shows the settling time against the objective function weighting ratio. Although an overshoot was observed in scenario 16, it was not a significant overshoot (Figure 4-10). The trend has a similar inverse relationship between the output and input weights as the batch results. It can be concluded that by increasing the weight of Q relative to R, the settling time of the controller can be decreased, as should be expected. The selected values of Q and R are 5 and 1, respectively, from scenario 13. A similar justification is made as the prior case, whereby increasing Q from 5 to 10, for a 1-minute gain in settling time does not satisfy the criterion. The objective function is again prioritising reference trajectory tracking but the MPC input moves are also weighted.

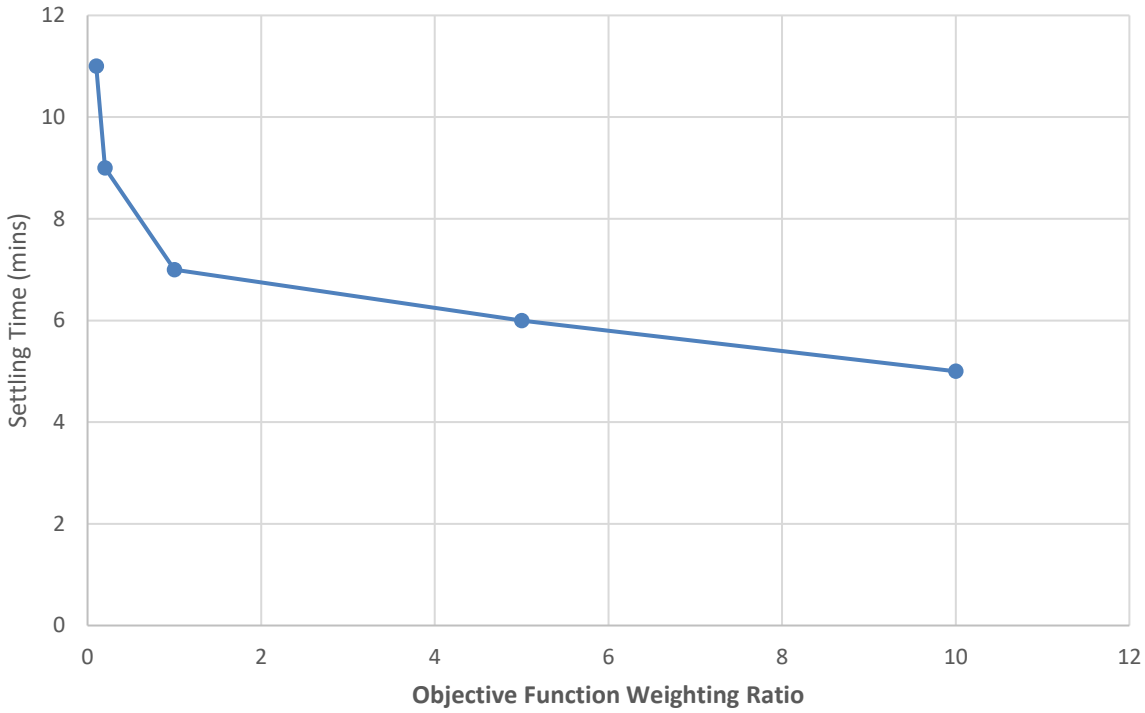

Figure 4-9 Settling Time against Objective Function Weighting Ratio for Continuous Crystallization

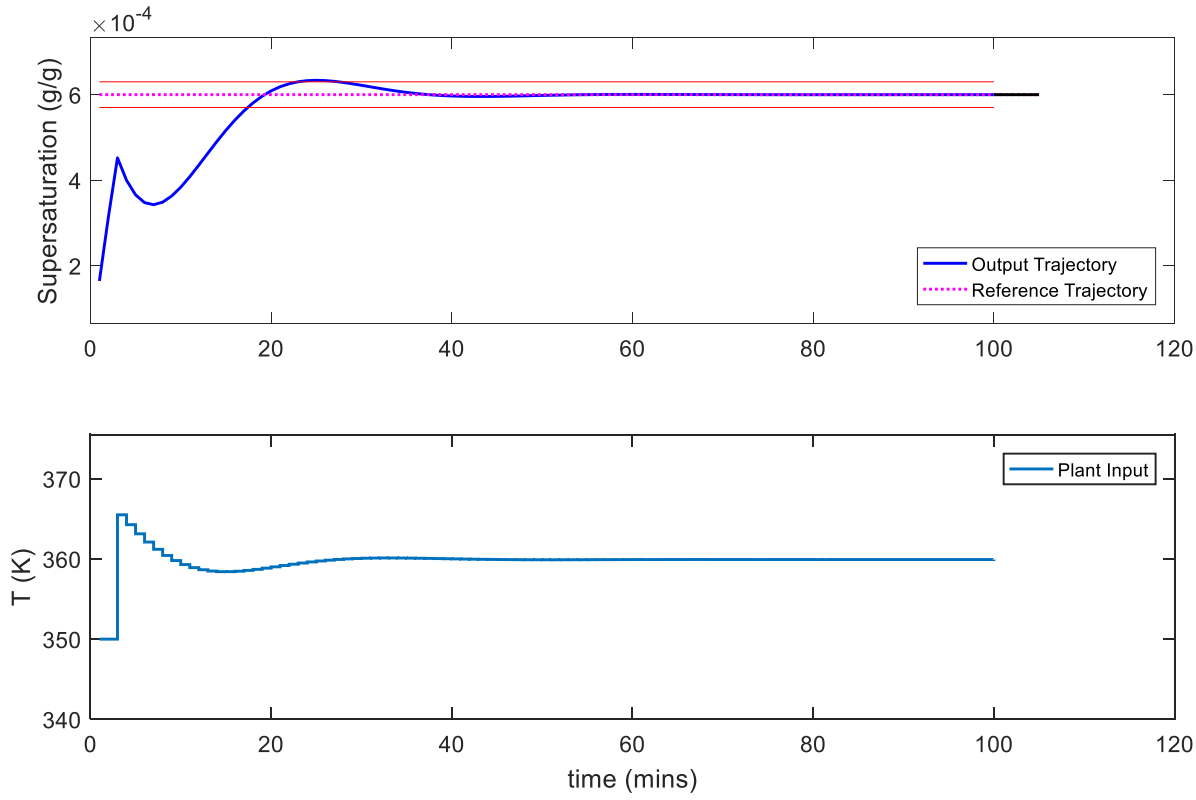

Figure 4-10 – Continuous MSMPR Seeded Crsytallization Output (Supersaturation) Response and Corresponding Input (Coolant Temperature) Profile for Scenario 16

4.7.6 SFL-MPC Tuning Conclusions

Using an iterative tuning approach, it was possible to select values for the SFL β parameters and objective functions for the batch seeded and continuous MSMPR seeded crystallization systems that were linearized with SFL. It was also possible to determine how different pairs of β tuning parameters affected the controller response to converging the crystallization process onto a setpoint. There do remain some areas to explore later, including the effects of disturbances on the continuous crystallization feed, or the effects of changes in the seed distribution, which will be explored in the next chapter. The selected parameters that will be used for the batch and continuous SISO SFL MPC for supersaturation control using the coolant temperature are declared in Table 4-6. The constraints handling will be discussed next and using the tuning parameters obtained from this section, it will be determined if these parameters can be used universally for the respective batch and continuous MSMPR crystallization control with different crystallization seed conditions.

	$\boldsymbol{\beta_0}$	$\boldsymbol{\beta_1}$	$\boldsymbol{Q}$	$\boldsymbol{R}$
Batch	2.5	5	5	1
Continuous	0.5	1	5	1

Table 4-6 – Results from Batch and Continuous Tuning Parameter Selection

4.8 SFL Bounds and Constraints Handling

This section will discuss one of the key developments in this research which is a new method of handling bounds and constraints on an SFL system. The main background has already been given on this area in section 2.12.3. It was discussed how Kurtz and Henson (1996, 1998) introduced the methods for constant constraints technique (CCT) and variable constraint technique (VCT) which were later adopted and improved by others. The main drawback which can be explained further now is the uncertainty in the constraints beyond the horizon. The SFL model as shown in Equation 4-48 is again shown here:

$$\boldsymbol{\xi}(k+1) = A_d\boldsymbol{\xi}(k) + B_d\boldsymbol{v}(k)$$
$$\boldsymbol{y}(k) = C_d\boldsymbol{\xi}(k)$$

Equation 4-48

With this structure in mind, and also expanding the vector $\boldsymbol{\xi}$:

$$\boldsymbol{\xi} = [y, \frac{dy}{dt}, \frac{d^2y}{dt^2}, \dots, \frac{d^ry}{dt^r}] \qquad \textit{Equation 4-59}$$

The model is formed of SFL tuning parameters and the derivatives of the outputs. Other than the plant output y, there is no other information from the plant in the SFL model, but there is in the control law (Kravaris and Chung, 1987):

$$u = \frac{v - \sum_{k=0}^{r} \beta_k L_f^k h(x)}{\beta_r L_g L_f^{r-1} h(x)} = \frac{v - \beta_0 h(x) - \beta_1 L_f h(x)}{\beta_1 L_g h(x)} \qquad \textit{Equation 4-60}$$

Therefore, the main method for constraints handling has leveraged the inverse of the control law to use the plant input and states and determine the inputs on the MPC input v through transformation. However, the plant states are measured variables and time-varying, so the Lie derivatives are also time-varying, thus even if the bounds or constraints on u are fixed, it does not result in a fixed set of bounds or constraints for v (Kurtz and Henson, 1998). In the CCT technique, the strategy is to use the current measured states of the plant and use the control law to transform the constraints on u to v using the current measurement, and apply it over the whole horizon. This guarantees that the constraints on the first input in the horizon is always valid, because it is obtained using the current plant state, but the future states which are not known will likely be different and therefore the horizon constraints may be unreliable. In contrast, the VCT technique uses an alternative approach where the inputs from the last sampling time are used to calculate the constraints at the current sampling time by propagating the inputs and current measured states through the control law to determine the values of u, and then performing an optimization to obtain the constraints of v using the constraint on u.

The CCT and VCT techniques both guarantee the first input in the horizon will be feasible, and because that is the only input in an MPC that is implemented, the techniques enable the use of model-based control on a process, even though the constraints applied beyond the first value of the horizon are likely to be unreliable. One important statement from Kurtz and Henson (1997) is that the VCT technique could be achieved through an iterative and nonlinear program, but this approach would not be computationally efficient. However, recent developments show that iterative approaches are now more usable than at the time of the

original writing because of the advances in computational efficiency. This has led to the use of artificial neural networks (ANNs) to map nonlinear constraints in single input and multiple-input SFL (Deng *et al.* 2009), and more recently by Schnelle and Eberhard (2015) the use of iterative techniques to calculate the constraints using state estimators and future state predictions (Chang and Chen, 2014). There is a possibility of using an iterative approach with the SQP algorithm (Boggs and Tolle, 1995), with two important features of the SQP being the ability to apply a nonlinear constraints function which can be supplied with parameters beyond the traditional states and inputs in traditional optimization, but also can be initialised at an infeasible point and can iteratively find a feasible route to an optimal solution. The importance of these is that the SQP algorithm can be supplied with any set of v regardless of whether the initial vector is feasible. Moreover, the nonlinear constraints function does not need to be used to constrain v, but can be supplied with the values of v from the optimizer, and have an iterative routine which incorporates the nonlinear plant, current states $\boldsymbol{x}$ and MPC inputs $\boldsymbol{v}$ to calculate the future plant inputs $\boldsymbol{u}$ using the control law, and therefore constrain the plant states and plant inputs directly. The iterative routine is shown in Figure 4-11 The output of the function is the feasibility of the solution, so the structure for the SFL MPC scheme with SFL-Plant constraints appears as shown in Figure 4-12, and this scheme is structurally similar to that which was provided by Schnelle and Eberhard (2015)

1. Optimizer creates a set of $\boldsymbol{v}$
    a. Constraints handling function is supplied with:
        i. The set $\boldsymbol{v}(k,\ k+N_c)$
        ii. $\boldsymbol{x}(k)$ from the nonlinear plant
    b. Calculates $u(k)$ using control law and $\boldsymbol{v}(k)$ and $\boldsymbol{x}(k)$
    c. Uses $u(k)$ to calculate $\boldsymbol{x}(k+1)$ at the next time step
    d. Iterates through steps 2 and 3 until $v(k+N_c)$ by which point:
        i. $x(k)$ to $x(k+N_c)$ are calculated
        ii. $u(k)$ to $u(k+N_c)$ are calculated
    e. Checks all $\boldsymbol{x}$ and $\boldsymbol{u}$ for feasibility against constraints on $\boldsymbol{x}$ and $\boldsymbol{u}$ respectively and returns feasibility to optimizer
2. Optimizer evaluates the objective function

Figure 4-11 – Iterative Routine for Constraints handling using Nonlinear Plant

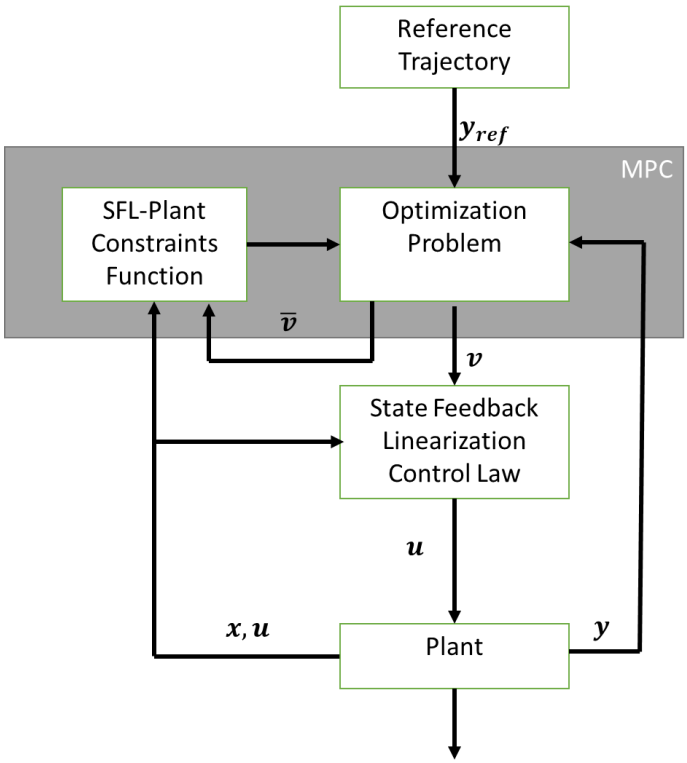

Figure 4-12 – SFL-MPC Scheme with SFL-Plant Constraints

This strategy for constraint handling will be referred to as SFL-Plant constraints, so named because the SFL model and the plant model are combined to calculate the plant inputs and states and determine the feasibility of the MPC input over the whole horizon. The optimization cost function will also be modified now to represent the SFL-Plant constraints. Traditional optimisation problems with constraint handling often appear in a form where the inputs and states are subject to the constraints.

$$\max_{x,u} f(x)$$
$$subject\ to: g(x,u) \geq 0 \qquad \text{Equation 4-61}$$
$$h(x,u) = 0$$

In the objective function in Equation 4-61 the inequality function $g(x)$ and the equality function $h(x)$ can either be explicit linear constraints on the values of x and u or they can be some nonlinear function of x and u. This is the traditional method of constraints handling. Applying this same objective function to the SFL would yield the following:

$$\begin{aligned} \max_{v} y \\ subject\ to: g(\xi, v) \geq 0 \\ h(\xi, v) = 0 \end{aligned}$$ Equation 4-62

With the new SFL-Plant constraints, the new optimization function with constraints changes to the following form:

$$\begin{aligned} \max_{v} y \\ subject\ to: k(x, u) \geq 0 \\ l(x, u) = 0 \\ \dot{x} = f(x) + g(x)u \\ y = h(x) \end{aligned}$$ Equation 4-63

There is a drawback to this method in that each step in the optimization now has an iterative nonlinear programming strategy to calculate the feasibility of the MPC input with plant inputs and constraints, which adds to the computational effort for control. However, for the ability to determine an accurate horizon and apply real constraints to a crystallization control, as intended by MPC, this extra computation is an acceptable trade-off because it makes possible the ability to find feasible control solutions which are paramount to a successful control strategy. Furthermore, the prediction and control horizons which were previously 5 samples have been increased to 10 (10 minutes using a time step of 1 minute) because in preliminary tests at the shorter horizon length a solution was found in a very short time for each instant the MPC was invoked. The increase in horizon length resulted in slightly longer time to converge a solution but not to the detriment of the controller, it could still be applied in real-time, but also it was possible to gain a better trajectory of the prediction horizon in simulation. This constraints method and implementation appears to be unique at time of writing and thus will be assessed to see if it is a reliable method of constraint handling for SFL applications on crystallization.

4.9 SFL-MPC Performance with SFL-Plant Constraints

In this section a series of test scenarios are devised to assess the SFL-MPC performance between unconstrained crystallization control and SFL-Plant constrained crystallization control. The test scenarios are split into two sets, one set for batch crystallization and one set for continuous MSMPR crystallization from start-up.

4.9.1 Key Performance Indicators for SISO MPC with SFL

Key performance indicators (KPIs) are used to quantify the performance of each scenario in the batch and continuous SFL-MPC scenarios with SFL-Plant constraints. Two sets of comparison are made using the KPIs:

1) The difference in KPI values of all scenarios based on a selected reference scenario.
2) The relative difference in KPI values of SFL-Plant constraints scenarios relative to their unconstrained counterpart scenarios.

The reference scenarios are used as a way of standardising the results of all scenarios based on a fixed reference. The scenario chosen for this standardisation is that which was used to identify the tuning parameters and objective function weights. Therefore, it was scenario 15 from the batch tuning study and scenario 13 from the continuous tuning study. These were chosen as the reference because they were originally used to determine the tuning. The comparison between the constrained and unconstrained studies is performed by solving the same control problem in 2 scenarios, one with constraints and one without constraints. The KPIs from the constrained scenario are divided by the respective KPIs from the unconstrained to show the difference between the two control problems which arose from implementation of SFL-Plant constraints. A difference in KPIs will result from a difference in evaluating the control problem.

4.9.2 SFL-MPC Control Problem

The SFL-MPC control problems are described in Equation 4-64 for batch and continuous MSMPR unconstrainted crystallization, Equation 4-65 for batch crystallization with SFL-Plant constraints and Equation 4-66 for continuous MSMPR crystallization with SFL-Plant constraints. Furthermore, for the scenarios with SFL-Plant constraints, successful constraint implementation will be determined based on feasible input profiles which satisfy the following criteria:

1) The plant input is bounded and the upper and lower limits are provided as Plant constraints. The plant input profile must not exceed the limits.
2) The plant input moves (changes in plant input over sample times) are bounded and the upper and lower limits provided as Plant constraints. The plant input moves must not exceed the move limit.

The unconstrained objective function is defined as follows using the previously determined values for Q and R:

$$\min_{v} J = 5\sum_{i=1}^{5}\left(y_i - y_{i,setpoint}\right)^2 + \sum_{k=1}^{5}\Delta v_k^2 \qquad \textit{Equation 4-64}$$

Meanwhile, the SFL-Plant constraints function for batch crystallization is:

$$\min_{v} J = 5\sum_{i=1}^{5}\left(y_i - y_{i,setpoint}\right)^2 + \sum_{k=1}^{5}\Delta v_k^2 \qquad \textit{Equation 4-65}$$

Subject to: $$273\ K \leq u = \varphi(\boldsymbol{x}, v) \leq 340\ K$$

$$-1 \leq \Delta u(Kmin^{-1}) = \varphi(\boldsymbol{x_i}, v_i) - \varphi(\boldsymbol{x_{i+1}}, v_{i+1}) \leq 1$$

Given: $$\boldsymbol{x}$$
$$\dot{\boldsymbol{x}} = \boldsymbol{f}(\boldsymbol{x}) + \boldsymbol{g}(\boldsymbol{x})u$$

Finally, for SFL-Plant constraints for continuous MSMPR crystallization:

$$\min_{v} J = 5\sum_{i=1}^{5}\left(y_i - y_{i,setpoint}\right)^2 + \sum_{l=1}^{5}\Delta v_l^2 \qquad \textit{Equation 4-66}$$

Subject to: $$273\ K \leq u = \varphi(\boldsymbol{x}, v) \leq 360\ K$$

$$-1 \leq \Delta u(Kmin^{-1}) = \varphi(\boldsymbol{x_i}, v_i) - \varphi(\boldsymbol{x_{i+1}}, v_{i+1}) \leq 1$$

Given: $$\boldsymbol{x}$$
$$\dot{\boldsymbol{x}} = \boldsymbol{f}(\boldsymbol{x}) + \boldsymbol{g}(\boldsymbol{x})u$$

The difference between the batch and continuous unconstrained objective functions is the upper limit on u which is 340 K for batch and 360 K for continuous, selected based on the dynamics of each respective system because the continuous crystallization temperature is affected by the feed conditions too, and may require a higher temperature in the jacket to maintain the supersaturation target. Though this may not be directly applicable to a real system whose coolant temperature will have a truly fixed limit on upper and lower bounds, a specific coolant medium has not been defined, but it is assumed that this range of temperature would be possible for a system using water as a coolant.

4.9.3 SFL-MPC and SFL-Plant Constraint Scenarios

A set of batch and continuous scenarios are presented where the batch scenarios have different initial conditions, and the continuous scenarios have different operating conditions. The purpose of this is to introduce some variation into the control scenarios and observe if the designed SFL-MPC is capable of controlling the problem. The same procedure is followed as prior where the first 2 minutes of simulation are open-loop to initialise the SFL-MPC, and from the 3rd minute each process enters closed loop control. The simulation time is 100 minutes in total for each scenario.

4.9.4 Batch Supersaturation SFL-MPC Scenarios and Results

The batch crystallization scenarios consist of 16 scenarios as described in Table 4-7. The first 8 scenarios are unconstrained and the last 8 have SFL-Plant constraints. Scenarios 1, 2, 9 and 10 are unseeded, while the remaining scenarios are seeded, and the seed moments are calculated from the seed size and loading. Scenario 3 is used as the reference batch for the first performance comparison. There is a larger supersaturation setpoint ($y_{setpoint}$) for the unseeded systems because they need to generate crystals through nucleation, whereas the nucleation must be suppressed in the seeded systems.

Scenario	Seed mean size (µm)	Seed loading (g L^{-1})	$y_{setpoint}$ (g/g)	SFL-Plant Input Constraints Active
1	0	0	0.0005	No
2	0	0	0.0008	No
3 (Ref.)	10	0.5	0.0002	No
4	10	1	0.0002	No
5	20	0.5	0.0002	No
6	50	2	0.0002	No
7	100	5	0.0002	No
8	50	5	0.0002	No
9	0	0	0.0005	Yes
10	0	0	0.0008	Yes
11	10	0.5	0.0002	Yes
12	10	1	0.0002	Yes
13	20	0.5	0.0002	Yes
14	50	2	0.0002	Yes
15	100	5	0.0002	Yes
16	50	5	0.0002	Yes

Table 4-7 – Summary of all Batch Supersaturation Control Scenarios

The results of the KPIs for all batch scenarios are shown in Table 4-8. The results show that scenario 10, the unseeded batch with the higher setpoint target of 0.008 g/g and SFL-Plant constraints is the only one that had an overshoot in the output response, which also led to the longest settling time of 24 minutes. The other unseeded batch with SFL-Plant constraints was scenario 9 which had a setpoint of 0.0005 g/g and the second longest settling time. This suggests that the tuning parameters, which were identified from a seeded unconstrained scenario, can be applied to unseeded batch crystallization scenarios but the output response will be different from that which was obtained during tuning. Additionally, the only difference between scenarios 9 and 10 is the setpoint, but for the higher supersaturation setpoint there was an overshoot and longer settling time, so the choice of setpoint also appears to affect the controller response.

Scenario	**Seed mean size (µm)**	**Seed loading (g L^{-1})**	**ISE**	**IAE**	**ITAE**	**t_{set} (min)**	**Over-shoot**	**t_{sim} (s)**
1	0	0	9.51E-07	2.29E-03	7.00E-03	9	No	15.2
2	0	0	2.40E-06	3.64E-03	1.12E-02	9	No	15.1
3 (Ref.)	10	0.5	1.62E-07	9.38E-04	3.09E-03	9	No	15.5
4	10	1	1.63E-07	9.65E-04	5.21E-03	9	No	18
5	20	0.5	1.61E-07	9.34E-04	2.90E-03	9	No	15.8
6	50	2	1.61E-07	9.34E-04	2.90E-03	9	No	15.5
7	100	5	1.62E-07	9.34E-04	2.91E-03	9	No	15.6
8	50	5	1.63E-07	9.36E-04	2.89E-03	9	No	17.5
9	0	0	2.00E-06	4.68E-03	2.57E-02	14	No	31.5
10	0	0	5.90E-06	9.18E-03	6.58E-02	24	Yes	34.4
11	10	0.5	2.68E-07	1.50E-03	6.75E-03	12	No	41.4
12	10	1	2.80E-07	1.80E-03	3.30E-02	12	No	44.44
13	20	0.5	2.67E-07	1.49E-03	6.52E-03	12	No	31.5
14	50	2	2.67E-07	1.49E-03	6.54E-03	12	No	32.1
15	100	5	2.68E-07	1.50E-03	6.59E-03	12	No	30.2
16	50	5	2.72E-07	1.53E-03	6.81E-03	12	No	31.9

Table 4-8 – Batch Scenarios – KPI data for all results

All unconstrained scenarios had the same settling time and a simulation time (t_{sim}) of 15 to 18 seconds to compute the 100-minute simulation. The settling time for all seeded scenarios with SFL-Plant constraints was consistent at 12 minutes. In all cases with SFL-Plant constraints, the input profiles were all feasible too, meaning the constraints were satisfied throughout the simulation. This is shown in a selection of output responses from scenarios in the order 9, 1,

10, 2, 12 and 4 have been provided from Figure 4-13 to Figure 4-18, respectively. This order is provided to show the SFL-Plant constraints solution with the unconstrained solution for the same crystallization system. In the figures related to the unconstrained system, the output response (supersaturation) and input profile (coolant temperature) are shown. The same plots are shown for the SFL-Plant constraints scenarios with an additional trend for the change in input Δu which is also constrained. The constraint limits in the SFL-Plant scenarios are also plotted as red dashed lines.

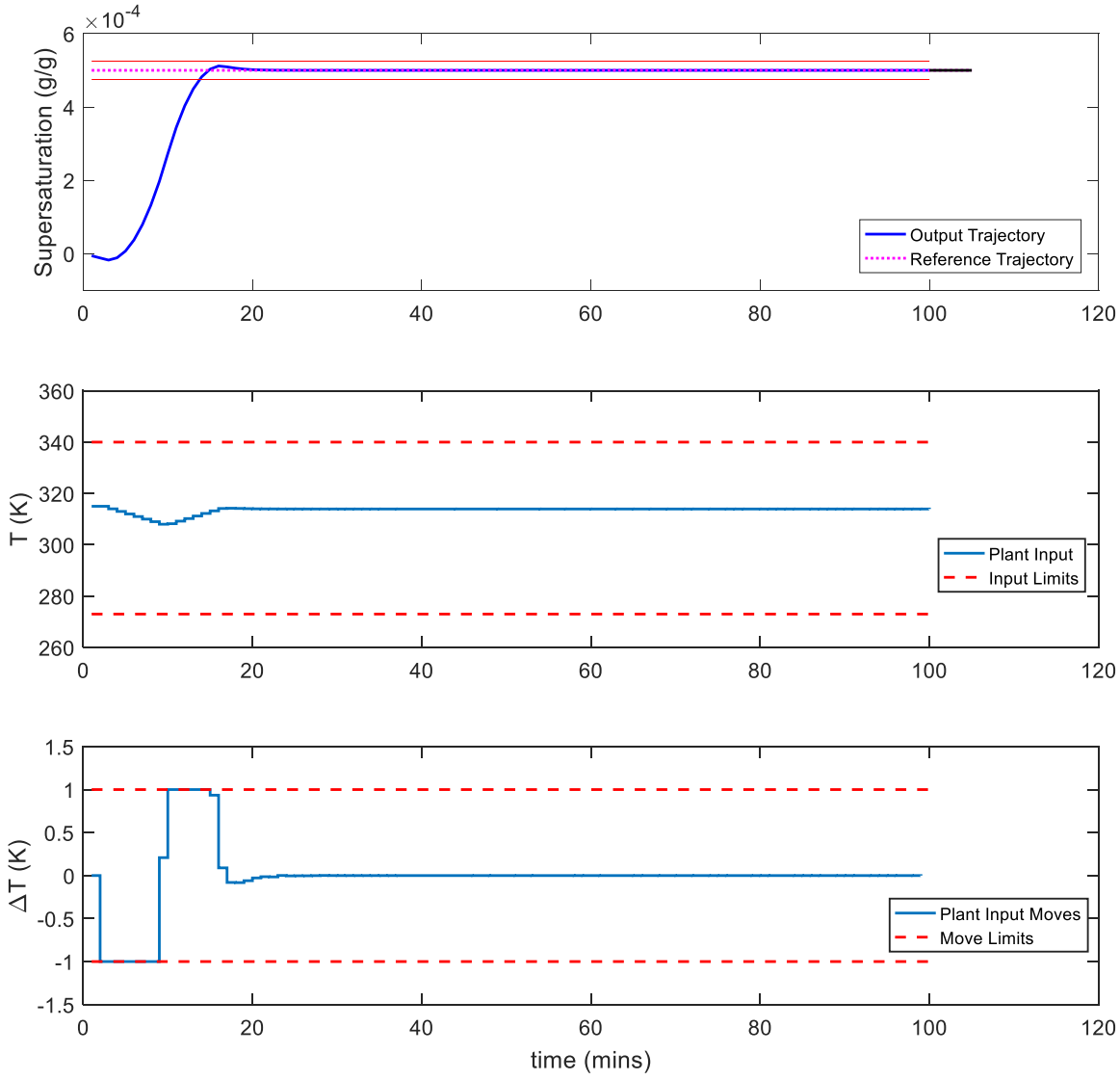

Figure 4-13 Batch Scenario 9 – Unseeded and reference setpoint 0.0005 g/g with SFL-Plant constraints

The trajectory of the output in scenario 9 (Figure 4-14) is much smoother with the SFL-Plant constraints present than that of scenario 1 (Figure 4-15), this smoothness is attributed to the temperature profile which changes more gradually in scenario 9 due to the controller

reaching the constraint limits on rate of change of the input. The output trajectory does increase beyond the reference but does not overshoot beyond the acceptance limits. This behaviour can be explained from the input profile because the crystallizer is cooling to increase the supersaturation when it is under target, but 5 minutes before the supersaturation enters the acceptance region, the MPC begins to heat the jacket to reduce the rate of increase in supersaturation and land on the reference trajectory. It appears that the limit on the input change Δu hinders slow-down of the output change, causing it to pass the reference before then settling on the reference trajectory. Comparing this to scenario 1, as soon as the MPC comes online in the third minute there is an instantaneous temperature drop to increase the supersaturation, followed by subsequent increases to converge onto the reference.

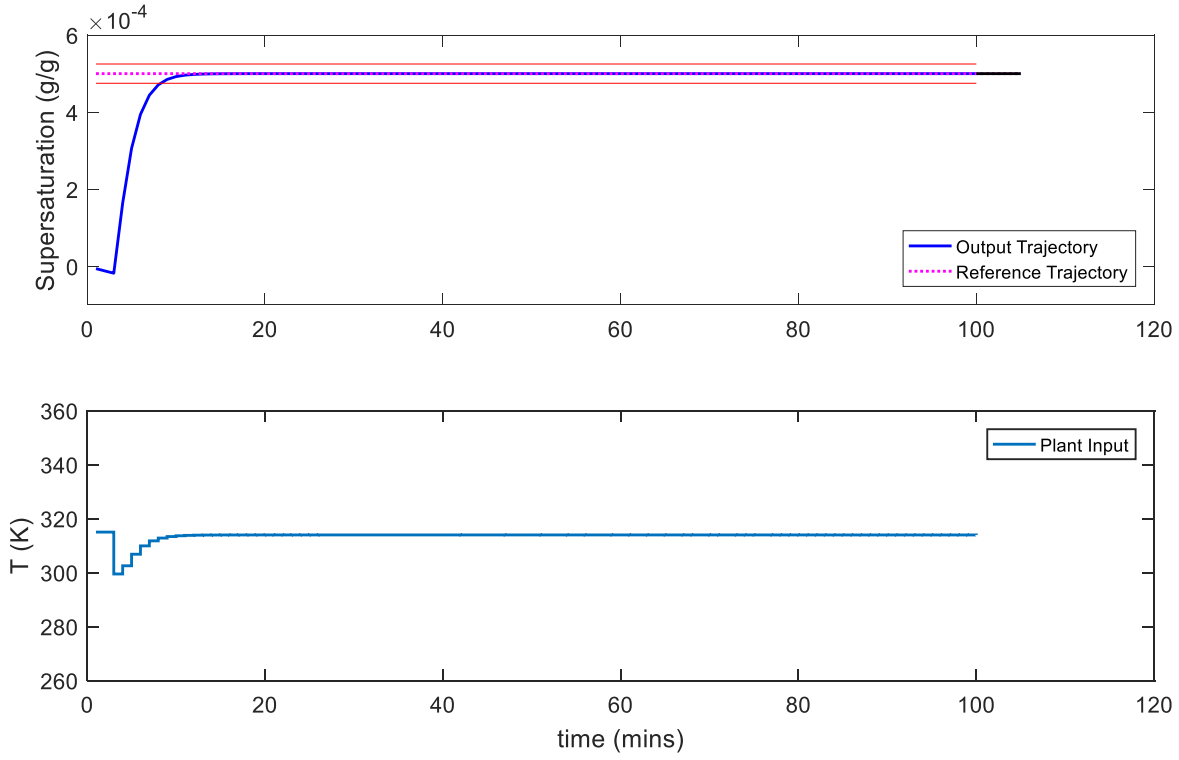

Figure 4-14 Batch Scenario 1 – Unseeded and reference setpoint 0.0005 g/g without constraints

The results from scenario 9 also apply to scenario 10 as seen Figure 4-15, the input profile is cooling the system to increase the supersaturation as quickly as feasible given the SFL-Plant constraints and the input change limits are reached. However, the larger supersaturation setpoint results in a larger decrease in temperature to drive the supersaturation up to target in a short period of time. Therefore, when the MPC's model prediction sees the

supersaturation begin to approach the reference trajectory 5 minutes before entering the acceptance region, the overshoot is inevitable because the rate of change in supersaturation is already very big and heating the jacket at the fastest rate of 1 K/min will not slow the supersaturation rate of increase enough to prevent the overshoot. Comparing this to scenario 2 in Figure 4-16 shows how the unconstrained system has almost an identical output trajectory to that of scenario 1, achieved by a larger heating and cooling rate in the input profile.

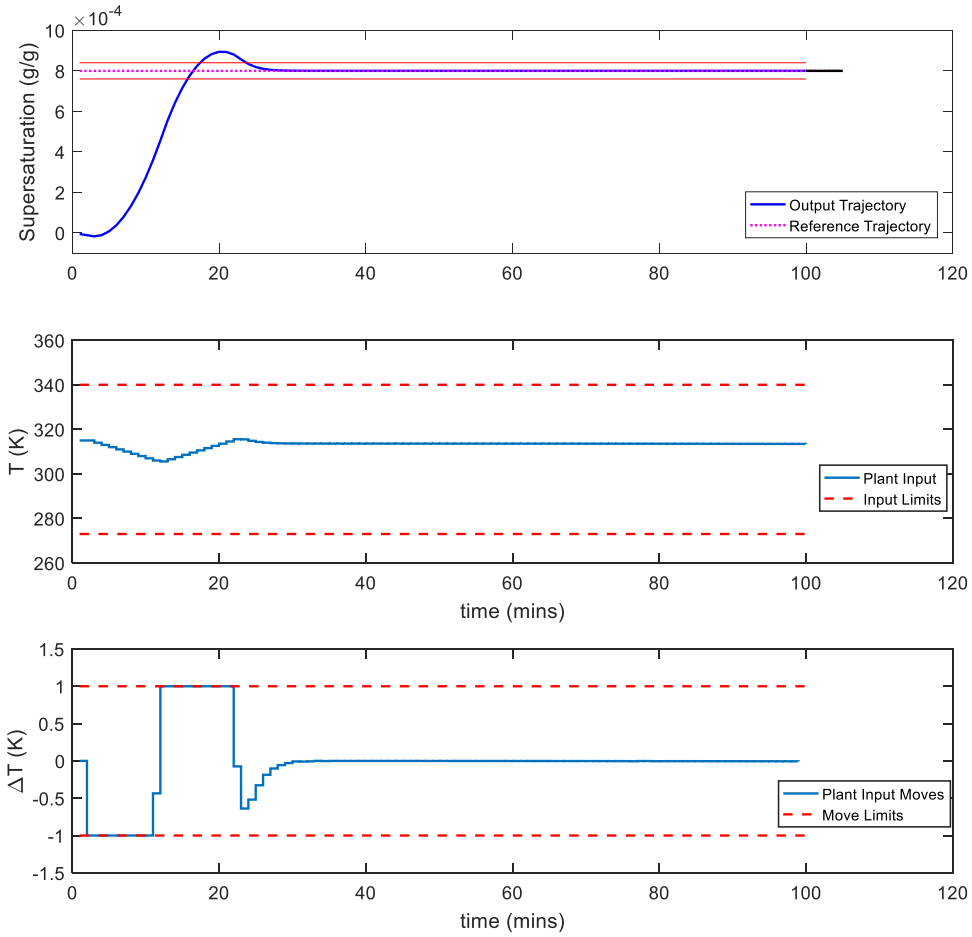

Figure 4-15 Batch Scenario 10 – Unseeded and reference setpoint 0.0008 g/g with SFL-Plant constraints

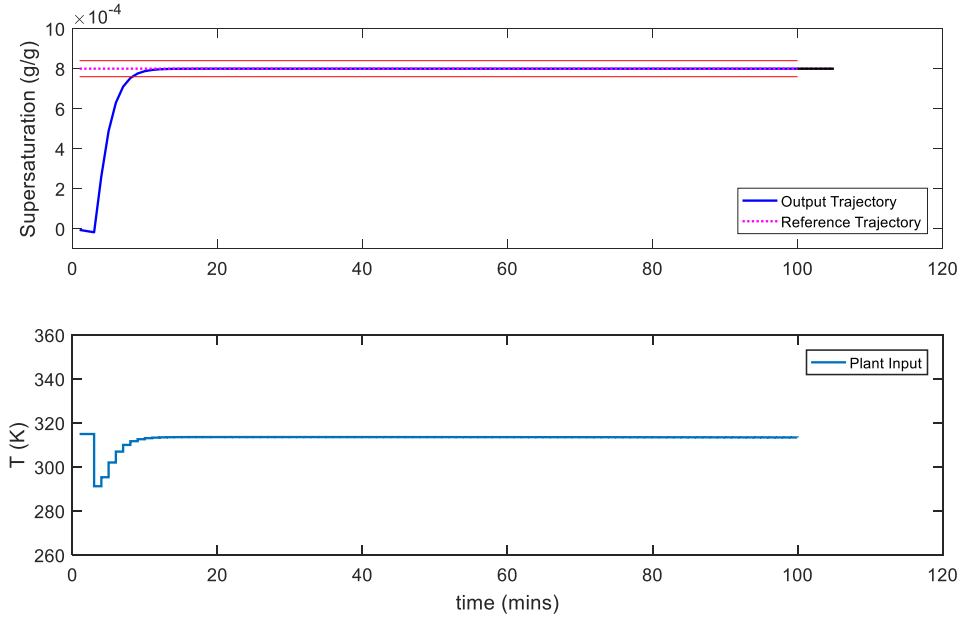

Figure 4-16 Batch Scenario 2 – Unseeded and reference setpoint 0.0008 g/g without constraints

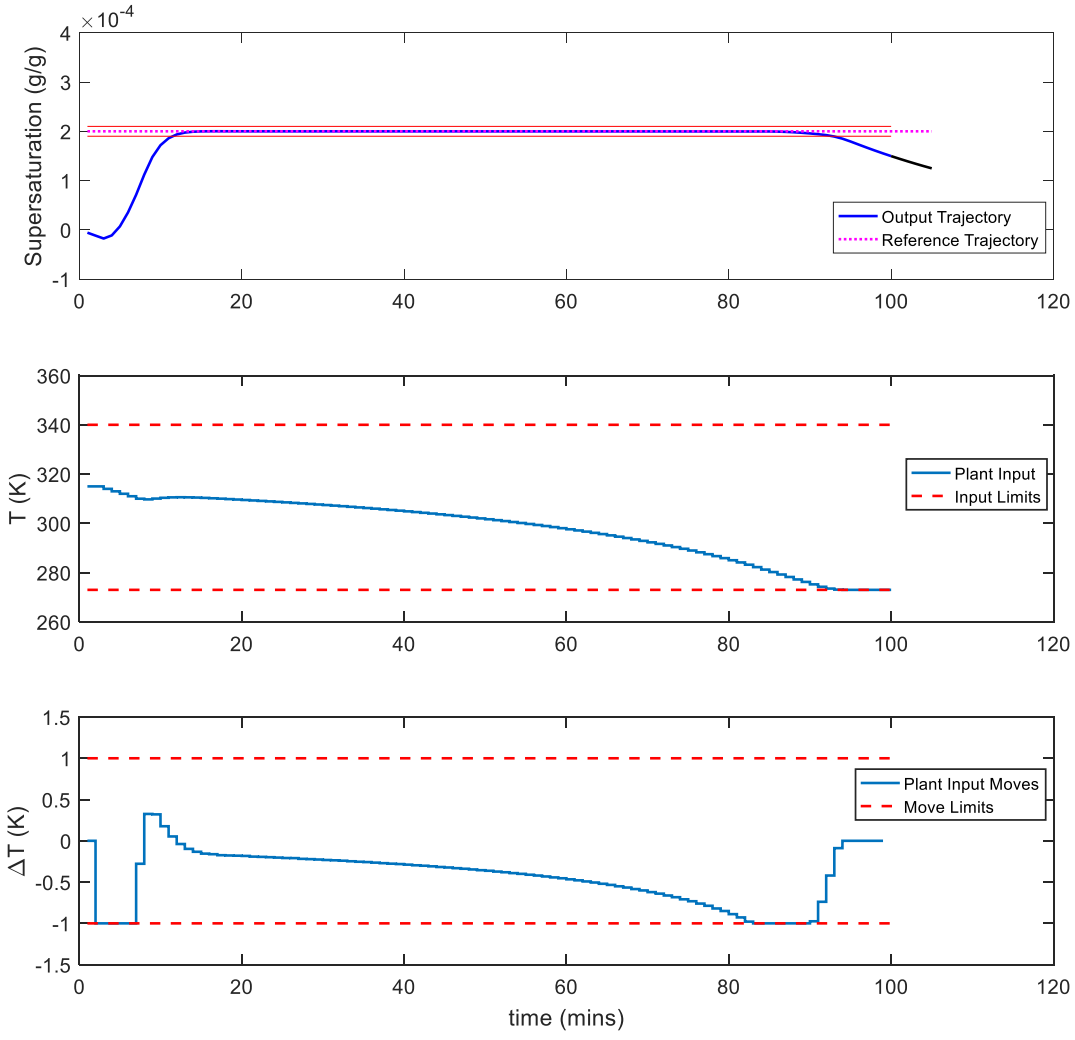

Figure 4-17– Batch Scenario 12 – 10 µm seed and 1 g L^{-1} seed loading with SFL-Plant constraints

Finally, scenario 12 is shown in Figure 4-17 because it too exhibited a unique output response which converged to the reference trajectory quickly but then after 90 minutes began to diverge. This scenario was seeded with a large seed loading of 1 g/L of small seeds with a mean size of 10 µm. The significance of this is that the supersaturation is a function of concentration, which itself is a function of the growth rate and second moment. The second moment is a measure of the crystal surface area and for a defined mass loading of crystals, if the mean crystal size is smaller there will be a larger surface area of crystals and therefore a larger 2nd moment. This results in a faster rate of change of dissolved solute, so to keep the supersaturation on target a faster cooling rate is also required. At 82 minutes, the rate of change in the cooling rate reaches the lower limit, and subsequently at 91 minutes the coolant temperature reaches its lower limit. At this point it is not possible to cool the system further to maintain the supersaturation, so the supersaturation begins to drop and diverge from the reference trajectory. Comparing this to scenario 4 which is the same system without constraints in Figure 4-18, the cooling rate progressively becomes faster at the end of the 100-minute simulation and the temperature drops to 240 K, far lower than the lower limit of 273 K defined in the SFL-Plant constraints. The resulting output trajectory also remains on the reference throughout although towards the end the trajectory does begin to diverge slightly, thus showing the importance of the constraints in a real system and also demonstrating how the SFL-Plant constraints method has indeed produced feasible control.

Onto the comparisons of the KPIs, Table 4-9 shows the results of the first comparison with scenario 3 as the reference. The KPIs from each scenario have been divided by the same KPI value from scenario 3 and presented in this table. The first conclusion that is drawn here is that all KPI values for scenarios 4 to 8 (unconstrained) are close to 1. This suggests that for the seeded batch crystallization the controller performance is consistent across a wide range of seed size and loading. The notable difference is for scenario 4 the ITAE is 1.69 and this is a consequence of the seed loading, the slight divergence of the output trajectory from the reference towards the end of the simulation is captured in the ITAE value because of the time weighting on the error.

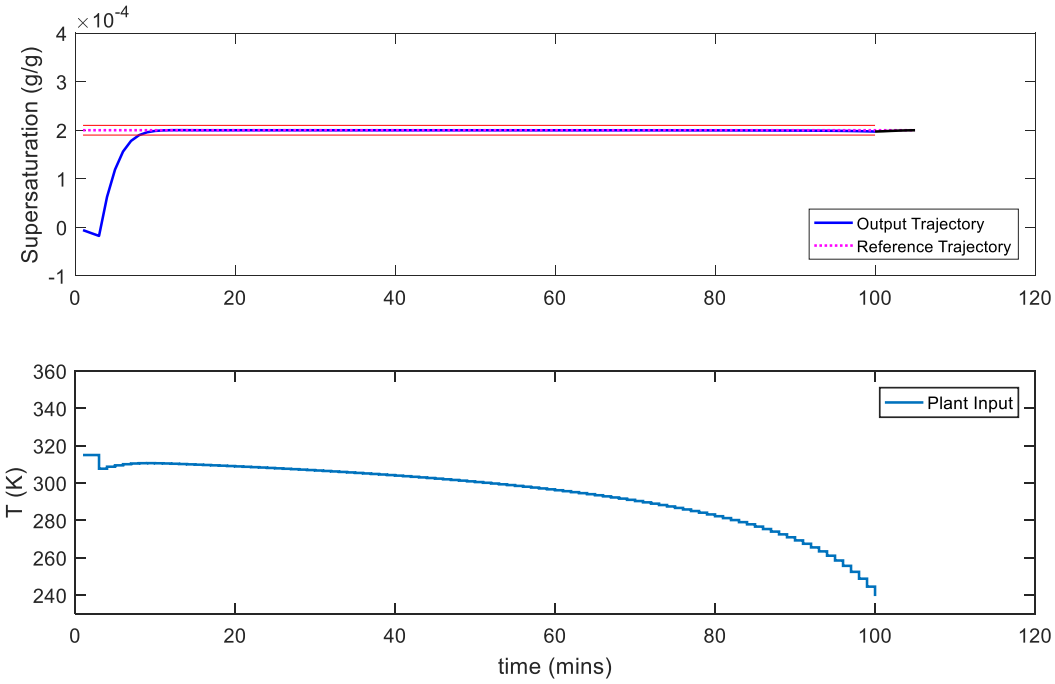

Figure 4-18 – Batch Scenario 4 – 10 µm seed and 1 g L^{-1} seed loading without constraints

Scenarios (Standaridised)	SD SP Error	ISE	IAE	ITAE	t_{set}	t_{sim}
1	2.43	5.89	2.44	2.27	1.00	0.98
2	3.85	14.86	3.88	3.63	1.00	0.97
4	1.00	1.01	1.03	1.69	1.00	1.16
5	1.00	1.00	1.00	0.94	1.00	1.02
6	1.00	1.00	1.00	0.94	1.00	1.00
7	1.00	1.00	1.00	0.94	1.00	1.01
8	1.00	1.01	1.00	0.94	1.00	1.13
9	3.42	12.35	4.99	8.32	1.56	2.03
10	5.86	36.49	9.79	21.28	2.67	2.22
11	1.27	1.66	1.60	2.18	1.33	2.67
12	1.27	1.73	1.92	10.67	1.33	2.87
13	1.26	1.65	1.59	2.11	1.33	2.03
14	1.27	1.65	1.59	2.12	1.33	2.07
15	1.27	1.66	1.60	2.13	1.33	1.95
16	1.27	1.68	1.63	2.20	1.33	2.06

Table 4-9 – Continuous Scenarios – Relative Performance to reference scenario 1

The unseeded scenarios 1, 2, 9 and 10 have significantly larger errors than the seeded scenarios mainly because the supersaturation setpoints are larger for the unseeded systems and require more time to converge onto these setpoints, also resulting in larger errors at the

beginning of the batch. The scenarios with SFL-Plant constraints consistently have a larger error than the reference scenario as expected, and these results can be explained when comparing the provided output response and input profile results as has already been explained for scenarios 9, 10 and 12. The SFL-Plant constraints impose strict limits on the input profile and input moves, so the larger input steps seen in the unconstrained scenarios will not be achieved, resulting in longer time to achieve the setpoints and thus greater error.

For the second comparison between the SFL-Plant constraints scenarios and their counterpart unconstrained scenarios, the comparison in KPIs is presented in Table 4-10. The scenarios are labelled as "$x\ vs\ y$" where the KPIs in scenario x are divided by those of scenario y, and the results disclosed in the table. The relative errors for seeded batch systems is consistent, so the SFL-Plant constraints scenarios appear to have very similar impact on error irrespective of the seeding conditions for a given set of initial seed conditions. The exception to this trend is scenario 12 where the ITAE is significantly larger than the other seeded system, attributed to the divergence from setpoint as already discussed.

Scenario	**SD SP Error**	**ISE**	**IAE**	**ITAE**	t_{set} (min)	t_{sim} **(s)**
9 vs 1	1.41	2.10	2.05	3.67	1.56	2.07
10 vs 2	1.52	2.46	2.52	5.87	2.67	2.28
11 vs 3	1.27	1.66	1.60	2.18	1.33	2.67
12 vs 4	1.27	1.73	1.86	6.33	1.33	2.47
13 vs 5	1.27	1.65	1.60	2.25	1.33	1.99
14 vs 6	1.27	1.65	1.60	2.25	1.33	2.07
15 vs 7	1.27	1.66	1.60	2.26	1.33	1.94
16 vs 8	1.27	1.67	1.63	2.35	1.33	1.82

Table 4-10 – Batch Scenario Relative Performance of SFL-Plant constraints vs Unconstrained

For the unseeded systems, the relative errors of the SFL-Plant constraints were much greater but this can also be explained from the output responses. For scenario 10 (Figure 4-15), the rate of change in the input was at the move limit which caused an overshoot when compared to case 2 (Figure 4-16) where the input profile has larger steps. Finally, the SFL-Plant constraints scenarios took between 2 and 2.7 times longer to simulate the 100-minute batch control than the unconstrained system. However, in terms of real-time this difference was from 15 seconds to calculate 100 MPC moves as compared to 40 seconds with SFL-Plant

constraints. Consequently, SFL-Plant constraints appear to be a viable option for real-time MPC.

4.9.5 Continuous Crystallization SFL-MPC Scenarios and Results

The continuous crystallization scenarios shown in Table 4-11 consist of 12 scenarios which are all seeded. The first 6 scenarios are unconstrained while the last 6 have SFL-Plant constraints. Scenario 1 is used as the reference batch for the first performance comparison. The effects of disturbances to continuous operation have also been simulated as detailed in the table. The disturbances are applied to feed flow rate and/or feed temperature, where the disturbance type is a normally-distributed random disturbance within the specified boundaries in Table 4-11. The disturbance interval is defined as the interval time between each disturbance, so an interval of 10 means the disturbance affects the process every 10th time-interval, or every 10 minutes in this case because the time interval is set to 1 minute. The disturbances are active from the beginning of startup and throughout the 100-minute simulation.

Scenario	Seed mean size (µm)	Seed loading (g L^{-1})	Feed Flow rate (mL min^{-1})	Feed Temp. (K)	Disturb. type	Disturb. interval (mins)	$y_{setpoint}$ (g/g)	SFL-Plant Input Constraints Active
1 (Ref.)	10	0.5	70	305	-	-	0.0006	No
2	10	1	70	305	-	-	0.0006	No
3	20	0.5	70	305	-	-	0.0006	No
4	10	0.5	70 ± 7	305	Random	10	0.0006	No
5	10	0.5	70	305 ± 3	Random	10	0.0006	No
6	10	0.5	70 ± 7	305 ± 2	Random	5	0.0006	No
7	10	0.5	70	305	-	-	0.0006	Yes
8	10	1	70	305	-	-	0.0006	Yes
9	20	0.5	70	305	-	-	0.0006	Yes
10	10	0.5	70 ± 7	305	Random	10	0.0006	Yes
11	10	0.5	70	305 ± 3	Random	10	0.0006	Yes
12	10	0.5	70 ± 7	305 ± 2	Random	5	0.0006	Yes

Table 4-11 – Summary of all Continuous Supersaturation Control Scenarios

The results of the KPIs for all continuous scenarios are shown in Table 4-12. The settling times have not been calculated for the results with disturbances because at each interval the

disturbance causes the output trajectory to diverge from the reference. Scenario 8 did not settle in the acceptance region and hence a settling time was not determined. This was a result of the SFL-Plant constraints preventing the MPC from implementing large changes in the input profile which were necessary for the output to quickly converge onto the setpoint and remain converged. The results for scenario 8 are shown in Figure 4-19 that can be compared alongside scenario 2 which is the equivalent but without constraints (Figure 4-20). There was a similar magnitude of error in the ISE, IAE and SDE between all scenarios. The SFL-MPC controller produced feasible results in all cases with SFL-Plant constraints. Figure 4-19 to Figure 4-24 are provided for scenarios 8, 2, 9, 3, 12 and 6 respectively.

Scen-ario	Seed mean size (µm)	Seed loading (g L^{-1})	Feed flow rate (ml min^{-1})	Feed Temp (K)	ISE	IAE	ITAE	SDE	t_{set}	t_{sim}
1 (Ref.)	10	0.5	70	305	4.14E-07	1.32E-03	3.54E-03	6.33E-05	6	18.3
2	10	1	70	305	4.44E-07	1.39E-03	4.14E-03	6.56E-05	6	18.9
3	20	0.5	70	305	4.03E-07	1.29E-03	3.24E-03	6.25E-05	6	19.1
4	10	0.5	70±7	305	4.14E-07	1.33E-03	4.53E-03	6.33E-05	-	18.3
5	10	0.5	70	305±3	4.14E-07	1.32E-03	3.54E-03	6.33E-05	-	18.2
6	10	0.5	70±7	305±2	4.14E-07	1.34E-03	4.79E-03	6.33E-05	-	19.5
7	10	0.5	70	305	3.67E-07	1.29E-03	3.71E-03	5.95E-05	7	78.5
8	10	1	70	305	1.14E-06	8.49E-03	2.75E-01	6.54E-05	-	30.1
9	20	0.5	70	305	3.25E-07	1.14E-03	3.10E-03	5.64E-05	6	99.4
10	10	0.5	70±7	305	4.49E-07	2.91E-03	7.84E-02	6.25E-05	-	66.8
11	10	0.5	70	305±3	1.06E-06	5.94E-03	2.95E-01	1.01E-04	-	61.4
12	10	0.5	70±7	305±2	9.49E-07	6.50E-03	2.12E-01	8.95E-05	-	58.5

Table 4-12 – Continuous Scenarios – KPI data for all results

The effect of the high seed loading on the output trajectory is shown for scenario 8 in Figure 4-19. From the beginning when MPC is active and the system is in closed-loop, the lower constraint limit on the input moves is reached, and while the MPC cools the system as fast as it can with the SFL-Plant constraints, the rate of consumption of supersaturation through growth is dominant. While the output trajectory does enter the acceptance region at 75 minutes, shortly thereafter the lower limit for the input is also reached resulting in no further possibility of cooling the system, resulting in divergence from the reference. Though this performance is not ideal for crystallization control to the desired setpoint, the SFL-MPC

produces a feasible control inputs over the supersaturation trajectory given the SFL-Plant constraints which are imposed. This scenario demonstrates that operating under these conditions with the prescribed SFL-Plant constraints would result in a system where supersaturation control to this setpoint would be difficult to achieve. Comparing this to the results from the same system without constraints in Figure 4-20 (scenario 2) it is clear that the system is indeed controllable by the MPC, but the temperature required to sustain the supersaturation is much lower than can be achieved with the SFL-Plant constraints on the input.

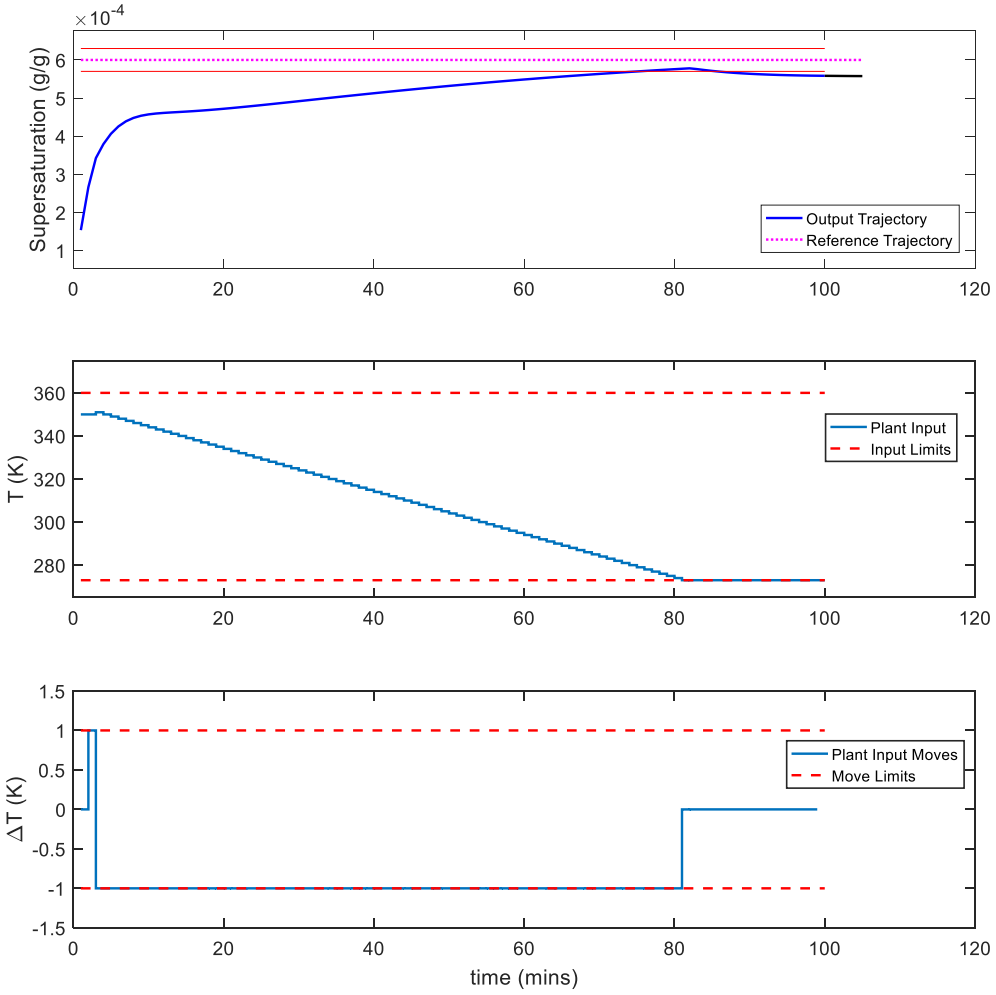

Figure 4-19 – Continuous scenario 8 – 10µm seed size and 1 g L^{-1} seed loading with SFL-Plant Constraints

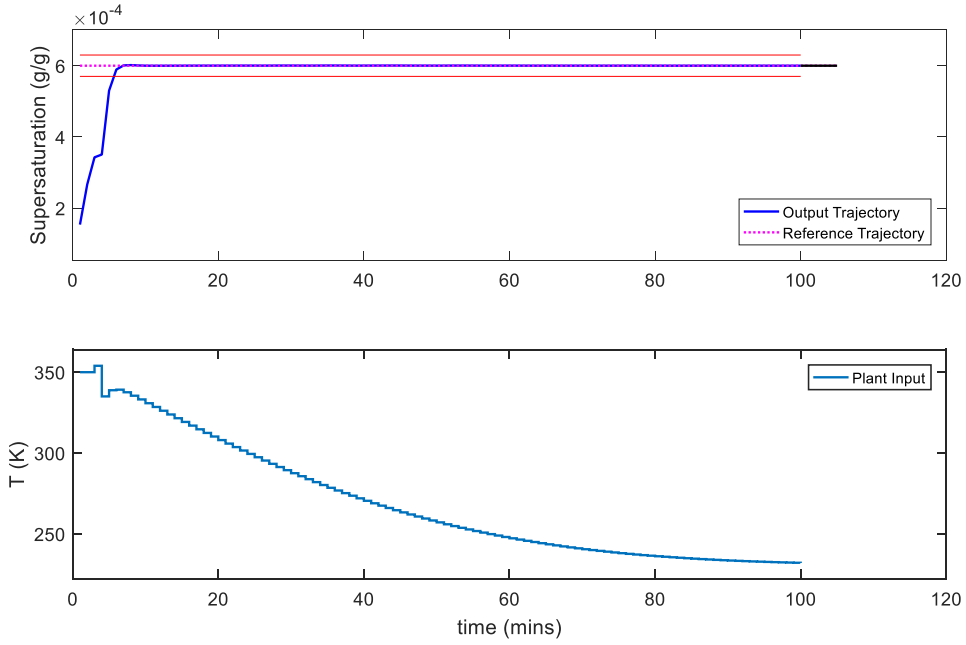

Figure 4-20 – Continuous scenario 2 – 10µm seed size and 1 g L^{-1} seed loading without constraints

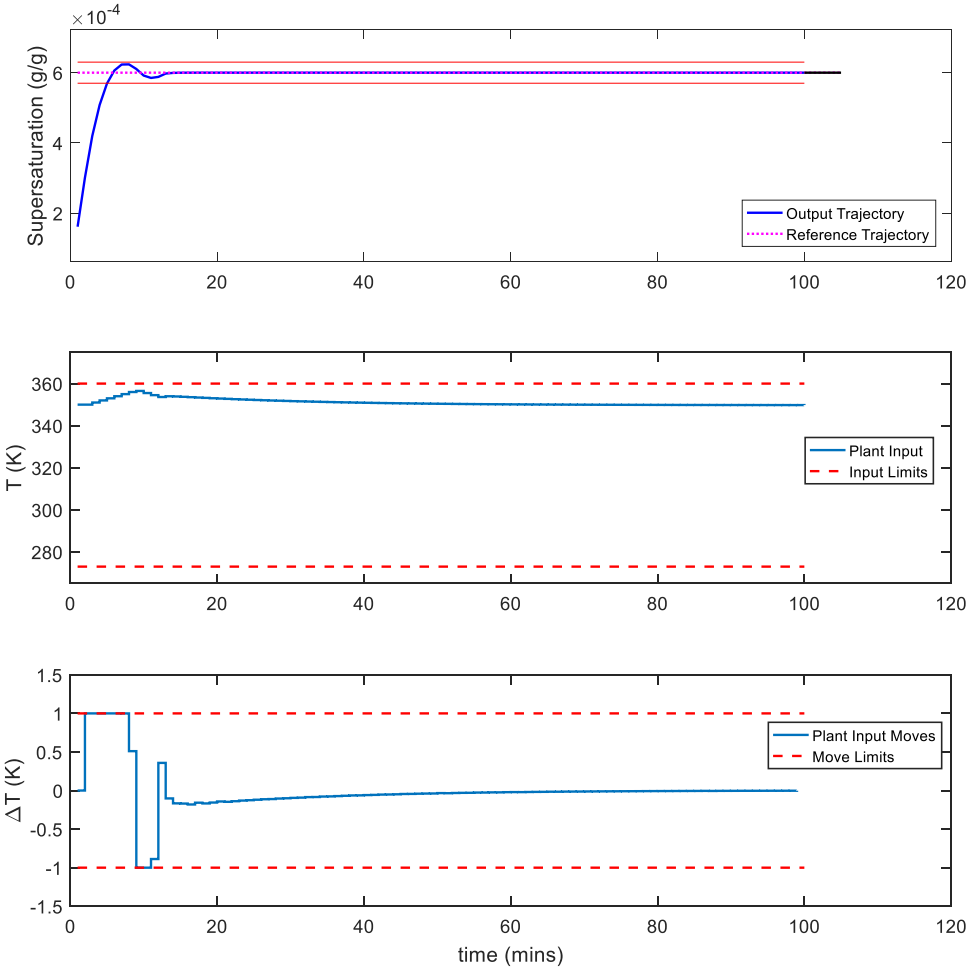

Figure 4-21– Continuous scenario 9 – 20µm seed size and 0.5 g L^{-1} seed loading with SFL-Plant constraints

The output response for scenario 9 is shown in Figure 4-21 and with a larger seed size of 20 µm and a smaller seed loading of 0.5 g/L; this system is more controllable than scenario 8. During the first two minutes in open-loop, the supersaturation in the system is increasing and this can be attributed to the feed temperature being at 305 K, lower than the initial temperature of the system. When the MPC is enabled, the input profile begins to heat the system to slow the rate of change in supersaturation and this does result in the output trajectory passing the reference trajectory but the controller is able to converge the output onto the setpoint. The input moves in the initial heating phase are also at the move limit, so the system was heating as quickly as feasible, it just was not sufficient to overcome the rate of increase in supersaturation to prevent the output exceeding the reference. Comparing this to the unconstrained scenario (3) of the same system in Figure 4-22, the results show a large change in temperature at the beginning of the batch followed by a smooth temperature profile to steady state. The output response shows the supersaturation decreases for one time period but this is a result of the sharp increase in temperature to slow down the rate of increase in the supersaturation.

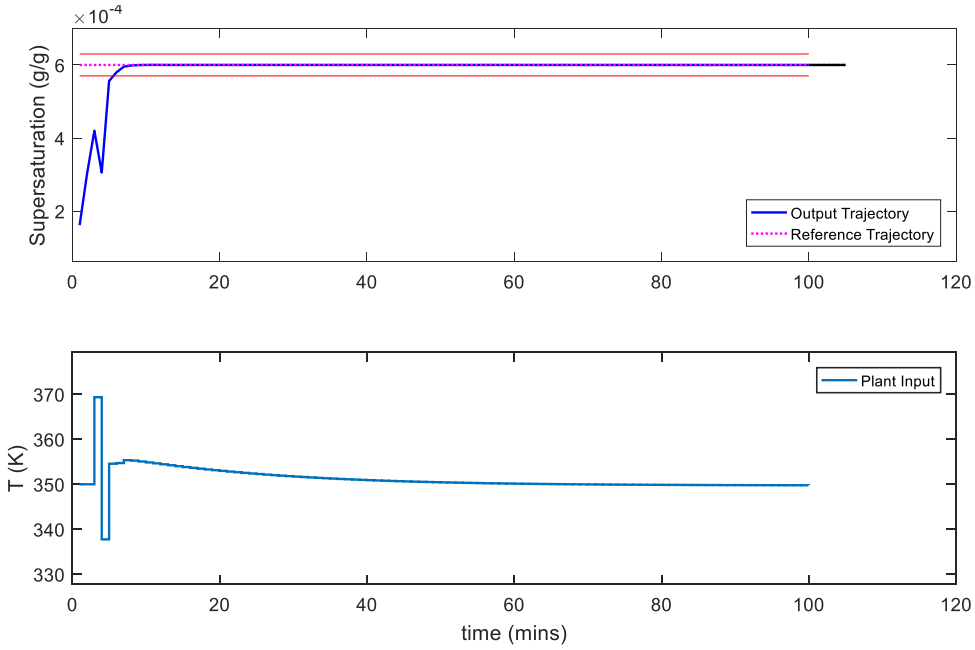

Figure 4-22– Continuous scenario 3 – 20µm seed size and 0.5 g L^{-1} seed loading without constraints

Two final scenarios shown in Figure 4-23 and Figure 4-24 are scenario 12 and 6, respectively. These scenarios experienced a combination of feed flow and feed temperature disturbances at 5-minute intervals and were included in the study to establish how disturbances would

affect the SFL-MPC performance. Scenario 12 with the SFL-Plant constraints shows how the output trajectory does appear to be converging onto the reference despite the numerous disturbances affecting the process. The input profile shows the temperature is on an upward or downward ramp throughout the 100-minute simulation, and the temperature changes coincide with the disturbances to the feed. The input moves are constrained at the high and low limits for most of the simulation too, so the MPC has again shown a feasible control solution. At each point when a disturbance affects the system, the MPC is always attempting to bring the output back onto the reference trajectory, which is the expected behaviour. In scenario 6, the output trajectory is less affected by the same magnitude of disturbances, this is because the input profile makes large unconstrained step changes in the temperature at the occurrence of each disturbance, to immediately counteract the effects. Overall, this concludes that the SFL-MPC with SFL-Plant constraints has the capability for disturbance rejection.

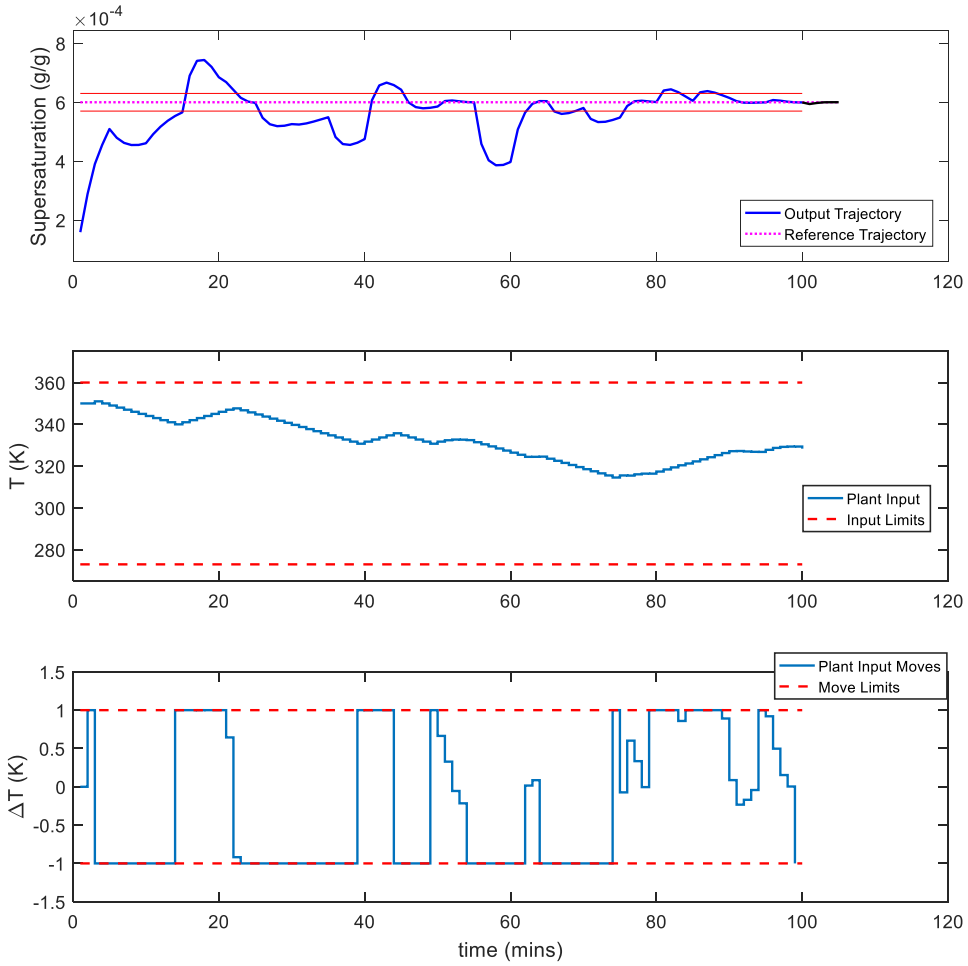

Figure 4-23– Continuous scenario 12 – feed flow rate and temperature disturbances with SFL-Plant constraints

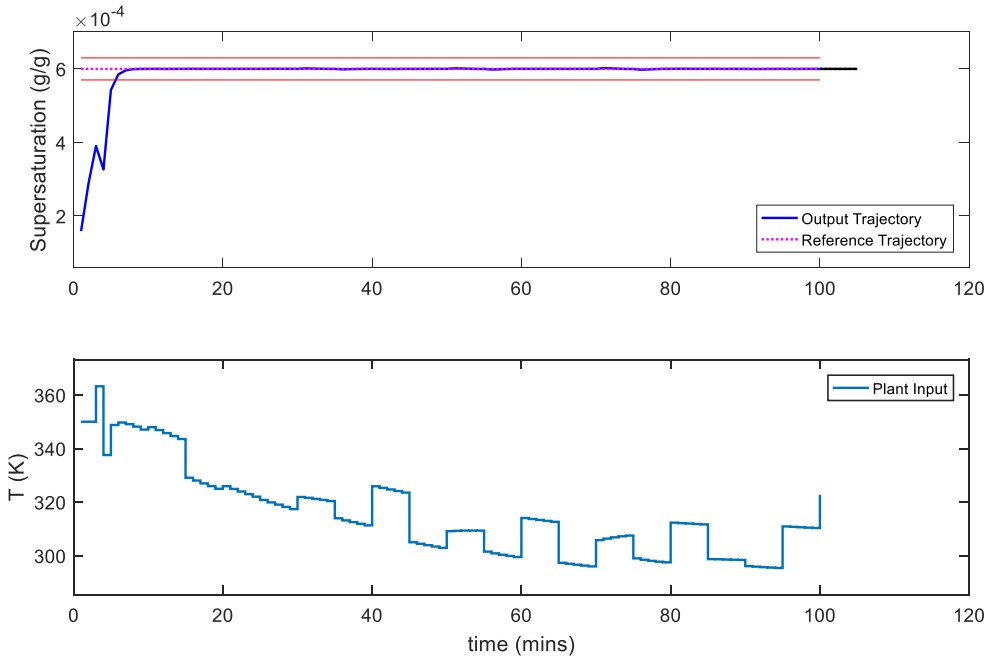

Figure 4-24 – Continuous scenario 6 – feed flow rate and temperature disturbances without constraints

The results from using scenario 1 as a reference to standardise the KPIs for all other scenarios are shown in Table 4-13. Scenarios 3 and 9 had a smaller error than scenario 1 which can be explained by scenarios 3 and 9 having a larger seed size. The interpretation of this is that the larger seed size at the same seed mass loading there will be fewer but larger crystals in the system. Therefore, the zeroth moment and the 2nd moment will both have a smaller value for scenarios 3 and 9 compared to the reference. Consequently, the mass balance which is also dependent on 2nd moment will result in a lower rate of crystallization, so maintaining the supersaturation trajectory would require less aggressive cooling. Considering the errors of the SFL-Plant constraints scenarios relative to the reference, all errors are larger for the feed temperature disturbance scenarios 11 and 12, and scenario 8 with the higher seed loading.

Finally, comparing the each SFL-Plant constraint scenario using the equivalent unconstrained scenario as a reference, the adjusted KPIs are shown in Table 4-14. One observation made here is that for scenarios 7 and 9, the SFL-Plant constraints simulations had a smaller error than scenarios 1 and 3 respectively. To understand this behaviour, scenarios 9 and 3 are provided in Figure 4-21 and Figure 4-22, respectively. The error differences can be explained by the output response for scenario 9 directly increasing from the start of simulation and converging onto the reference, whereas in scenario 3 the trajectory changes direction for 1 time-step which increases the error. On the other hand, the SFL-Plant constraints error was

larger in the other simulations. Furthermore, the simulation time is anywhere between 3 and 5.2 times longer for the SFL-Plant constraints calculation, but the longest overall time for the 100-minute simulation was 99.4 seconds, so in the context of real-time applications with a 1-minute plant interval, the SFL-Plant constraints remain a viable option for continuous MSMPR crystallization.

Scenario	ISE	IAE	ITAE	SDE	t_{set} (-)	t_{sim}(-)
2	1.07	1.05	1.17	1.04	1.00	1.03
3	0.97	0.97	0.91	0.99	1.00	1.04
4	1.00	1.01	1.28	1.00	-	1.00
5	1.00	1.00	1.00	1.00	-	1.00
6	1.00	1.02	1.35	1.00	-	1.06
7	0.89	0.97	1.05	0.94	1.17	4.29
8	2.76	6.43	77.71	1.03	12.67	1.64
9	0.79	0.87	0.87	0.89	1.00	5.43
10	1.09	2.20	22.14	0.99	-	3.65
11	2.57	4.50	83.19	1.59	-	3.35
12	2.29	4.92	59.84	1.41	-	3.19

Table 4-13 – Continuous Scenarios – Relative Performance to reference scenario 1

Scenario	ISE	IAE	ITAE	SDE	t_{set}(-)	t_{sim}(-)
7 vs 1	0.89	0.97	1.05	0.94	1.17	4.29
8 vs 2	2.57	6.11	66.57	1.00	12.67	1.59
9 vs 3	0.81	0.89	0.96	0.90	1.00	5.21
10 vs 4	1.09	2.18	17.32	0.99	-	3.66
11 vs 5	2.57	4.50	83.20	1.59	-	3.37
12 vs 6	2.29	4.85	44.26	1.41	-	3.01

Table 4-14 – Continuous Scenario Relative Performance of SFL-Plant constraints vs Unconstrained

4.10 SISO SLF MPC Applied to Batch and Continuous Crystallization

This section will focus on the use of the SISO SFL MPC with SFL-Plant constraints on a series of full batch and prolonged continuous MSMSPR crystallization scenarios. The focus in this section will be on the effects of the MPC on the overall crystallization process and the KPIs will be focussed on critical quality attributes of crystallization process. In addition to supersaturation control, the control of number-weighted mean-size control will also be performed.

4.10.1 Crystallization Critical Quality Attributes (CQAs)

In these crystallization studies, the CQAs that have been chosen are the mean crystal length (number weighted), coefficient of variation (COV) and yield. These three attributes have been

chosen because the mean size and COV provide two important characteristics of the CSD from the process, and the yield can be used to determine how much material is recovered from the process. The mean size can be calculated as follows:

$$L_{10} = \frac{\mu_1}{\mu_0}$$ *Equation 4-67*

Similarly, the coefficient of variation can be calculated:

$$COV = \sqrt{\frac{\mu_2 \mu_0}{\mu_1^2} - 1}$$ *Equation 4-68*

The recovery is the amount of paracetamol that is recovered from the system as a percentage of the amount of paracetamol in the system, and can be calculated as follows:

$$Recovery\ (\%) = \frac{C_{initial} - C_{final}}{C_{initial}}$$ *Equation 4-69*

Finally, the yield is the amount of paracetamol that is recovered in the desired form as a percentage of the theoretical amount which could theoretically be recovered at the same conditions, and can be calculated as follows:

$$yield(\%) = \frac{C_{initial} - C_{final}}{C_{initial} - C_{final}^*}$$ *Equation 4-70*

In the context of batch crystallization, the CQAs will be calculated at the end of the batch. For the continuous crystallization they will be calculated when the process has reached steady-state operation. In the continuous crystallization scenarios where disturbances are present, the CQAs will be represented as a mean-centred range of sizes, calculated from steady state.

4.10.2 Crystallization Control Scenarios

Three case studies are simulated using the SISO SFL MPC. The simulations will also address how the crystallization quality attributes differ across a series of simulations with and without SFL-Plant constraints. The following case studies will be considered:

- Seeded batch supersaturation control
- Seeded continuous MSMPR supersaturation control
- Seeded continuous mean size control.

4.10.3 Batch supersaturation Control Scenarios

The batch supersaturation control scenarios are detailed in Table 4-15 the SFL-MPC application on six scenarios will be shown. These scenarios are chosen because they show how the mean size, seed loading and constraints will affect the overall batch CQAs.

Scenario	Seed mean size (µm)	Seed loading (g L^{-1})	$y_{setpoint}$ (g/g)	SFL-Plant Input Constraints Active
1	10	0.5	0.0002	No
2	10	0.5	0.0002	Yes
3	10	0.75	0.0002	No
4	10	0.75	0.0002	Yes
5	20	0.5	0.0002	No
6	20	0.5	0.0002	Yes

Table 4-15 – Batch Supersaturation Control Scenarios for SFL-MPC with SFL-Plant Constraints

There are no disturbances implemented in the batch seeded crystallization scenarios. The objective function for the unconstrained batch scenarios is:

$$\min_{v} J = 5\sum_{i=1}^{5}\left(y_i - y_{i,setpoint}\right)^2 + \sum_{l=1}^{5}\Delta v_l^2 \qquad \textit{Equation 4-71}$$

And for the constrained batch scenarios the objective function is:

$$\min_{v} J = 5\sum_{i=1}^{5}\left(y_i - y_{i,setpoint}\right)^2 + \sum_{l=1}^{5}\Delta v_l^2 \qquad \textit{Equation 4-72}$$

Subject to:

$$273\ K \leq u = \varphi(\boldsymbol{x}, v) \leq 340\ K$$

$$-1 \leq \Delta u(Kmin^{-1}) = \varphi(\boldsymbol{x_i}, v_i) - \varphi(\boldsymbol{x_{i+1}}, v_{i+1}) \leq 1$$

Given:

$$\boldsymbol{x}$$

$$\dot{\boldsymbol{x}} = \boldsymbol{f}(\boldsymbol{x}) + \boldsymbol{g}(\boldsymbol{x})u$$

The batch simulations have a definitive end-point, which is triggered when the system temperature drops to 295K, at which point the batch is ended by switching the supersaturation setpoint to 0 g/g thus ending the batch contents at the solubility curve, the switch in setpoint results in the jacket temperature increasing at the end of the batch to prevent the requirement for a long hold-time to end at the solubility curve.

4.10.4 Batch Supersaturation Control Results and Discussion

In all the batch scenarios, the results are shown in 4 plots. The middle plot is the supersaturation (output), the bottom plot is the corresponding MPC input profile, and the two graphs at the top of the figures show the evolution of the number-weighted crystal mean-size (L_{10}) and the phase diagram. In the first batch scenario results are shown in Figure 4-25. This unconstrained scenario resulting in the MPC successfully tracking the supersaturation trajectory for 142 minutes, at which point the end-point of the batch was triggered because the system temperature dropped to 295 K. Then the setpoint was changed to 0 g/g supersaturation to end the batch, and the batch crystallization process terminated at 160 minutes. The system was seeded with 10 µm seed crystals with a loading of 0.5 g/L. In the phase diagram, the operating profile of the batch is shown to be very close to the solubility curve throughout production and there was little secondary nucleation throughout the process as a result. The crystals in the system did grow from the 10 µm seed size to 32 µm at the end of the batch. This may not appear to be significant growth, but the small seed size coupled with the seed loading results in many small seed crystals in the system, which results in a high surface area per mass of crystals when compared to a larger seed size for the same loading. Therefore, the growth to 33 µm is a reasonable outcome. Increasing the final seed size would be achievable through a smaller seed loading for the same size, or a larger seed size for the same loading.

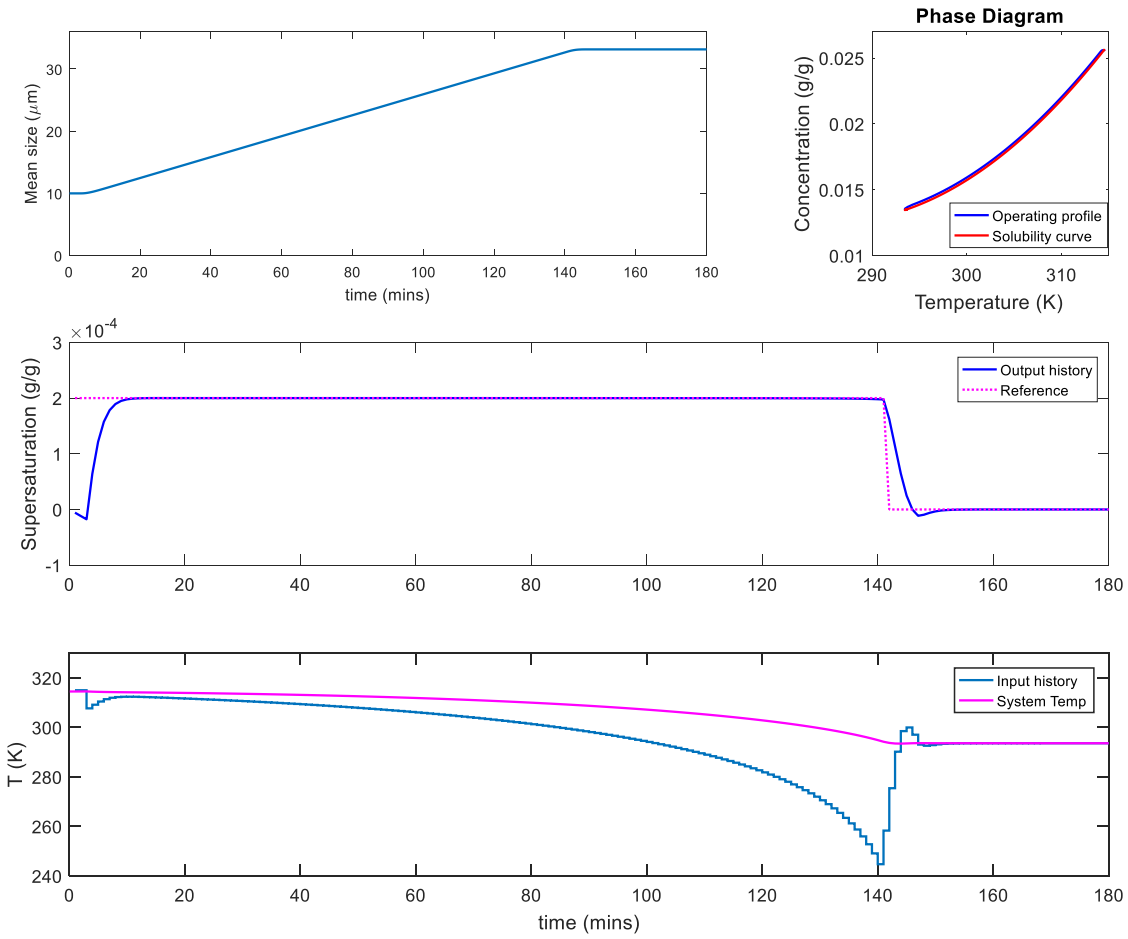

Figure 4-25. – Batch Scenario 1 - 10μm seed size and 0.5 g L^{-1} seed loading unconstrained

The second scenario shown in Figure 4-26 complements the results from the first scenario as it is the same crystallization system but with SFL-Plant constraints. The main differences seen here are that the plant input minimum temperature constraint is reached at 135 minutes, so no further cooling of the system is possible. The supersaturation profile coincidentally begins to diverge from the setpoint and the supersaturation is reduced as the dissolved concentration of paracetamol in the system continues to be consumed by growth. The system temperature does reach the 295 K end-point at 150 minutes, at which point the batch is ended. In this system, the crystal mean size also reached 33 μm from the initial 10 μm seed size, and a similar operating profile as scenario 1 is observed in the phase diagram plot, but a noticeable different is the mean-size trajectory from 135 to 150 minutes in scenario 2 appears to plateau smoothly and gradually, as compared to the almost instantaneous change seen in scenario 1.

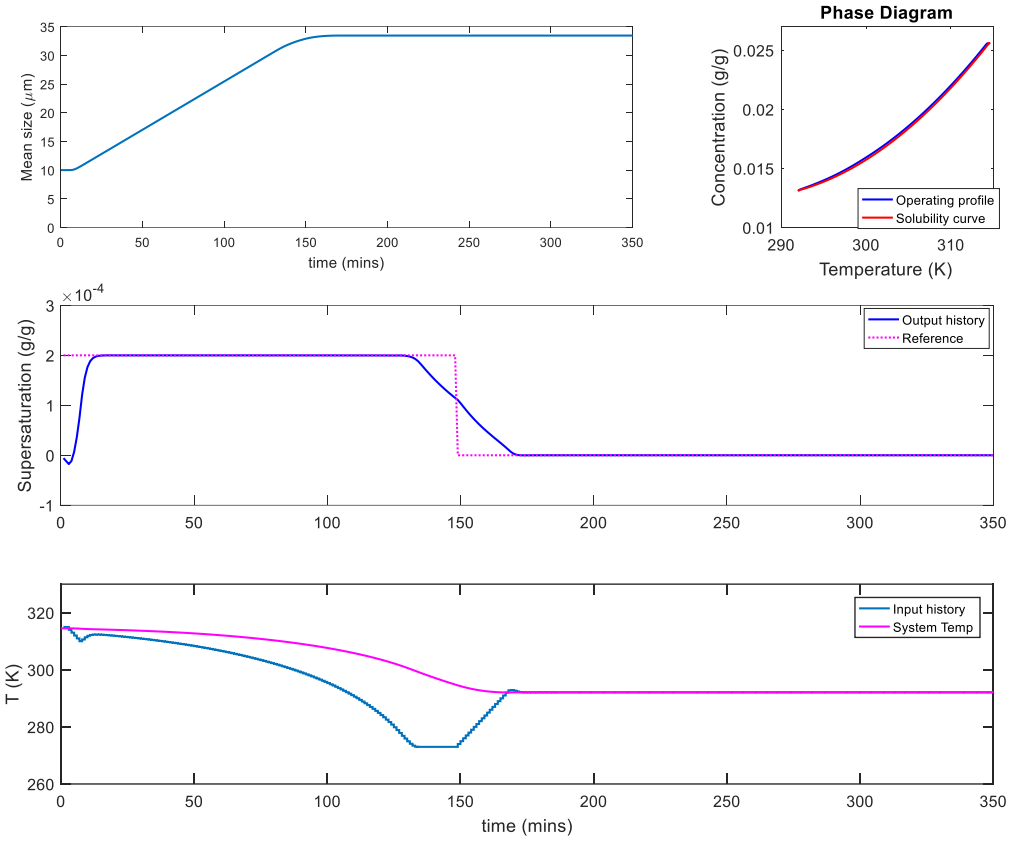

Figure 4-26 – Batch Scenario 2 Results - 10µm seed size and 0.5 g L^{-1} seed loading with SFL-Plant constraints

Scenario 3 shows a variation of scenario 1 where the seed loading is increased. Insights that can be gained from the model equations and the PBE would suggest then that for an increased mass of crystals in the same batch system, there would be more crystals and therefore a larger surface area and the resulting mean-size at the end of the batch should be smaller. Furthermore, the time to complete a batch should also be shorter because the growth rate is independent of size and dependent on supersaturation, thus dependent on concentration and the 2nd moment (related to surface area). This is clearly seen in the results for scenario 3 in Figure 4-27, with a shorter batch time of 119 minutes and smaller mean-size of 29.5 µm.

Comparing these results to scenario 4 in Figure 4-28 with the SFL-Plant constraints active, there is again a noticeable different in the operation of the batch. As the 2nd moment is larger in this system, therefore crystallization of dissolved paracetamol will be larger according to

the mass balance. So, when the low limit on the input temperature is reached at 108 minutes, the supersaturation diverges from the setpoint at a faster rate than in scenario 2. This batch also ends later than the unconstrained system, at 130 minutes, because the system temperature reaches 295 K at a later time than scenario 3. However, the mean-size is similar in scenario 3 and 4 so it appears there is little effect on the overall size of crystals at the end of the batch.

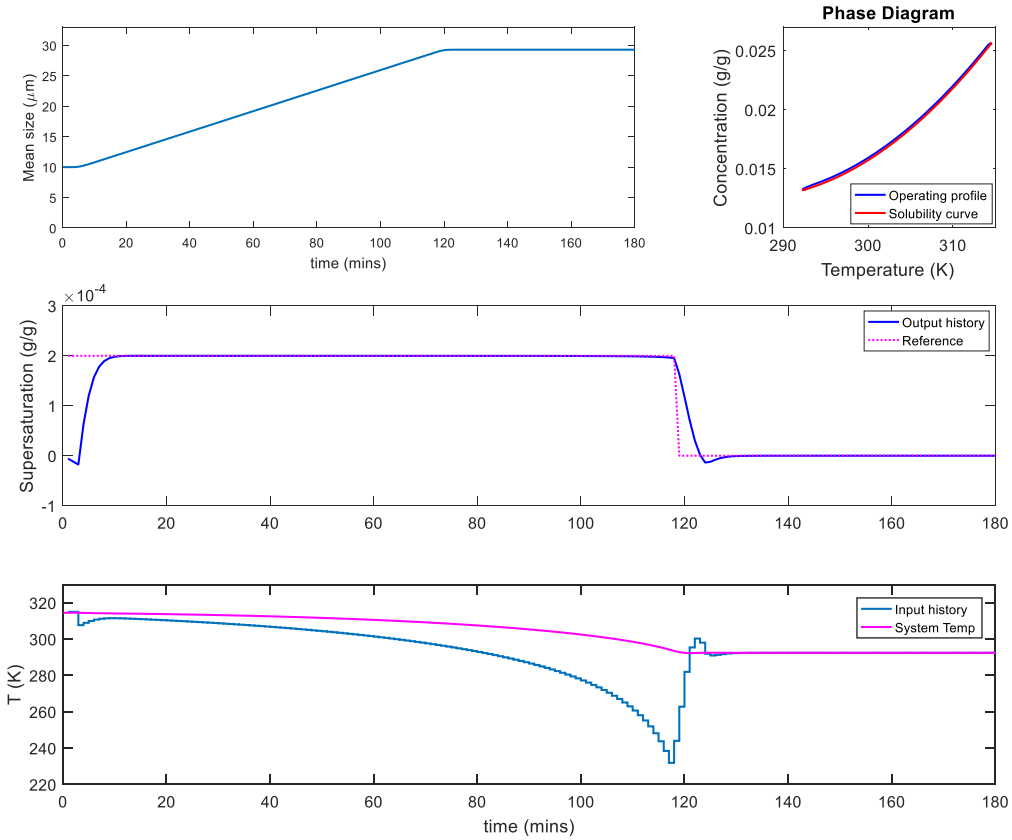

Figure 4-27 – Batch Scenario 3 Results - 10μm seed size and 0.75 g L^{-1} seed loading unconstrained

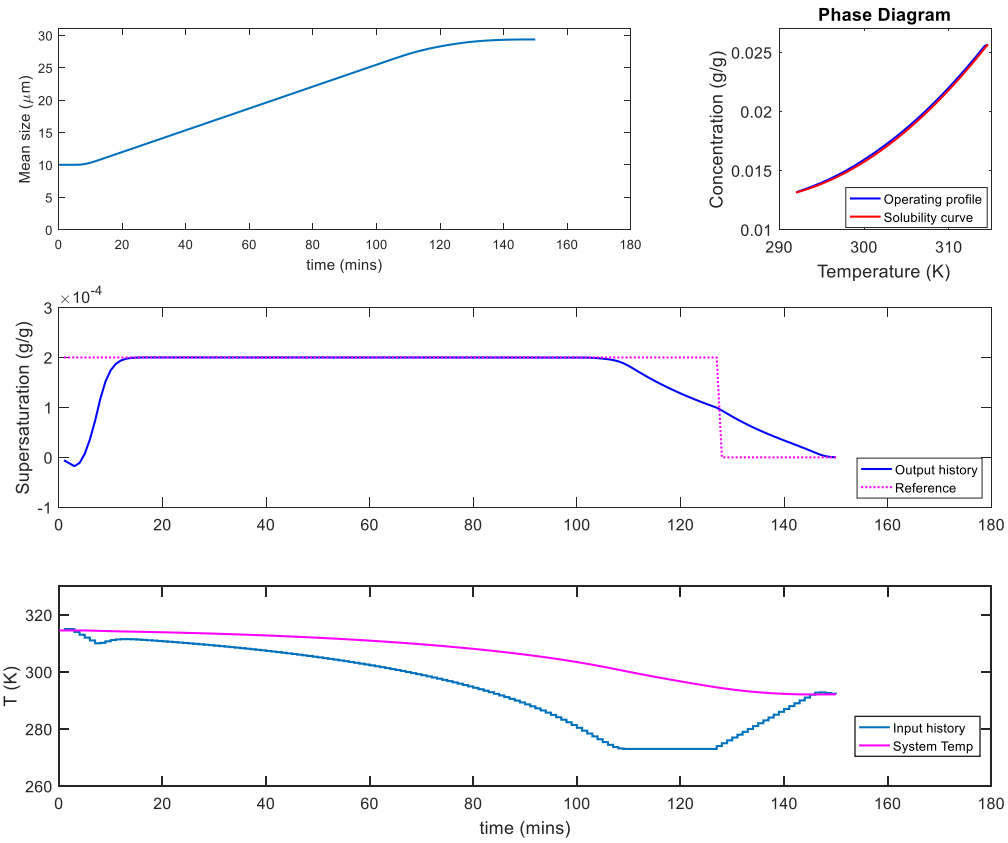

Figure 4-28. – Batch Scenario 4 Results - 10μm seed size and 0.75 g L^{-1} seed loading with SFL-Plant constraints

Scenario 5 is also similar to scenario 1 but the seed size is doubled from 10 µm to 20 µm with the same seed loading. The resulting seed conditions in the model have a smaller zeroth moment and 2nd moment, because the same mass of larger crystals results in fewer crystals in the system and a smaller surface area. Therefore, it is expected that the batch will require a longer time to complete to the same end-point as previous cases due to a relatively lower consumption of dissolved paracetamol in the system. Also, it is expected that the final mean size of crystals will be larger than the previous cases too. This is seen in the results in Figure 4-29 where the batch time is 277 minutes and the final crystal size reached 65 µm.

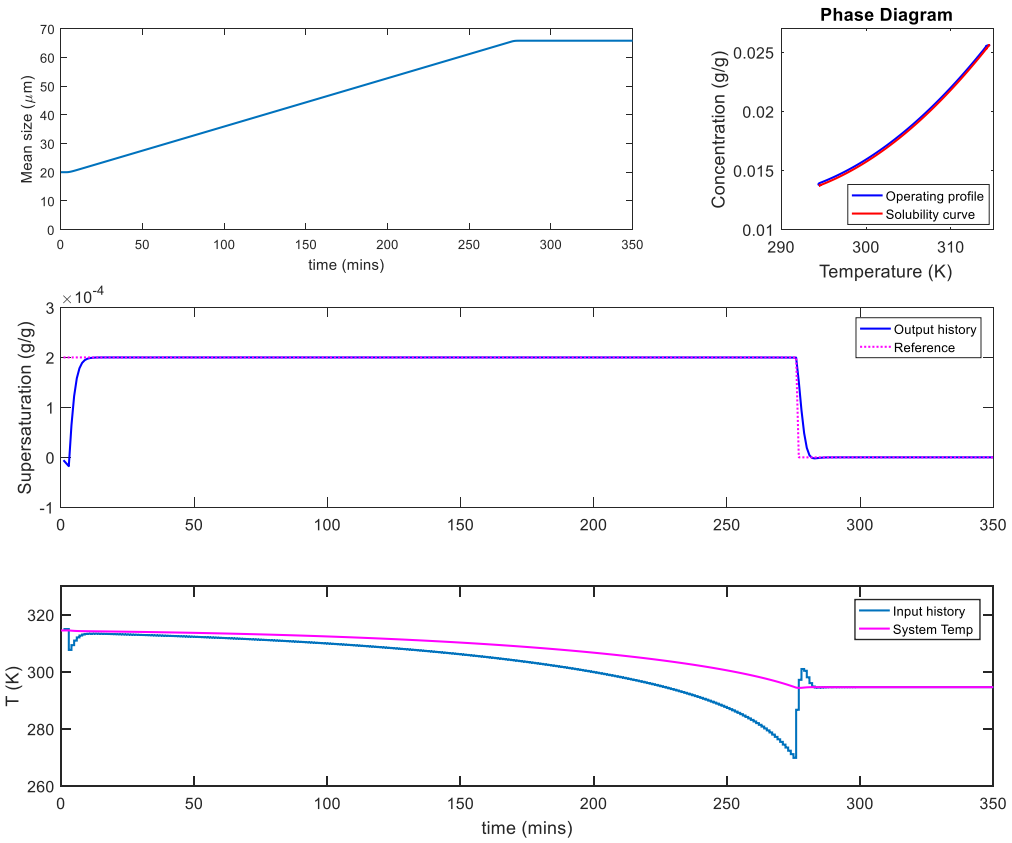

Figure 4-29. – Batch Scenario 5 Results - 20µm seed size and 0.5 g L^{-1} seed loading unconstrained

In the final batch scenario shown in Figure 4-30, a slightly longer batch time is observed from scenario 5 but because the consumption of supersaturation for growth is slower in this system, the SFL-Plant constraints do not have a significant effect on the overall batch time or supersaturation trajectory. It was possible for the SFL-MPC to maintain the supersaturation target and only reached the low limit for the input at 275 minutes, the batch ended at 278 minutes. The input profile is certainly less aggressive towards the end of the batch in scenario 6 than scenario 5. The mean size was also similar, but slightly larger again in the SFL-Plant constraints scenario. It is suspected that the increased batch time which results from reaching the MPC input limits results in more time for crystal growth and therefore marginally larger crystals at the end of the batch.

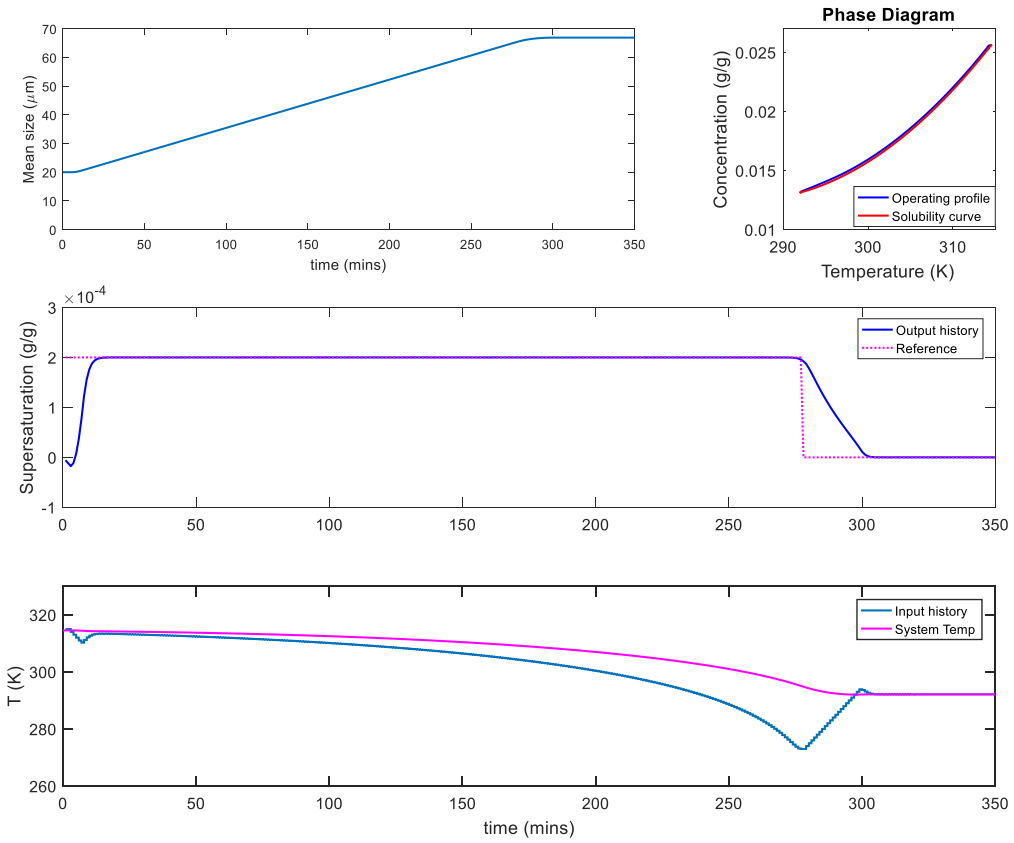

Figure 4-30. . – Batch Scenario 6 Results - 20μm seed size and 0.5 g L^{-1} seed loading with SFL-Plant constraints

Finally, the CQAs for the six scenarios have been summarised in Table 4-16. The main conclusions from these KPIs are that the mean-size for the SFL-Plant constraints scenarios were marginally larger than their counterpart unconstrainted scenarios, and the COVs are the same, although in practice it would likely not be possible to distinguish the differences seen between scenarios 1 and 2 or 3 and 4 through in-line process measurements.

Scenario	Mean Size (μm)	COV	Recovery (%)	Yield (%)
1	33.15	0.022	47.30	100.00
2	33.45	0.022	48.61	100.00
3	29.29	0.024	48.32	100.00
4	29.34	0.024	48.60	100.00
5	65.82	0.013	46.22	100.00
6	66.90	0.013	48.59	100.00

Table 4-16 – Summary of KPIs for Batch Supersaturation Control Scenarios

The yield from all scenarios was 100 % because every batch ended at the solubility curve, but the recovery was between 46 % and 49 %. Therefore, a large quantity of paracetamol remains dissolved in the system at the end of the batch, but this is a good outcome for this batch crystallization system because the solubility curve that was used (Nagy $et\ al.$, 2008a) is only feasible from system temperature of 320 K to 290 K, and the batch end-point was close to this limit.

4.10.5 Continuous Supersaturation Control Scenarios

The continuous MSMPR supersaturation control study consists of 7 scenarios detailed in Table 4-17. The SFL-Plant constraints are active for all scenarios and the first three aim to compare the differences in continuous crystallization production based on differences in seed parameters, while the last four also consider the impacts of disturbances on the feed conditions.

Scenario	Seed mean size (µm)	Seed loading (g L^{-1})	Feed Flow rate (mL min^{-1})	Feed Temp. (K)	Disturb. type	Disturb. interval (mins)	$y_{setpoint}$ (g/g)
1	10	0.5	70	305	-	-	0.0006
2	10	0.75	70	305	-	-	0.0006
3	20	0.5	70	305	-	-	0.0006
4	10	0.5	70	305 ± 2	Random	1	0.0006
5	10	0.5	70 ± 7	305 ± 2	Random	1	0.0006

Table 4-17 – Summary of all Continuous Supersaturation Control Scenarios

The cost function for the continuous case is as shown in Equation 4-66 and the supersaturation setpoint is held throughout production.

$$\min_{v} J = 5\sum_{i=1}^{5}\left(y_i - y_{i,setpoint}\right)^2 + \sum_{l=1}^{5}\Delta v_l^2 \qquad \textit{Equation 4-73}$$

Subject to:

$$273\ K \leq u = \varphi(\boldsymbol{x}, v) \leq 360\ K$$

$$-1 \leq \Delta u(Kmin^{-1}) = \varphi(\boldsymbol{x_i}, v_i) - \varphi(\boldsymbol{x_{i+1}}, v_{i+1}) \leq 1$$

Given:

$$\boldsymbol{x}$$

$$\dot{\boldsymbol{x}} = \boldsymbol{f}(\boldsymbol{x}) + \boldsymbol{g}(\boldsymbol{x})u$$

Each continuous MSMPR crystallization scenario is initialised at the same conditions as provided in section 4.6, and the initial conditions are not the same as the steady-state of each scenario, so there is a transient phase during the start of the simulation where the MPC converges the supersaturation profile to the setpoint and the system then converges to steady state operation. The disturbances applied to scenarios 4 through 7 are normally distributed and random disturbances to the feed conditions in the defined ranges in the Table 4-17, and each disturbance has an interval of 1 so every minute of simulation, a new disturbance is experience in the system.

4.10.6 Continuous Supersaturation Control Results

The graphs for the continuous supersaturation control scenarios consist of 5 plots. The first row of plots are the feed flow rate and temperature trend and the phase diagram, followed by the supersaturation (output) trend, the temperature (input) profile and finally the crystal mean size. The results of the first scenario are shown in Figure 4-31. The feed conditions are constant in this scenario and the supersaturation target of 0.0006 g/g is reached quickly by the controller. The reason for this is because the feed temperature is at 305 K and during the first two minutes of open-loop simulation, the feed is reducing the temperature of the system and increasing the supersaturation. The system is initialised with the jacket temperature at 350 K for this reason, to prevent the supersaturation of the open-loop simulation overshooting the reference trajectory before the MPC is enabled. Then, the input profile shows a steady decrease for the first 100 minutes over which the system is in a transient phase where the MPC is cooling the MSMPR to maintain the supersaturation trajectory, thus changing the point of steady state operation that would be converged in open-loop. The controller settles on steady-state production after 100 minutes. The transient period also results in a change in the crystal mean size from the seed size of 10 µm to 20.6 µm, so at steady state there is a mean growth of 10.6 µm experienced. Furthermore, the phase diagram shows the trajectory of the operating profile and unlike the long batch trajectories which end at a low temperature and saturated, the MSMPR converges to a point of operation at a temperature above 306 K and operates in a supersaturated location in the phase diagram, thus the amount of recovered paracetamol in a single stage MSMPR is much smaller than that of batch.

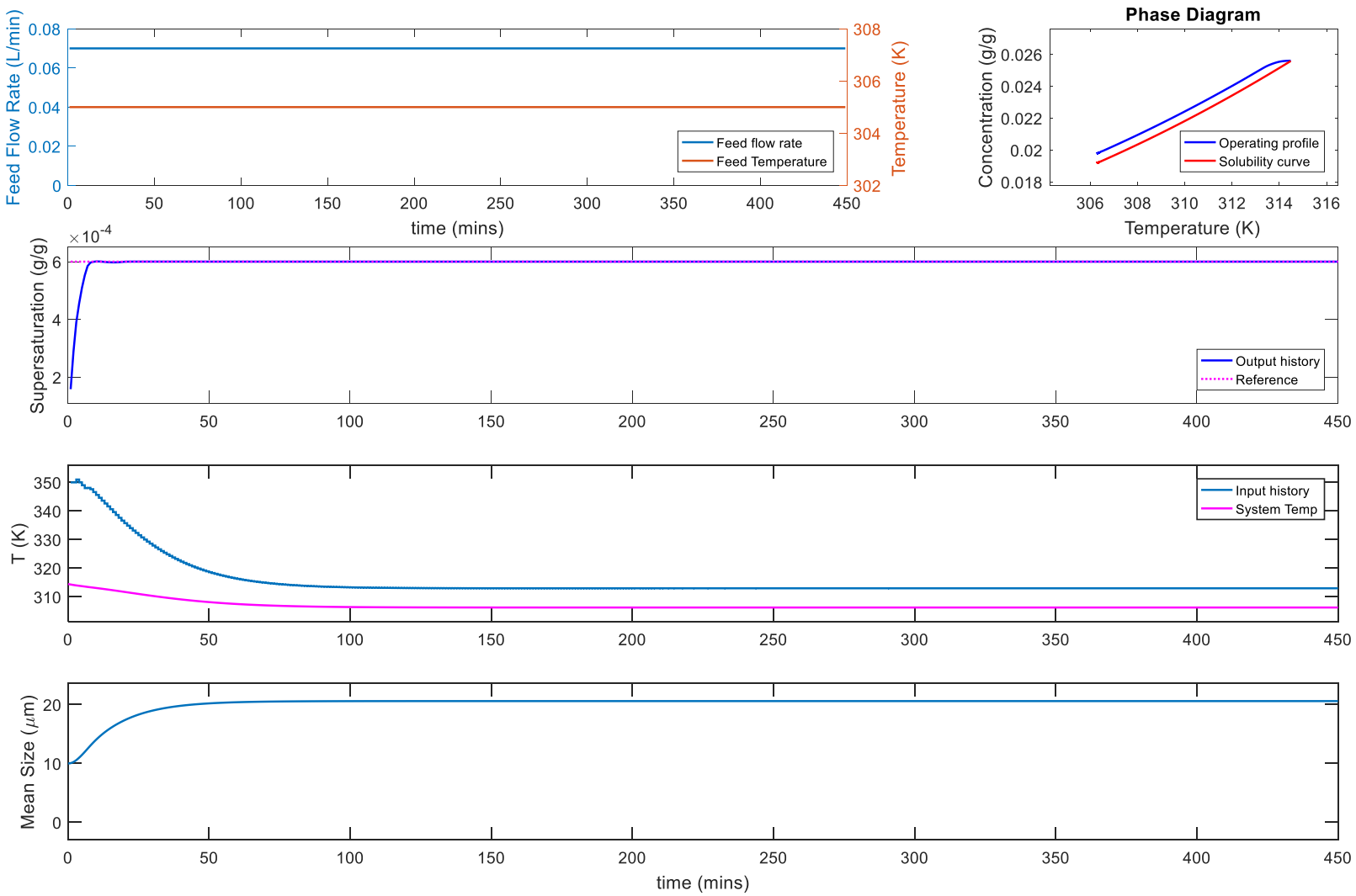

Figure 4-31 – Continuous MSMPR Supersaturation Control Scenario 1 - 10µm seed size and 0.5 g L^{-1} seed loading and no disturbances

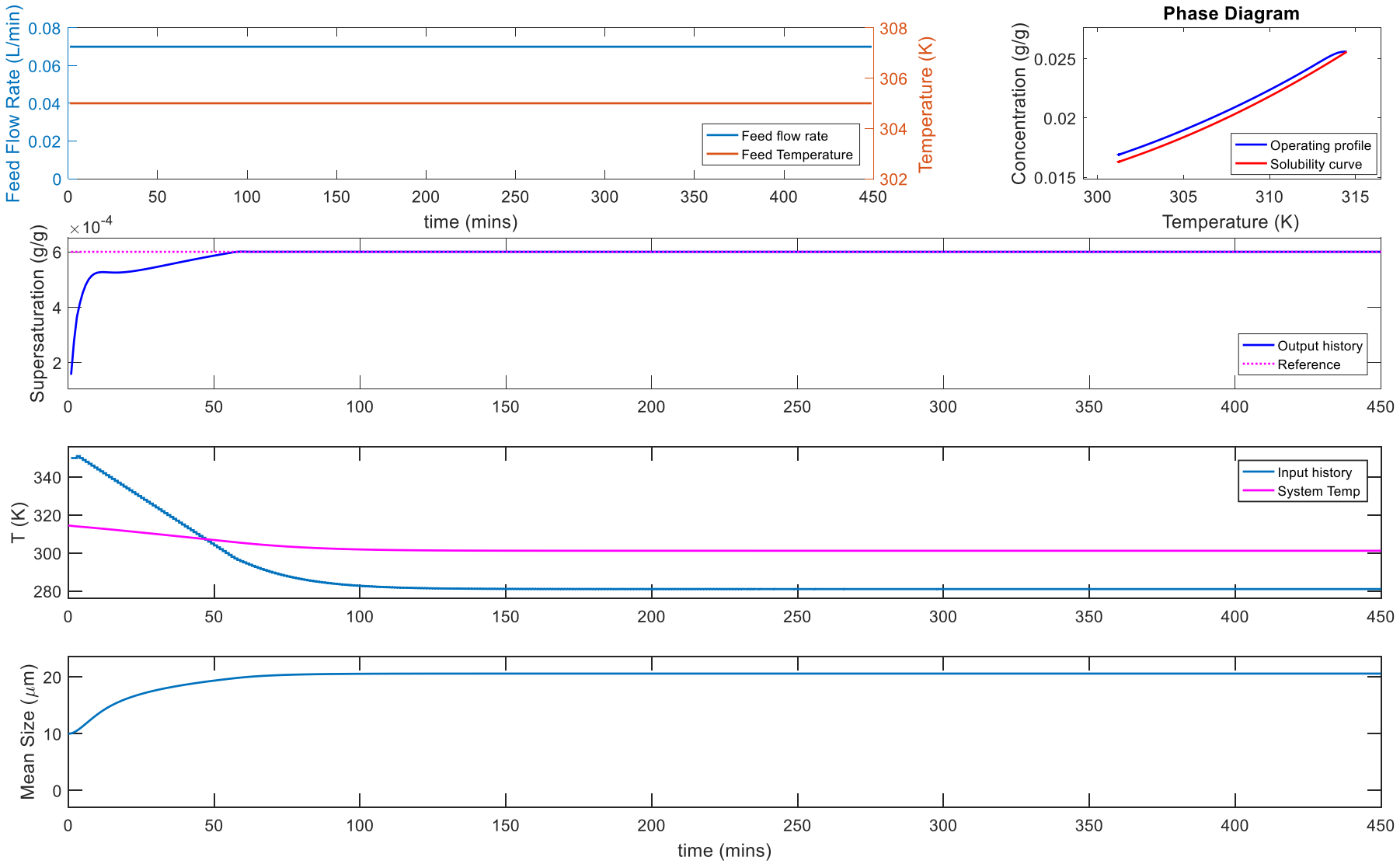

Figure 4-32 – Continuous MSMPR Supersaturation Control Scenario 2 - 10μm seed size and 0.75 g L^{-1} seed loading no disturbances

The next scenario shown in Figure 4-32 has a 50% larger seed loading than scenario 1. This again results in a higher depletion rate of supersaturation which requires a faster cooling rate to maintain the supersaturation target. As seen in the first 55 minutes of the simulation results, the output does not appear to converge onto the target immediately. This is caused by the SFL-Plant constraints which have an imposed move-limit on the inputs of 1 K/min, the system cannot cool fast enough to maintain the supersaturation rate. However, unlike the batch case, the continuous MSMPR production is at a steady-state position and the temperature limit of the system happens to be low enough that eventually steady state production will be reached and supersaturation control will be possible to the desired target. The feed flow rate is the same as the previous scenario so again the system reaches the steady state in a similar time after 100 minutes. The phase diagram also shows that this system's steady state position is at a lower temperature but still supersaturated. This will result in a higher recovery of material. The crystal mean-size in the outlet of the MSMPR is also the same as the previous scenario, once steady state is reached.

The final scenario without disturbances is scenario 3 (Figure 4-33) where the seed loading is the same as scenario 1 (0.5 g/L) but the seed size is doubled from 10 µm to 20 µm. The resulting system shows a slight overshoot in the supersaturation trajectory which is related again to a smaller 2^{nd} moment because the seed size is increased for the same seed loading. Thus the rate of supersaturation consumption is smaller than scenario 1. This results in immediate heating of the system from the initial jacket temperature of 350 K. Furthermore, the steady state operating point is reached in the same time as the previous scenarios but the operating point is at a higher temperature in the phase diagram, over 312 K, thus the recovery of material will be low at steady state in this single-stage MSMPR. The crystal mean-size grows from the 20 µm seed to 30.6 µm crystals though. Overall, these scenarios that are absent of disturbances demonstrate the ability of SFL-MPC to control continuous MSMPR crystallization with SFL-Plant constraints and the output trajectories are reasonable. The next stage is to consider the four scenarios where feed disturbances are applied.

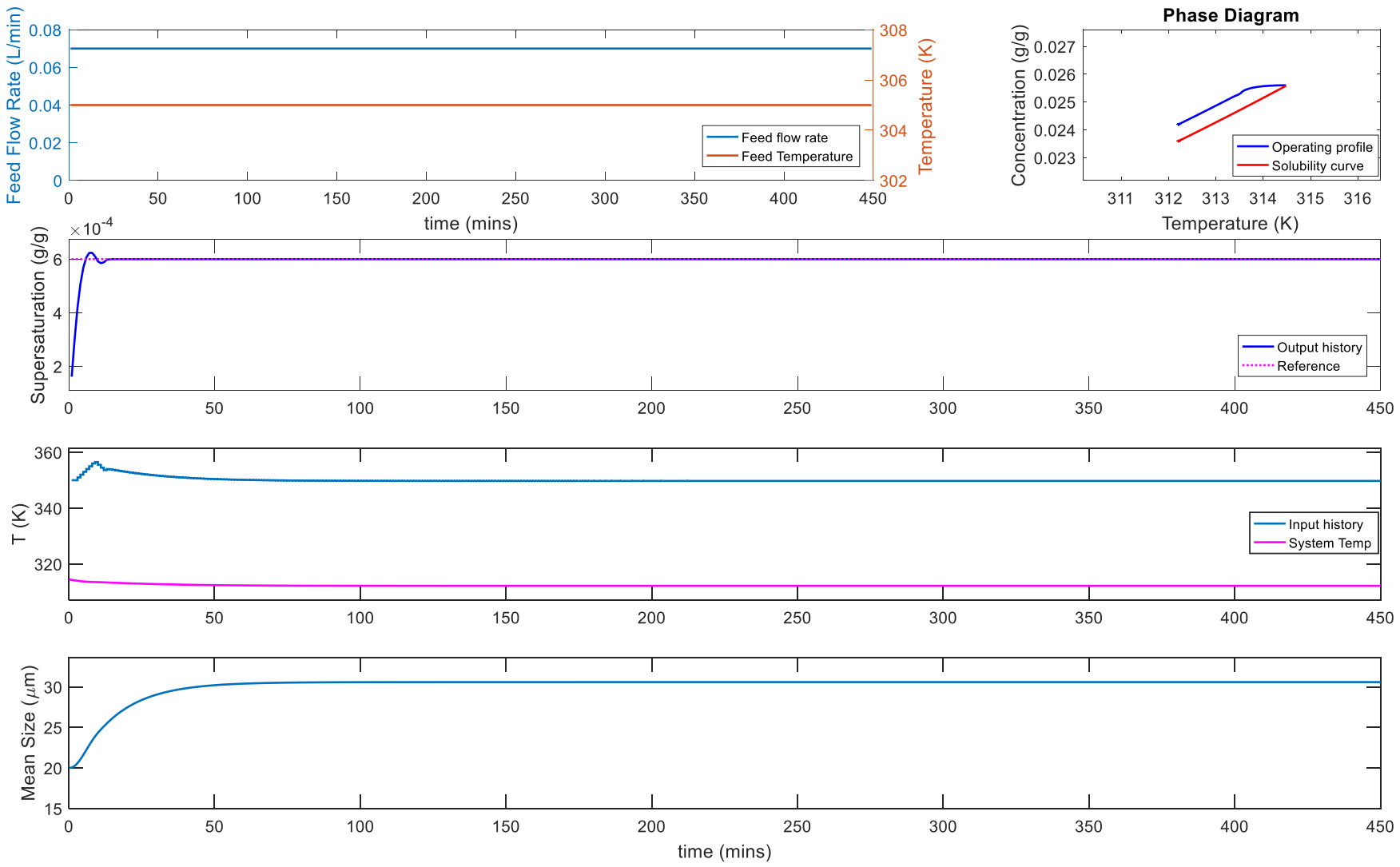

Figure 4-33 – Continuous Supersaturation Control Scenario 3 - 20μm seed size and 0.5 g L^{-1} seed loading no disturbances

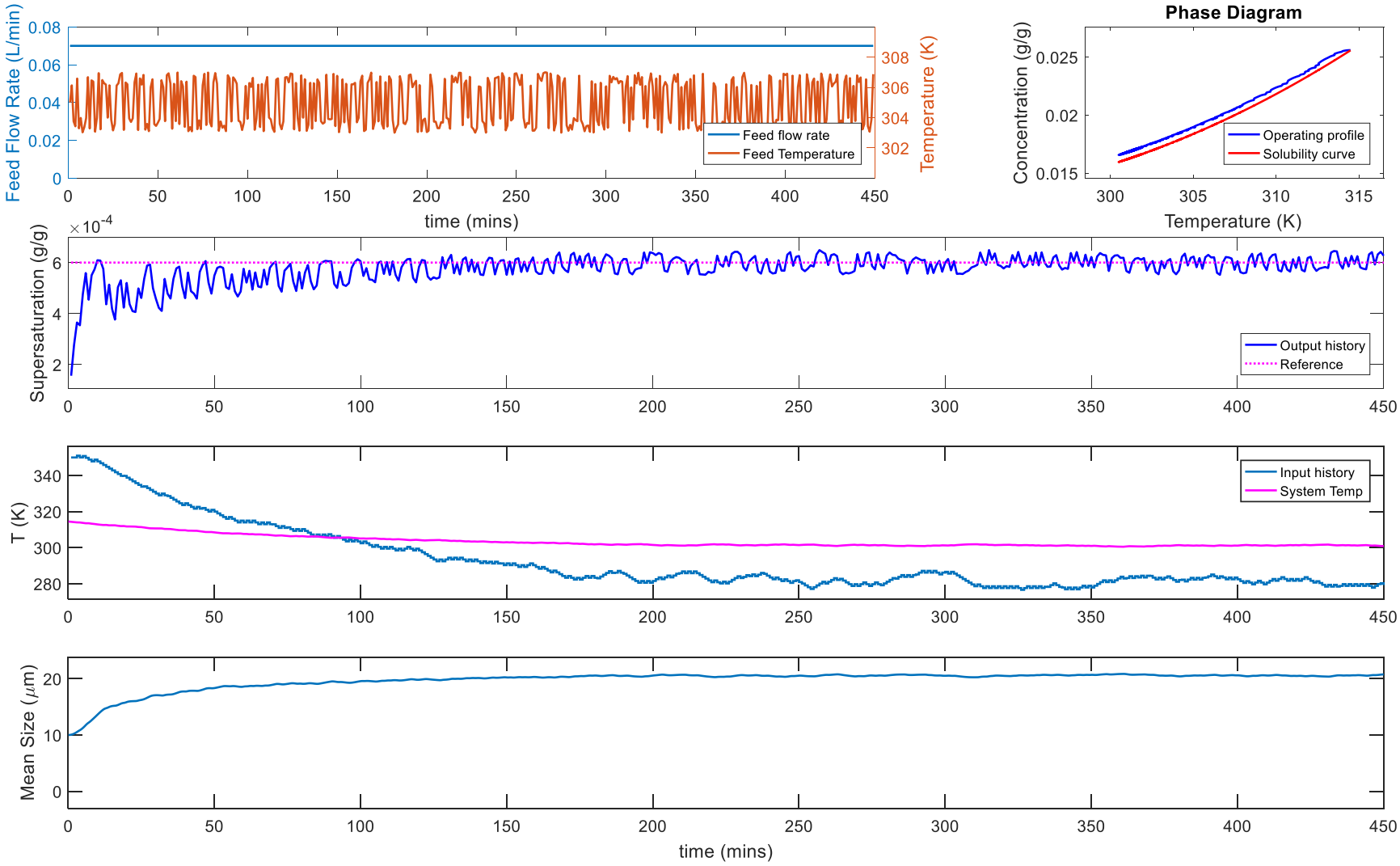

Figure 4-34 – Continuous MSMPR Supersaturation Control Scenario 4 - 10μm seed size and 0.5 g L^{-1} seed loading with feed temperature disturbances

Scenario 4 with the feed temperature disturbances for the 10 µm seed size and 0.5 g/L seed loading is shown in Figure 4-34. The main difference between this trajectory and that of scenario 1 is that the temperature disturbances in the feed have a significant impact on the supersaturation profile. The SFL-MPC does indeed converge onto the setpoint, but the converged appears to require more time than prior cases. The input moves are mostly at their move limit between each implementation of the MPC, which suggests that the cooling rate limit imposed on the inputs is not sufficient enough to completely counteract the disturbances, but is sufficient to ensure the process still operates around the same target supersaturation. The resulting system also appears to operate at a lower temperature in the phase diagram, but this cannot be concluded through the operating profile because the system temperature is fluctuating throughout operation. The crystal mean-size in the outlet does appear to be similar to that of scenario 1 but the mean-size fluctuates in the range of 20 $\pm$ 3 µm.

Scenario 5 shown in Figure 4-35 aims to combine disturbances to both the feed temperature and feed flow rate to establish is the effects of multiple disturbances on the continuous process. The main conclusions from these results are that the process does not appear to require as long a time to settle near steady-state as scenario 4, but the effects of the combined disturbances do cause greater fluctuations in the supersaturation profile. However, the supersaturation remains centred on the setpoint, so given the limitations imposed by the SFL-Plant constraints on the inputs, the results in this scenario are also acceptable for the control problem. The outlet crystal mean size is also similar to that of scenario 4.

Finally, the CQA results for continuous MSMPR crystallization control are disclosed in Table 4-18. The results show that for the larger seed size, a larger mean size is obtained and a smaller COV is also achieved. For all scenarios with a 10 µm seed size, the outlet crystal number-weighted mean size appears to be similar and in the region of 20.6 µm. The yield also appeared to be larger for the 10 µm seeds size than for the scenario with a 20 µm seed size, and the recovery follows a similar trend too. This is expected though because the larger seed size will not consume as much supersaturation during the transient phase when at the supersaturation setpoint. This can be aided by adjusting the supersaturation setpoint based on the seed size and seed loading. To determine the best supersaturation setpoint to maximise the recovery and yield from given initial conditions, it is recommended to perform

an offline optimization to maximise recovery and/or yield given the seed conditions using the setpoint as the decision variable. Alternatively, a multi-stage MSMPR approach can also be used to increase the paracetamol recovery.

Scenario	**Mean Size (µm)**	**COV**	**Recovery (%)**	**Yield (%)**
1	20.59	0.515	22.7	90.6
2	20.59	0.515	34.1	93.6
3	30.59	0.347	5.5	70.3
4	20.15 ± 2.99	0.496 ± 0.17	20.7	90.3
5	20.38 ± 2.72	0.501 ± 0.19	23.5	90.3

Table 4-18 – Summary of KPIs for all Continuous Supersaturation Control Scenarios

Another approach is to select a different control problem and try to control one of the CQAs directly. This leads into the following section where instead of continuous MSMPR supersaturation control, the crystal mean-size will be used for control. The optimization of crystal mean-size in batch has been performed in chapter 3 of this research and by other authors too (Sarkar, Rohani and Jutan, 2006; Hemalatha *et al.*, 2018). The crystal mean-size has also been used for control problems in various research, but the use of SFL-MPC to control mean-size has not been reported.

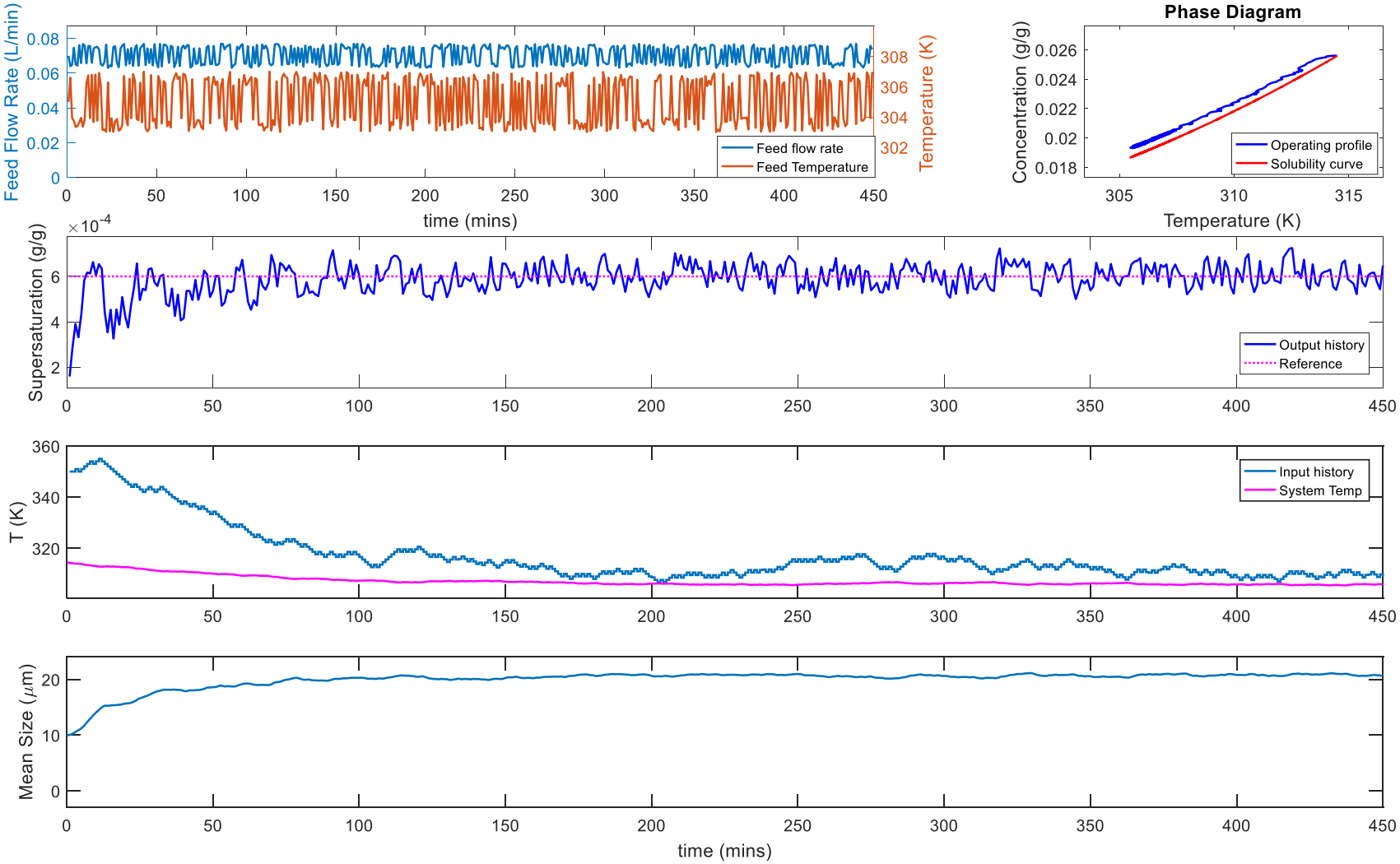

Figure 4-35 – Continuous supersaturation Control Scenario 5 - 10μm seed size and 0.5 g L^{-1} seed loading with feed temperature and flow disturbances

4.10.7 SFL MPC for Mean Size Control

The case of mean-size control requires a new SFL model which is obtained using the same procedure as earlier in this chapter. The following is disclosed regarding the mean-size control system. The output is (Ramkrishna, 2000):

$$y = h(x) = \frac{\mu_1}{\mu_0} \qquad \textit{Equation 4-74}$$

Meanwhile, the plant input u is the jacket temperature. The resulting linearization from the nonlinear model into an input-output linear model has a relative order of 2. Thus, the control law for the new system is defined:

$$u = \frac{v - \beta_0 h(x) - \beta_1 L_f h(x) - \beta_2 L_f^2 h(x)}{\beta_2 L_g L_f h(x)} \qquad \textit{Equation 4-75}$$

Subsequent tuning of this system using the approach described in section 4.7 resulted in the tuning parameters detailed in Table 4-20:

	$\boldsymbol{\beta_0}$	$\boldsymbol{\beta_1}$	$\boldsymbol{Q}$	$\boldsymbol{R}$
Continuous	1	10	5	1

Table 4-19 – Summary of Continuous Mean Size Control Tuning Parameters

Finally the cost function is defined as follows:

$$\min_{v} J = 5\sum_{i=1}^{5}\left(y_i - y_{i,setpoint}\right)^2 + \sum_{l=1}^{5}\Delta v_l^2 \qquad \textit{Equation 4-76}$$

Subject to:

$$100\ K \leq u = \varphi(\boldsymbol{x}, v) \leq 360\ K$$

$$-2 \leq \Delta u(Kmin^{-1}) = \varphi(\boldsymbol{x_i}, v_i) - \varphi(\boldsymbol{x_{i+1}}, v_{i+1}) \leq 2$$

Given:

$$\boldsymbol{x}$$
$$\dot{\boldsymbol{x}} = \boldsymbol{f}(\boldsymbol{x}) + \boldsymbol{g}(\boldsymbol{x})u$$

This information is sufficient to describe the full design of the SFL-MPC for mean size control which will be used later in the chapter.

4.10.8 Continuous Mean Size Control Scenarios

The SISO SFL MPC for continuous MSMPR mean-size control has been defined, and for this study two scenarios will be presented as shown in Table 4-20. Both scenarios are seeded with the same size seed at 20 µm and the same loading of 0.5 g/L. Scenario 2 is subjected to feed

temperature disturbances each minute. The aim of the SFL-MPC is to reach a setpoint of 40 µm crystal size in the outlet. This is an ambitious target for the existing control problem as it was already seen that the 20 µm seed can grow to 30.6 µm crystals by operating close to the low temperature limit of the MPC input. For this reason, the control problem for mean-size control is relaxed to allow a wider temperature range and though this may not be realistic in practice, the aim of this study is to observe if mean-size control is a viable control problem for the SFL-MPC and to also assess if the SFL-Plant constraints are also upheld and if SFL-MPC control produces feasible results.

Scenario	Seed mean size (µm)	Seed loading (g L^{-1})	Feed Flow rate (mL min^{-1})	Feed Temp. (K)	Disturb. type	Disturb. interval (mins)	$y_{setpoint}$ (µm)
1	20	0.5	70	305	-	-	40
2	20	0.5	70	305 ± 2	Random	1	40

Table 4-20 – Summary of Continuous Mean Size Control Scenarios

4.10.9 Continuous Mean-Size Control Results and Discussion

The first scenario is absent of any feed condition disturbances to establish how the controller performs. The results in Figure 4-36 show that the process converges to steady at around 100 minutes and does indeed achieve the 40 µm crystal size target. The input profile over the first 100 minutes shows a cycling behaviour where the temperature change is at the move-limit of 2 K/min for most of the first 100 steps. The coolant temperature reaches as low as 105 K, but eventually stabilises at 155 K, these temperatures are likely not feasible in crystallization coolant systems which concludes that the target mean size of 40 µm from a seed size of 20 µm and loading of 0.5 g/L is likely not realistic. A feasible input profile may be possible at a lower seed loading, or using a cooling medium which has more effective heat transfer to the system and thus doesn't need drop to such low temperatures seen in this simulation. However, the system temperature stabilises at 304 K, so the heat transfer parameters in the energy balance cause this large difference and may be overcome with a more effective method of heating and cooling the crystallizer. Initially the process is cooled quickly to converge the mean size onto the target, and there is a slight overshoot in size which causes the cycling of heating and cooling in the input profile until the mean-size is converged on the target.

The second scenario extends the first by including feed temperature disturbances each minute, in the range of 310 $\pm$ 3 K. This range was chosen to exaggerate the potential disturbances in the feed temperature and to observe the controllability of this system. The results shown in Figure 4-37 show the mean size appeared to be affected by disturbances with the outlet crystal size fluctuating in the range of 40 $\pm$ 2 μm. However, the mean size is indeed converged onto the setpoint within the first 100 minutes and appears to remain converged despite the effects of disturbances. Thus, the results show feasible control of continuous MSMPR mean-size using SFL-MPC with SFL-Plant constraints.

Concluding the mean size control cases, it appears that the SISO SFL MPC is able to control a seed to a desired mean size in the presence of process disturbances, though careful considerations should be made about the target mean size so that it is attainable by the system and controller. The SFL MPC has been tested for multiple crystallization configurations in this chapter and in all cases the simulation results appear to follow the expected trends, the behaviour of the controller can be explained down to the low-level detail and changes, and the SFL-plant constraints method also holds up across a wide selection of cases. These results allow the conclusion to be made that the SISO SFL MPC is a suitable controller for crystallization where an accurately identified model for the crystallization system exists and where there are real world constraints that must be adhered.

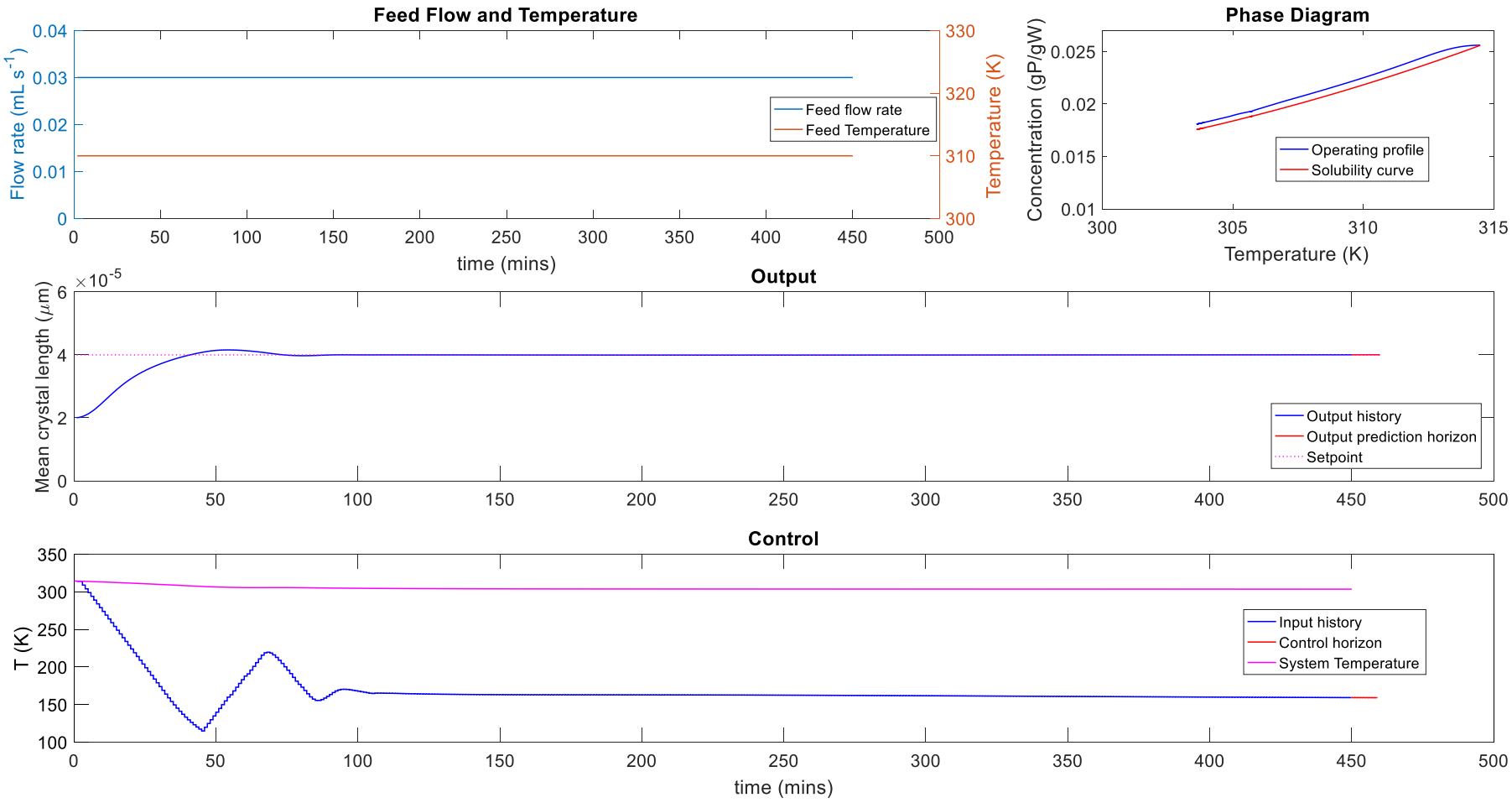

Figure 4-36 – Continuous mean-size control case 1 without disturbances.

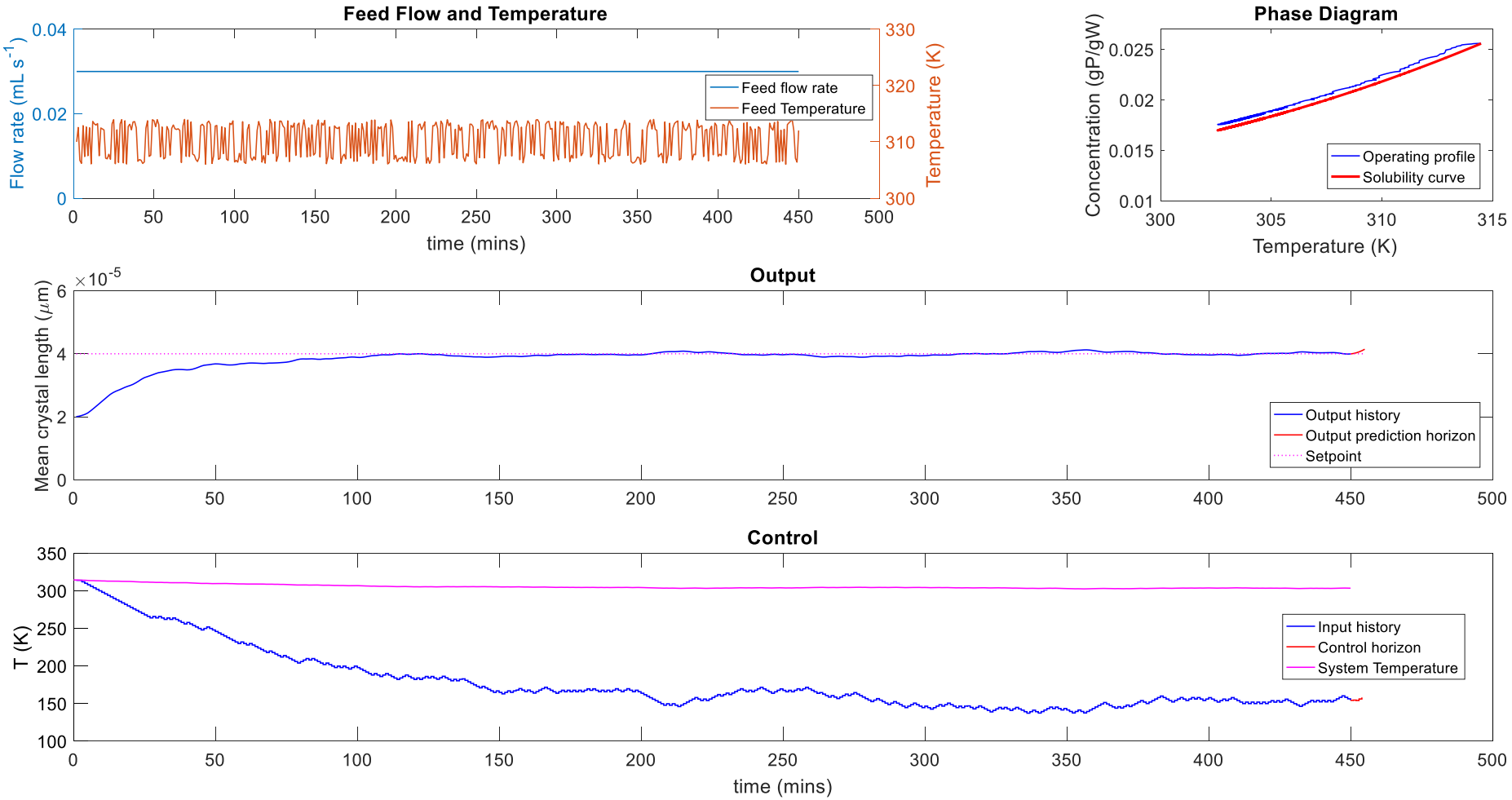

Figure 4-37 – Continuous mean-size control case 2 with temperature disturbance and input constraints of 2 K/min ramp.

4.11 Conclusion

This chapter introduced state space modelling and detailed the methodology for transforming a nonlinear state-space model into a linear model using the global input/output state feedback linearization method (Kravaris and Chung, 1987). The SFL model structure was also identified model predictive control introduced. The implementation of the SFL model into the MPC was a key part of this chapter for SISO control of batch and continuous MSMPR crystallization supersaturation control by manipulating the coolant temperature.

This chapter introduced the nonlinear crystallization model used for batch and continuous crystallization. Subsequent linearization of the model for supersaturation control successfully converted the nonlinear input-output model into a linear input-output model, using the SFL procedure. The subsequent linear model was implemented into the SFL-MPC. The tuning parameters for the SFL-MPC were selected iteratively with the aim to prevent overshoot in the output trajectory and reduce the settling time for output response. The selected parameters were used to identify objective function weights, and a set of tuning parameters and weights were obtained for batch and continuous MSMPR crystallization systems for supersaturation control.

The difficulties of constraint handling in SFL-MPC is introduced and a novel method for handling constraints is described, name SFL-Plant constraints. The SFL-MPC tuning and weight parameters were then used in a study to establish controller performance and feasibility across a set of batch and continuous scenarios with and without SFL-Plant constraints. The first outcome was that the SFL-Plant constraints were successfully implemented, and every scenario produced feasible results subject to the constraints, satisfying both the input limit and input move limit criteria. Secondly, KPIs were used to quantify the differences in error between similar scenarios and it was found that the tuning parameters were transferrable across many different crystallization conditions of the same paracetamol/water batch and continuous crystallization system. Finally, the relative performance of the SFL-Plant constraints simulations against the unconstrained equivalent simulations was consistent throughout the results, with an average simulation time increase of between 2 to 6 times across all batch and continuous simulations.

This chapter demonstrates the successful application of SFL-Plant constraints for SISO supersaturation control on batch supersaturation control, continuous MSMPR supersaturation control and continuous MSMPR number-weighted mean size control. The SFL-MPC with SFL-Plant constraints in a SISO control strategy demonstrated feasible controller performance and stability for all simulated case studies presented in this chapter. The next step from the SISO control is to explore MIMO control because in a realistic control scenario it would be useful to control multiple outputs or quality attributes instead of one. The following chapter introduces the MIMO SFL technique and MPC for crystallization control.

5 Multiple-Input Multiple-Output Model Predictive Control with State Feedback Linearization and Decoupling for Crystallization

5.1 Introduction

The state feedback linearization technique demonstrated in a single input single output configuration (Kravaris and Chung, 1987) has been successful in controlling supersaturation and crystal mean size. This chapter extends the SISO controller to multiple-input multiple-output (MIMO) systems (Kravaris and Soroush, 1990) to further explore the capabilities of the SFL MPC controller with the SFL-Plant constraints technique. The SFL extension to MIMO will first be defined and then applied to a continuous MSMPR crystallization problem. A similar MIMO control has been applied to the continuous MSMPR elsewhere which includes the use of agitation rate in the kinetic equations for growth and nucleation, and successfully demonstrates how the agitation rate and feed flow rate can be used to control the third moment and temperature of the system, but the application is not of an MPC controller but a PID (Quintana-hern, Tututi-avila and Hern, 2012). In this chapter, a MIMO MPC will be applied to the supersaturation and crystal mean size control by manipulation of crystallizer jacket temperature and seed loading and the overarching aim is to test the applicability of SFL-Plant constraints.

5.2 State-Feedback Linearization MIMO

The exploration of MIMO MPC stems from the desire to control multiple outputs in a process. The procedure for applying SFL to a MIMO system is a direct extension of the SISO SFL technique as detailed by Kravaris and Chung (1987) and the technique will be described here, this technique is fully described by Kravaris and Soroush (1990). To perform MIMO SFL, first the characteristic matrix must be defined (Ha and Gilbert, 1986):

$$C = \begin{bmatrix} L_{g1}L_f^{r_1-1}h_1 & \cdots & L_{g_m}L_f^{r_1-1}h_1 \\ \vdots & \ddots & \vdots \\ L_{g_1}L_f^{r_m-1}h_m & \cdots & L_{g_m}L_f^{r_m-1}h_m \end{bmatrix} \qquad \textit{Equation 5-1}$$

Where the Lie derivatives have their usual meanings. This matrix is valid for an $m \times m$ system of inputs and outputs. The characteristic matrix is used for decoupling every combination of input/output using the same technique described in chapter 4. An important condition must be met to define the characteristic matrix is that each output must have a relative order for

every input. Therefore, the relative orders r_i must be found using the SFL technique for all possible input/output combinations. Plant testing techniques used for cause-effect analysis can be used to ensure that the selected inputs do indeed affect each of the outputs in the system, thus guaranteeing this condition is satisfied. When relative orders have been obtained to populate the characteristic matrix, the next stage is to decouple the system such that each output is controlled exactly by 1 unique input, the process of selecting the pairings of unique inputs to outputs will be described in the following section. A special form of the characteristic matrix Equation 5-1 is used for decoupling as shown here:

$$E = \begin{bmatrix} \beta_{1,r} L_{g1} L_f^{r_1-1} h_1 & \cdots & \beta_{1,r} L_{g_m} L_f^{r_1-1} h_1 \\ \vdots & \ddots & \vdots \\ \beta_{m,r} L_{g_1} L_f^{r_m-1} h_m & \cdots & \beta_{m,r} L_{g_m} L_f^{r_m-1} h_m \end{bmatrix} \quad \textit{Equation 5-2}$$

Where the included β parameters are identified using tuning, but follow the same rules as seen in the SISO SFL case. Thus, to guarantee closed-loop stability, these tuning parameters must have positive real values. The decoupling matrix shows that one value of relative order is used in each row of the matrix. This order is the lowest that exists for that output, which means if the first output y_1(otherwise, h_1) is linearized with respect to two inputs u_1 and u_2, if the relative order for the linearization is r = 1 and 2 respectively, the value of 1 is used in the row. The physical meaning of this is that the input which has the lowest relative order will have the greatest impact on the output, thus the output will be paired with the respective input for control. This can be proved by referring to the following conditions for input/output decoupling, where the relative order is found when the input/output linearization yields a non-zero value:

$$L_g L_f^k \boldsymbol{h}(\boldsymbol{x}) = 0 \qquad k = 0, 1, \ldots, r-2 \quad \textit{Equation 5-3}$$

$$L_g L_f^{r-1} \boldsymbol{h}(\boldsymbol{x}) \neq 0 \quad \textit{Equation 5-4}$$

Extending the example above, when the relative order r is 1 for u_1 and 2 for u_2, if the value of 1 is used in row of the decoupling matrix, the Lie derivative with respect to u_2 will be reduced to 0, thus y_1 will be controlled by u_1 and decoupled from u_2. This principle applies to all inputs and outputs in the decoupling matrix, and hence the inputs and outputs are decoupled (Ha and Gilbert, 1986) and set of pairings between inputs and outputs will emerge.

In cases where inputs have the same relative order when linearized to the same output, further selection criteria are required and then more advanced techniques such as input-output selection (Van De Wal and De Jager, 2001) or sensitivity analyses (Saltelli *et al.*, 2008; Fysikopoulos *et al.*, 2018) can be performed.

Once Equation 5-1 has been populated, it can be implemented into a control law that is specifically designed for MIMO systems but again is an extension of the SISO system. In fact, by setting the number of inputs and outputs to 1, the SISO SFL case will emerge, hence the SISO SFL system appears to be a special case of the MIMO system:

$$u = -E^{-1}\begin{bmatrix} \sum_{k=0}^{r_1} \beta_{1_k} L_f^k x_1 \\ \vdots \\ \sum_{k=0}^{r_n} \beta_{n_k} L_f^k x_n \end{bmatrix} + E^{-1} v \qquad \textit{Equation 5-5}$$

The MIMO SFL control law uses the inverted decoupling matrix is referred to herein as SFLD. For Equation 5-5 to be used to control, the decoupling matrix must be square and invertible (non-singular). The determination of the relationships between inputs and outputs are all performed offline and must be performed only once, following this the tuning can be performed as detailed in chapter 4. The tuning for MIMO is more laborious than for SISO because of the number of additional parameters involved in the SFLD. To simplify the tuning, each decoupled input/output pair will be tuned first in a SISO configuration which follows the method from chapter 4, and the resulting tuning parameters will be combined and applied for MIMO control. There is a drawback in this technique as described by Kravaris and Soroush (1990) which disclose the design of this MIMO linearization based on decoupling the closed-loop response may not yield satisfactory control results, especially when the plant is ill-conditioned or when the β parameters are chosen to uphold closed-loop stability, there will be cases where process performance may deteriorate or yield undesirable results. However, the emphasis of using this technique remains on evaluation of the application of SFL-Plant constraints in MIMO SFLD MPC.

5.2.1 Lie derivatives and controller setup

To populate the decoupling matrix E, first the inputs and outputs must be defined. In this case the outputs are supersaturation and number-weighted crystal mean-size and the first input is the jacket temperature because these have already been studied in the prior chapter. The second input requires some further knowledge of the system to understand the other properties that can be manipulated. From the plant model, the seed moments can be manipulated alongside the inlet conditions for temperature, flow rate and concentration. Considering the control of mean-size and the prior discussions of the results in chapter 4 which describe the effects of seed size and loading on mean-size, it appears the seed loading will be a suitable input. The seed loading is represented in the plant as part of the seed moments, because the moments are defined on the basis of a gram of solvent. The SFL for all four combinations of input/output is performed and the relative orders are summarised in Table 5-1. The lowest order for mean size and supersaturation were both 1, therefore the value of r_1 and r_2 is set to 1 and the decoupling matrix is populated. Hence, the pairings of this MIMO system are the jacket temperature controlling supersaturation and seed loading controlling the mean size. Furthermore, once the decoupling matrix is populated it is then important to ensure the matrix is invertible for use in the SFLD control law, in this case it is invertible. The next step in this procedure is tuning but first some open-loop simulations will be performed on the plant model.

	Mean Size	Super-saturation
Seed Loading	**1**	**2**
Jacket Temperature	**2**	**1**

Table 5-1 – Summary of the relative order from SFL for every input/output pairing

5.2.2 Open-Loop Input-Output Testing

The plant model will be open-loop tested because it is known that the MIMO MPC has been decoupled using SFLD, but the impact of seed loading on mean size and supersaturation has not been established clearly. A simple study on an open-loop simulation of the MSMPR can be performed to assess how changing the jacket temperature and seed loading will affect the steady state position of the MSMPR in the phase diagram and thus the trajectories for the mean size and supersaturation can also be deduced. In the first case, the seed loading is held constant at 0.5 g/L and the jacket temperature set to a fixed value of 305 K, 310 K and 315 K.

The results of the open-loop MSMSPR start-up are shown in Figure 5-1. The second case holds the jacket temperature at 310 K while the seed loading of 0.4, 0.5 and 0.6 g/L are used for the same MSMPR start-up, results shown in Figure 5-2.

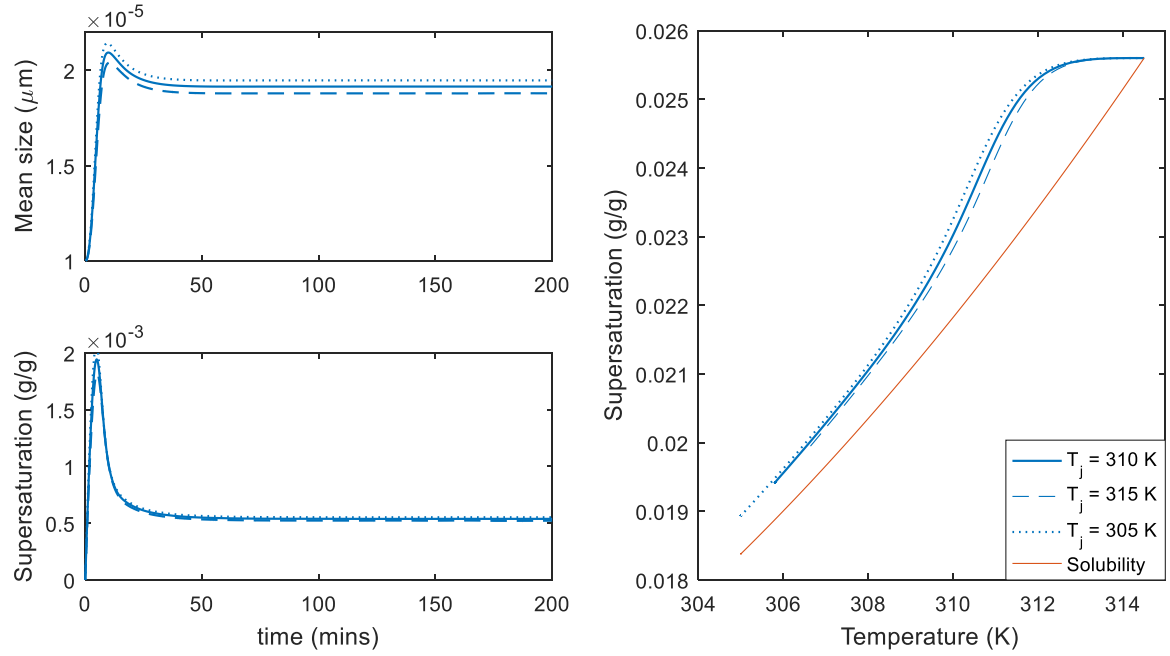

Figure 5-1 - Effect of coolant temperature on mean size and supersaturation

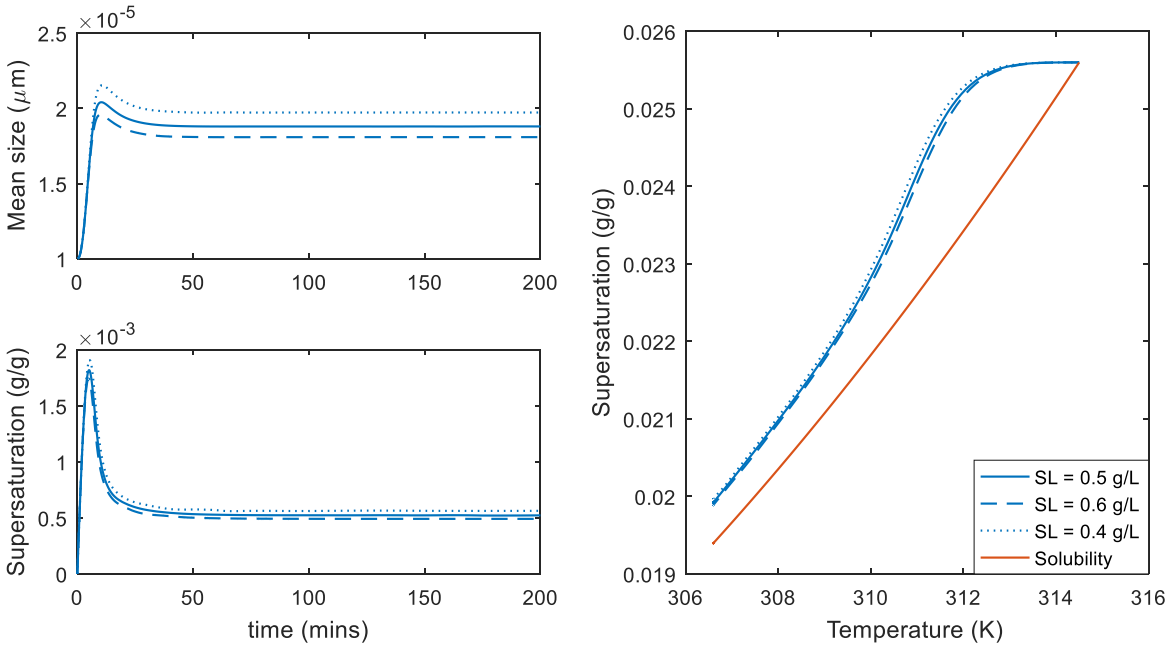

Figure 5-2 - Effect of seed loading on mean size and supersaturation

In both cases it is evident that both inputs affect both outputs. The steady-state mean size and supersaturation values are determined from each case, and using 310 K and 0.5 g/L as

the base case, the change in mean size and supersaturation as a result of changes to seed loading and jacket temperature are shown in Table 5-2, to confirm that each input does indeed affect both outputs. This information is important when considering the closed-loop MIMO MPC with SFLD because although the MPC has decoupled the effects of these inputs, there does exist an interrelationship in the dynamics which will not be captured by the controller, which could lead to undesirable crystallization performance.

	Δ mean size (m)	Δ super-saturation (g/g)
Δ seed loading (g/L)	**-0.0087**	**-0.3815**
Δ jacket temperature (K)	**-6.64E-08**	**-2.90E-06**

Table 5-2 – Summary of the sensitivity of mean size and supersaturation to changes in seed loading and jacket temperature.

5.2.3 MIMO MPC with SFLD Control

This section will detail the MIMO MPC with SFLD starting with defining the control problem and performing tuning on two SISO systems to then complete the tuning of the MIMO system and determine if the SFL-Plant constraints can be applied successfully; the criteria for successful constraint application is feasible input profiles.

5.2.3.1 Objective Function and Constraints

The objective function for the MIMO MPC with SFLD control problem is:

$$\min_{v} J = Q_1 \sum_{i=1}^{N_p} \left(y_{1,i} - y_{1,i,setpoint}\right)^2 + R_1 \sum_{l=1}^{N_c} \Delta v_{1,l}^2 + Q_2 \sum_{i=1}^{N_p} \left(y_{2,i} - y_{2,i,setpoint}\right)^2 + R_2 \sum_{l=1}^{N_c} \Delta v_{2,l}^2 \qquad \text{Equation 5-6}$$

Subject to:

$$273 \leq u_1 = \varphi(\boldsymbol{x}, v) \leq 360$$

$$-2 \leq \Delta u_1 (Kmin^{-1}) = \varphi(\boldsymbol{x_i}, v_i) - \varphi(\boldsymbol{x_{i+1}}, v_{i+1}) \leq 2$$

$$0.25 \leq u_2 = \varphi(\boldsymbol{x}, v) \leq 2.5$$

Given:

$$\boldsymbol{x}$$

$$\dot{\boldsymbol{x}} = f(x) + g(x)u$$

Where u_1 is the jacket temperature, u_2 is seed loading, $y_1$is the supersaturation and y_2 is the crystal mean size. The SFL-Plant constraints are also applied to the absolute value and relative change of the jacket temperature, and also to the absolute value of the seed loading.

The simulation data is from the P/W system as shown in Table 5-3 (Nagy, Chew, *et al.*, 2008a; Nagy, Fujiwara, *et al.*, 2008), meanwhile the initial conditions for the crystallizers are a temperature of 315 K, concentration of 0.0256 g/g initialised with seed moments corresponding to a mean-size of 20 µm and seed loading of 0.5 g/L.

	Value	Units
k_b	$e^{45.8}$	$min^{-1}g^{-1}$
b	6.2	-
k_g	$e^{-4.1}$	$m\ min^{-1}$
g	1.5	-
ρ	1000	kgm^{-3}
k_v	0.24	-
ρ_c	1296	kgm^{-3}
V	1	L
C_{in}	0.0256	g/g
F_{in}/F_{out}	0.07	L/min
K	0.1	-
UA_c	54521	$J\ min^{-1}\ K^{-1}$
T_{in}	305	K

Table 5-3 – Crystallization Data

5.2.3.2 Tuning MIMO MPC with SFLD using SISO MPC

The tuning procedure used will first consider the two decoupled input/output systems as SISO systems to perform the tuning, and the chosen parameters will be combined for the MIMO MPC. The objective function weights for Q and R are set to 1 for the SISO tuning.

5.2.3.2.1 SISO Supersaturation Control Tuning

The SISO supersaturation control tuning was fully detailed in chapter 4. The resulting tuning parameters values of 0.5 and 1 were used for β_0 and β_1, respectively.

5.2.3.2.2 Seed loading

The SISO case for seed loading and mean size has also been evaluated using a similar iterative approach. It was determined that the seed loading should not be less than 0.25 g/L or larger

than 2.5 g/L, thus these constraints were defined using the SFL-Plant constraints method. The MPC objective function used for tuning is:

$$\min_{v} J = \sum_{i=1}^{5} \left(y_i - y_{i,setpoint}\right)^2 + \sum_{l=1}^{5} \Delta v_l^2 \qquad \textit{Equation 5-7}$$

Subject to: $$0.25 \leq u = \varphi(\boldsymbol{x}, v) \leq 2.5$$

Given: $$\boldsymbol{x}$$
$$\dot{\boldsymbol{x}} = f(x) + g(x)u$$

The main results from this tuning were that the seed size appears to be very sensitive to the seed loading and many combinations of tuning parameters needed to be used to establish a stable and desirable control response. It was found that the value of β_0 had significantly less impact on the overall control response than β_1. For the latter, a value less than 25 resulted in significant oscillations in the seed loading throughout the simulation and values over 50 resulted in a very slow response and convergence to setpoint, longer than the 300-minute simulation used for tuning. Three tuning simulations are shown where β_1 is 30, 40 and 50 in Figure 5-3, Figure 5-4 and Figure 5-5 respectively.

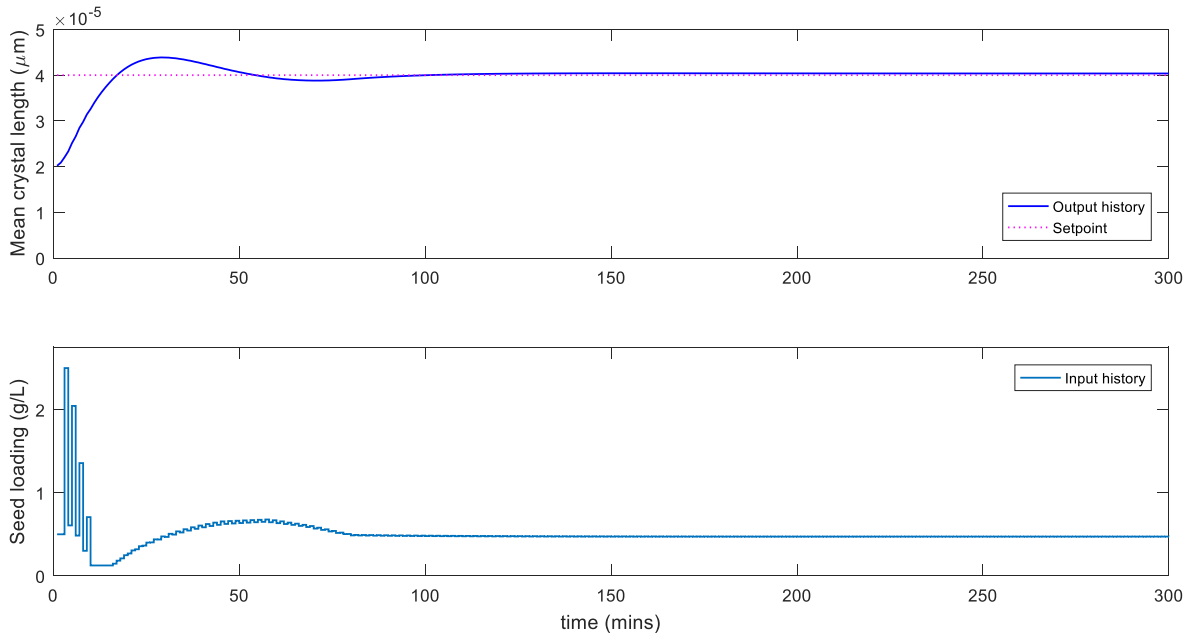

Figure 5-3 - Mean size control – β_1 = 30

The results in Figure 5-3 show the mean size of crystals increasing from 20 µm, overshooting the set-point of 40 µm and finally converging to within 2% of the target at 82 minutes and stabilized within 1% of the target after 125 minutes. The corresponding seed loading sees

some oscillations at the beginning, including saturation at the highest and lowest allowed seed loading as per the bounds, but this subsided after 15 minutes and was common to all three results that are presented here. The oscillation could not be avoided despite efforts to change the tuning parameters, this is one of the inherent difficulties with this form of input/output linearization; tuning parameters can be chosen to ensure a convergence but in comparison to traditional linear systems with linear MPC, the parameters cannot be chosen intuitively (Kravaris and Soroush, 1990; Kravaris, 1988). There is a transient change in the loading up to 82 minutes, beyond which the loading stabilizes with some minor oscillations. Finally, the trajectory is smooth after 125 minutes, simultaneously the output trajectory also stabilises. Though the result was considered acceptable as the mean size difference between the set-point and trajectory was 0.04 µm, other controller tuning parameters were tested to see if a value closer to 40 µm could be obtained.

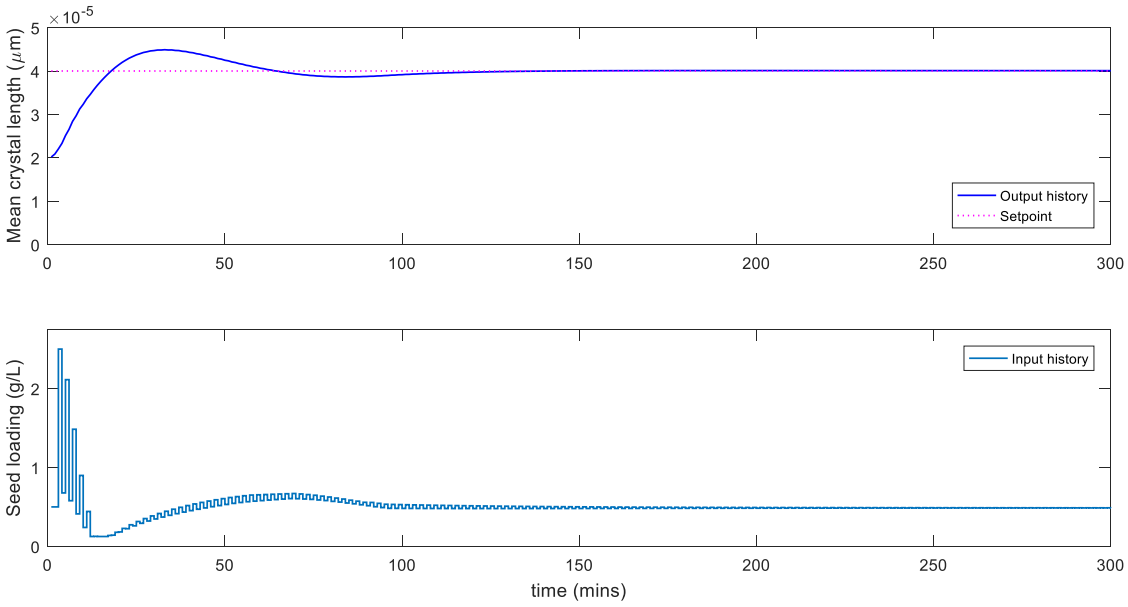

Figure 5-4 - Mean size control – $\beta_1 = 40$

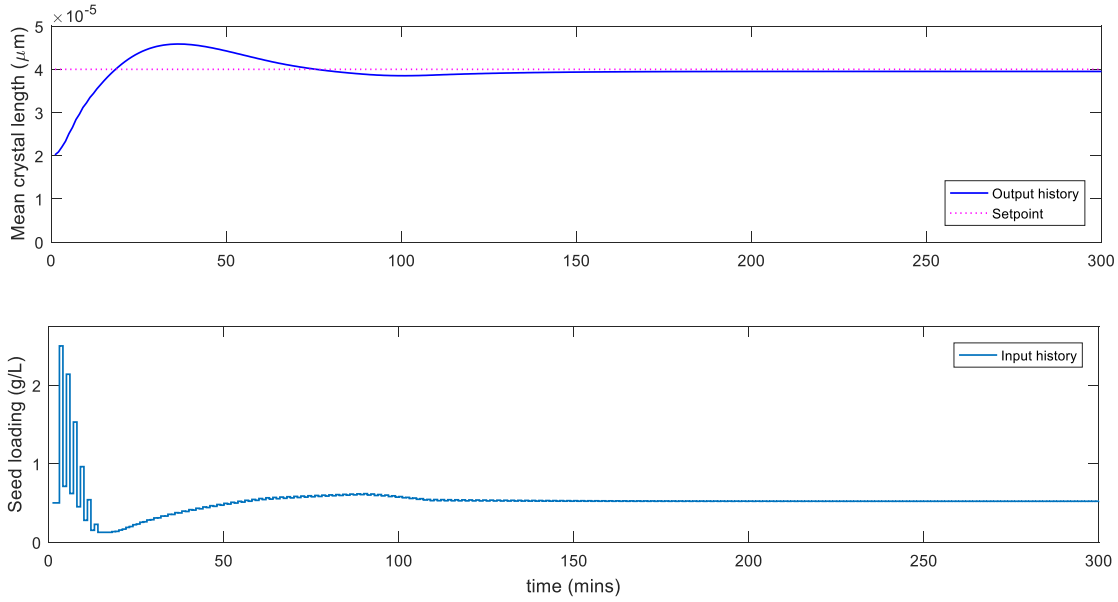

Figure 5-5 - Mean size control – β_1= 50

Subsequently, the results in Figure 5-4 show the best case for set-point convergence where β_1 is 40, the mean size was within 2% at 100 minutes and the trajectory finally stabilised to within 0.25% of the set-point at 130 minutes. In addition to requiring more time to reach steady state, the seed loading trajectory has a noticeably greater magnitude in oscillation which would require the seeding mechanism to change the loading every minute. The oscillations were more pronounced as compared to the previous tuning settings but eventually the input oscillations did stabilize and disappear after 250 minutes. For a final comparison, the case where β_1 is 50 shows the mean size within 2% of the set-point at 135 minutes and stabilizing within 1.25% after 190 minutes. In conjunction to this, the seed loading sees some oscillatory behaviour again followed by a transient change to seed loading through the start-up procedure in the first 120 minutes and the seed loading is stabilized at 190 minutes. The larger value of β_1 in this range resulted in longer time to reach steady state. There was no direct correlation between the tuning value to the set-point error, because when the value of 40 was chosen the mean size at steady state was closest to the set-point, but it was further from setpoint at 30 and furthest at 50.

This decaying oscillatory response at the beginning of these simulations could be due to some plant-model mismatch which causes an instability in the control moves, but further actions could be taken to mitigate these. The first option would be to apply significantly larger input weights on the seed loading to prevent the oscillations. Another way to prevent the

oscillations would be to apply an input rate limit, thus preventing the seed loading from changing significantly from one-time step to the next. It is possible to facilitated these constraints in the constraints handling function. Furthermore, there may be a need for more complex linear models to capture the input/output behaviour for seed loading onto crystal mean size, and a further analysis on the plant-model mismatch is likely to indicate this; alternatively it may be more suitable to select a different input instead of seed loading to control the mean size.

Though these results demonstrate the impact of the controller tuning parameters for SFL, the decision was made to use the value of 40 for β_1 despite the oscillatory behaviour in the input trajectory. The SFL-Plant constraints applied to the seed loading in all three simulations were also satisfied, so all the input trajectories were again feasible. Therefore, with the two separate SISO test cases, a starting point for MIMO MPC with SFLD is now established.

5.2.4 MIMO MPC with SFLD Framework

The MIMO SFLD framework is an extended version of the SISO framework as seen in Figure 5-6. The SFL control law is replaced with the SFLD law and for each input/output mapping there is a unique linearization model. The MPC handles these models internally and the optimisation for MIMO is handled as a single weighted objective function with all inputs and outputs integrated into one objective. The weightings require consideration to ensure that one objective isn't favoured over another due to differences in the order of magnitude of the values.

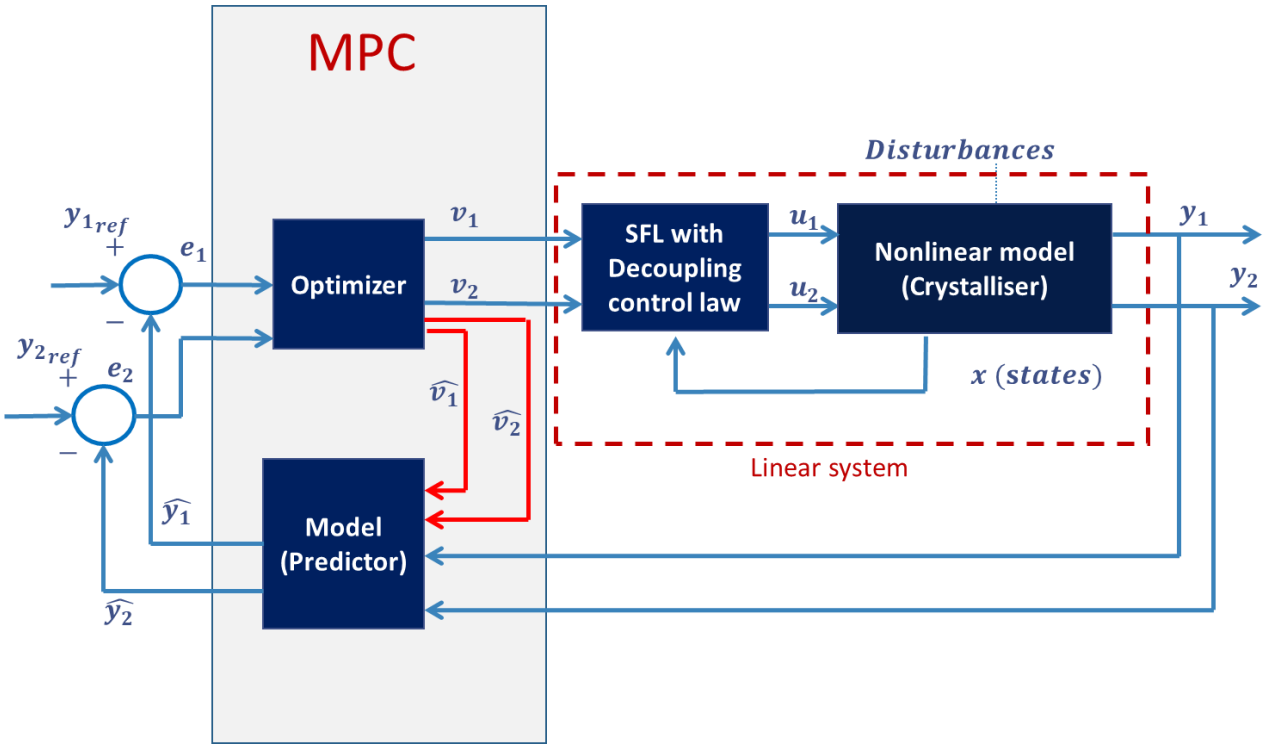

Figure 5-6 – MIMO MPC with SFLD Framework

5.2.5 MPC data

The control set points, weightings and tuning parameters are summarised in Table 5-4. The initial conditions of the MSMPR consist of moments which are all equal to the seed moments obtained using the initial seed loading of 0.5 g L^{-1} for a 10 µm seed with 1 µm standard deviation, normally distributed. The concentration is 0.0256 g/g and the temperature is 315 K. The tuning parameters shown in the table are from the SISO results, but further tuning was required when they were implemented into the MIMO case so the changes have been indicated with (MIMO) in the table. the mean size β_1 is adjusted in the results section to observe the impact on controllability of the crystallizer. The set-point for mean size (y_{ref_2}) of 21 µm and 20 µm are used and clearly indicated in the respective results discussion. The crystallizer volume is 1 L and with a flow rate of 0.07 L min^{-1}, the resulting mean residence time is 14.28 mins. The prediction and control horizons are set to 10.

	Value	Units
Supersaturation β_0	0.5	-
Supersaturation β_1	1	-
Mean size β_0	1	-
Mean size β_1	40, 18 (MIMO)	-
Q (supersat)	1	-
R (supersat)	1	-

Q (Mean size)	1	-
R (Mean size)	1	-
Q_1 (MIMO)	0.1	-
R_1 (MIMO)	50000	-
Q_2 (MIMO)	0.1	-
R_2 (MIMO)	100000	-
y_{ref_1}	0.0006	g/g
y_{ref_2}	20, 21(MIMO)	µm

Table 5-4 – Controller data

5.2.6 MIMO MPC with SFLD Results

The objective function for the MIMO study combines the objectives of both outputs and inputs into a single cost function, the weighting matrices ($Q_1, Q_2, R_1 \; and \; R_2$) needed to be assigned with appropriate values to ensure the numerical values from one objective did not dominate the objective function. The weighting was first adjusted based on the magnitude of the inputs and outputs. For MIMO tuning, the parameter for β_1 for the seed loading which was tuned to 40 resulted in instability for MIMO MPC. Therefore, while the SISO supersaturation tuning parameters were directly transferrable to MIMO, the mean size controller parameters were not, so further tuning of a β_1 was required. Then to test the sensitivity of the mean size tuning parameter to changes in the setpoint, the mean size set-point was changed from 20 µm to 21 µm. A greater change than this would not be suitable given the strong coupling between the supersaturation and mean size as determined from open-loop simulation. Three sets of results are shown whose tuning parameters are in Table 5-5.

Case	$\beta_{0,ss}$	$\beta_{1,ss}$	$\beta_{0,ms}$	$\beta_{1,ms}$	y_{ref1}	y_{ref2}
1	0.5	1	1	18	0.0006	20 µm
2	0.5	1	1	18	0.0006	21 µm
3	0.5	1	1	24	0.0006	21 µm

Table 5-5 – Overview of tuning parameters and setpoints for MIMO results

The value of β_1 for mean-size is referred to as $\beta_{1,ms}$. After iteratively tuning $\beta_{1,ms}$ for the 20 µm setpoint, the value of 18 for was found to show good control with a reasonable seed loading profile. The results are shown in Figure 5-7. The supersaturation converged to within 1% of the set-point after 50 minutes and remained there throughout the simulation, and the coolant temperature during start-up did reach the upper limit of 320 K but then gradually decreased as the system attempted to approach steady state. The mean size stabilized to within 3% of the set-point after 100 minutes but the seed loading exhibited small oscillatory

behaviour after 50 minutes. The seed loading appeared to be increasing at the end of the simulation, so the steady state of the MSMPR was likely not reached in the 450-minute simulation and will require more time to reach steady state. However, given the input changes were very small towards the end, the MSMPR was likely to be close to the steady state in the phase diagram. Consequently, the simulation was ended at 450 minutes. The SFL-Plant constraints were upheld throughout this simulation

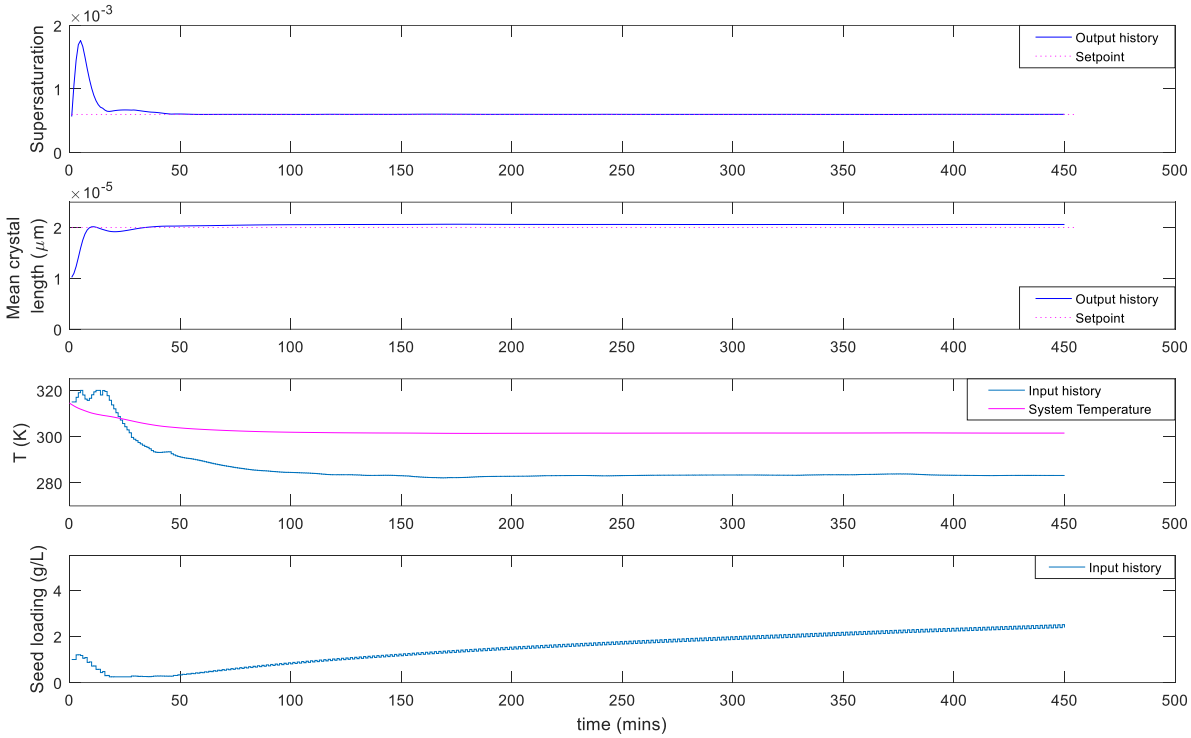

Figure 5-7 – MIMO control – β_1= 18, y_{ref_2}= 20μm

Using the same tuning parameters and changing the mean size target to 21 μm, the resulting simulation is shown in Figure 5-8. The main differences here from the previous simulation are that the seed loading immediately had oscillations which never converged to a stable value or trajectory, although the general shape of the trajectory is similar to that of the previous case. The input profile for the coolant temperature was smooth at the beginning but only up to 140 minutes, coincidentally this is where the upper limit of seed loading is encountered. When the seed loading is saturated at the upper limit, the coolant temperature profile is affected by some oscillatory behaviour, but the magnitude of these oscillations is likely limited by the rate of change constraint on the temperature input, therefore the SFL-Plant constraints are upheld. The supersaturation was within 1% of the set-point until the seed loading reached the high limit and then there were minor deviations throughout the remainder of the

simulation. The supersaturation did remain within 5% of the set-point despite the coolant temperature fluctuations. Similarly, the mean size was within 2% of the target at 140 minutes. These results suggest that as the MSMPR is cooling and crystal growth is taking place, there is an increase in the seed loading to increase the number of crystals being seeded into the system, the controller does this to remain close to the mean size target. There appear to be some coupled effects between the two input/output pairings and when one input reaches the constraint limit, the MPC appears to manipulate the second input more aggressively. Adding this to the difficulty of establishing adequate tuning parameters across a wider range of setpoints does make MIMO MPC with SFLD of this system a difficult control procedure to recommend. The sensitivity to these tuning parameters does suggest that there is a requirement for conditional tuning parameters with this MIMO MPC with SFLD. The suggested improvements from the previous section, including the addition of input rate limits, may be a better control approach for this system.

In the final simulation (Figure 5-9) an attempt was made to re-tune the controller parameter for the mean size target of 21 µm and a value of 24 had the best control response for both mean size and supersaturation. The supersaturation was within 1% of target after 80 minutes and the mean size within 2% at the same time. The temperature profile performed a cooling ramp at the beginning of simulation, reaching the bottom limit, and then there was an increase in coolant temperature to 280.5 K where it stabilized after 190 minutes. Similarly, the seed loading decreased down to the lower limit but then exhibited some oscillatory behaviour throughout the process after 50 minutes. After 190 minutes, the seed loading remained within the range of 0.253 and 0.289 gL^{-1} for the remainder of the simulation. This set of results also shows that the temperature of the coolant is as low as the first case in Figure 5-7, but where the seed loading was increased to maintain 20 µm previously, it is now remaining low to maintain 21 µm target, which is reasonable. The controller performance for this case is therefore acceptable and the SFL-Plant constraints are again feasible.

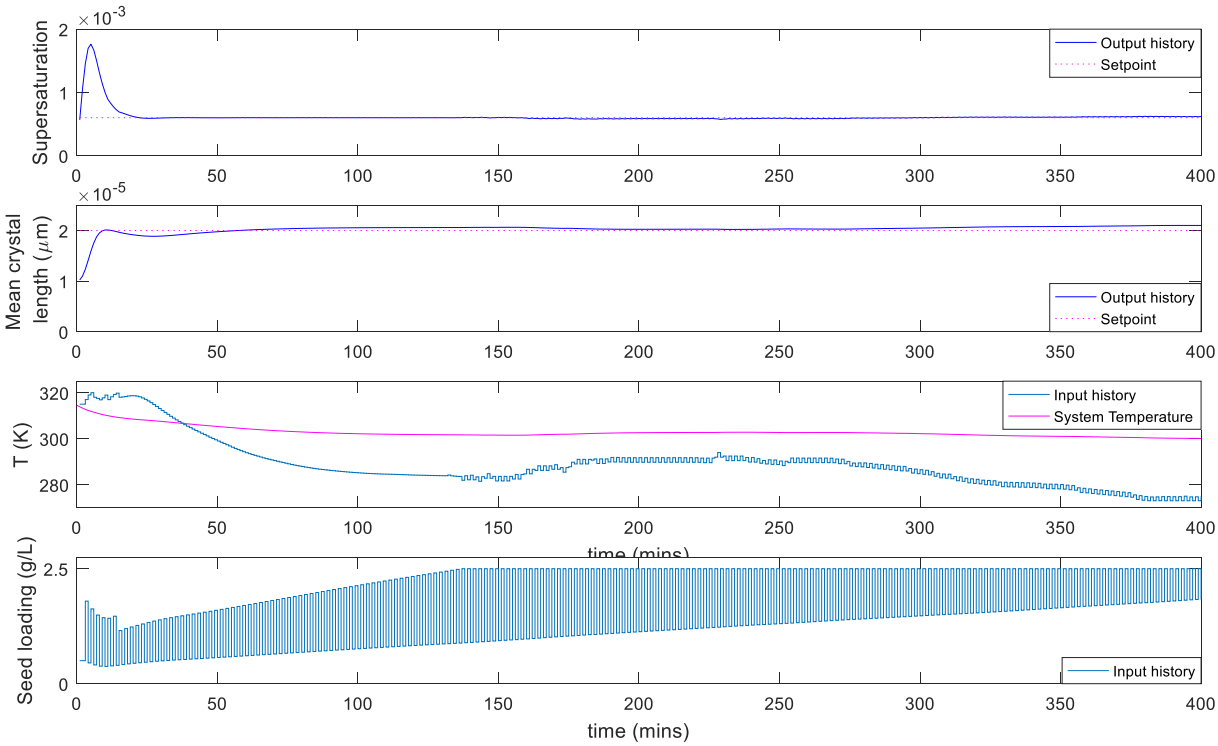

Figure 5-8 – MIMO control – β_1= 18, y_{ref_2}= 21µm

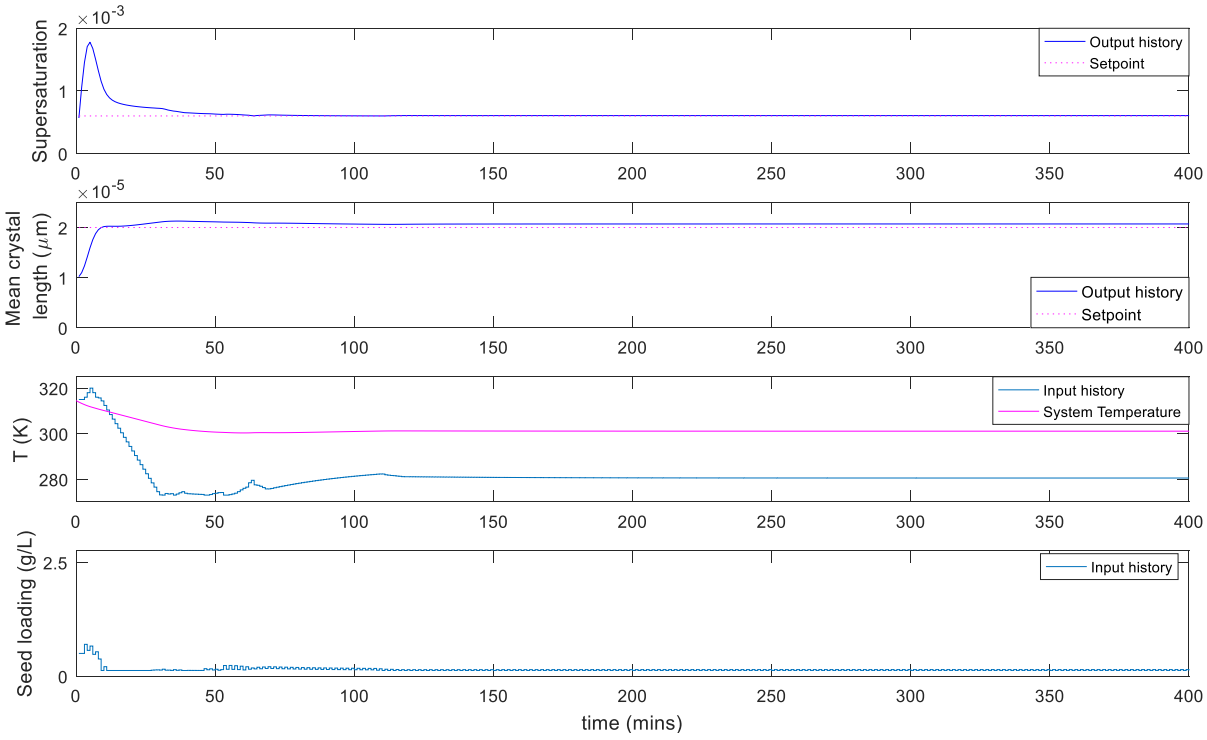

Figure 5-9 – MIMO control – β_1= 24, y_{ref_2}= 21µm

In all the MIMO cases, it was not possible to achieve both output targets exactly given the highly coupled nature of supersaturation and mean size in the crystallization system being simulated, this is one of the disadvantages that was mentioned by Kravaris and Soroush

(1990). The decoupling in SFLD attempts to decouple as best possible the two input and output pairings, but when one of the inputs becomes saturated there has been an observed impact on the other input. The exact origin of this has not been determined mainly because with the presence of linearization, decoupling, control tuning and optimisation problem solving; it is very difficult to trace the cause. Overall, the results show the importance of selecting controller tuning and objective function weights in a MIMO MPC with SFLD scheme as these can have a significant impact on the simulation results, especially when seed loading is used to control mean size. Significant effort is also required to find the best tuning parameters and likely will not be transferable to different setpoints, which is a drawback to this technique. If a good set of tuning parameters exist for a decoupled system, they would best be found through a global optimisation method. Otherwise, a unique set of tuning parameters will need to be identified each time there is a change to setpoints. In all the cases of MIMO MPC with SFLD that were simulated, the SFL-Plant constraints were used successfully and therefore this technique for is indeed usable for SISO and MIMO SFL MPC.

5.3 Conclusions

This chapter covers the development process of a MIMO MPC with SFLD for a cooling MSMPR crystallization process. The development workflow begins with the MIMO SFLD methodology which extends the SISO SFL methodology from the previous chapter. Two inputs (jacket temperature and seed loading) and two outputs (supersaturation and crystal mean size) are then selected for performing SFLD, resulting in the pairing of jacket temperature to control supersaturation and seed loading to control mean-size. Subsequent open-loop simulations demonstrated the highly coupled relationship of seed loading and temperature to both outputs and the MIMO MPC was tuned.

It was found that while it was possible to transfer the tuning parameters from SISO supersaturation control to MIMO, the transferal from the SISO mean-size control using seed-loading did not yield stable results in a MIMO configuration. Thus, the MIMO MPC required retuning and it was found that the mean-size control was sensitive to changes in setpoint too of as little as 20 µm to 21 µm. Overall, these limitations were expected because various limitations were stated prior by Kravaris and Soroush (1990), but the successful application of MIMO SFLD on crystallization was shown by Quintana-Hernandez $et\ al.$ (2015) for a system where agitation rate was also used in the model, so there may be other systems for which the

MIMO SFLD can be successfully applied without the limitations seen in the configuration detailed in this chapter. The main outcome from this chapter is that the SFL-Plant constraints were successfully applied to the MIMO SFLD framework and have shown the same success in application as for the SISO case, but it would be important to consider alternative control problems which either limit the seed loading input rate, or consider the use of a different input to control mean size.

6 Comparative Study of SFL-MPC and ARX-MPC applied to Seeded Batch Crystallization

6.1 Introduction

The contributions in previous chapters have focussed on the use of mechanistic models with successful application of the SFL MPC in SISO configurations for batch and continuous MSMPR crystallization with SFL-Plant constraints. This now leads into a comparison of the SFL MPC with other modelling and MPC techniques used in industry. Comparisons of MPC techniques for crystallization have been performed and the results disclosed in literature, the most significant publication relevant to crystallization MPC comparison was from Shen *et al.* (1999) who compared SFL (named global linearizing control) with multi-model MPC, generic model control with a PI regulator, and PID control. The focus of this chapter is to compare the SISO MPC with SFL against a data driven modelling technique that is commonly used for MPC in industrial applications (Qin and Badgwell, 1997, 2003). Furthermore, in all of the prior SFL MPC case studies disclosed in this research the plant and model were a perfect match and the MPC simulation was performed in MATLAB. This chapter will introduce the implementation of the SFL MPC in a new environment, to be used in an industrial software used for data analysis, optimization, monitoring and process control, PharmaMV (PMV), from Perceptive Engineering Ltd. The plant will be a batch crystallization simulation built in gPROMS Formulated Products (gFP), solved using a higher order finite volume method (FVM), thus introducing a plant-model mismatch. The use of separate platforms for MPC and plant simulation also introduces the need to form an interface between both platforms. This is a common requirement in industry when controlling process equipment through a distributed control system (DCS). The performance of the SISO MPC with SFL is compared with a SISO MPC with autoregression model with exogenous input (ARX) (Jensen, Lindholm and Henneberg, 1996).

This chapter will begin by introducing the new crystallization system and the separate software platforms used for plant simulation and control. The model identification discussion will follow because the ARX model identification is performed using both software platforms.

6.2 Crystallization System

The crystallization system in this study is paracetamol crystallization in isopropyl alcohol (IPA) referred to as P/IPA herein. As Granberg and Rasmuson (1999) reports, paracetamol has a higher solubility in IPA than in water, and is another common crystallization system for paracetamol, making the P/IPA system a good candidate system for this study. The chemical and thermodynamic data used for P/IPA is shown in Table 6-1 (Ålander, Uusi-Penttilä and Rasmuson, 2004). The solubility, heat capacity of the crystal (c) and solvent (s) and density of the solvent are determined using Euqation 6-1 to 6-4, respectively.

$$C^* = A_0 + A_1 T + A_2 T^2 \qquad \textit{Equation 6-1}$$

$$c_{p,c} = B_0 + B_1 T \qquad \textit{Equation 6-2}$$

$$c_{p,s} = C_0 + C_1 T \qquad \textit{Equation 6-3}$$

$$\rho_s = D_0 + D_1 T \qquad \textit{Equation 6-4}$$

Parameter	Value	Units
Solubility Coefficients		
$\boldsymbol{A_0}$	1.03992	kg/m^3
$\boldsymbol{A_1}$	-7.24E-03	kg/m^3K
$\boldsymbol{A_2}$	1.27E-05	kg/m^3K^2
Heat capacity coefficients		
$\boldsymbol{B_0}$	531.04	J/kgK
$\boldsymbol{B_1}$	6.458	J/kgK^2
$\boldsymbol{C_0}$	-403.71	J/kgK
$\boldsymbol{C_1}$	1.31E+01	J/kgK^2
Density coefficients		
$\boldsymbol{D_0}$	1066.36	J/kgK
$\boldsymbol{D_1}$	-8.96E-01	J/kgK^2
$\boldsymbol{\rho_c}$	1200	kg/m^3
$\boldsymbol{\Delta H_c}$	0	J/kg
$\boldsymbol{k_v}$	0.24	

Table 6-1 – Batch Crystallization Properties for Paracetamol/IPA

The seeded batch crystallization plant model is a defined in Equation 6-5 to Equation 6-11. The full size-distribution is calculated using finite volume method with 50 grid points, and the

system only has growth kinetics and no nucleation. In this crystallization model it is the supersaturation ratio (S_r) which is the output, changed to represent a new control problem, and furthermore the input is the coolant temperature (T_j)

$$\frac{\partial f_n(L)}{\partial t} = G\frac{\partial [f(L)]}{\partial L} \quad \text{Equation 6-5}$$

$$\frac{dC}{dt} = -k_v\rho_c(3G\mu_2 + Br_0^3) \quad \text{Equation 6-6}$$

$$\frac{dT}{dt} = -\frac{3\rho_c k_v G\mu_2 \Delta H}{\rho c_p} - \frac{UA_c}{\rho V c_p}(T - T_j) \quad \text{Equation 6-7}$$

$$G = k_g(S)^g \quad \text{Equation 6-8}$$

$$S = C - C^* \quad \text{Equation 6-9}$$

$$C^*(T) = A_0 + A_1T + A_2T^2 \quad \text{Equation 6-10}$$

$$y = S_r = C/C^* \quad \text{Equation 6-11}$$

6.3 Model Identification

The aim of this study is to compare the performance of an ARX MPC and SFL MPC. The ARX modelling in PharmaMV is applied to input-output discrete-time data, obtained using a black box system identification approach, otherwise referred to as plant-testing, by applying some inputs to a process and observing the output at discrete points in time (Johansson, 1993). In this case the plant is the batch crystallization model defined in Equation 6-5 to 6-10 solved using the finite volume method and the input-output data is obtained from this virtual plant, but the same identification approach can be used on a real plant in practice. The following sub-sections will discuss ARX modelling.

6.3.1 ARX Model

The ARX is a polynomial input-output regression model used to describe dynamic systems and can be applied to discrete-time data. Identification of an ARX system model is commonplace for process dynamics and control analysis (Jensen, Lindholm and Henneberg, 1996) and has been used across the oil and gas, fine chemicals, wastewater treatment and pharmaceutical industries for system identification and modelling for process control (Swaanenburg *et al.*, 1985; García, Prett and Morari, 1989a; Simani, Fantuzzi and Beghelli, 2000; Casanova-Peláez

et al., 2012; Rincón, Roux and Lima, 2015). The widespread use of this technique is the reason for performing the comparison with SFL-MPC. A linear ARX model will be identified for the batch crystallization system. The ARX model is of the form shown in Equation 6-12.

$$y_k = \Sigma_{i=1}^{n_a} a_i y_{k-i} + \Sigma_{i=1}^{n_b} b_i u_{k-i} + e_k \qquad \textit{Equation 6-12}$$

In this form, a_i is the i^{th} coefficient for the output term and b_i is the i^{th} coefficient for the input term, with the error residuals being stored in the error term, e, and n_b is the number of past inputs (u) used to determine the output prediction. The linear first order ARX model has one coefficient for a, thus n_a is 1, but higher order ARX models can also be identified using this same method. This type of modelling requires input-output data which can collected by subjecting the plant to a series of inputs and observing the outputs (Mullen and Jebwab, 1995; Qin and Badgwell, 1997). The input and output data are time-aligned and using a least-squares approach the coefficients of a and b are identified. The significance of both coefficients will now be discussed.

The b coefficient is the extent to which the inputs will affect the output. The a coefficient represents the extent to which a model prediction is based on past values of the output, thus larger values of a relative to b will result in the model prediction being greatly influenced by the output value instead of the input. The significance of this is the ARX model has the ability to reject disturbances. This can be proved when compared to a simple Finite Impulse Response (FIR) model whose structure is shown in Equation 6-13 and can be achieved when the ARX coefficient a is set to 0 in Equation 6-12.

$$y_k = \Sigma_{i=1}^{n_b} b_i u_{k-i} + e_k \qquad \textit{Equation 6-13}$$

In the FIR model (Nikolaou and Vuthandam, 1998), the output prediction is solely dependent on the inputs and the coefficients of b_i, irrespective of the current measured output value. Consequently, when a fixed sequence of inputs is supplied to the FIR model, the output prediction will always be the same, whereas for an ARX model the output prediction will be different for the same set of inputs if the previous value of the output, y_k, is also different. This results in the ARX model having the ability to reject disturbances more effectively if a is

nonzero, however there is a trade-off because very small values of a will behave closer to an FIR model, whereas very large values of a relative to b will dominate the output prediction and the inputs will have virtually no influence on the output prediction (Wise and Ricker, 1990).

In a process where a clear input-output (or cause-effect) relationship can be determined, obtaining suitable parameters for the ARX model for control will be dependent on the quality of the data used for modelling and the discrete time interval specified for modelling. For the modelling in this system, every sample point will be used to ensure the dynamics of the process output are fully captured when input changes are made. The time interval of the measurements being obtained from the plant is also set equal to the MPC interval, thus ensuring the plant data is not over-sampled as would be the case if multiple measurements were taken between each MPC intervention.

6.3.2 Input-Output Data Acquisition

The input-output data is obtained by using conventional plant-testing methods on the plant (Johansson, 1993) and PharmaMV has adopted a plant testing method for identifying system dynamics –pseudo-random binary sequence (PRBS). The PRBS is a random number generator for a sequence of two numbers, a high value and a low value. This tool allows the black-box process input-output data collection to be automated and the technique has been used in literature for identification of models for process control (Mullen and Jebwab, 1995). Each input value in the binary sequence must be held for sufficient time to determine the dynamics of the output. For a dynamic batch process, it must be ensured that the duration of each input change is long enough to obtain sufficient output data and identify the dynamics, so if a change in input requires 2 samples before the output begins to change and a further 4 samples for the output dynamics to be measured, a total of 6 samples would be required to define the input-output relationship. In this case it was determined that changing the input required a 1 sample delay before the output also began to change and by the 5th sample, the major dynamic changes in output had been fully observed. To clarify this further, in a batch crystallization if the cooling rate is set to 1 K/min the supersaturation change will indeed change at a nonlinear rate as the batch progresses due to the nonlinear supersaturation profile. However, if the cooling rate is suddenly changed to a heating rate of 1 K/min the supersaturation profile would quickly change direction and the dynamics of the direction

change will be captured. This is the information that will be used to identify the model. Multiple steps are necessary to capture any variability in the output response and gain statistical confidence in the model prediction (Marshall *et al.*, 1998).

The PRBS for the batch crystallization simulation is configured to target a crystallization temperature setpoint in the temperature controller, and the output is the supersaturation ratio which is calculated using the concentration and temperature information from the simulation. The PRBS is configured to apply temperature change rates of -1 and 1 K/min with a minimum time of 10 simulated minutes and the maximum time of 20 mins. The PRBS is run for a cycle of 15 changes in the ramp from -1 and 1 K/min. This configuration will ensure a sufficiently large dataset of dynamic data for modelling. Furthermore, the plant is initialised at a supersaturation ratio of 1.1 (see Table 6-5) and using the input conditions above, it was observed that the supersaturation profile remained centred around the region for a supersaturation ratio of 1.1; identifying the ARX model in this region will also allow a second comparison to be made with how the ARX-MPC performs when a model identified around supersaturation ratio target of 1.1 is applied to control the process at a supersaturation target up to 1.4.

ARX Coefficients	
a_1	-0.972
b_1	-0.0167
b_2	-1.3684
b_3	-0.0265
b_4	-0.0142
b_5	-0.0013

Table 6-2 – ARX Coefficients identified for ARX Model using PRBS testing on Batch Crystallization System

The ARX model coefficients are identified using a least squares algorithm in PharmaMV. The input and output data are provided to compute the ARX coefficients of the model. The sampling time for the model was set to 1 minute and is set based on the time that would be required to obtain new measured data from in-line sensors using in crystallization such as FBRM and other spectroscopic devices. The resulting ARX coefficients are shown in Table 6-2. This model has a large coefficient for a_1 and thus the supersaturation ratio prediction will be largely reliant on the previous value of supersaturation ratio. This is acceptable, because the same rate of cooling or heating can result in very different values of supersaturation ratio

depending on where the batch is currently operating. The supersaturation ratio trajectory for the crystallization process is a nonlinear curve in the phase diagram.

Given the growth rate is a function of supersaturation, maintaining the supersaturation ratio target trajectory will result in a fixed growth rate throughout the batch process. Therefore, to maintain the supersaturation ratio target as the dissolved solute concentration in the batch is crystallised, a progressively faster cooling rate is required. This behaviour is captured in the ARX model which relies heavily on the current value of the supersaturation ratio alongside the past inputs to predict the supersaturation ratio trajectory in the future.

6.3.3 SFL-MPC Model

The SFL model identified in previous chapters for supersaturation control using jacket temperature is used in the SFL MPC. The tuning parameters were re-identified for the SFL-MPC and it was found that for the new process model, a value of 1 and 80 are used for β_0 and β_1, respectively. The paracetamol-IPA system has different parameters to the previously discussed P/W system, consequently the SFL model will use the new parameters in Table 6-1. These data are sufficient to fully describe the SFL-MPC model.

6.4 Batch Crystallization Simulation

The software used for simulation is gPROMS Formulated Products (gFP). The batch crystallization model is created in gFP as shown in Figure 6-1. In the gFP environment, there is a flowsheet development environment and a set of blocks; the configured flowsheet is shown in the figure. The *vessel* block is the crystallizer. The *blank_inlet* and *blank_output* nodes attached to the vessel signify that there is no material entering or leaving the vessel, therefore it is a closed (batch) system. The *global_spec* block is a global specifications block holds the information for all the materials used in the flowsheet and contained all the thermodynamic data for the API and solvent used in this crystallization system. The *TC* block is a temperature controller attached to the vessel, allowing the vessel temperature to be controlled. There are two further blocks which are sensors: *liquid_composition_sensor* which is used to track the concentration of the batch solution, and the *PSD_sensor* to track the particle size distribution. This completes the flowsheet setup of the plant in the MPC framework.

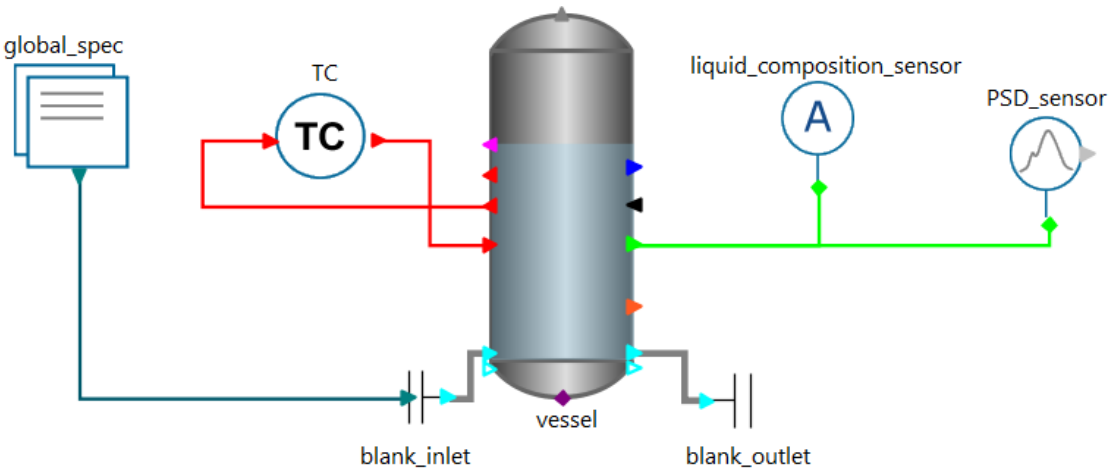

Figure 6-1 – Batch Crystallization Flowsheet in gPROMS Formulated Products

The paracetamol and isopropyl alcohol physical, chemical and thermodynamic parameters are shown in Table 6-1 and are contained within the *global_spec* block.

The crystallization process is seeded and operated batchwise with a growth mechanism represented by a power law relationship as a function of absolute supersaturation; other crystallization mechanisms (nucleation, agglomeration and breakage) have been disabled. The parameters that must be defined in this block are the growth equation parameters, the seed parameters, working volume, impeller parameters and initial conditions, all summarised in Table 6-3.

Batch Crystallizer Properties		
Vessel Volume	3	L
Impeller Diameter	0.1	m
Impeller Frequency	200	rpm
Impeller Power Number	0.4	
Growth Rate Constant	4.00E-06	m/s
Growth Order	1	
Seed loading	0.5	g/L
Seed Size	100	μm

Table 6-3 – Batch Crystallizer Properties in gFP

In the TC block, the minimum and maximum heat transfer rate to the system can be defined as well as the type of control applied to the crystallizer temperature. In this case, a Proportional-Integral (PI) controller is used, which will receive a cooling or heating temperature ramp from the MPC and will apply this to the batch crystallization. The parameters in the TC block are summarised in Table 6-4.

TC Properties		
TC Controller Type	PI	
Maximum Heat Transfer Rate	1000	W
Bias	0	W
Gain	1	W/K
Integral Time	6	s

Table 6-4 – TC Block Properties in gFP

The liquid composition sensor will analyse the solute concentration of the system and the PSD sensor is an ideal particle analyser which will track the CSD during the batch, an inherent limitation of this system is that the CSD will cannot be tracked in-line in a real system the same way the PSD sensor tracks the CSD. Other parameters that can be obtained from the PSD sensor are the moments calculated from the CSD, these moments ensure compatibility with the SFL-MPC technique which uses a mechanistic model based on moments. The gFP batch crystallization is set to report at an interval of 1 minute, meaning every instance that the gFP simulation is triggered, it will simulate 1 minute of the batch and the states and outputs at the end of the 1 minute period will be the measured/sampled data that is fed into PMV control software to represent plant measurements. The PharmaMV controller will also transfer a new process temperature setpoint at 1-minute intervals to the temperature controller. Once sent, over the duration of the 1 minute plant simulation, the TC will implement the crystallizer temperature setpoint using the built-in PI temperature controller (Figure 6-2). During the testing phase of this plant simulation, it was discovered that the TC can achieve perfect temperature control over the 1 minute interval for a temperature change of up to 2 K/min with the parameters defined in Tale 6-4. It is also important to note this is a form of supervisory control, where the PI temperature controller in the gFP block is the low-level controller to which the MPC sends supervisory setpoints of the temperature ramp rate. In this case y is the supersaturation ratio and x is the states which include the moments, temperature and concentration of the crystallizer.

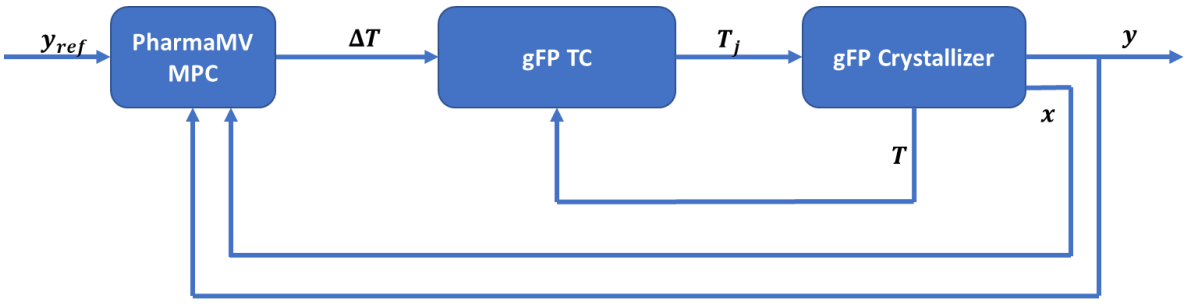

Figure 6-2 – PharmaMV MPC – gFP TC Control structure

6.5 Control Framework

The control software is the PharmaMV platform, which has built-in functionality to trigger the simulation environment in gFP, execute the plant testing and model identification for the built-in MPC functionality, execute python functions, and exchange data between python and gFP. PharmaMV is used as the master platform to drive the simulation in gFP and the scheduling of the controllers, either built-in or in python. The data are acquired and visualised in PharmaMV too. The communications between the platforms are shown in Figure 6-3.

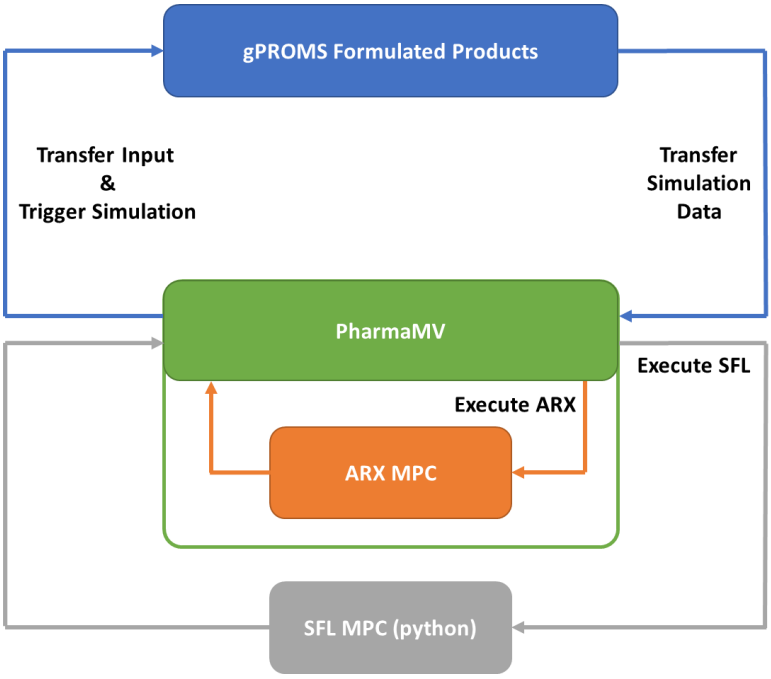

Figure 6-3 – PharmaMV – gFP Communication and Interfacing

The SFL-MPC technique with SFL-Plant constraints that has been developed in this research has been implemented into PharmaMV via a python script, and the ARX MPC is identified and tuned on the platform directly. The scheduling of the simulation is handled by PharmaMV which triggers the crystallization simulation each minute. Thus, the MPC application here is executed in real-time.

6.5.1 Case Study Comparing ARX and SFL MPC

The case study will compare the performance of the ARX MPC and the SFL MPC using a supersaturation ratio target of 1.1, 1.25 and 1.4 in 3 separate scenarios per controller. The criteria for comparison are the setpoint tracking capability using the RMSE of the setpoint error as defined by Equation 6-14. Additionally, the KPIs for comparing performance between the SFL-MPC and ARX-MPC are batch time, yield (%), RMSE and particle size properties (mean, D50 and span). The simulations for each of the six scenarios will be initialised at the desired supersaturation ratio target, so the batches will be initialised with the concentrations shown in Table 6-5.

$$RMSE = \sqrt{\frac{\sum_{i=1}^{n}\left(y_i - y_{ref}\right)^2}{n}} \qquad \textit{Equation 6-14}$$

S_r Target	Paracetamol (kg/kg)	IPA (kg/kg)
1.1	0.0720	0.9280
1.25	0.0817	0.9183
1.4	0.0915	0.9085

Table 6-5 – Initial Conditions for Simulations Based on Supersaturation Target

The performance criterion is quantified by the root mean square error shown in Equation 6-14. It is expected that the SFL-MPC would be applicable over a wider operating range than the ARX-MPC because the former is a global linearization technique whereas the latter was identified around a local region of the phase diagram. However, the performance difference will depend on how well each model matches or predicts the plant behaviour. A greater tracking performance will be quantified through a smaller value for RMSE. The original ARX-MPC has been identified over the region where the supersaturation ratio is close to 1.1, so it is suspected that the ARX-MPC will perform best at these conditions and the performance may deteriorate at a ratio of 1.4. All scenarios are described in Table 6-6.

Scenario	Model Type	Supersaturation Target
1	SFL	1.1
2	ARX	1.1
3	SFL	1.25
4	ARX	1.25
5	SFL	1.4
6	ARX	1.4

Table 6-6 – SFL and ARX Control Scenarios

6.6 Comparison of SFL-MPC and ARX-MPC – Results and Discussion

The results from the MPC comparison will be presented with respect to the target supersaturation, comparing the performance at relative supersaturation of 1.1 followed by 1.25 and finally at 1.4. The KPIs of the seeded batch crystallization MPC scenarios will be compared after the results have been discussed.

6.6.1 Comparison of SFL-MPC and ARX-MPC at Supersaturation Ratio 1.1

The results from the SFL-MPC and ARX-MPC control of the crystallization at supersaturation 1.1 are shown with the phase diagram operating profiles in Figure 6-4 and 6-5, respectively. The operating profiles both follow the desired trajectory, which is to be expected given the ARX model was identified in a region where the supersaturation ratio was 1.1.

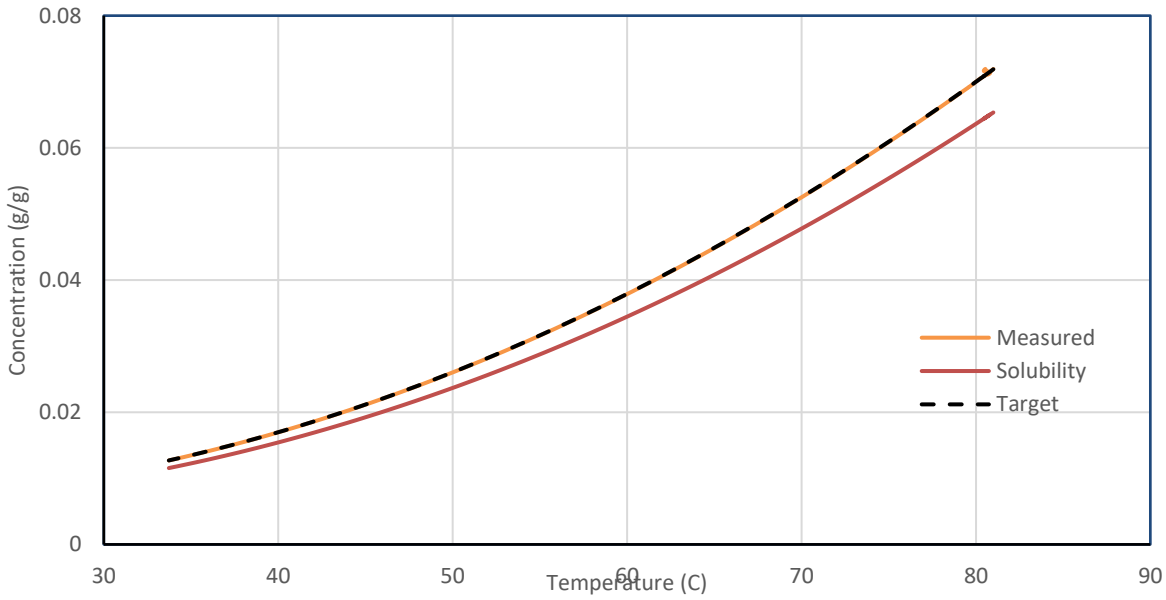

Figure 6-4 – Phase Diagram for SFL MPC with Supersaturation = 1.1

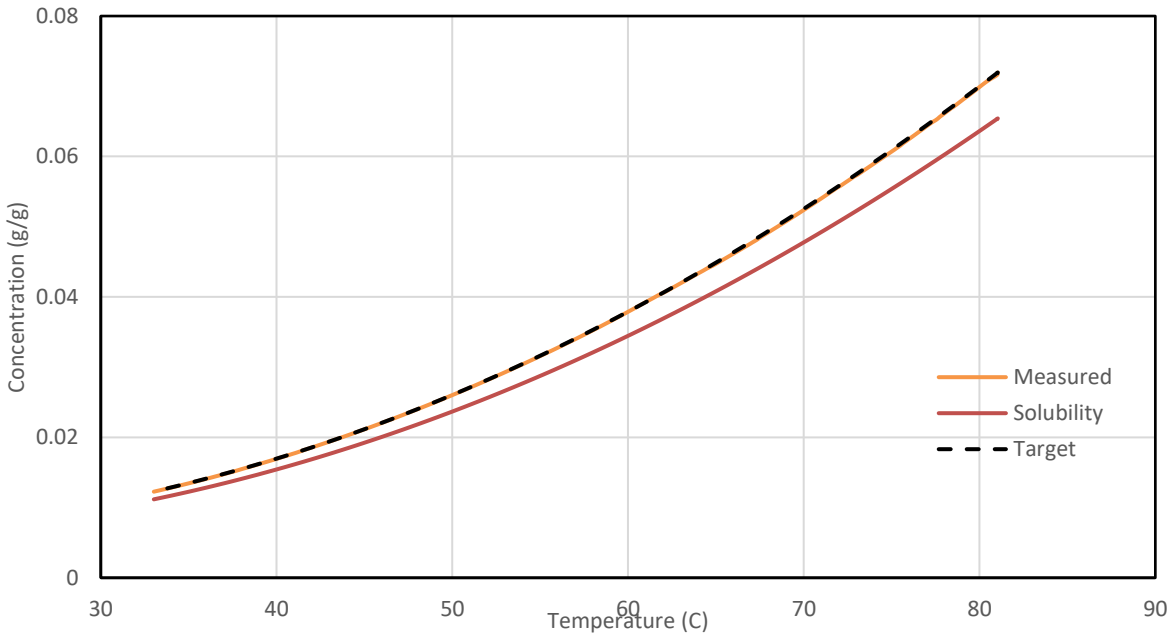

Figure 6-5 – Phase Diagram for ARX MPC with Supersaturation = 1.1

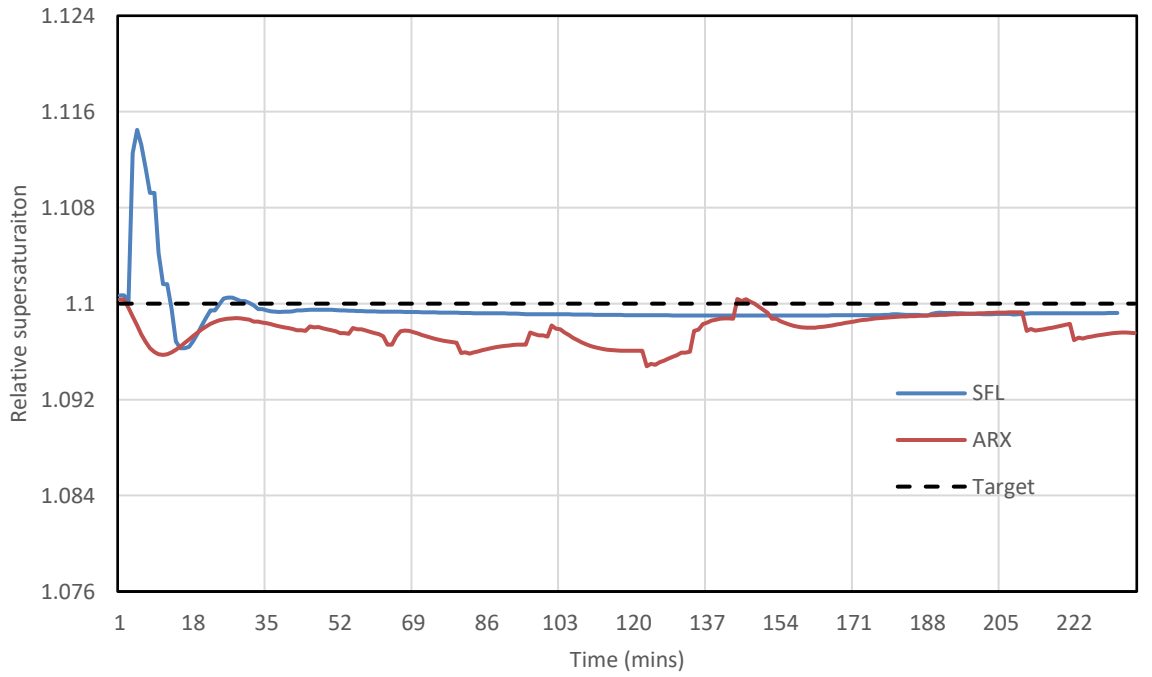

Figure 6-6 – Supersaturation Tracking Comparison for SFL and ARX at Supersaturation = 1.1

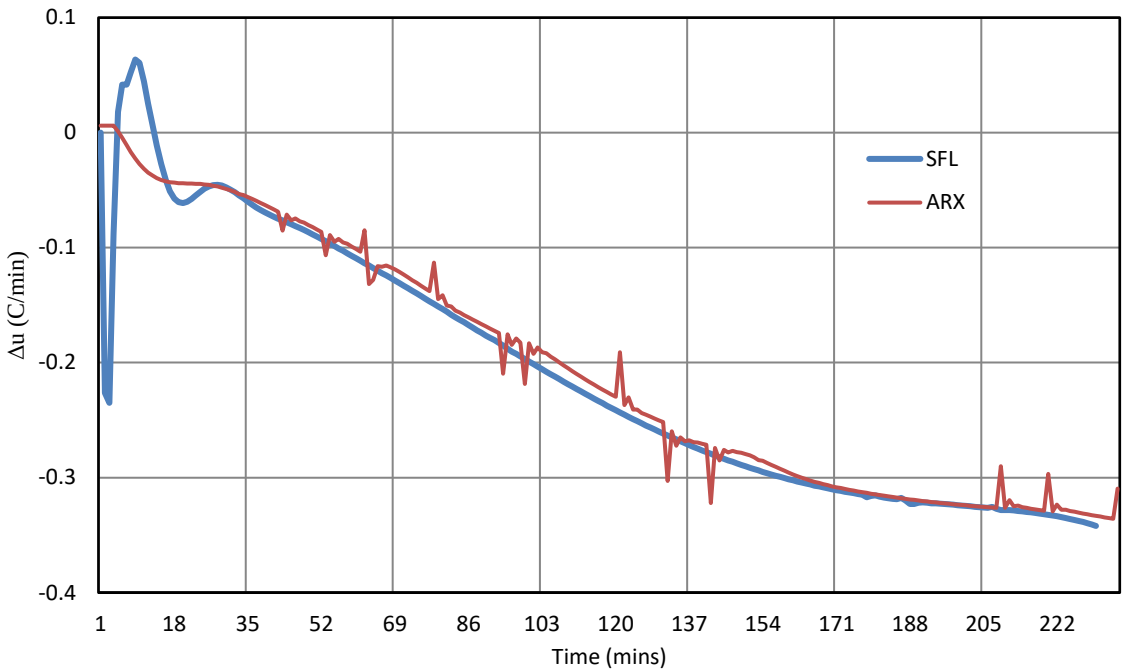

Figure 6-7 – Input Profile Comparison for SFL and ARX at Supersaturation = 1.1

Comparing both trajectories, supersaturation trajectory is shown in Figure 6-6, while the corresponding input profile from the MPC is also seen in Figure 6-7. There is an overshoot in the SFL-MPC trajectory at the beginning of the batch which is not seen in the ARX-MPC trajectory, but after the first 20 minutes, the SFL-MPC appears to track the supersaturation trajectory much closer with less offset than the ARX-MPC. The ARX-MPC does recover after 137 minutes and demonstrates similar tracking.

In the input profile plot, the SFL-MPC has a much smoother profile than the ARX-MPC and the latter also has some significant spikes in the cooling rate profile. The origin of these are a result of delayed communication between the gFP and PharmaMV platforms as can be seen when the change in concentration from both scenarios is plotted as per Figure 6-8. All the data shown here are from PharmaMV, so the gFP data that is plotted is that which has been transferred to PharmaMV. It is worth noting that the gFP simulation trajectories did appear smooth when viewed using the gFP reporting tool built into the platform, hence it was concluded that the source of these discontinuities is the communication between platforms.

The spikes occur where there is a large change in data in one interval followed by no change in the following interval. These are an anomaly caused by the co-simulation of the two

environments where one data point from gFP is missed, but subsequently datapoint is a repeat, which consequently results in a return of the operating trajectory to the expected trajectory for each simulation. The ARX-MPC is more sensitive to these changes than the SFL-MPC, but the trajectories of each simulation have not been significantly affected by these anomalies, as will be shown in the results that follow. Therefore, the effects of these anomalies are not regarded as having a significant impact on the final outcome from this case study and the results are regarded as acceptable to form a conclusion in comparison of ARX-MPC and SFL-MPC.

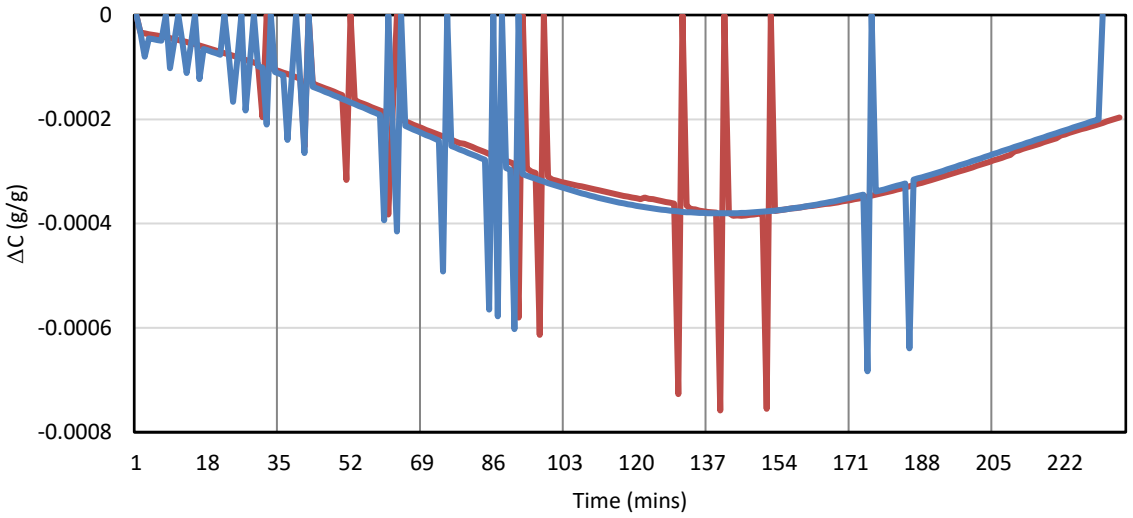

Figure 6-8 – Trend of change in concentration to demonstrate communication issues

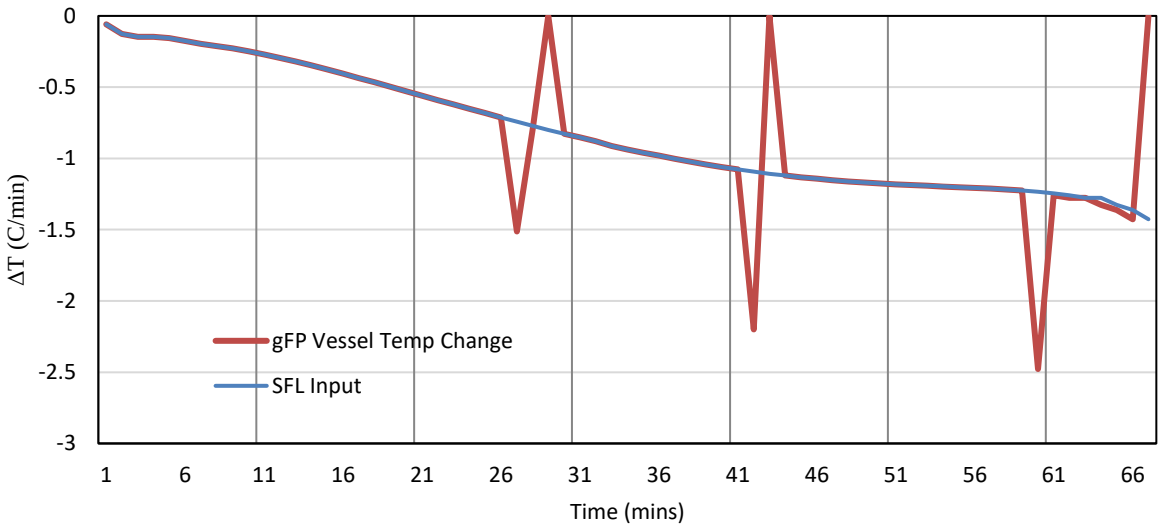

Figure 6-9 – gFP temperature compared to SFL input temperature

The smoothness in the SFL input profile can be seen clearly in Figure 6-9 where the change in vessel temperature of the gFP plant is demonstrating the same spikes as the change in concentration in the prior figure, but the SFL input remains smooth. Overall, the SFL-MPC appeared to track the supersaturation closer than the ARX-MPC but both scenarios demonstrated acceptable control.

6.6.2 Comparison of SFL-MPC and ARX-MPC at Supersaturation Ratio 1.25

The phase diagram operating profiles for the SFL-MPC and ARX-MPC are shown in Figure 6-10 and 6-11, respectively. The profile for SFL-MPC appears to track the supersaturation just as well as in the first scenario at the lower supersaturation target, but the ARX-MPC appears to deviate slightly from the reference profile. This is supported by the supersaturation profile comparison in Figure 6-12 which shows the tracking of both controllers. The SFL-MPC in this case appears to remain below the supersaturation target throughout and there is no overshoot, whereas for the ARX-MPC there is an overshoot at the beginning and then a larger offset from the target than the SFL-MPC. Though the ARX-MPC tracking does again improve towards the end of the batch, the improvement does not show better tracking performance than the SFL-MPC. In the corresponding input profiles shown in Figure 6-13, once again the SFL input trajectory is much smoother than the ARX input trajectory and the latter suffers from the spikes in the rate of change of cooling. These two scenarios show the superior performance of the SFL-MPC at the higher supersaturation setpoint with a deterioration in performance of the ARX-MPC when compared to the target of 1.1.

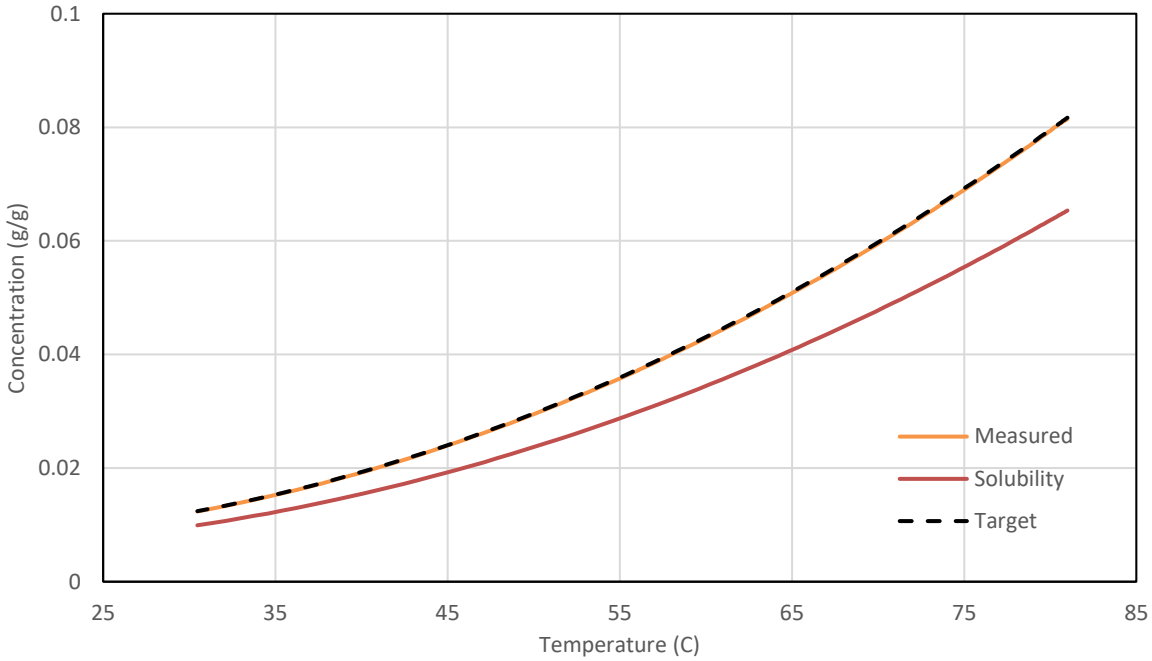

Figure 6-10 – Phase Diagram for SFL MPC with Supersaturation = 1.25

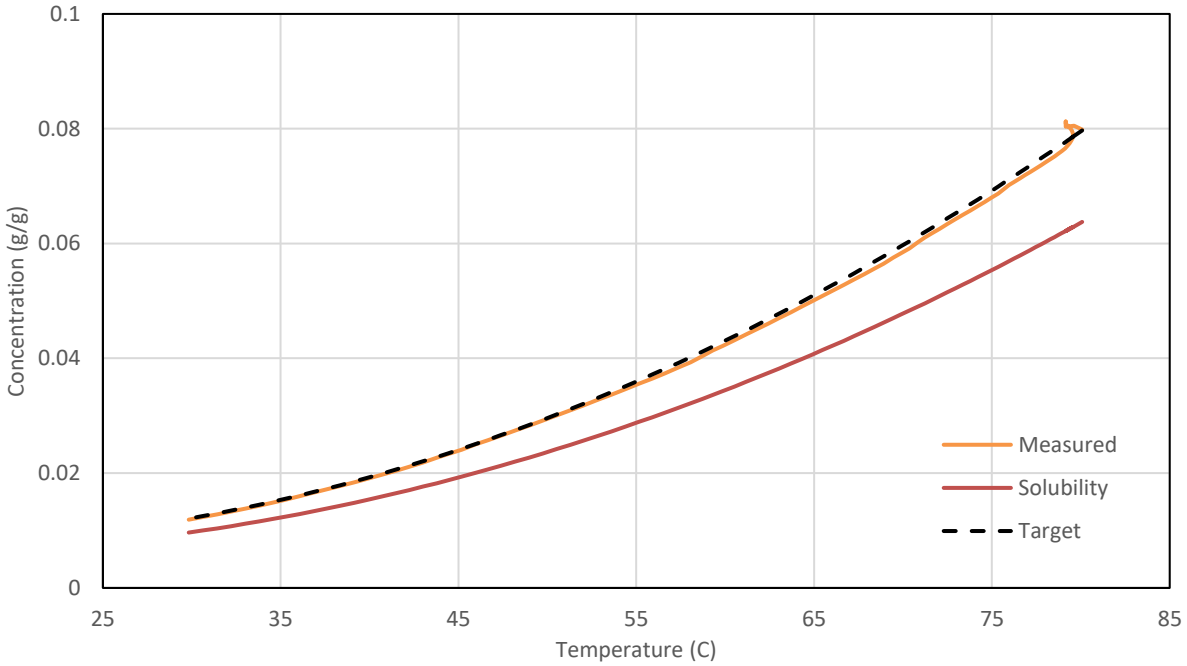

Figure 6-11 – Phase Diagram for ARX MPC with Supersaturation = 1.25

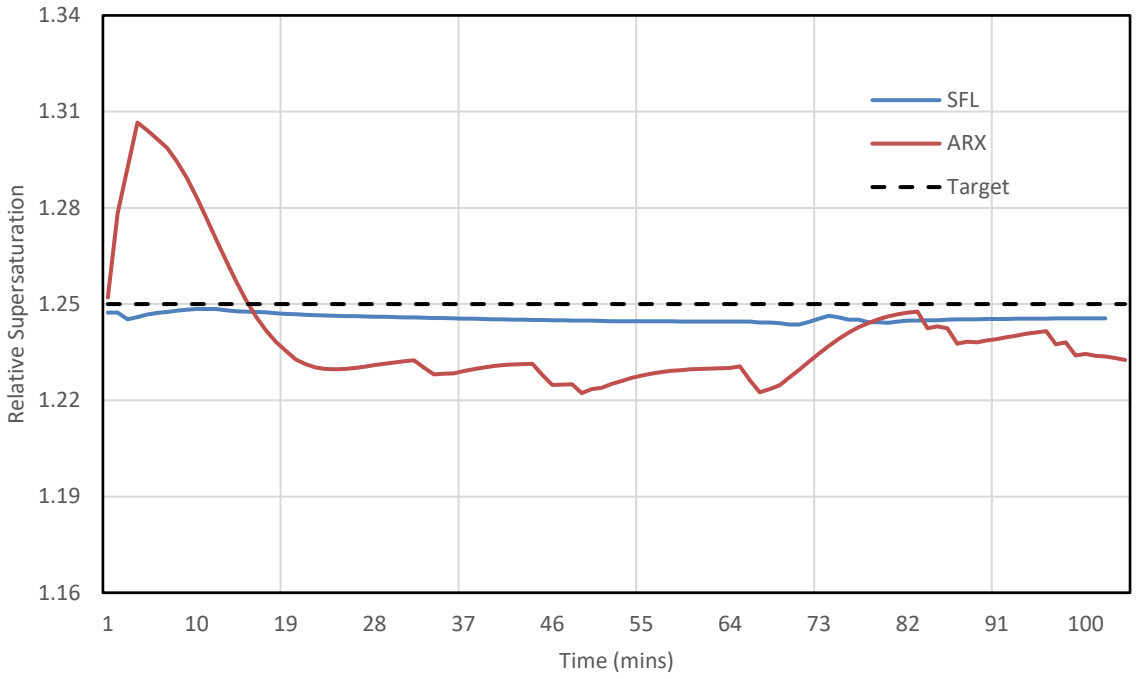

Figure 6-12 – Supersaturation Tracking Comparison for SFL and ARX at Supersaturation = 1.25

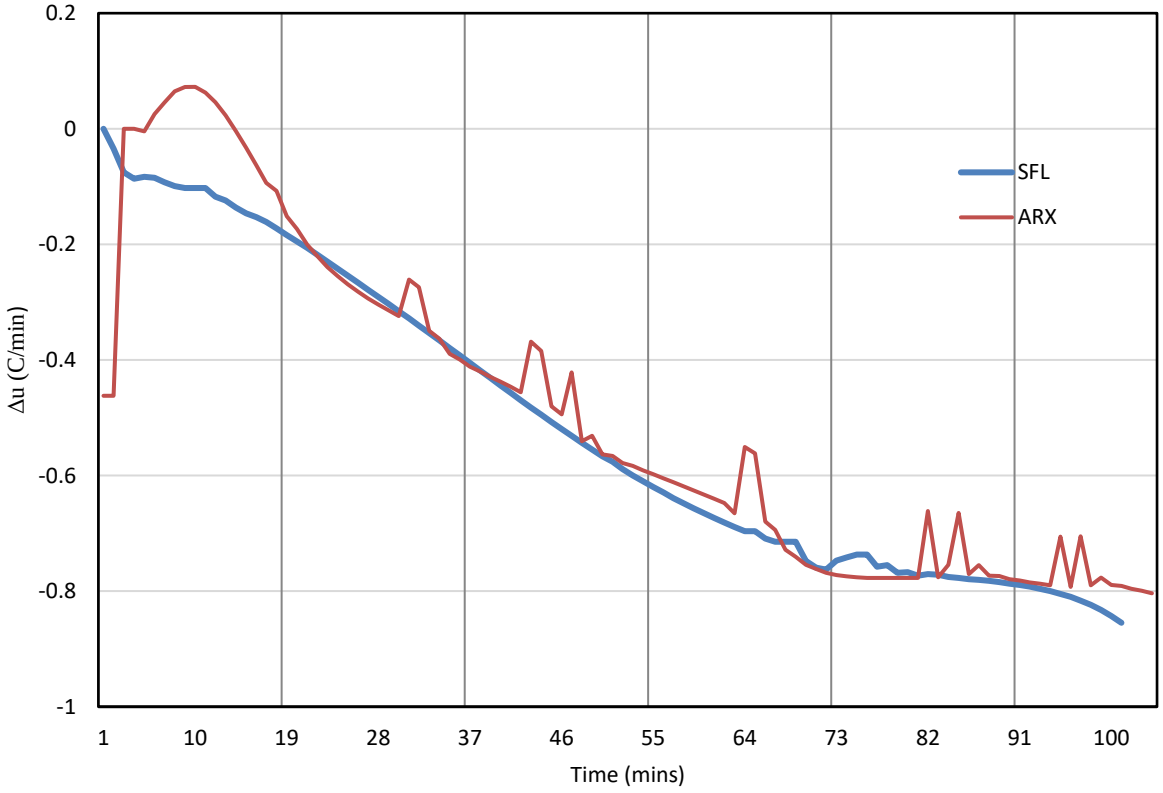

Figure 6-13 – Input Profile Comparison for SFL and ARX at Supersaturation = 1.25

6.6.3 Comparison of SFL-MPC and ARX-MPC at Supersaturation Ratio 1.4

The final comparison is of the supersaturation tracking at a setpoint of 1.4, the phase diagram trajectory for SFL-MPC is shown in Figure 6-14 and the ARX-MPC is shown in Figure 6-15 In the SFL-MPC trajectory there does appear to be a slight deviation from the reference profile, but not as large a deviation as the one seen for ARX-MPC. The comparison of supersaturation tracking in Figure 6-16 shows again that the SFL-MPC tracks the supersaturation trajectory much closer than the ARX-MPC, but even in the case of SFL-MPC there is a sustained offset. The input profile (Figure 6-17) also shows a smooth SFL input profile and the same issues seen with the spikes in the ARX inputs. At these conditions the SFL-MPC shows a clear advantage over the ARX-MPC for tracking control, this will be confirmed in the following section when discussing the KPIs in the following section.

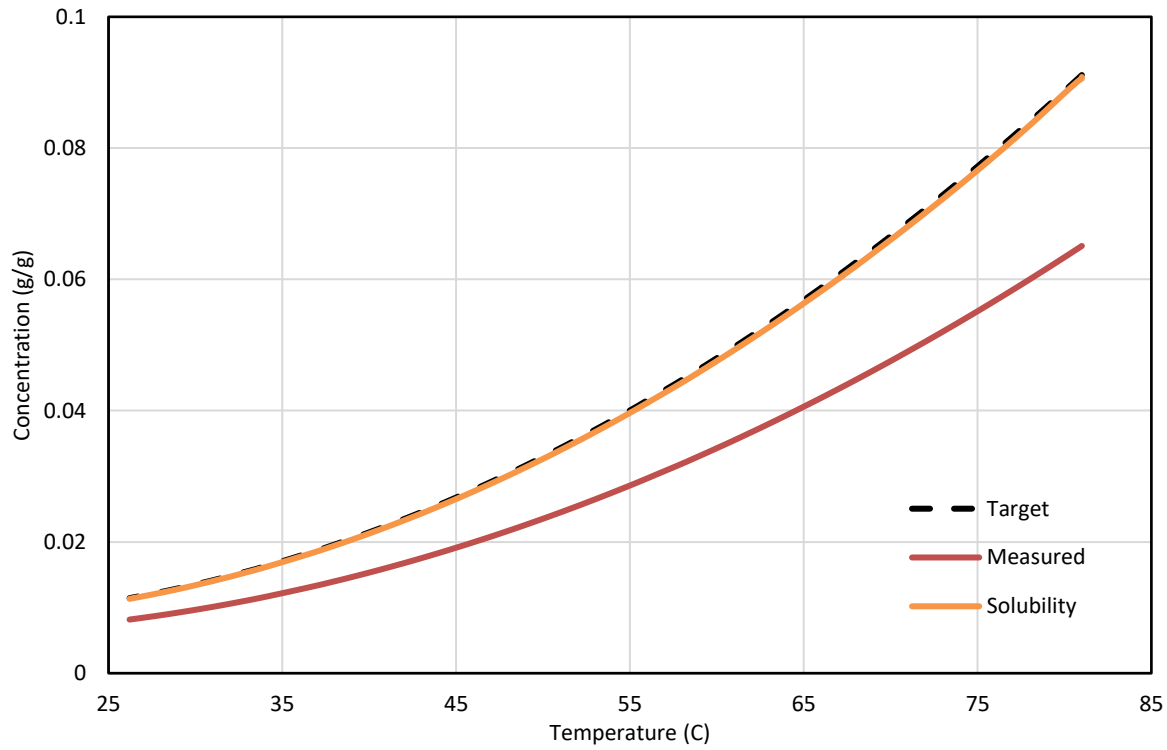

Figure 6-14 – Phase Diagram for SFL MPC with Supersaturation = 1.4

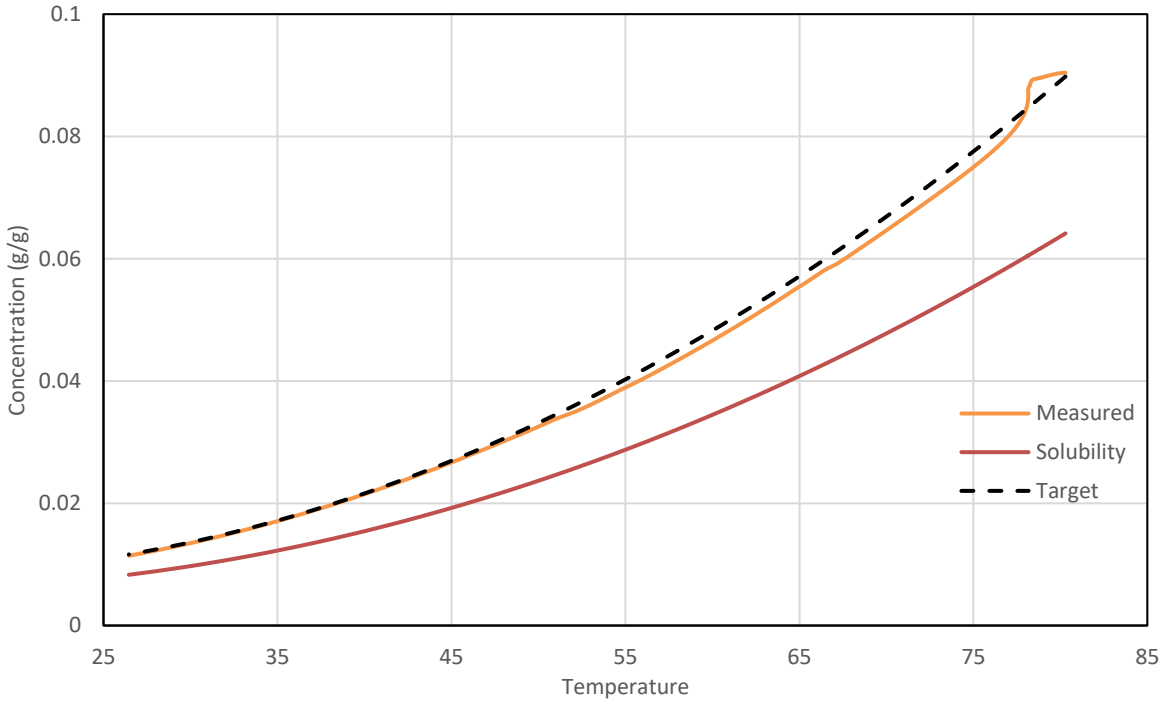

Figure 6-15 – Phase Diagram for ARX MPC with Supersaturation = 1.4

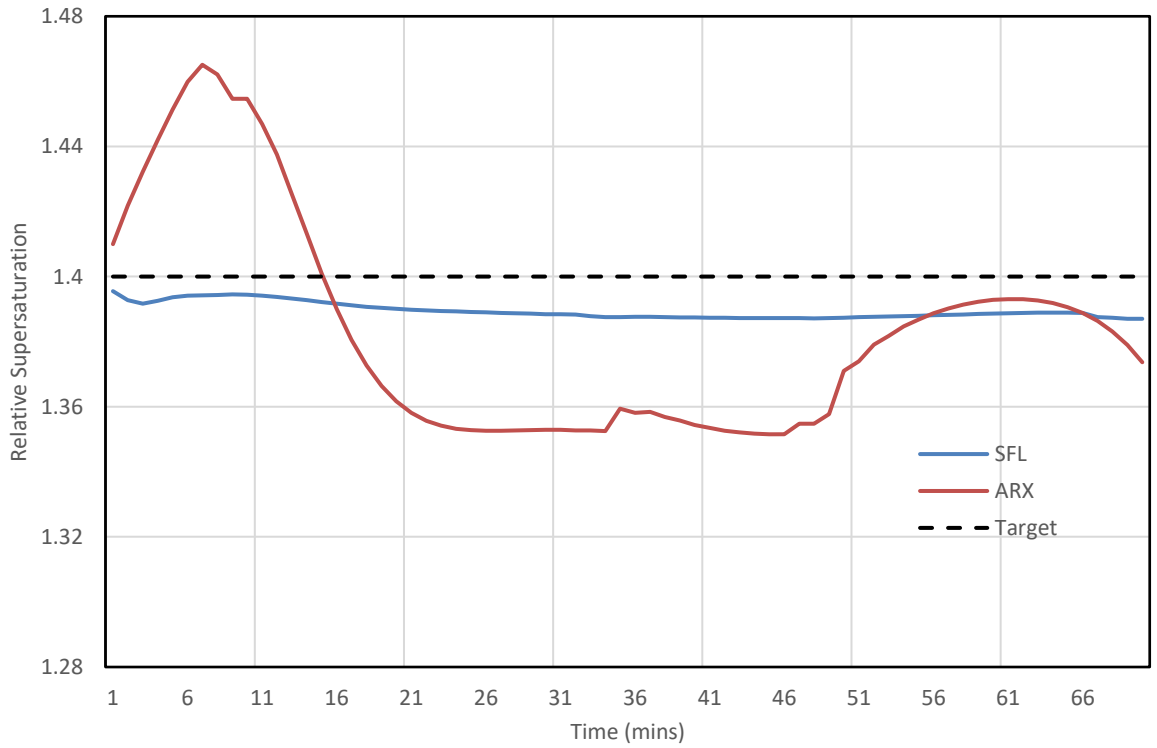

Figure 6-16 – Supersaturation Tracking Comparison for SFL and ARX at Supersaturation = 1.4

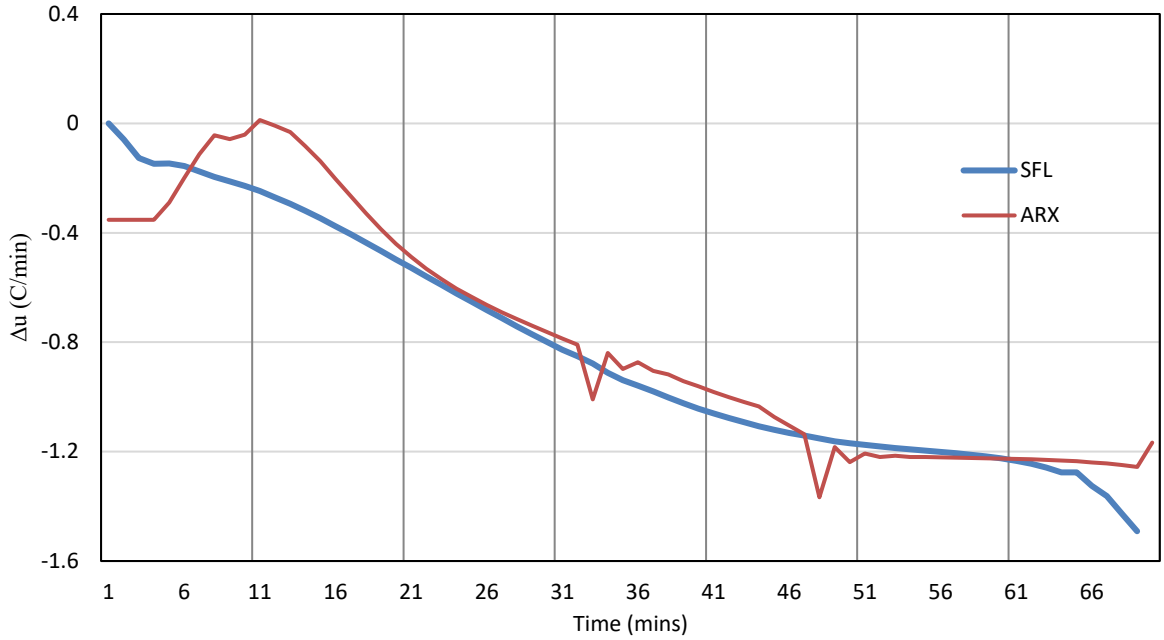

Figure 6-17 – Input Profile Comparison for SFL and ARX at Supersaturation = 1.4

6.6.4 Comparison of KPIs from SFL-MPC and ARX-MPC

The main KPI used for comparison of tracking performance is the RMSE which is shown in Figure 6-18. The RMSE at supersaturation of 1.1 is similar for both the SFL and ARX. The RMSE does increase for both MPC strategies as the supersaturation target is increased, but the rate of increase is much greater for ARX-MPC than SFL-MPC, thus allowing the conclusion to be made that the SFL-MPC is the superior strategy. The errors may be reduced for ARX-MPC if the model was identified at a higher supersaturation target, but that would require a new model to be identified to improve tracking performance. Considering the other KPIs, the yield is larger for lower supersaturation target and similar for both MPC strategies (Figure 6-19). Furthermore, the batch times are similar (Figure 6-20) between the two forms of MPC, as are the particle size characteristics shown in Table 6-7, finally all other KPIs are shown in Table 6-8. Reverting to the comparison that was made by Shen *et al.* (1999), the author concluded that the global linearizing control (equivalent to SFL) was superior to PID control but outperformed by generic model control or multi-model MPC. From this study of batch crystallization, it appears that SFL-MPC performs better than data-driven low order model-based controllers such as ARX-MPC.

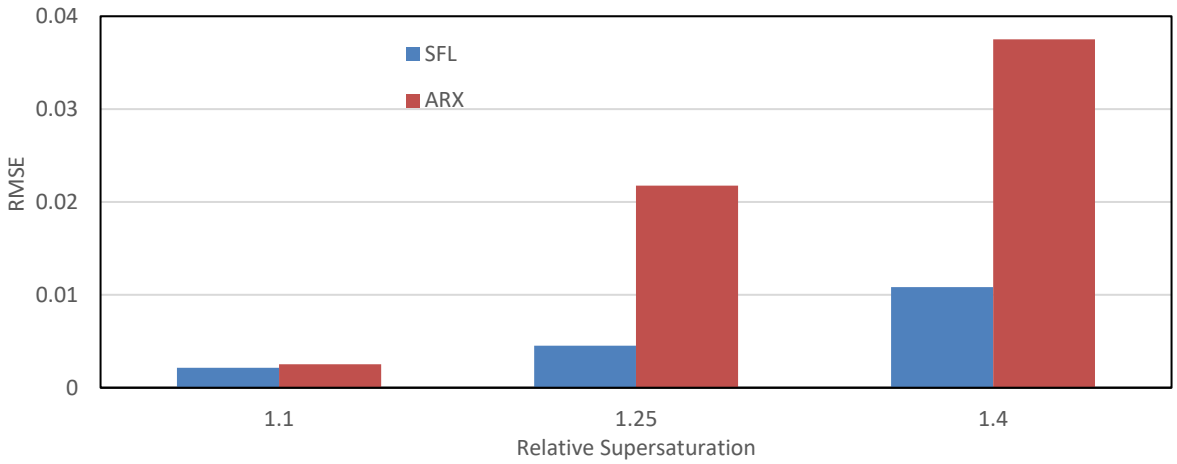

Figure 6-18 - SFL-MPC vs ARX-MPC - RMSE Comparison

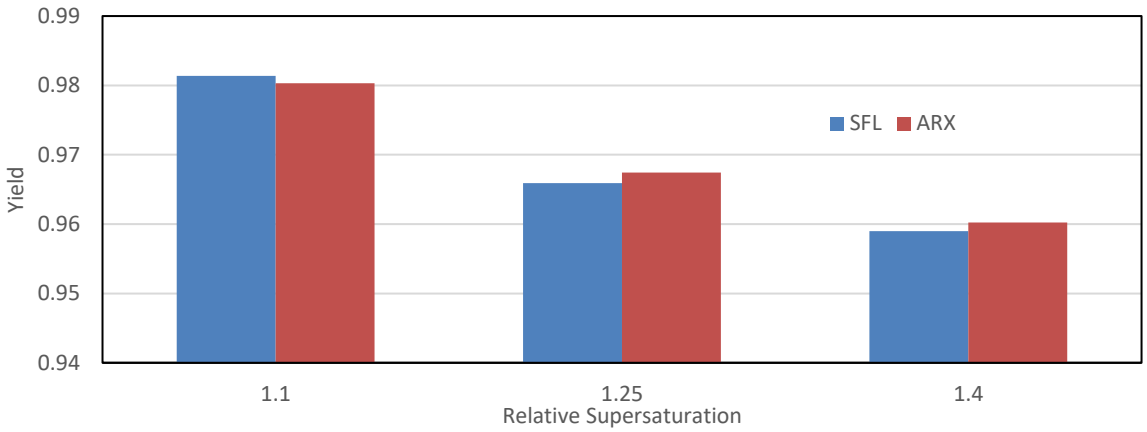

Figure 6-19 – SFL-MPC vs ARX-MPC - Yield Comparison

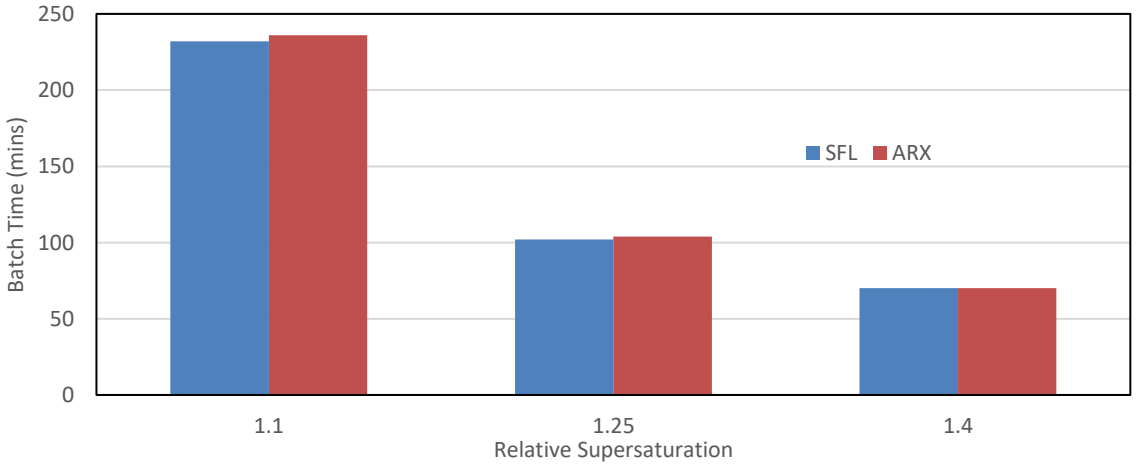

Figure 6-20 – SFL-MPC vs ARX-MPC - Batch Time Comparison

Target S	Model	Particle Size Mean (L_4/L_3)	Particle size D50	Particle Size CV
1.1	***SFL***	297.1	278.7	33.9
	ARX	297.2	278.8	33.9
1.25	***SFL***	284.1	266.7	34.2
	ARX	284.7	266.8	34.1
1.4	***SFL***	270.7	254.0	34.5
	ARX	271.3	254.1	34.4

Table 6-7 – Particle Size Data from End of Batch for all Scenarios

Target S	Model	Yield (%)	ISE	Time (mins)	RMSE
1.1	***SFL***	98.1	0.00108	232	0.00216
	ARX	98.0	0.00151	236	0.00253
1.25	***SFL***	96.6	0.00210	102	0.00453
	ARX	96.7	0.0493	104	0.0218
1.4	***SFL***	95.9	0.00822	70	0.0108
	ARX	96.0	0.0984	70	0.0375

Table 6-8 – Summary of KPIs for all Scenarios

6.7 Conclusion

This chapter forms a comprehensive comparison between SFL-MPC and ARX-MPC. The linear ARX is first identified from plant testing on the gFP plant, and the identified model is then used in a controller to perform supersaturation control at 3 targets of 1.1, 1.25 and 1.4. A plant mismatch is introduced between the SFL model and plant model because the plant-model is a higher order PBE model solved using FVM to track the full-size distribution from which the moments are calculated, whereas the SFL model is solved using SMOM and only tracking the moments. A multi-platform control system is also configured using PharmaMV, an industrial process control software, and gPROMS Formulated Products, an industrial software for mechanistic modelling to represent the plant. The challenges of communication issues in interfacing were faced between the platforms and the ARX model appeared more sensitive to these changes than the SFL-MPC. The root mean square error was used as the main KPI to calculate the tracking error between the SFL-MPC and ARX-MPC, the results concluded that the SFL-MPC had the superior supersaturation tracking performance with

smaller offset from the desired supersaturation in all cases. The other KPIs included yield, batch time and particle size characteristics which were all similar between the two MPC strategies.

Despite the direct comparison between strategies, it is worth noting that the SFL-MPC performance is subject to the identification of a reliable mechanistic model, so this control strategy may not be as widely applicable as the ARX-MPC. It is possible to identify an ARX-MPC for any plant from which input (jacket temperature)-output (supersaturation ratio) data can be generated. Despite the reduction in tracking performance seen with the ARX-MPC, it is possible to also re-identify the model at different operating conditions too using the same general model structure. Therefore, there are some advantages for the ARX-MPC technique too.

7 Conclusions

The research in this thesis focusses on optimization and control for batch and continuous (MSMPR) crystallization. The use of a global input/output linearization technique referred to as state-feedback linearization (SFL) triggered the initial study of whether a global optimization approach needs to be used in the controller or whether a local approach is capable on converging onto a global solution with great confidence and short time. This defined the first objective of the research to develop single and multi-objective optimization strategies for crystallization. After testing a global genetic algorithm against a local deterministic SQP approach and a combined hybrid approach, it was determined that the quality of the optimization solution from the local approach was better than the genetic algorithm alone, and the time of solution convergence was much shorter, hence giving confidence to recommend exploring the use of the SQP solver for optimization of a batch crystallization model. The benefits of multi-objective optimisation were also studied to understand if there existed a wider applicability of these techniques in control. As an offline optimisation approach the multi-objective optimization is useful for gaining insight into the process, and has been used in this way in published research from others, but for online or real-time application it is not an efficient optimization method to implement into a control system and would also require a decision-making process to select one of the Pareto profiles.

With a suitable and efficient optimization technique (SQP) identified, the focus was then changed to model predictive control, particularly the use of SFL and the objective was to develop an SFL-MPC for both SISO and MIMO control schemes. A state-space nonlinear model of the crystallizer in continuous MSMPR and batch forms were then identified in the SFL form for supersaturation and mean size as outputs; and jacket temperature and seed loading as inputs in various SISO and MIMO configurations. Each were successfully identified, demonstrating the wide applicability of this technique on the model system that was chosen. The next and main objective with the SFL was to address the inherent and widely reported difficulties to hand constraints. The previous attempts at constraints handling had limitations, and all focussed on transforming the real system constraints onto the linearized system. Using the most recently published framework for constraints handling, it appeared possible that rather than transforming the real constraints to the transformed system, that it should be possible to use the MPC inputs of the transformed system to estimate future inputs using a

nonlinear constraints routine and then apply the constraints to the estimated plant, directly. This was the main objective from the SFL-MPC research, and it was found that the devised nonlinear constraints routine – name SFL-Plant constraints, because it couples the SFL model with the plant – was indeed a viable constraints handling approach. In all simulations of SISO and MIMO MPC disclosed, where the SFL-Plant constraints were implemented, the resulting simulation results were all feasible and did not violate the prescribed constraints. The use of SQP algorithm which facilitates the use a nonlinear constraints function plays an important role in the successful application of this technique. From a crystallization processing perspective, it was found that some scenarios did not demonstrate good control because SFL-Plant constraints prevented the system from reaching or maintaining the setpoint, or the inputs required unrealistically low temperatures. However, these limitations can be overcome by ensuring appropriate setpoints are set for the system.

The successful use of SFL-MPC on batch and continuous MSMPR simulations then drove the next and final objective which was to compare this mechanistically-derived technique to a data-driven technique that is commonly used in industry, and to extend the comparison by using a cross-platform setup such that there is one platform for the control environment and one for the simulated plant. This is more representative of applying control onto a real system. The data-driven approach that was used is a black-box modelling approach to determine an input-output relationship of system. In this case it was the jacket temperature as the input and the supersaturation ratio as the output for a batch crystallization system, and the model identified was an autoregressive model with exogenous input (ARX). The comparison focussed on the SFL-MPC and ARX-MPC abilities to track a batch supersaturation ratio setpoint across a full batch. The results demonstrated that the SFL-MPC had a similar performance to the ARX-MPC in tracking the supersaturation ratio at low target of 1.1, and that both models demonstrated deteriorating performance as the supersaturation ratio target was increased to 1.25 and further to 1.4. However, the SFL-MPC demonstrated a significantly smaller tracking error (root mean square error between the measured output and trajectory) than the ARX-MPC model. One noted benefit of SFL over a local linearization technique is that the global transformation should have wider applicability without loss of prediction reliability, and this benefit was demonstrated in the results, quantified by the smaller tracking error.

8 Recommendations and Future work

This section discusses some areas for future work. The main recommendation from this thesis is the extension of these *in-silico* techniques to a real system. The chosen crystallization systems here are of paracetamol in water and paracetamol in isopropyl alcohol, using models which have been validated in literature. This allows for the ability to extend the SFL-MPC applications in this thesis directly onto the equivalent physical crystallization systems to further validate the SFL-Plant constraints and the general applicability of the SFL-MPC for control.

The SISO application of SFL-MPC disclosed in this research will be immediately transferrable to a real system, but the MIMO application does present some limitations with regards to the tuning. Therefore, two areas could be explored for SFL-MPC. The first is to determine global tuning parameters through a global linearization technique such as the NSGA-II that was disclosed in the optimization work. This is recommended because even though it was found in the SISO systems that tuning parameters could be used over a wide operating range, for the MIMO system the tuning parameters for seed loading input to control mean size appeared to be very sensitive to small changes in the setpoint. The second recommendation is to use a different MSMPR model with different objectives that are less coupled than mean-size and supersaturation to the temperature and seed loading. One example would be the exploration of mean size control using impeller speed to control attrition, while maintaining supersaturation control using jacket temperature.

In the comparison for SFL-MPC with ARX-MPC, this would also be useful to determine in a real system and be extended to other techniques of local linearization using the mechanistic model and using state of the art nonlinear MPC. It would be very useful to gain an understanding of the benefits and drawbacks in terms of tracking performance of these techniques, especially applied to a practical setup.

9 References

Aamir, E. *et al.* (2009) 'Combined Quadrature Method of Moments and Method of Characteristics Approach for Efficient Solution of Population Balance Models for Dynamic Modeling and Crystal Size Distribution Control of Crystallization Processes', *Ind. Eng. Chem. Res.*, 48, pp. 8575–8584.

Aamir, E. (2010) *Population Balance Model-Based Optimal Control of Batch Crystallisation Processes for Systematic Crystal Size Distribution Design*, *Loughborough University's Institutional Repository*.

Acevedo, D. *et al.* (2017) 'Model-Based Evaluation of Direct Nucleation Control Approaches for the Continuous Cooling Crystallization of Paracetamol in a Mixed Suspension Mixed Product Removal System', *Crystal Growth & Design*. ACS Publications, 17(10), pp. 5377–5383.

Acevedo, D., Tandy, Y. and Nagy, Z. K. (2015) 'Multiobjective Optimization of an Unseeded Batch Cooling Crystallizer for Shape and Size Manipulation', *Industrial & Engineering Chemistry Research*, 54(7), pp. 2156–2166. doi: 10.1021/acs.iecr.5b00173.

Akaike, H. (1974) 'A new look at the statistical model identification', in *Selected Papers of Hirotugu Akaike*. Springer, pp. 215–222.

Ålander, E. M. and Rasmuson, Å. C. (2005) 'Mechanisms of crystal agglomeration of paracetamol in acetone− water mixtures', *Industrial & engineering chemistry research*. ACS Publications, 44(15), pp. 5788–5794.

Ålander, E. M., Uusi-Penttilä, M. S. and Rasmuson, Å. C. (2004) 'Agglomeration of paracetamol during crystallization in pure and mixed solvents', *Industrial & engineering chemistry research*. ACS Publications, 43(2), pp. 629–637.

Allgöwer, F., Findeisen, R. and Nagy, Z. K. (2004) 'Nonlinear Model Predictive Control : From Theory to Application', *J. Chin. Inst. Chem. Engrs.,* 35(3), pp. 299–315.

Antonyuk, S., Palis, S. and Heinrich, S. (2011) 'Breakage behaviour of agglomerates and crystals by static loading and impact', *Powder Technology*. Elsevier, 206(1–2), pp. 88–98.

Antwerp, J. G. Van and Braatz, R. D. (2000) 'Model predictive control of large scale processes',

Journal of Process Control, 10, pp. 1–8.

Bakar, M. R. A. *et al.* (2009) 'The Impact of Direct Nucleation Control on Crystal Size Distribution in Pharmaceutical Crystallization Processes', *Crystal Growth & Design*, 9(3), pp. 1378–1384.

Bakar, M. R. A., Nagy, Z. K. and Rielly, C. D. (2009) 'Seeded Batch Cooling Crystallization with Temperature Cycling for the Control of Size Uniformity and Polymorphic Purity of Sulfathiazole Crystals', *Organic Process Research & Development*, 13(3), pp. 1343–1356.

Beck, R. *et al.* (2009) 'The effect of crystallization conditions, crystal morphology and size on pressure filtration of l-glutamic acid and an aromatic amine', *Separation and Purification Technology*, 66(3), pp. 549–558. doi: 10.1016/j.seppur.2009.01.018.

Beckmann, J. R. and Randolph, A. D. (1977) 'Crystal size distribution and dynamics in a classified crystallizer. Part II. Simulated control of crystal size distribution', *American Institution of Chemical Engineers Journal*, 23, pp. 510–520.

Benyahia, B. *et al.* (2011) 'Multicriteria dynamic optimization of an emulsion copolymerization reactor', *Computers and Chemical Engineering*. Elsevier Ltd, 35(12), pp. 2886–2895. doi: 10.1016/j.compchemeng.2011.05.014.

Benyahia, B., Lakerveld, R. and Barton, P. I. (2012) 'A plant-wide dynamic model of a continuous pharmaceutical process', *Industrial and Engineering Chemistry Research*, 51(47), pp. 15393–15412. doi: 10.1021/ie3006319.

Boggs, P. T. and Tolle, J. W. (1995) 'Sequential Quadratic Programming', *Acta Numerica*, 4, pp. 1–51. doi: 10.1017/S0962492900002518.

Borsos, A., Majumder, A. and Nagy, Z. K. (2015) 'Multi-impurity adsorption model for modeling crystal purity and shape evolution during crystallization processes in impure media', *Crystal Growth & Design*. ACS Publications, 16(2), pp. 555–568.

Borsos, Á., Majumder, A. and Nagy, Z. K. (2014) 'Model development and experimental validation for crystal shape control by using tailored mixtures of crystal growth modifiers', in *Computer Aided Chemical Engineering*. Elsevier, pp. 781–786.

Boukouvala, F. and Ierapetritou, M. G. (2013) 'Surrogate-based optimization of expensive flowsheet modeling for continuous pharmaceutical manufacturing', *Journal of Pharmaceutical Innovation*, 8(2), pp. 131–145. doi: 10.1007/s12247-013-9154-1.

Braatz, R. D. (2004) 'Open-loop and closed-loop robust optimal control of batch processes using distributional and worst-case analysis processes using distributional and worst-case analysis', *Journal of Process Control*, 14, pp. 411–422. doi: 10.1016/j.jprocont.2003.07.004.

Briuglia, M. L., Sefcik, J. and ter Horst, J. H. (2018) 'Measuring secondary nucleation through single crystal seeding', *Crystal Growth & Design*. ACS Publications, 19(1), pp. 421–429.

Brown, C. J. and Ni, X.-W. (2012) 'Determination of metastable zone width, mean particle size and detectable number density using video imaging in an oscillatory baffled crystallizer', *CrystEngComm*. Royal Society of Chemistry, 14(8), pp. 2944–2949.

Casanova-Peláez, P. J. *et al.* (2012) 'RBF–ARX model of an industrial furnace for drying olive pomace', *Energy conversion and management*. Elsevier, 64, pp. 106–112.

Castagnoli, C. *et al.* (2010) 'Application of quality by design principles for the definition of a robust crystallization process for casopitant mesylate', *Organic Process Research & Development*. ACS Publications, 14(6), pp. 1407–1419.

Chang, L.-Y. and Chen, H.-C. (2014) 'Linearization and Input-Output Decoupling for Nonlinear Control of Proton Exchange Membrane Fuel Cells', *Energies*, 7(2), pp. 591–606. doi: 10.3390/en7020591.

Chianese, A., Di Berardino, F. and Jones, A. G. G. (1993) 'On the effect of secondary nucleation on the crystal size distribution from a seeded batch crystallizer', *Chemical Engineering Science*. Pergamon, 48(3), pp. 551–560. doi: 10.1016/0009-2509(93)80309-E.

Choong, K. L. and Smith, R. (2004) 'Optimization of batch cooling crystallization', *Chemical Engineering Science*. Elsevier, 59(2), pp. 313–327.

Cornehl, B. *et al.* (2014) 'Breakage of lysozyme crystals due to compressive stresses during cake filtration', *Chemical Engineering Science*. Elsevier, 111, pp. 324–334. doi: 10.1016/j.ces.2014.02.016.

Corriou, J. R. and Rohani, S. (2002) 'Nonlinear control of a batch crystallizer', *Chemical Engineering Communications*, 189(10), pp. 1415–1436. doi: 10.1080/00986440214062.

Coulson, J. M. *et al.* (1964) *Chemical Engineering: Fluid flow, heat transfer and mass transfer*. Pergamon press.

Damour, C. *et al.* (2010) 'Nonlinear predictive control based on artificial neural network model for industrial crystallization', *Journal of Food Engineering*, 99(2), pp. 225–231. doi: 10.1016/j.jfoodeng.2010.02.027.

David, R. *et al.* (2003) *Modelling of multiple-mechanism agglomeration in a crystallization process*, *Powder Technology - POWDER TECHNOL*. doi: 10.1016/S0032-5910(02)00213-9.

Davis, L. (1991) 'Handbook of genetic algorithms'. CUMINCAD.

Deb, K. *et al.* (2000) 'A fast elitist non-dominated sorting genetic algorithm for multi-objective optimization: NSGA-II', *Lecture Notes in Computer Science (including subseries Lecture Notes in Artificial Intelligence and Lecture Notes in Bioinformatics)*, 1917, pp. 849–858.

Deb, K., Lele, S. and Datta, R. (2007) 'A hybrid evolutionary multi-objective and SQP based procedure for constrained optimization', in *International Symposium on Intelligence Computation and Applications*. Springer, pp. 36–45.

Diaconis, P. (1987) 'Application of the method of moments in probability and statistics', *Moments in mathematics*. Amer. Math. Soc.: Providence, RI, 37, pp. 125–142.

Diehl, M. *et al.* (2002) 'Real-time optimization and nonlinear model predictive control of processes governed by differential-algebraic equations', *Journal of Process Control*, pp. 577–585. doi: 10.1016/S0959-1524(01)00023-3.

Eggers, J. *et al.* (2009) 'Monitoring size and shape during cooling crystallization of ascorbic acid', *Chemical Engineering Science*, 64, pp. 163–171. doi: 10.1016/j.ces.2008.08.007.

Eymard, R., Gallouët, T. and Herbin, R. (2000) 'Finite volume methods', *Handbook of numerical analysis*. Elsevier, 7, pp. 713–1018.

Faria, N. *et al.* (2008) 'Modelling agglomeration degree in sucrose crystallisation', *Chemical Engineering and Processing: Process Intensification*, 47(9–10), pp. 1666–1677. doi:

10.1016/j.cep.2007.09.008.

Forgione, M. *et al.* (2015) 'Control Engineering Practice Batch-to-batch model improvement for cooling crystallization', *Control Engineering Practice*. Elsevier, 41, pp. 72–82. doi: 10.1016/j.conengprac.2015.04.011.

Fujiwara, M. *et al.* (2002) 'Paracetamol crystallization using laser backscattering and ATR-FTIR spectroscopy: metastability, agglomeration, and control', *Crystal Growth & Design*. ACS Publications, 2(5), pp. 363–370.

Fysikopoulos, D. *et al.* (2018) 'A framework for model reliability and estimability analysis of crystallization processes with multi-impurity multi-dimensional population balance models', *Computers & Chemical Engineering*. Pergamon. doi: 10.1016/J.COMPCHEMENG.2018.09.007.

Gao, X. *et al.* (2008) 'Multi-objective optimization for the periodic operation of the naphtha pyrolysis process using a new parallel hybrid algorithm combining NSGA-II with SQP', *Computers & Chemical Engineering*. Elsevier, 32(11), pp. 2801–2811.

Gao, Z. *et al.* (2017) 'Recent Developments in the Crystallization Process: Toward the Pharmaceutical Industry', *Engineering*, 3(3), pp. 343–353. doi: 10.1016/J.ENG.2017.03.022.

García, C. E., Prett, D. M. and Morari, M. (1989a) 'Model predictive control: Theory and practice-A survey', *Automatica*, 25(3), pp. 335–348. doi: 10.1016/0005-1098(89)90002-2.

García, C. E., Prett, D. M. and Morari, M. (1989b) 'Model predictive control: Theory and practice—A survey', *Automatica*. Pergamon, 25(3), pp. 335–348. doi: 10.1016/0005-1098(89)90002-2.

Garside, J. (1984) 'Advances in the characterization of crystal growth', in *AIChE symposium series*. American institute of chemical engineers, pp. 23–38.

Garside, J. and Davey, R. J. (1980) 'Invited Review Secondary Contact Nucleation: Kinetics, Growth and Scale-up', *Chemical Engineering Communications*. Taylor & Francis, 4(4–5), pp. 393–424. doi: 10.1080/00986448008935918.

Garside, J. and Jančić, S. J. (1978) 'Prediction and measurement of crystal size distributions for size-dependent growth', *Chemical Engineering Science*. Elsevier, 33(12), pp. 1623–1630.

Georgieva, P., Meireles, M. J. and Feyo de Azevedo, S. (2003) 'Knowledge-based hybrid modelling of a batch crystallisation when accounting for nucleation, growth and agglomeration phenomena', *Chemical Engineering Science*, 58(16), pp. 3699–3713. doi: 10.1016/S0009-2509(03)00260-4.

Gimbun, J., Nagy, Z. K. and Rielly, C. D. (2009) 'Simultaneous Quadrature Method of Moments for the Solution of Population Balance Equations, Using a Differential Algebraic Equation Framework | Jolius Gimbun - Academia.edu', *Ind. Eng. Chem. Res.*, 48, pp. 7798–7812.

Gordon, R. G. (1968) 'Error Bounds in Equilibrium Statistical Mechanics', *Journal of Mathematical Physics*, 9(5), p. 655. doi: 10.1063/1.1664624.

Granberg, R. A. and Rasmuson, Å. C. (1999) 'Solubility of paracetamol in pure solvents', *Journal of Chemical & Engineering Data*. ACS Publications, 44(6), pp. 1391–1395.

Granberg, R. A. and Rasmuson, Å. C. (2005) 'Crystal growth rates of paracetamol in mixtures of water+ acetone+ toluene', *AIChE journal*. Wiley Online Library, 51(9), pp. 2441–2456.

Grof, Z. *et al.* (2011) 'Computational and experimental investigation of needle-shaped crystal breakage', *International journal of pharmaceutics*. Elsevier, 407(1–2), pp. 12–20.

Groppi, G. *et al.* (1995) 'A comparison of lumped and distributed models of monolith catalytic combustors', *Chemical Engineering Science*. Elsevier, 50(17), pp. 2705–2715.

Gunawan, R. *et al.* (2004) 'Optimal control of rapid thermal annealing in a semiconductor process', *Journal of Process Control*, 14, pp. 423–430. doi: 10.1016/j.jprocont.2003.07.005.

Gunawan, R., Fusman, I. and Braatz, R. D. (2004) 'High Resolution Algorithms for Multidimensional Population Balance Equations', *AIChE*, 50(11), pp. 2738–2749. doi: 10.1002/aic.10228.

Haber, R. (1992) 'Transformation of the absolute descriptions of linear and non-linear processes to their incremental forms', *International journal of systems science*. Taylor & Francis, 23(6), pp. 935–955.

Haddad, A. H. (2008) *Applied optimal estimation*, *Proceedings of the IEEE*. doi: 10.1109/proc.1976.10175.

Hartman, P. (1963) 'On the local linearization of differential equations', *Proceedings of the American Mathematical Society*. JSTOR, 14(4), pp. 568–573.

Hefter, G. T. and Tomkins, R. P. T. (2003) *The experimental determination of solubilities*. John Wiley & Sons.

Helt, J. E. and Larson, M. A. (1977) 'Effects of temperature on the crystallization of potassium nitrate by direct measurement of supersaturation', *AIChE Journal*. John Wiley & Sons, Ltd, 23(6), pp. 822–830. doi: 10.1002/aic.690230608.

Hemalatha, K. *et al.* (2018) 'Multiobjective optimization and experimental validation for batch cooling crystallization of citric acid anhydrate', *Computers and Chemical Engineering*. Elsevier Ltd, 112, pp. 292–303. doi: 10.1016/j.compchemeng.2018.02.019.

Henrion, D. and Lasserre, J.-B. (2004) 'Solving nonconvex optimization problems', *IEEE Control Systems Magazine*. IEEE, 24(3), pp. 72–83.

Hofmann, S. and Raisch, J., (2010). Application of optimal control theory to a batch crystallizer using orbital flatness. In *16th Nordic Process Control Workshop, Lund, Sweden* (pp. 25-27). Lund Institute of Technology.

Hojjati, H. and Rohani, S. (2006) 'Measurement and prediction of solubility of paracetamol in water− isopropanol solution. Part 1. Measurement and data analysis', *Organic Process Research & Development*. ACS Publications, 10(6), pp. 1101–1109.

Hreiz, R. *et al.* (2015) 'Chemical Engineering Research and Design Multi-objective optimal control of small-size wastewater treatment plants', *Chemical Engineering Research and Design*. Institution of Chemical Engineers, 102, pp. 345–353. doi: 10.1016/j.cherd.2015.06.039.

Hulburt, H. M. and Katz, S. (1964) 'Some problems in particle technology', *Chemical Engineering Science*, 19(8), pp. 555–574. doi: 10.1016/0009-2509(64)85047-8.

Izmailov, A. F., Myerson, A. S. and Arnold, S. (1999) 'A statistical understanding of nucleation', *Journal of Crystal Growth*, 196, pp. 234–242.

Jang, H. *et al.* (2014) 'Fast moving horizon estimation for a two-dimensional distributed

parameter system', *Computers and Chemical Engineering*. Elsevier Ltd, 63, pp. 159–172. doi: 10.1016/j.compchemeng.2013.12.005.

Jansen, P. (2011) 'State Feedback Linearization of a Seeded Batch Cooling Crystallizer for Supersaturation Control', pp. 1–13.

Jansens, P. J. and Hof, P. M. J. Van Den (2009) 'Chemical Engineering Research and Design A model-based control framework for industrial batch crystallization processes', *Chemical Engineering Research and Design*. Institution of Chemical Engineers, 88(9), pp. 1223–1233. doi: 10.1016/j.cherd.2009.09.010.

Jansson, M. (2003) 'Subspace identification and ARX modeling', *IFAC Proceedings Volumes*. Elsevier, 36(16), pp. 1585–1590.

Jensen, E. W., Lindholm, P. and Henneberg, S. W. (1996) 'Autoregressive modeling with exogenous input of middle-latency auditory-evoked potentials to measure rapid changes in depth of anesthesia', *Methods of information in medicine*. Schattauer GmbH, 35(03), pp. 256–260.

Jiang, M. *et al.* (2012) 'Towards achieving a flattop crystal size distribution by continuous seeding and controlled growth', *Chemical Engineering Science*. Elsevier, 77, pp. 2–9. doi: 10.1016/j.ces.2011.12.033.

Johansson, R. (1993) *System modeling and identification*. Prentice Hall Englewood Cliffs, NJ.

John, V. and Thein, F. (2012) 'On the efficiency and robustness of the core routine of the quadrature method of moments (QMOM)', *Chemical Engineering Science*. Elsevier, 75, pp. 327–333. doi: 10.1016/j.ces.2012.03.024.

Kadam, S. S., Kramer, H. J. M. and ter Horst, J. H. (2011) 'Combination of a single primary nucleation event and secondary nucleation in crystallization processes', *Crystal Growth & Design*. ACS Publications, 11(4), pp. 1271–1277.

Kazerounian, K. and Wang, Z. (1987) 'Optimization Redundancy Manipulators Local in Resolution of Robotic', *Optimization*, (1984), pp. 3–12.

Kitak, T. *et al.* (2015) 'Determination of solubility parameters of ibuprofen and ibuprofen

lysinate', *Molecules*. Multidisciplinary Digital Publishing Institute, 20(12), pp. 21549–21568.

Koren, B. (1993) 'A robust upwind discretization method for advection, diffusion and source terms', *Notes on Numerical Fluid Mechanics*, pp. 117–138. Available at: http://www.narcis.nl/publication/RecordID/oai:cwi.nl:2269%5Cnhttp://repository.tue.nl/737323.

Kravaris, C. and Chung, C. (1987) 'Nonlinear State Feedback Synthesis by Global Input / Output Linearization', *AIChE*, 33(4), pp. 592–603.

Kravaris, C. and Soroush, M. (1990) 'Synthesis of multivariable nonlinear controllers by input/output linearization', *AIChE Journal*, 36(2), pp. 249–264. doi: 10.1002/aic.690360211.

Kulkarni, S. A., Meekes, H. and Ter Horst, J. H. (2014) 'Polymorphism control through a single nucleation event', *Crystal Growth & Design*. ACS Publications, 14(3), pp. 1493–1499.

Kurtz, M. J. and Henson, M. A. (1998) 'Feedback linearizing control of discrete-time nonlinear systems with input constraints', *International Journal of Control*. Taylor & Francis, 70(4), pp. 603–616.

Kurtz, R. J. and Henson, M. A. (1996) 'Feedback linearizing control of discrete-time nonlinear systems with constraints', in *Proceedings of 28th Southeastern Symposium on System Theory*. IEEE, pp. 23–27.

Lakerveld, R. *et al.* (2015) 'The Application of an Automated Control Strategy for an Integrated Continuous Pharmaceutical Pilot Plant', *Organic Process Research and Development*, 19(9), pp. 1088–1100. doi: 10.1021/op500104d.

Lawton, S. *et al.* (2009) 'Continuous crystallization of pharmaceuticals using a continuous oscillatory baffled crystallizer', *Organic Process Research and Development*, 13(6), pp. 1357–1363. doi: 10.1021/op900237x.

Lekhal, A. *et al.* (2004) 'The effect of agitated drying on the morphology of l-threonine (needle-like) crystals', *International journal of pharmaceutics*. Elsevier, 270(1–2), pp. 263–277.

Liu, X. *et al.* (2011) 'Monitoring of antisolvent crystallization of sodium scutellarein by

combined FBRM–PVM–NIR', *Journal of pharmaceutical sciences*. Elsevier, 100(6), pp. 2452–2459.

Liu, Y. C. *et al.* (2019) 'A Comparative Study of Continuous Operation between a Dynamic Baffle Crystallizer and a Stirred Tank Crystallizer', *Chemical Engineering Journal*. Elsevier. doi: 10.1016/J.CEJ.2019.02.129.

Ma, D. L., Tafti, D. K. and Braatz, R. D. (2002) 'Optimal control and simulation of multidimensional crystallization processes', *Computers and Chemical Engineering*, 26, pp. 1103–1116.

Ma, L. and Braatz, R. D. (2003) 'Robust identification and control of batch processes', *Computers and Chemical Engineering*, 27, pp. 1175–1184. doi: 10.1016/S0098-1354(03)00045-0.

Majumder, A. *et al.* (2012a) 'Lattice Boltzmann method for multi-dimensional population balance models in crystallization', *Chemical Engineering Science*. Elsevier, 70, pp. 121–134. doi: 10.1016/j.ces.2011.04.041.

Majumder, A. *et al.* (2012b) 'Lattice Boltzmann method for population balance equations with simultaneous growth , nucleation , aggregation and breakage', *Chemical Engineering Science*. Elsevier, 69(1), pp. 316–328. doi: 10.1016/j.ces.2011.10.051.

Majumder, A. and Nagy, Z. K. (2013) 'Prediction and control of crystal shape distribution in the presence of crystal growth modi fi ers', *Chemical Engineering Science*. Elsevier, 101, pp. 593–602. doi: 10.1016/j.ces.2013.07.017.

Manrique, J. and Martinez, F. (2007) 'Solubility of ibuprofen in some ethanol+ water cosolvent mixtures at several temperatures', *Latin American Journal of Pharmacy*. COLEGIO DE FARMACEUTICOS, 26(3), p. 344.

Marchisio, D. L. and Fox, R. O. (2005) 'Solution of population balance equations using the direct quadrature method of moments', *Journal of Aerosol Science*, 36(1), pp. 43–73. doi: 10.1016/j.jaerosci.2004.07.009.

Marchisio, D. L., Vigil, R. D. and Fox, R. O. (2003a) 'Implementation of the quadrature method

of moments in CFD codes for aggregation – breakage problems', 58, pp. 3337–3351. doi: 10.1016/S0009-2509(03)00211-2.

Marchisio, D. L., Vigil, R. D. and Fox, R. O. (2003b) 'Quadrature method of moments for aggregation – breakage processes', 258, pp. 322–334. doi: 10.1016/S0021-9797(02)00054-1.

Marshall, T. C. *et al.* (1998) 'Statistical confidence for likelihood-based paternity inference in natural populations', *Molecular ecology*. Wiley Online Library, 7(5), pp. 639–655.

Matthews, H. B., Miller, S. M. and Rawlings, J. B. (1996) 'Model identification for crystallization: Theory and experimental verification', *Powder Technology*. Elsevier, 88(3), pp. 227–235. doi: 10.1016/S0032-5910(96)03125-7.

Mazzarotta, B. (1992) 'Abrasion and breakage phenomena in agitated crystal suspensions', *Chemical Engineering Science*. Elsevier, 47(12), pp. 3105–3111.

McDonald, D. B. *et al.* (2007) 'Global and local optimization using radial basis function response surface models', *Applied Mathematical Modelling*, 31(10), pp. 2095–2110. doi: 10.1016/j.apm.2006.08.008.

McGraw, R. (1997) 'Description of Aerosol Dynamics by the Quadrature Method of Moments', *Aerosol Science and Technology*, 27(2), pp. 255–265. doi: 10.1080/02786829708965471.

Meimaroglou, D., Roussos, a. I. and Kiparissides, C. (2006) 'Part IV: Dynamic evolution of the particle size distribution in particulate processes. A comparative study between Monte Carlo and the generalized method of moments', *Chemical Engineering Science*, 61(17), pp. 5620–5635. doi: 10.1016/j.ces.2006.05.001.

Mesbah, A. *et al.* (2009) 'A control oriented study on the numerical solution of the population balance equation for crystallization processes', *Chemical Engineering Science*. Elsevier, 64(20), pp. 4262–4277. doi: 10.1016/j.ces.2009.06.060.

Mesbah, A. *et al.* (2010) 'A model-based control framework for industrial batch crystallization processes', *Chemical Engineering Research and Design*, 88(9), pp. 1223–1233. doi: 10.1016/j.cherd.2009.09.010.

Mitchell, N. A. and Frawley, P. J. (2010) 'Nucleation kinetics of paracetamol–ethanol solutions

from metastable zone widths', *Journal of Crystal Growth*. Elsevier, 312(19), pp. 2740–2746.

Mitchell, N. A., Frawley, P. J. and Ó'Ciardhá, C. T. (2011) 'Nucleation kinetics of paracetamol–ethanol solutions from induction time experiments using Lasentec FBRM®', *Journal of Crystal Growth*. Elsevier, 321(1), pp. 91–99.

Mohan, R. and Myerson, A. S. (2002) 'Growth kinetics : a thermodynamic approach', *Chemical Engineering Science*, 57, pp. 4277–4285.

Mullen, S. F. and Jebwab, J. (1995) 'Methods and apparatus for generating pseudo-random binary patterns'. Google Patents.

Mullin, J. W. (2001) 'Crystallization', in. Butterworth-Heinemann, pp. 181–284. doi: 10.1021/op0101005.

Mullin, J. W. and Nývlt, J. (1988) 'Programmed cooling of batch crystallizers', *Chemical Engineering and Processing*, 24(4), pp. 217–220. doi: 10.1016/0255-2701(88)85005-0.

Mumtaz, H. S. *et al.* (1997) 'Orthokinetic Aggregation During Precipiations: A Computational Model for Calcium Oxalate Monohydrate', *Institution of Chemical Engineers*, 75, pp. 152–159.

Nagy, Z. and Agachi, S. (1997) 'Model predictive control of a PVC batch reactor', *Computers and Chemical Engineering*, 21(6), pp. 571–591.

Nagy, Z. K. (2003) 'Robust Nonlinear Model Predictive Control of Batch Processes Robust Nonlinear Model Predictive Control of Batch Processes', (February). doi: 10.1002/aic.690490715.

Nagy, Z. K., Chew, J. W., *et al.* (2008a) 'Comparative performance of concentration and temperature controlled batch crystallizations', *Journal of Process Control*, 18(3–4), pp. 399–407. doi: 10.1016/j.jprocont.2007.10.006.

Nagy, Z. K., Chew, J. W., *et al.* (2008b) 'Comparative performance of concentration and temperature controlled batch crystallizations', *Journal of Process Control*, 18(3–4), pp. 399–407. doi: 10.1016/j.jprocont.2007.10.006.

Nagy, Z. K., Fujiwara, M., *et al.* (2008) 'Determination of the kinetic parameters for the crystallization of paracetamol from water using metastable zone width experiments',

Industrial and Engineering Chemistry Research, 47(4), pp. 1245–1252. doi: 10.1021/ie060637c.

Nagy, Z. K. *et al.* (2013) 'Chemical Engineering Research and Design Recent advances in the monitoring , modelling and control of crystallization systems', *Chemical Engineering Research and Design*. Institution of Chemical Engineers, 91(10), pp. 1903–1922. doi: 10.1016/j.cherd.2013.07.018.

Nagy, Z. K. and Braatz, R. D. (2003) 'Robust Nonlinear Model Predictive Control of Batch Processes', *AIChE*, 49(7), pp. 1776–1786.

Nagy, Z. K. and Braatz, R. D. (2004) 'Open-loop and closed-loop robust optimal control of batch processes using distributional and worst-case analysis', *Journal of Process Control*, 14, pp. 411–422. doi: 10.1016/j.jprocont.2003.07.004.

Nagy, Z. K. and Braatz, R. D. (2012) 'Advances and New Directions in Crystallization Control', *Annual Review of Chemical and Biomolecular Engineering*, 3, pp. 55–75. doi: 10.1146/annurev-chembioeng-062011-081043.

Ni, X. and Liao, A. (2008) 'Effects of cooling rate and solution concentration on solution crystallization of L-glutamic acid in an oscillatory baffled crystallizer', *Crystal Growth and Design*. ACS Publications, 8(8), pp. 2875–2881.

Nikolaou, M. and Vuthandam, P. (1998) 'FIR model identification: parsimony through kernel compression with wavelets', *AIChE Journal*. Wiley Online Library, 44(1), pp. 141–150.

Ochsenbein, D. R. *et al.* (2015) 'Modeling the facet growth rate dispersion of β L -glutamic acid — Combining single crystal experiments with n D particle size distribution data', *Chemical Engineering Science*. Elsevier, 133, pp. 30–43. doi: 10.1016/j.ces.2015.02.026.

Ogata, K. (1995) *Discrete-time control systems*. Prentice Hall Englewood Cliffs, NJ.

Oguchi, T., Watanabe, A. and Nakamizo, T. (2002) 'Input-output linearization of retarded non-linear systems by using an extension of Lie derivative', *International Journal of Control*. Taylor & Francis, 75(8), pp. 582–590.

Onyemelukwe, I. I. *et al.* (2018) 'The heat transfer characteristics of a mesoscale continuous

oscillatory flow crystalliser with smooth periodic constrictions', *International Journal of Heat and Mass Transfer*. Elsevier Ltd, 123, pp. 1109–1119. doi: 10.1016/j.ijheatmasstransfer.2018.03.015.

Pardalos, P. M. and Romeijn, H. E. (2013) *Handbook of global optimization*. Springer Science & Business Media.

Peiró, J. and Sherwin, S. (2005) 'Finite difference, finite element and finite volume methods for partial differential equations', in *Handbook of materials modeling*. Springer, pp. 2415–2446.

Pöllänen, K. *et al.* (2006) 'Dynamic PCA-based MSPC charts for nucleation prediction in batch cooling crystallization processes', *Chemometrics and Intelligent Laboratory Systems*, 84(1-2 SPEC. ISS.), pp. 126–133. doi: 10.1016/j.chemolab.2006.04.016.

Porru, M. and Özkan, L. (2017) 'Monitoring of Batch Industrial Crystallization with Growth, Nucleation, and Agglomeration. Part 2: Structure Design for State Estimation with Secondary Measurements', *Industrial & engineering chemistry research*. ACS Publications, 56(34), pp. 9578–9592.

Powell, K A *et al.* (2015) 'Periodic steady-state flow crystallization of a pharmaceutical drug using MSMPR operation', *Chemical Engineering & Processing: Process Intensification*. Elsevier B.V., 97, pp. 195–212. doi: 10.1016/j.cep.2015.01.002.

Powell, Keddon A *et al.* (2015) 'Toward Continuous Crystallization of Urea-Barbituric Acid : A Polymorphic Co-Crystal System'. doi: 10.1021/acs.cgd.5b00599.

Qin, S. J. and Badgwell, T. A. (1997) 'An overview of industrial model predictive control technology', in *AIChE Symposium Series*. New York, NY: American Institute of Chemical Engineers, 1971-c2002., pp. 232–256.

Qin, S. J. and Badgwell, T. A. (2003) 'A survey of industrial model predictive control technology', *Control engineering practice*. Elsevier, 11(7), pp. 733–764.

Quintana-Hernandez, P. A., Tututi-avila, S. and Hern, S. (2012) 'Nonlinear MIMO Control of a Continuous Cooling Crystallizer', *Modelling and Simulation in Engineering*, 2012. doi:

10.1155/2012/912071.

Raff, T. *et al.* (2006) 'Nonlinear Model Predictive Control of a Four Tank System : An Experimental Stability Study', in *International Conference on Control Applications*, pp. 237–242.

Ramkrishna, D. (2000) 'Population Balances', in. Academic Press, pp. 47–192. doi: 10.1016/B978-012576970-9/50007-2.

Randolph, A. D. (1969) 'Effect of crystal breakage on crystal size distribution in mixed suspension crystallizer', *Industrial & Engineering Chemistry Fundamentals*. ACS Publications, 8(1), pp. 58–63.

Randolph, A. D. and Larson, M. A. (1971) 'Chapter 3 – THE POPULATION BALANCE', in *Theory of Particulate Processes*. Academic Press, pp. 41–63. doi: 10.1016/B978-0-12-579650-7.50008-7.

Rawlings, J. B., Miller, S. M. and Witkowski, W. R. (1993) 'Model identification and control of solution crystallization processes: a review', *Industrial & Engineering Chemistry Research*. ACS Publications, 32(7), pp. 1275–1296.

Rawlings, J. B., Witkowski, W. R. and Eaton, J. W. (1992) 'Modelling and control of crystallizers', *Powder Technology*, 69(1), pp. 3–9. doi: 10.1016/0032-5910(92)85002-D.

Rincón, F., Roux, G. and Lima, F. (2015) 'A novel ARX-based approach for the steady-state identification analysis of industrial depropanizer column datasets', *Processes*. Multidisciplinary Digital Publishing Institute, 3(2), pp. 257–285.

Saleemi, A. (2011) *Strategic feedback control of pharmaceutical crystallization systems*, *Loughborough University's Institutional Repository*.

Saleemi, A. N., Rielly, C. D. and Nagy, Z. K. (2012) 'Comparative Investigation of Supersaturation and Automated Direct Nucleation Control of Crystal Size Distributions using ATR-UV/vis Spectroscopy and FBRM', *Crystal Growth & Design*, 12, pp. 1792–1807.

Saleemi, A., Rielly, C. and Nagy, Z. K. (2012) 'Automated direct nucleation control for in situ dynamic fines removal in batch cooling crystallization', *CrystEngComm*, 14, pp. 2196–2203.

doi: 10.1039/c2ce06288g.

Saltelli, A. *et al.* (2008) *Global sensitivity analysis: the primer*. John Wiley & Sons.

Sanzida, N. and Nagy, Z. K. (2013) 'Iterative learning control for the systematic design of supersaturation controlled batch cooling crystallisation processes', *Computers and Chemical Engineering*. Elsevier Ltd, 59, pp. 111–121. doi: 10.1016/j.compchemeng.2013.05.027.

Sarkar, D., Rohani, S. and Jutan, A. (2006) 'Multi-objective optimization of seeded batch crystallization processes', *Chemical Engineering Science*, 61(16), pp. 5282–5295. doi: 10.1016/j.ces.2006.03.055.

Schnelle, F. and Eberhard, P. (2015) 'Constraint mapping in a feedback linearization/MPC scheme for trajectory tracking of underactuated multibody systems', *IFAC-PapersOnLine*, 48(23), pp. 446–451. doi: 10.1016/j.ifacol.2015.11.319.

Schorsch, S., Vetter, T. and Mazzotti, M. (2012) 'Measuring multidimensional particle size distributions during crystallization', *Chemical Engineering Science*. Elsevier, 77, pp. 130–142. doi: 10.1016/j.ces.2011.11.029.

Shen, J.-X., Chiu, M.-S. and Wang, Q.-G. (1999) 'A comparative study of model-based control techniques for batch crystallization process', *Journal of chemical engineering of Japan*. The Society of Chemical Engineers, Japan, 32(4), pp. 456–464.

Shinskey, F. G. (1996) *Process control systems: application, design, and tuning*. McGraw-Hill New York.

Simani, S., Fantuzzi, C. and Beghelli, S. (2000) 'Diagnosis techniques for sensor faults of industrial processes', *IEEE Transactions on Control Systems Technology*. IEEE, 8(5), pp. 848–855.

Van Soest, W. R., Chu, Q. P. and Mulder, J. A. (2006) 'Combined feedback linearization and constrained model predictive control for entry flight', *Journal of guidance, control, and dynamics*, 29(2), pp. 427–434.

Söhnel, O. and Garside, J. (1988) 'Solute clustering and nucleation', *Journal of Crystal Growth*. North-Holland, 89(2–3), pp. 202–208. doi: 10.1016/0022-0248(88)90403-4.

Su, Q., Nagy, Z. K. and Rielly, C. D. (2015) 'Pharmaceutical crystallisation processes from batch to continuous operation using MSMPR stages: Modelling, design, and control', *Chemical Engineering and Processing: Process Intensification*. Elsevier B.V., 89, pp. 41–53. doi: 10.1016/j.cep.2015.01.001.

Suh, K. and Hollerbach, J. (1987) 'Local versus global torque optimization of redundant manipulators', in *Proceedings. 1987 IEEE International Conference on Robotics and Automation*. IEEE, pp. 619–624.

Swaanenburg, H. A. C. *et al.* (1985) 'Practical aspects of industrial multivariable process identification', *IFAC Proceedings Volumes*. Elsevier, 18(5), pp. 201–206.

Szilágyi, B., Agachi, P. Ş. and Lakatos, B. G. (2015) 'Numerical analysis of crystallization of high aspect ratio crystals with breakage', *Powder Technology*, 283, pp. 152–162. doi: 10.1016/j.powtec.2015.05.029.

Törn, A. and Žilinskas, A. (1989) *Global optimization*. Springer.

Tretter, S. A. (1976) *Introduction to discrete-time signal processing*. Wiley New York.

Trifkovic, M., Sheikhzadeh, M. and Rohani, S. (2008) 'Kinetics estimation and single and multi-objective optimization of a seeded, anti-solvent, isothermal batch crystallizer', *Industrial and Engineering Chemistry Research*, 47(5), pp. 1586–1595. doi: 10.1021/ie071125g.

Tulleken, H. J. A. F. (1993) 'Grey-box modelling and identification using physical knowledge and bayesian techniques', *Automatica*, 29(2), pp. 285–308. doi: 10.1016/0005-1098(93)90124-C.

Ulrich, J. *et al.* (2001) 'Crystallization', *Kirk-Othmer Encyclopedia of Chemical Technology*, pp. 1–63. doi: 10.1002/0471238961.0318251918152119.a01.pub3.

Veesler, S. and Puel, F. (2015) 'Crystallization of Pharmaceutical Crystals', *Handbook of Crystal Growth*. Elsevier, pp. 915–949. doi: 10.1016/B978-0-444-56369-9.00021-6.

Vissers, J., Jansen, P. and Weiland, S. (2011) 'Control of Supersaturation in Batch Cooling Crystallization by Robust State Feedback Linearization', *IEEE International Conference on Control and Automation*, pp. 1114–1120.

Vollmer, U. and Raisch, J., (2003). Control of batch cooling crystallization processes based on orbital flatness. *International Journal of Control*, *76*(16), pp.1635-1643.

Vollmer, U. and Raisch, J. (2006) 'Control of batch crystallization-A system inversion approach', *Chemical Engineering and Processing: Process Intensification*, 45(10), pp. 874–885. doi: 10.1016/j.cep.2006.01.012.

Van De Wal, M. and De Jager, B. (2001) 'A review of methods for input/output selection', *Automatica*. Elsevier, 37(4), pp. 487–510.

Wang, L. (2009) *Model Predictive Control System Design and Implementation Using MATLAB*, *Engineering*. doi: 10.1007/978-1-84882-331-0.

Winston, P. (2015) *6.034 Artificial Intelligence, Fall 2010*. (Massachusetts Institude of Technology: MIT OpenCourseWare). Available at: http://ocw.mit.edu.

Wise, B. M. and Ricker, N. L. (1990) 'The effect of biased regression on the identification of FIR and ARX models', *Recent Advances in Process Control*.

Xiong, L. *et al.* (2018) 'Determination of metastable zone widths and nucleation behavior of aspirin in acetic acid and acetic anhydride binary solvent mixture', *Journal of Molecular Liquids*. Elsevier, 269, pp. 805–815. doi: 10.1016/J.MOLLIQ.2018.08.055.

Yang, Y., Ma, C. Y. and Wang, X. Z. (2012) *Optimisation and Closed-loop Control of Crystal Shape Distribution in Seeded Cooling Crystallisation of L-Glutamic Acid*, *IFAC Proceedings Volumes*. IFAC. doi: 10.3182/20120710-4-SG-2026.00112.

Yang, Y. and Nagy, Z. K. (2014a) 'Advanced control approaches for combined cooling and antisolvent crystallization (CCAC) in continuous mixed suspension mixed product removal (MSMPR) cascade crystallizers', *Computing and Systems Technology Division 2014 - Core Programming Area at the 2014 AIChE Annual Meeting*. Elsevier, 1, pp. 260–264. doi: 10.1016/j.ces.2015.01.060.

Yang, Y. and Nagy, Z. K. (2014b) 'Model-based systematic design and analysis approach for unseeded combined cooling and antisolvent crystallization (CCAC) systems', *Crystal Growth and Design*, 14(2), pp. 687–698. doi: 10.1021/cg401562t.

Yang, Y. and Nagy, Z. K. (2015) ‘Advanced control approaches for combined cooling / antisolvent crystallization in continuous mixed suspension mixed product removal cascade crystallizers’, *Chemical Engineering Science*. Elsevier, 127, pp. 362–373. doi: 10.1016/j.ces.2015.01.060.

Zhang, X. *et al.* (2015) ‘Nucleation kinetics of lovastatin in different solvents from metastable zone widths’, *Chemical Engineering Science*. Pergamon, 133, pp. 62–69. doi: 10.1016/J.CES.2015.01.042.